Molecular diversity of neurons in the ventral tegmental area and substantia nigra pars compacta

A thesis submitted for the degree of Doctor of Philosophy

Eleanor Jane Paul

Supervisor: Dr Mark Ungless

Neurophysiology Group

Imperial College London - Institute of Clinical Sciences

MRC London Institute of Medical Sciences

Abstract

Neurons in the ventral tegmental area (VTA) and substantia nigra pars compacta (SNc) are central to motivation and reward processing. These nuclei contain three core neuronal cell types: dopamine, GABA and glutamate (as well as combinatorial neurons). Dopamine neurons - the largest population - have been intensely studied, but little is known about the GABA neurons- the second largest population. They provide local inhibitory control of dopamine neurons with behavioural consequences, as well as sending long-range projections. It is unknown whether these are distinct populations of interneurons and projection neurons, or axon collaterals from the same population. Given what is known about interneurons and their control over principal cells in other networks, we hypothesised that diverse populations of interneurons are likely to be present in the VTA/SNc. However, there is no way of distinguishing them from projecting GABA populations, because there are no known molecular markers of GABA subpopulations in the VTA/SNc. My aim was to uncover novel molecular markers of subpopulations of GABA neurons in the VTA/SNc to provide new genetic entry points for future investigation of their function.

First, I investigated the expression of two cardinal interneuron markers, neuronal nitric oxide synthase (nNOS) and parvalbumin (PV), in the VTA/SNc using immunostaining and viral tracing. nNOS+ neurons are present throughout the VTA/SNc and neuronal phenotype is sub-region specific. PV+ neurons are also present and they are likely to be GABA interneurons.

Next, I isolated and sequenced mRNA from GABA and dopamine neurons in the midbrain using tagged polyribosomes. A comparison of transcriptomes revealed genes that are enriched in GABA neurons, offering novel candidates for subpopulation markers. These candidates were then validated through immunostaining. In conclusion, I have uncovered molecular markers of subpopulations of GABA neurons in the VTA/SNc as well as a novel population of nNOS+ glutamate neurons.

Contents

Declaration of Originality **6**

Copyright Declaration **7**

Acknowledgements **8**

List of Figures **9**

Chapter 4 – An unbiased approach: Isolating and sequencing mRNA from midbrain GABA and dopamine neurons **10**

List of Tables **12**

Chapter 2 – A biased approach: Investigating the expression of neuronal nitric oxide synthase in the VTA and SNc **12**

List of abbreviations 13

Chapter 1 – Introduction **18**

1.1 Introduction to the VTA and SNc 18

1.1.1 The early identification of dopamine cell groups throughout the brain 19

1.1.2 Anatomy of the VTA and SNc 21

1.2 Neuronal populations of the VTA and SNc 23

1.2.1 Dopamine neurons 24

1.2.2 GABA neurons 28

1.2.3 Glutamate neurons 29

1.2.4 Co-releasing neurons 30

1.3 Neuronal projections of the VTA and SNc 33

1.3.1 Dopamine neuron projections 33

1.3.2 GABA neuron projections 35

1.3.3 Local GABA neuron connections of the VTA and SNc 37

1.3.4 Glutamate neuron projections 38

1.3.5 Local glutamate neuron connections 39

1.3.6 Co-releasing projections 39

1.4 Inputs into the VTA and SNc 41

1.5 VTA and SNc circuits and behaviour 42

1.5.1 VTA and SNc dopamine neurons and behaviour 42

1.5.2 VTA and SNc GABA neurons and behaviour 44

1.5.3 VTA and SNC glutamate neurons and behaviour 46

1.6 Molecular diversity of neurons in the VTA and SNc 47

1.7 Selectively targeting neuronal populations 49

1.8 Project outline 50

Chapter 2 – A biased approach: Investigating the expression of neuronal nitric oxide synthase in the VTA and SNc 53
2.1 Introduction 53
2.1.1 The diversity of GABAergic interneurons 53
2.1.2 The expression of GABAergic interneuron markers in the VTA and SNc 55
2.1.3 Introduction to neuronal nitric oxide synthase 58
2.1.4 nNOS as a molecular marker in the brain 59
2.1.5 nNOS expression in the VTA and SNc 60
2.2 Experimental Procedures 63
2.2.1 Animals 63
2.2.2 DNA extraction 63
2.2.3 Genotyping 65
2.2.4 Perfusion fixation and tissue preparation 65
2.2.5 Immunocytochemistry 66
2.2.6 Viral vectors 67
2.2.7 Stereotaxic surgery for circuit tracing 68
2.2.8 Confocal Imaging, image processing and analysis 68
2.3 Results 71
2.3.1 Neurons in the VTA and SNc express nNOS 71
2.3.2 nNOS expressing neurons in the midbrain contain projecting and non-projecting populations 80
2.3.3 The degree of ChR2-mCherry and nNOS co-localisation is region specific 86
2.3.4 nNOS neurons are GABAARα1+ 89
2.3.5 Neurochemical identity of nNOS+ interneurons in the VTA and SNc 91
2.3.6 Neuronal phenotype of nNOS+ projection neurons in the VTA 96
2.4 Discussion 102
2.4.1 Validation of anti-nNOS antibodies in the VTA and SNC 102
2.4.2 There are at least three distinct populations of nNOS+ neurons in the VTA and SNc 102
2.4.3nNOS+ glutamate projection neurons 105
2.4.4 nNOS+ TH+ interneurons 108
Chapter 3 – A biased approach: Investigating the expression of parvalbumin in the VTA and SNc 111
3.1 Introduction 111
3.1.1 Parvalbumin as a molecular marker in the brain 111
3.1.2 Evidence of parvalbumin expression in the VTA and SNc 113
3.2 Experimental procedures 115

3.2.1 Animals 115
3.2.2 DNA extraction 115
3.2.3 Genotyping 115
3.2.4 Perfusion fixation and tissue preparation 116
3.2.5 Immunocytochemistry 117
3.2.6 Viral vectors 118
3.2.7 Stereotaxic surgery for circuit tracing 118
3.2.8 Confocal Imaging, image processing and analysis 118
3.3 Results 119
3.3.1 Neurons in the VTA and SNc that express PV 119
3.3.2 PV+ neurons are GABA neurons 122
3.3.3 Parvalbumin expressing neurons and nNOS expressing neurons are distinct populations in the VTA and SNc 125
3.3.4 PV+ neurons of the VTA and SNc do not send long-range projections 125
3.3.5 Most ChR2-mCherry + neurons are PV+ and GABAARα1+ 127
3.3.6 ChR2-mCherry+ neurons fibres and axon terminals are present in the VTA and SNc 129
3.4 Discussion 131
3.4.1 There are PV+ GABA neurons in the VTA and SNc 131
3.4.2 Preliminary tracing experiments suggests PV+ neurons in the VTA and SNc are interneurons 132
Chapter 4 – An unbiased approach: A comparison of the transcriptomes from GABA and dopamine neurons 134
4.1 Introduction 134
4.1.1 The isolation of ribosome associated mRNA from complex tissues 134
4.1.2 RiboTag technology 135
4.2 Experimental procedure 137
4.2.1 Animals 137
4.2.2 DNA extraction 137
4.2.3 Genotyping 137
4.2.4 Perfusion fixation and tissue preparation 138
4.2.5 Immunostaining 138
4.2.6 Preparation of fresh tissue for immunoprecipitation 140
4.2.7 Immunoprecipitation of tagged polyribosomes 140
4.2.8 RNA extraction 143
4.2.9 Assessment of RNA quality and quantity 143
4.2.10 Reverse transcription 144

4.2.11 Quantitative-RT-PCR 144
4.2.12 Statistical comparisons 145
4.2.13 RNA-library preparation and sequencing 145
4.2.14 RNA-Seq Analysis 146
4.2.15 Confocal Imaging, image processing and analysis 146
4.3 Results 147
4.3.1 Expression of RPL22^{HA} in target neurons 147
4.3.2 Assessment of purified RNA samples 149
4.3.3 Enrichment of cell type specific mRNAs 150
4.3.4 RNA-sequencing library preparation 154
4.3.5 A direct comparison of the transcriptomes of GABA and dopamine neurons 156
4.3.6 The selection of candidate markers 158
4.3.7 Validation of candidates 163
4.4 Discussion 183
4.4.1 Verification of RNA isolated via immunoprecipitation 183
4.4.2 Selection of candidate markers for GABA neuron subpopulations 183
4.4.3 Limitations to the candidate selection process 184
4.4.4 Validation of candidates 185
4.4.5 Future directions 186
References 191
Appendix 1: RNA-Seq candidate checklist 220

Declaration of Originality

The data presented in this thesis are a result of my own work and experimentation unless explicitly stated. Contributions made by others are appropriately acknowledged and referenced within the text.

No part of this thesis has been submitted for any other degree or professional qualification.

Copyright Declaration

The copyright of this thesis rests with the author and is made available under a Creative Commons Attribution Non-Commercial No Derivatives licence. Researchers are free to copy, distribute or transmit the thesis on the condition that they attribute it, that they do not use it for commercial purposes and that they do not alter, transform or build upon it. For any reuse or redistribution, researchers must make clear to others the licence terms of this work.

Acknowledgements

First and foremost, I would like to express my gratitude to my supervisor Mark Ungless. I thank you not only for the opportunity to take on this PhD but for the constant encouragement and direction I have received under your supervision. As a result of your guidance I was able to develop not only my skills as scientist but also my confidence. I cannot thank you enough for the all the lessons in both neuroscience and grammar. I hit the jackpot.

I owe a huge thank you to Kyoko Tossell. No matter how busy you were you always had the time to provide training, answer my questions and give general encouragement and support. Without your confocal microscopy lessons my thesis would not look so pretty. I would also like to thank Elaine Irvine for teaching me stereotaxic surgery and to Mel Clements for always answering my RNA-related questions and readily giving advice. I have thoroughly enjoyed my time at the LMS and that is down to the host of wonderful colleagues and friends I have made along the way. I would particularly like to thank all past and present members of the neurophysiology group, Michelle, Eleanor, Anushka, Katlyn, Eliza, Rebecca, Azhaar, Raj and Emilie and all who work in office 2008.

I am incredibly grateful to Dan. You have experienced the best and worst of my PhD journey alongside me. Thank you for being there to celebrate the successes however small, but also knowing when not ask about my day. I thank my brother Jon for bringing out the competitive streak that has driven me to work harder. Thank you for the interest and support you have always shown.

Finally, with the utmost gratitude I thank my parents. I inherited my interest in science from you both and without your unwavering encouragement I never would have made it to this point. I will be forever grateful for all the support, both moral and financial, that you have provided throughout my entire time in education. I owe you both so much.

List of Figures

Chapter 1 – Introduction

Figure 1: A sagittal schematic of the mouse brain illustrating the distribution of dopamine cell groups in the brain (A8-A16)..... 20

Figure 2: Schematics illustrating the anatomy of the VTA and SNc in mouse brain..... 22

Figure 3: Schematics illustrating the distribution of the three core neuronal groups throughout the VTA and SNc..... 23

Figure 4: Schematics illustrating the distribution of dopamine neurons that differentially express dopamine neuron marker genes..... 27

Figure 5: Schematics illustrating the distribution of neurons that express markers for different neuronal groups..... 32

Figure 6: Schematic showing some of the projections of dopamine neurons from the VTA and SNc..... 34

Figure 7: Schematic illustrating some of the established (anatomical) projections from GABA neurons in the VTA..... 36

Figure 8: Schematic illustrating some of the established (anatomical) projections from glutamate neurons in the VTA..... 38

Figure 9: Schematic showing the long-range projections of different co-releasing neurons of the VTA..... 40

Chapter 2 – A biased approach: Investigating the expression of neuronal nitric oxide synthase in the VTA and SNc

Figure 10: Molecular markers of GABA interneurons and evidence of their expression in the VTA and SNc..... 57

Figure 11: A comparison of three anti-nNOS antibodies in the midbrain of WT and NOS1-KO.... 74

Figure 12: Dual immunostaining for nNOS and TH in the VTA and SNc..... 75

Figure 13: Triple immunostaining for nNOS, HA and TH in VGATCre:RiboTag..... 78

Figure 14: Schematic illustrating localisation of nNOS+ GABA and nNOS+ glutamate in sub regions of the VTA and the SNc..... 79

Figure 15: Representative images showing the ChR2-mCherry cell body expression exhibited by each injected group..... 84

Figure 16: Representative images showing the presence or absence of ChR2-mCherry+ axon terminals in different brain regions of each injected group..... 85

Figure 17: The degree of co-localisation between ChR2-mCherry+ and nNOS+ neurons in each sub-region..... 87

Figure 18: ChR2-mCherry+ neurons are GABAARα1+..... 90

Figure 19: ChR2-mCherry+ neurons form synapses in the VTA…… 92

Figure 20: There is some co-localisation between ChR2-mCherry+ cell bodies and VGLUT2 immunostaining in the PBP…… 93

Figure 21: ChR2-mCherry, TH, and VGAT+ co-localisation in the SNc…….. 95

Figure 22: There is co-localisation between all imaged ChR2-mCherry+ cell bodies and VGLUT2 immunostaining in the RLi. …… 96

Figure 23: ChR2-mcherry+ axon terminals in the VP…….. 98

Figure 24: ChR2-mcherry+ axon terminals in the raphe…… 100

Figure 25: A summary of the three types of nNOS+ neurons discovered in the VTA and SNc…… 105

Chapter 3 – A biased approach: Investigating the expression of parvalbumin in the VTA and SNc

Figure 26: Tile-scans from different rostro-caudal levels of the VTA and SNc showing the distribution of PV+ neurons…….. 120

Figure 27: Double immunostaining for PV and TH in sub-regions of the VTA and SNc…… 121

Figure 28: Triple immunostaining for PV, HA and TH in VGATCre:RiboTag mice…… 123

Figure 29: Schematic illustrating the distribution of parvalbumin+ cells observed throughout the VTA and SNc…… 124

Figure 30: Triple immunostaining for PV, NOS1 and TH in the VTA…….. 125

Figure 31: Schematic illustraiting the precence of ChR2-mCherry+ cells (magenta dots) in the midbrian of injected mice…….. 126

Figure 32: Triple immunostaining for PV, NOS1 and TH in the VTA…….. 128

Figure 33: ChR2-mCherry+ neurons co-localise with GABAARα1…… 129

Figure 34: Examples of ChR2-mCherry+ processes and terminals within the VTA and SNc……. 130

Figure 35: CHR2-mCherry+ terminals co-localise with VGAT…… 130

Chapter 4 – An unbiased approach: Isolating and sequencing mRNA from midbrain GABA and dopamine neurons

Figure 36: Schematic illustrating the RiboTag and Cre-Driver line cross…… 136

Figure 37: Schematic illustrating the protocol for the isolation of ribosomal associated mRNA from neurons in the midbrain…….. 142

Figure 38: Immunohistochemistry for the HA-tag to verify expression in the target neuronal populations…….. 148

Figure 39: Assessment of RNA quality…… 151

Figure 40: Assessment of RNA quantity…… 152

Figure 41: Enrichment of transcripts expressed in GABA and dopamine neurons…… 153

Figure 42: Examples of High sensitivity-DNA electropherograms of libraries prepared from IP-RNA…… 155

Figure 43: The fold enrichment in GABA-IP relative to dopamine-IP RNA subjected to RNA-seq for transcripts specific to GABA neurons and dopamine neurons…… 156

Figure 44: A direct comparison of the transcriptomes of GABA and dopamine neurons…… 157

Figure 45: Flowchart summarising the steps taken in selecting novel candidates for markers of GABA neurons in the midbrain…… 159

Figure 46: Quantitative data from the Allen Brain Atlas for 1102 genes extracted from PANTHER…… 161

Figure 47: ISH data from the ABA showing the expression of GPR101 in the VTA and SNc…… 165

Figure 48: Immunohistochemistry showing the expression of GPR101 in relation to GABA neurons in the VTA and SNc…… 165

Figure 49: ISH data from the ABA showing the expression of CBLN4 in the VTA and SNc…… 166

Figure 50: Immunohistochemistry showing the expression of CBLN4 in in relation to GABA neurons of the VTA and SNc…… 169

Figure 51: ISH data from the ABA showing the expression of RXFP3 in the VTA and SNc…… 171

Figure 52: Immunohistochemistry showing the expression of RXFP3 in in relation to GABA neurons of the VTA and SNc…… 172

Figure 53: ISH data from the ABA showing the expression of RORA in the VTA and SNc…… 174

Figure 54: Immunohistochemistry showing the expression of RORA in in relation to GABA neurons of the VTA and SNc…… 175

Figure 55: ISH data from the ABA showing the expression of TRH in the VTA and SNc…… 177

Figure 56: Immunohistochemistry showing the expression of TRH in the hypothalamus and in the VTA…… 178

Figure 57: ISH data from the ABA showing the expression of S100B in the VTA and SNc…… 180

Figure 58: Immunohistochemistry showing the expression of S100B in relation to GABA neurons of the VTA and SNc…… 180

Figure 59: ISH data from the ABA showing the expression of NRP2 in the VTA and SNc…… 182

Figure 60: Immunohistochemistry showing examples of NRP2 expressing dendrites in the VTA…… 182

List of Tables

Chapter 2 – A biased approach: Investigating the expression of neuronal nitric oxide synthase in the VTA and SNc

Table 1: Summary of the publications investigating the presence of nNOS in the VTA and SNc..... 62

Table 2: Mouse strain information..... 63

Table 3: Genotyping information..... 64

Table 4: Primary antibody information..... 66

Table 5: Secondary antibody information..... 67

Table 6: Injections details, cell body detection and axon terminal detection in all injected mice..... 81

Table 7: A summary of five groups of expression patterns observed in the injected mice.... 82

Chapter 3 – A biased approach: Investigating the expression of parvalbumin in the VTA and SNc

Table 8 Summary of the publications investigating the presence of PV in the VTA and SNc... 114

Table 9 Mouse strain information..... 115

Table 10 Genotyping information..... 116

Table 11 Primary antibody information..... 117

Table 12 Secondary antibody information..... 117

Chapter 4 – An unbiased approach: Isolating and sequencing mRNA from midbrain GABA and dopamine neurons

Table 13 Mouse strain information..... 133

Table 14 Genotyping information..... 138

Table 15 Primary antibody information..... 139

Table 16 Secondary antibody information..... 139

Table 17 Oligonucleotides used in quantitative RT-PCR experiments..... 144

Table 18 Final RNA-sequencing library information..... 154

Table 19 Details of the final 12 candidates identified as potential novel markers for subpopulations of midbrain GABA neurons..... 162

List of abbreviations

5-HT	Serotonin/5-hydroxytriptamine
AA	Amydaloid area
AADC/DDC	Aromatic amino acid decarboxylase/Dopa decarboxylase
AAV	Adeno-associated virus
ABA	Allen brain atlas
ALDH1A1	Aldehyde dehydrogenase family 1 member A1
AP	Antero-Posterior
Atg	Anterior tegmental nucleus
AV	Anterior ventral nucleus of the thalamus
BLA	Basal lateral amygdala
BNST	Bed nucleus of the stria terminalis
CA	Catecholamine
CALB2	Calretinin
CBLN4	Cerebellin 4
CCK	Cholecystokinin
cDNA	copy DNA
cGMP	Cyclic guanosine monophosphate
ChR2	Channel rhodopsin
Cli	Caudal linear nucleus
CNP	2',3'-Cyclic-nucleotide 3'-phosphodiesterase
Cre	Cre recombinase
DAT/Slc6a3	Dopamine transporter/Solute Carrier Family 6 Member 3
DBH	Dopamine beta-hydroxylase
DM	Dorsomedial nucleus of the hypothalamus
DMTg	Dorsal medial tegmental nucleus
DNA	Deoxyribonucleic acid
DR	Dorsal raphe
DV	Dorso-ventral
EDTA	Ethylenediaminetetraacetic acid
Eng2	Engrailed-2

eNOS	Endothelial nitric oxide synthase
EPSC	Excitatory postsynaptic current
FACs	Fluorescence-activated cell sorting
FIF	Formaldehyde induced-fluorescence
Flp	Flp recombinase
GABA	Gamma-amino butyric acid
GABAARα1	GABA A receptor alpha 1
GAD1/67	Glutamic acid decarboxylase 1/67
GAD2/65	Glutamic acid decarboxylase 2/65
GAT1	GABA transporter 1
GAT4	GABA transporter 4
GATA3	GATA Binding Protein 3
gDNA	genomic DNA
GFAP	Glial fibrillary acidic protein
GIRK	G-Protein inwardly rectifying potassium
GP	Globus pallidus
GPR101	G-protein couple receptor 101
HA	Haemagglutinin
HDB	horizontal limb of the diagonal band
IF	Interfasciuclar nucleus
iNOS	inducible nitric oxide synthase
IP	Immunoprecipitation
IPN	Interpeduncular nucleus
IPSC	Inhibitory postsynaptic potential
ISH	In situ hybridisation
LC	Locus coeruleus
LCM	Laser capture microdissection
LD	Laterodorsal thalamic nucleus
LDTg	Laterodorslal tegmental nucleus
LH	Lateral hypothalamus
LHb	Lateral habenula
LPO	Lateral preoptic area
LS	Lateral speptum

MCPO	Magnocellular preoptic area
MD	Medio-dorsal nucleus of the thalamus
ML	Medio-lateral
MnR	Median raphe nucelus
mPFC	Medial prefrontal cortex
Mrt	mesencephalic reticular formation
MS	Medial septum
NAc	Nucleus accumbens
NDS	Normal donkey serum
NMDA	N-Methyl-D-aspartic acid
NO	Nitric oxide
NOS1/nNOS	Neuronal nitric oxide synthase
NPY	Neuropeptide Y
NRP2	Neuropillin 2
NTS	Neurotensin
OCT	Optical cutting temperature
OT	Olfactory tubercle
oxR1	orexin receptor type 1
PAG	Periaqueductal grey
PANTHER	Protein analysis through evolutionary relationships
PBP	Parabrachial pigmented area
PBS	Phosphate buffered saline
PBSTx	Triton-x in phosphate buffered saline
PCR	Polymerchase chain reaction
PFA	Paraformaldehyde
PFC	Prefrontal cortex
PH	Posteror hypothalamus
PHA-L	*Phaseolus vulgaris* leucoagglutinin
PMnR	Paramedian raphe nucleus
PN	paranigral nucleus
Pn	Pontine nucleus
PnC	Pontine reticular nucleus, caudal part
PO	Preoptic area

PPTg	Pedunculopontine tegmentum
PV	Parvalbumin
qRT-PCR	Quantitative real time polymerase chain reaction
RELN	Reelin
RIN	RNA integrity number
RIP	Raphe interpositus nucleus
RLi	Rostral linear nuclei
RMg	Raphe magnus
RMTg	Rostro-medial tegmental nucleus
RORA	RAR Related Orphan Receptor A
RRF	Retrorubro field
RXFP3	Relaxin/insulin-like family peptide receptor 3
S100B	S100 calcium-binding protein B
SI	Substantia innominata
SNc	Substantia Nigra pars compacta
SNL	Lateral substanti nigra
SNr	Substantia Nigra pars reticulata
SOM	Somatostatin
ST	Bed nucleus of the stria terminalis
SUM	Supramamillary nucleus
Tac1	Tachykinin
TH	Tyrosine Hydroxylase
TRAP	Translating affinity ribosome purification
TRH	Thyrotropin-releasing hormone
Tz	Trapezoid nucleus
UV	Ultra-violet
VGAT/Slc32a1	Vesicular GABA transporter/Solute Carrier Family 32 Member 1
VGLUT2/Slc17a6	Vesicular glutamate transporter 2/Solute Carrier Family 17 Member 6
VIP	Vasoactive intestinal polypeptide
VM	Ventromedial thalamus
VMAT2/Slc18a2	Vesicular monoamine transporter 2/Solute Carrier Family 18 Member A2
VP	Ventral pallidum
VTA	Ventral Tegmental Area

VTAR	Rostral ventral tegmental area
WAG	Wheat germ agglutinin
WT	Wild-type
ZI	Zona inserta

Chapter 1 – Introduction

1.1 Introduction to the VTA and SNc

The ventral tegmental area (VTA) and the substantia nigra pars compacta (SNc) are found in the ventral midbrain. They are the two core nuclei of the midbrain dopamine system. Neurons whose cell bodies lie within these nuclei send long range, diverse projections to multiple different brain regions (Bjorklund and Dunnett, 2007; Lammel *et al*., 2014a; Morales and Margolis, 2017). It is in part due to their widespread connections that the dopamine system is central to the control of a wide range of normal brain functions; and conversely, why it is implicated in multiple neuropsychiatric disorders (Parkinson's disease, schizophrenia and drug addiction). These normal brain functions include voluntary movement, working memory, motivation and reward processing. (Bao *et al*., 2001; Bariselli *et al*., 2016; Bjorklund and Dunnett, 2007; Bromberg-Martin *et al*., 2010; Comoli *et al*., 2003; Di Chiara, 2002; Frank, 2005; Grace, 1991; Hikida *et al*., 2010; Hikosaka, 2007; Hochbaum *et al*., 2014; Kapur, 2003; Kravitz *et al*., 2010; Lammel *et al*., 2014a; Marshall *et al*., 1976; Matsumoto and Hikosaka, 2009; Meyer-Lindenberg *et al*., 2005; Morales and Root, 2014; Redgrave *et al*., 2008; Robinson and Berridge, 1993; Satoh *et al*., 2003; Schultz, 1986; Tzschentke and Schmidt, 2000; Wang *et al*., 2004; Zahniser and Sorkin, 2004). Dopamine neurons have been studied intensely, they are a heterogeneous group of cells that form subpopulations with different electrophysiological properties, as well as having distinct target regions (Bariselli *et al*., 2016; Brown *et al*., 2009; Lammel *et al*., 2011; Morales and Margolis, 2017; Poulin *et al*., 2014). In the VTA and SNc dopamine neurons make up the largest neuronal population, but their cell bodies lie intermingled with gamma-aminobutyric acid (GABA) neurons and a small population of glutamate neurons (German and Manaye, 1993a; Hnasko et al., 2012; Li et al., 2013; Margolis et al., 2012; Nair-Roberts et al., 2008; Olson and Nestler, 2007; Yamaguchi et al., 2011)

. GABA and glutamate populations regulate the activity of dopamine neurons by forming local connections, (Dobi *et al.,* 2010; Omelchenko and Sesack, 2009; Tan *et al.,* 2012; van Zessen *et al.,* 2012; Wang *et al.,* 2015b), and by sending long range projections to dopamine neuron target areas (Brown *et al.,* 2009; Hnasko *et al.,* 2012; Qi *et al.,* 2014; Root *et al.,* 2014b; Taylor *et al.,* 2014). There is also small populations of neurons that co-release GABA and glutamate (Root *et al.,* 2014b), dopamine and glutamate (Stuber *et al.,* 2010; Tecuapetla *et al.,* 2010; Zhang *et al.,* 2015), or dopamine and GABA (Berrios *et al.,* 2016; Kim *et al.,* 2015; Root *et al.,* 2014b; Tritsch *et al.,* 2014). In this introductory chapter I will introduce the VTA and SNc and describe what we know about the neurons whose cell bodies reside here.

1.1.1 The early identification of dopamine cell groups throughout the brain

Dopamine is a member of the catecholamine (CA) family of neurotransmitters, along with noradrenaline and adrenaline. CAs were originally visualised in the early 1960s with the development of the formaldehyde histofluorescence method (Falck, 1962). This was the first microscopic method that allowed the sensitive visualisation of neurotransmitters within neurons. The original formaldehyde-induced fluorescence (FIF) method was based on the exposure of freeze-dried tissue to formaldehyde vapour. This then triggered the conversion of dopamine and noradrenaline into isoquinoline molecules that emit a yellow-green fluorescence under the microscope. It was by using this method that two CAs were first identified (noradrenaline and dopamine) in discrete neuronal systems in the brain (Bjorklund and Dunnett, 2007; Carlsson *et al*., 1962; Dahlstrom and Fuxe, 1964).

The basic organisation of the dopaminergic system was established a decade later when it became possible to specifically detect dopamine synthesising enzymes using antibodies. These enzymes included tyrosine hydroxylase (TH) and aromatic amino acid decarboxylase (AADC) - sometimes referred to as DOPA decarboxylase (DDC). These early studies identified nine distinct dopamine neuron cell groups in the brain (termed A8-A16), which are distributed from the mesencephalon to

the olfactory bulb. Three are found in the ventral midbrain (A8-10) **(Figure 1)** (Bjorklund and Dunnett, 2007; Hokfelt *et al*., 1973). It is these three cell groups which make up the midbrain dopamine system.

A9 and A10 form the two major subgroups of midbrain dopamine neurons, with a small population in A8. The A10 group spans the VTA, A9 is found in the SNc and A8 lies in the retrorubral field (RRF) (Bjorklund and Dunnett, 2007). These three cell groups are conserved across mammalian species. However, with increasing size and complexity of primates there is a corresponding increase in dopaminergic cell density - most clearly observed in the SNc.

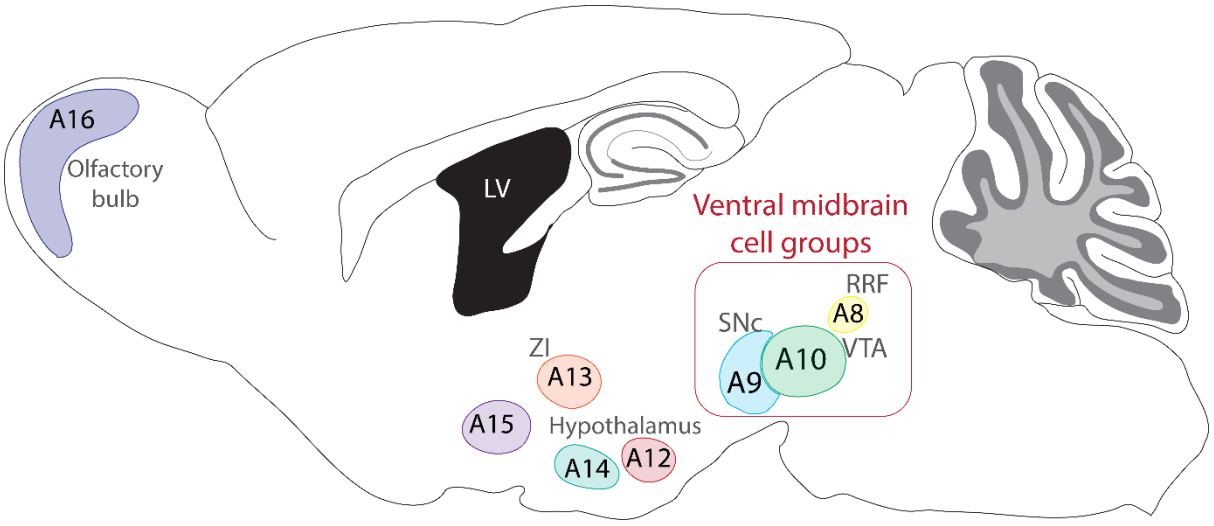


Figure 1: A sagittal schematic of the mouse brain illustrating the distribution of dopamine cell groups in the brain (A8-A16). *Adapted from (Bjorklund and Dunnett, 2007) Outlines adapted from (Franklin and Paxinos, 2008).*

1.1.2 Anatomy of the VTA and SNc

These two nuclei are usually defined using immunostaining for TH, which has become the gold standard for identification of dopamine neurons. The edge of the dopaminergic neuron cluster corresponds to the border of the nuclei. The VTA spans the largest anatomical area of the two nuclei. Its more caudal region sits above, and surrounds, the interpeduncular nucleus (IPN), and more rostrally it lies dorsal to the mammillary bodies. It extends bi-laterally from the midline to its boundary with the SNc. The VTA can be split into further sub-divisions based on neuroanatomical and functional differences. These sub-regions were first identified based on the different morphology and orientation of dopamine neuron cells bodies and their processes (Fu *et al*., 2012; Halliday and Tork, 1986; Oades and Halliday, 1987; Phillipson, 1979a, b; Sanchez-Catalan *et al*., 2014).

The parabrachial pigmented area (PBP) and the paranigral nucleus (PN) form the lateral parts of the VTA and are present over a large part of the rostro-caudal extent of the nucleus. The PN lies just dorso-lateral to the IPN (Franklin and Paxinos, 2008; Fu *et al*., 2012). It is mostly composed of fusiform cells with medium-sized cell bodies and of smaller cells with spiny dendrites. The PBP is located dorsally and dorsolateral to the PN, and extends laterally to border the SNc. The neurons in the PBP tend to be either fusiform or globular with numerous radial dendrites. Rostrally, the PBP becomes the wing-shaped rostral VTA (VTAR). The interfascicular nucleus (IF) and the rostral linear nuclei (RLi) make up the more medial regions of the VTA. The IF extends over the whole anterio-posterior extent of the VTA and is composed of round and densely packed cells that are smaller than those found in the other sub-regions (Fu *et al*., 2012; Phillipson, 1979b). The RLi lies above the IF and extends dorsally in the midline towards the dorsal raphe nucleus. The RLi continues posteriorly and medially from the VTA and extends dorsally in the midline towards the dorsal raphe nucleus (Del-Fava et al., 2007; Franklin and Paxinos, 2008; Fu et al., 2012; German and Manaye, 1993a; Halliday and Tork, 1986; Oades and Halliday, 1987; Phillipson, 1979b; Sanchez-Catalan et al., 2014). The SNc forms boundaries with the VTA and the substantia nigra pars reticulata (SNr) (Franklin and Paxinos, 2008; Fu et al., 2012; German and Manaye, 1993a). The SNr is a largely GABAergic nucleus that marks the lateral boundary of the

midbrain dopaminergic nuclei. GABA neurons in this region send collaterals into the SNc and VTA, as well as long-range projections (Zhou and Lee, 2011) **(Figure 2).**

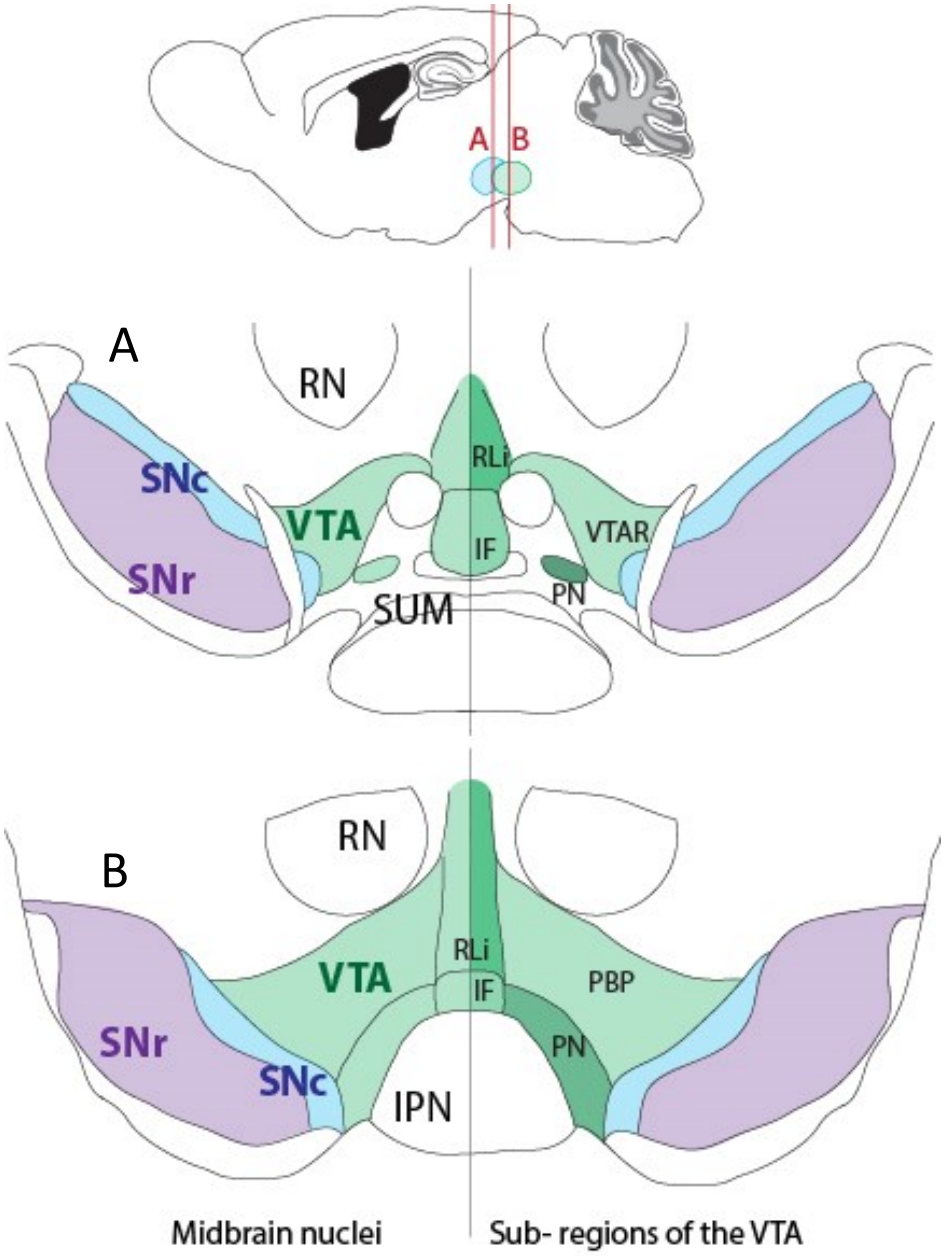


Figure 2: Schematics illustrating the anatomy of the VTA and SNc in mouse brain.

Coronal cross sections through the midbrain showing the anatomy of the VTA and SNc and surrounding region. The various sub-regions of the VTA are shown on the right hand side. *Outlines adapted from (Franklin and Paxinos, 2008).*

1.2 Neuronal populations of the VTA and SNc

Although dopamine neurons make up the primary neuronal population of the VTA and SNc, their cell bodies lie intermingled with GABA neurons and glutamate neurons **(Figure 3)**. In addition to these core neuronal identities, there is also evidence of neurons that can co-release more than one neurotransmitter. In this part of the introduction, I will introduce what we know about the organisation and distribution of these different neuronal populations within the VTA and SNc.

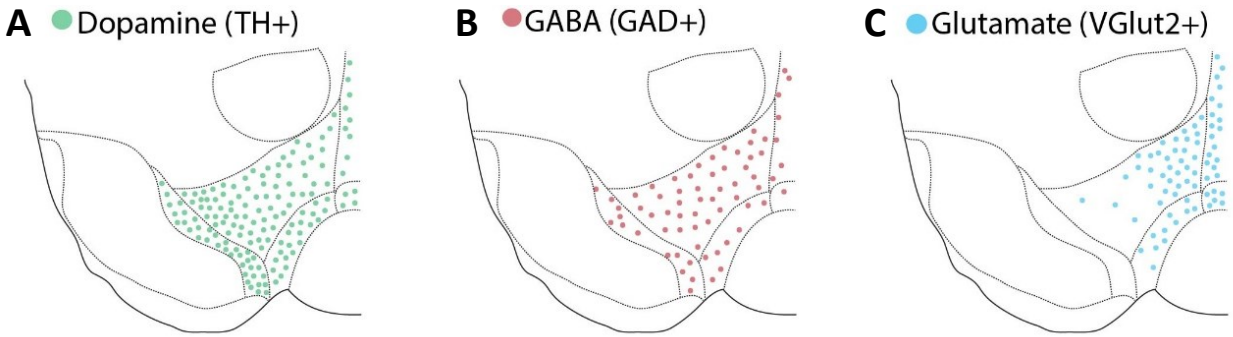


Figure 3: Schematics illustrating the distribution of the three core neuronal groups throughout the VTA and SNc. The distribution of dopamine **(A)**, GABA **(B)** and glutamate **(C)** neurons in the VTA and SNc, the diagrams are based on ISH data for TH, GAD and VGLUT2 (Nair-Roberts *et al.,* 2008). *Outlines adapted from (Franklin and Paxinos, 2008).*

1.2.1 Dopamine neurons

A neuron that synthesises and releases the neurotransmitter dopamine is defined as a dopamine neuron. For this reason, the expression of dopamine synthesising enzymes - TH in particular - is typically used to assign a dopaminergic phenotype (Bjorklund and Dunnett, 2007; Morales and Margolis, 2017). Dopamine is synthesised when phenylalanine hydroxylase converts phenylalanine to tyrosine which is the hydroxylated by TH, this is the rate limiting step in the dopamine synthesis pathway. The product, L-DOPA, is then converted to dopamine by lyase enzyme AADC/DDC (Morales and Margolis, 2017; Musacchio, 1975). In neurons that contain dopamine beta-hydroxylase (DBH), dopamine is converted to NA. These neurons make up catecholamine cell groups A1-A7 (Musacchio, 1975). In the dopamine cell groups A8-A16 (including the VTA and SNc, where DBH is not expressed) dopamine is packaged into vesicles by vesicular monoamine transporter 2 (VMAT2) for release at synapses (Eiden *et al*., 2004). Dopamine is released from axon terminals in long-range target areas where it binds to post-synaptic receptors (Beaulieu and Gainetdinov, 2011). In addition to this, dopamine neurons can release dopamine locally through their soma or dendrites in the VTA and SNc (Bjorklund and Lindvall, 1975; Cheramy *et al.,* 1981; Geffen *et al.,* 1976; Lacey *et al.,* 1987; Nieoullon *et al.,* 1977; Rice and Patel, 2015). Locally released dopamine binds to D2 autoreceptors (D2R) to regulate the rate and pattern of firing of the dopamine neurons, thereby regulating distal neurotransmitter release (Beckstead *et al.,* 2004; Pucak and Grace, 1994; Santiago and Westerink, 1991; Zhou *et al.,* 2009). Dendritically released dopamine also binds to D1 dopamine receptors on the terminals of neurons innervating the SNr from the striatum, enhancing GABA release from these terminals (Miyazaki and Lacey, 1998; Radnikow and Misgeld, 1998). After being released from the receptors dopamine undergoes re-uptake into the pre-synaptic neuron either by the dopamine transporter (DAT), or a non-specific monoamine transporter (Torres *et al*., 2003). DDC, VMAT, D2R and DAT are the other molecular markers used to identify dopamine neurons, along with TH.

The numbers and distribution of dopamine neurons in the VTA and SNc has been quantified extensively in rodents . Based on immunohistochemical labelling of TH (the rate limiting enzyme in

the dopamine synthesis pathway) there are approximately 65,000 dopamine neurons (bilaterally) across the VTA and SNc of the rat. The majority of these (>60%) lie in the VTA, but their distribution varies within different VTA sub-regions. The PBP and the PN nucleus contain much larger numbers of dopamine neurons than the RLi and IF in the more medial regions of the VTA (Fu *et al*., 2012; Nair-Roberts *et al*., 2008) **(Figure 3A).**

The presence of TH is often considered the gold standard method of dopamine neuron identification in the midbrain. In other brain regions, such as in the hypothalamic dopamine cell groups, the TH+ neurons far outweigh the number of dopamine neurons present (Bjorklund and Dunnett, 2007). In addition, TH containing interneurons that are not dopaminergic have been detected in the dorsal striatum (Cossette et al., 2005a; Cossette et al., 2005b; Cossette et al., 2004; Ibanez-Sandoval et al., 2010; Mao et al., 2001; Meredith et al., 1999; Petroske et al., 2001; Robinson et al., 2002a; Xenias et al., 2015b). These striatal TH+ interneurons do no express AADC, VMAT2 or DAT (Xenias et al., 2015b) and therefore lack the machinery required to synthesise and release dopamine. There is also a population of neurons in the bed nucleus of the stria terminalis (BNST) that transiently express TH in early adulthood (Carter, 2017). Despite their expression of TH, these neurons are not considered to be dopamine neurons. In the VTA and SNc immunohistochemical and in situ hybridisation (ISH) studies have shown that all TH expressing neurons in the VTA also express AADC, the two enzymes required for dopamine synthesis (Li *et al*., 2013). However, not all TH+ cells express the remaining three dopamine neuron 'markers': VMAT2, DAT or D2R. In fact, only 40% of dopamine neurons express all four of these classical markers. TH/VMAT2/DAT/D2R+ cells tend to lie in the more lateral regions of the PBP, this is also where the immunoreactivity of AADC appears strongest (Lammel *et al*., 2008; Li *et al*., 2013). As VMAT2 is thought to be required for packaging dopamine into vesicles release, it is unknown whether VMAT2 lacking neurons can actually release dopamine (Morales and Margolis, 2017). A population of TH+ neurons that project to the LHb are VMAT2- and have been shown to release GABA and not dopamine (Stamatakis *et al*., 2013). In addition to this, there is a subset of neurons in mice that produce mRNA for TH, but do not produce the enzyme itself and therefore cannot

synthesise dopamine. This means that detecting TH expression, through mRNA or gene expression can result in false positives (Lammel *et al.,* 2015; Yamaguchi *et al.,* 2015). This is a problem that has particularly come to light with the use of TH-Cre driver mouse lines for the targeting and studying of dopamine neurons (Lammel *et al.,* 2015; Lindeberg *et al.,* 2004; Min *et al.,* 1994; Savitt *et al.,* 2005). The genetic targeting of dopamine neurons using cre-recombinase expression driven by the TH promoter can result in transgene expression that extends beyond the boundary of the VTA and SN. Pronounced transgene expression has also been observed in TH and AADC neurons within the VTA and SNc. It is possible that this ectopic expression could have led to the stimulation of non-dopamine neurons concurrently along with the intended target cells, resulting in the misinterpretation of behavioural data (Lammel *et al*., 2015). The other Cre-driver line used to target dopamine neurons is the DATCre line, where cre-recombinase is under the control of the promoter for the slc6a3 (DAT) gene (Backman *et al*., 2006). A study comparing TH-Cre and DATCre mouse lines showed that the DATCre driver line exhibited a more selective transgene expression (Lammel *et al*., 2015). However, they are not without their problems. Dopamine neurons in more medial regions of the VTA that express lower levels of DAT or are DAT- could be omitted from studies using these mice (Lammel *et al*., 2015). The heterogeneity in expression of dopamine neuron marker genes indicates the possibility that regional bias may be unconsciously introduced into studies that use different combinations of markers to identify cells as dopaminergic. With this in mind, it is important that this molecular heterogeneity is taken into account when designing experiments.

Landmark studies of dopamine neurons in rats in the 1980s described their electrophysiological properties and identified a uniform set of features which became the classical 'functional fingerprint' of midbrain dopamine neurons (Grace and Bunney, 1980, 1984a; Grace et al., 1980; Ungless and Grace, 2012a). These features included action potentials with a unique broad waveform and either a low frequency and irregular firing rate, or transient high frequency bursting. This 'functional fingerprint', along with inhibition of firing after application of a D2 auto receptor agonist (for example, apomorphine), became the principal way of identifying dopamine neurons *in vivo* (Grace and Bunney,

1980, 1984a; Grace et al., 1980; Margolis et al., 2006b). More recent studies suggest that the criteria of a broad-waveform and slow firing rate alone may be inadequate to identify dopamine neurons in the VTA . It has been shown that the action potential duration of dopamine neurons varies with their projection target (Lammel *et al*., 2008; Margolis *et al*., 2006a; Margolis *et al*., 2008). In addition, a group of neurons in the rat VTA were excited by aversive stimuli and exhibited the functional properties of putative dopamine neurons, but were TH-. In this study all the identified TH+ neurons were inhibited by aversive stimuli (Ungless *et al.,* 2004). These data have highlighted the importance of using multiple modes of experimentation in order to confirm a neuronal phenotype before interpreting results (Ungless and Grace, 2012a).

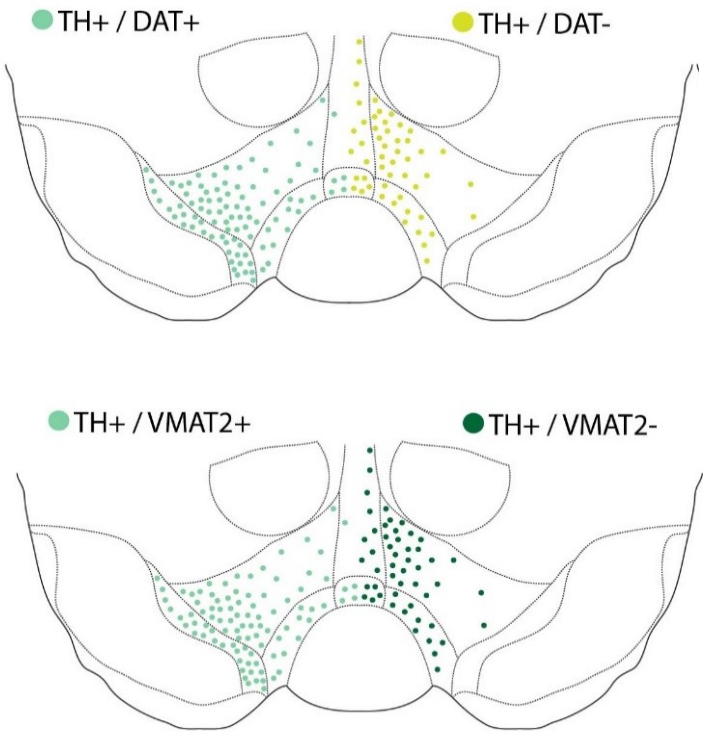


Figure 4: Schematics illustrating the distribution of dopamine neurons that differentially express dopamine neuron marker genes *Adapted from (Morales and Margolis, 2017). Outlines adapted from (Franklin and Paxinos, 2008)*

1.2.2 GABA neurons

Like dopamine neurons, GABA neuron cell bodies are distributed throughout the VTA and SNc where they lie intermingled with other cell types (Margolis *et al*., 2012; Nair-Roberts *et al*., 2008) **(Figure 3B).** GABA is synthesised from glutamate by the enzymes glutamate decarboxylase 1 and 2 (gad1 and gad2) also known as GAD67 and GAD65 respectively (Pinal and Tobin, 1998). It is packed into vesicles for release at synapses by vesicular GABA transporter (VGAT), transcribed from the solute carrier family 32 member 1 (slc32a1) (Jin *et al*., 2003; Morales and Margolis, 2017). The detection of the GAD enzymes, or of VGAT, is commonly used for the identification of GABA neurons. One major obstacle for the study of GABA neurons in the VTA and SNc is a lack of antibodies that reliably stain cell bodies in these nuclei. This makes the identification of GABA neurons using immunostaining a difficult undertaking. ISH to detect GAD or VGAT mRNA must be used to confirm a GABAergic phenotype (Margolis *et al*., 2012; Nair-Roberts *et al*., 2008). Alternatively, there are cre-driver lines available where Cre-recombinase enzyme is under the control of the promoter from the GAD2 gene, or the VGAT gene, that can then be crossed with a reporter line (Taniguchi *et al*., 2011; Vong *et al*., 2011). ISH for GAD1 and GAD2, has shown that GABAergic neurons make up a considerable proportion of the total number of neurons, 35% and 37% in the VTA and SNc respectively (Nair-Roberts *et al.,* 2008). This number was originally underestimated (Ford *et al.,* 1995). The proportion of GABA neurons in relation to TH expressing cells also varied within different sub regions of the VTA, with lower GAD+ cells visible in the IF and RLi (i.e. the more medial sub-regions). In general, greater numbers of GAD+ cells were observed in more caudal regions of the VTA (Nair-Roberts *et al.,* 2008). In early studies, neurons that did not fit the criteria of 'putative' dopamine neurons in terms of their electrophysiological activity and were not immunoreactive for TH were often assumed to be GABAergic or glutamatergic (Nagai *et al.,* 1983). In both neurobiotin-labelled, GABA containing cells in the rat, (Steffensen *et al.,* 1998) and GAD-GFP labelled cells in mice, it has been shown that GABA neurons in the VTA could be distinguished from dopamine neurons based on their shorter duration action potentials and faster firing frequency (Chieng *et al.,* 2011).

1.2.3 Glutamate neurons

The enzyme glutaminase produces glutamate from glutamine. It is then packaged into vesicles by vesicular glutamate transporter 2 (VGLUT2) which is encoded by the gene Slc17a6. Expression of VGLUT2 is often used as a glutamatergic identifier. Much like GABA neurons, glutamate neurons are hard to visualise due to a lack of available antibodies that reliably stain the cell bodies. This issue was overcome with ISH for VGLUT2 and later, with the use of a VLGUT2Cre driver line and fluorescent reporters. The activity of glutamatergic neurons was eluded to after recordings from single neurons that were immunonegative for TH did not fit the functional properties that distinguish GABA neurons at the time (Ungless *et al.,* 2004). It was also demonstrated that VTA neurons mediate rapid excitatory responses in the medial prefrontal cortex (mPFC) of rats after electrical stimulation of the VTA (Lavin *et al*., 2005). Later the detection of VGLUT2 mRNA in the VTA of the rat confirmed the prescence of glutamte neurons . Tracing studies have shown that these neurons also contain VGLUT2 in their axon terminals, and that they form asymmetric synapses and release glutamate as their neurotransmitter (Root *et al.,* 2014a; Zhang *et al.,* 2015). It is now widely accepted that VGLUT2 expressing neurons lie intermingled with dopamine and GABA neurons of the VTA in rats, mice, non-human primates and humans (Morales and Root, 2014; Nair-Roberts *et al.,* 2008; Root *et al.,* 2016; Yamaguchi *et al.,* 2015; Yamaguchi *et al.,* 2013).

ISH for VGLUT2 has revealed that glutamate neurons are far less abundant in the midbrain than either TH+ or GAD+ neurons. A relatively small population exists in the VTA with even fewer visible in the SNc. In the VTA these VGLUT2+ neurons are restricted to the more rostro-medial regions. In stark contrast to the GAD+ cells, a higher number can be observed in the medial subdivisions of the VTA, in particular, the RLi and medial PBP **(Figure 3C)** (Li et al., 2013; Nair-Roberts et al., 2008; Yamaguchi et al., 2007b). In these regions glutamate neurons outnumber dopamine neurons.

1.2.4 Co-releasing neurons

In addition to these three core neuronal groups there have been multiple reports of VTA neurons exhibiting the molecular markers of more than one neuronal phenotype (Poulin *et al.,* 2014; Sulzer *et al.,* 1998; Yamaguchi *et al.,* 2011; Zhang *et al.,* 2015). An additional layer of complexity was added to the midbrain dopamine system by the discovery that some neurons can co-release multiple neurotransmitters from their synapses. There have been reports of neurons from the VTA signalling via the release of multiple neurotransmitters with evidence of VTA neurons co-releasing dopamine and glutamate, dopamine and GABA or glutamate and GABA (Chuhma *et al.,* 2014; Kim *et al.,* 2015; Mingote *et al.,* 2015; Stuber *et al.,* 2010; Zhang *et al.,* 2015). To date, this has not been studied in SNc neurons to the same extent. A small proportion of TH expressing neurons in the VTA express VGLUT2 mRNA. These have been identified in the VTA of rats, mice, non-human primates and humans (Root et al., 2016; Yamaguchi et al., 2015; Yamaguchi et al., 2007b). TH+ VGLUT2+ neurons are much more abundant in the midline regions **(Figure 5A)**, all express AADC so have the ability to synthesise dopamine but some of them lack VMAT2 and DAT (Li *et al.,* 2013). In the VTA they constitute a small fraction of the total number of neurons expressing TH or VGLUT2 alone (Yamaguchi *et al.,* 2011), but are not present in the SNc (Yamaguchi *et al.,* 2013). Dopamine and glutamate co-release was first observed *in vitro* (Sulzer *et al*., 1998). Stimulation of individual dopamine neurons in cell culture evoked a fast glutamatergic excitatory postsynaptic current (EPSC) via autapse. Additionally, they showed presynaptic inhibition caused by simultaneous release of dopamine (Sulzer *et al.,* 1998). In brain slices, it has been demonstrated that optogenetic stimulation of dopamine terminals in the shell of the nucleus accumbens (NAc) evokes glutamate mediated EPSCs in medium spiny neurons (Stuber *et al.,* 2010; Tecuapetla *et al.,* 2010) and cholinergic interneurons (Chuhma *et al.,* 2014). These VTA terminals in the NAc have pools of separate vesicles containing either dopamine or glutamate, generally in different axon micro-domains (Zhang *et al.,* 2015). These glutamate terminals form asymmetric synapses - commonly associated with excitatory transmission - and lie next to axonal domains containing TH and VMAT2 (Zhang *et al*., 2015). This data suggests that a single dopamine

and glutamate neuron projecting to the NAc may signal via dopamine and glutamate (Chuhma *et al*., 2014; Mingote *et al*., 2015; Stuber *et al*., 2010; Zhang *et al*., 2015).

Single cell qPCRs on dopamine neurons have shown that up to 18% of dopamine neurons (TH+ DAT+) throughout the VTA express VGAT (Poulin *et al.,* 2014) **(Figure 5B).** In addition, a population of TH+ GAD+ neurons projects to the LHb. Optogenetic activation of these neurons evokes GABA release onto glutamate neurons in the LHb. However, there is no detectable release of dopamine (Root *et al*., 2014b; Stamatakis *et al*., 2013). This population of neurons do not express VMAT2 and they therefore lack the machinery needed to package dopamine into synaptic vesicles (Stamatakis *et al.,* 2013). In contrast, there are neurons that co-release both neurotransmitters (Kim *et al*., 2015; Tritsch *et al*., 2012; Tritsch *et al*., 2016; Tritsch *et al*., 2014). It is thought that this can occur via two different mechanisms: re-uptake and de-novo synthesis. GABA is released from TH+ dopamine containing axons in the dorsal striatum. These neurons lack expression of GAD1, GAD2 and VGAT. Instead of synthesising GABA, it undergoes re-uptake from the synaptic cleft via GABA transporters 1 or 4 (GAT1/GAT4) where it is packaged into vesicles by VMAT2 (Berrios *et al*., 2016; Tritsch *et al*., 2012; Tritsch *et al*., 2016; Tritsch *et al*., 2014). A separate population of dopamine neurons that also lack GAD1 and GAD2 have the ability to synthesis GABA through the activity of aldehyde dehydrogenase family 1 member A1 (ALDH1A1), an enzyme that synthesises GABA from putrescine (Kim *et al*., 2015). Selective inactivation of this enzyme in mice reduces GABA release by dopamine neurons in the dorsal striatum (Kim *et al.,* 2015). As well as dopamine co-release, some neurons of the VTA can also simultaneously release glutamate and GABA. These neurons express GAD1/2, VGAT and VGLUT2 (Root *et al.,* 2014b). The distribution of these neurons within the VTA and SNc has not yet been investigated (Morales and Margolis, 2017). However, it has been shown that single axon terminals in the LHb form both symmetric and asymmetric synapses and that those post-synaptic neurons express both GABAA receptors and GLuR1 receptors (Root *et al.,* 2014b). This co-transmission has been observed *in vivo* by specific activation of GABA and glutamate containing terminals (Root *et al.,* 2014b) . Finally, a small

population of neurons has been observed in the VTA of both rats and mice that express marker genes for all three core neuronal populations. These neurons express TH, VGLUT2, GAD1 and GAD2, but whether they co-release all three neurotransmitters is currently unknown (Root *et al.,* 2014b; Stamatakis *et al.,* 2013; Yamaguchi *et al.,* 2011)

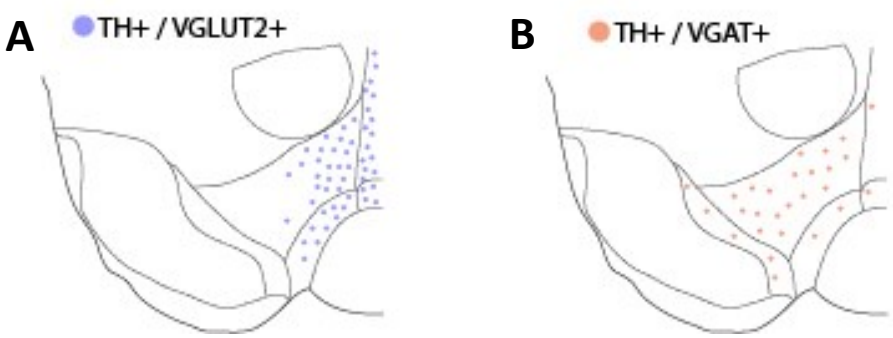


Figure 5 Schematics illustrating the distribution of neurons that express markers for different neuronal groups. A: The distribution of TH+ VGLUT2+ neurons in the VTA. **B:** The distribution of TH+ VGAT+ neurons in the VTA and SNc. *Outlines adapted from (Franklin and Paxinos, 2008).*

1.3 Neuronal projections of the VTA and SNc

1.3.1 Dopamine neuron projections

The classical view is that midbrain dopamine neurons in the VTA and SNc make up two distinct populations with different projection targets **(Figure 6)** (Bjorklund and Dunnett, 2007). Dopamine neurons of the VTA primarily send projections to regions of the limbic system and the prefrontal cortex (PFC), these make up the mesocorticolimbic pathway. VTA dopamine neurons target the NAc (Pickel *et al*., 1988), amygdala, cortex, hippocampus, ventral pallidum (VP), periaqueductal grey (PAG), BNST, olfactory tubercle (OT) and locus coeruleus (LC) (Aransay *et al*., 2015; Beier *et al*., 2015; Bjorklund and Dunnett, 2007; Ikemoto, 2007). These pathways play a critical role in reward processing; having been implicated in positive and negative reinforcement (Bromberg-Martin *et al*., 2010; Matsumoto and Hikosaka, 2009), decision making, working memory, salience and aversion . Mesocorticolimbic pathway dysfunction is implicated in drug addiction and schizophrenia (Cooper *et al*., 2017; Howes *et al*., 2017). The SNc dopamine neurons primarily send projections to the dorsal striatum; a main input nucleus of the basal ganglia (Bjorklund and Dunnett, 2007; Ikemoto, 2007). These neurons are involved in the control of voluntary movement and their loss leads to the motor symptoms observed in Parkinson's disease (Frank, 2005; Hikida *et al.,* 2010; Hikosaka, 2007; Jin and Costa, 2010; Kravitz *et al.,* 2010; Marshall *et al.,* 1976; Matsuda *et al.,* 2009; Schultz, 1986). Whilst this classical view is still widely accepted, it is somewhat of an over simplification. This is because cells from the VTA sometimes target the dorsal striatum, and SNc neurons sometimes project to limbic or cortical regions (Beier *et al*., 2015; Bromberg-Martin *et al*., 2010; Cragg *et al*., 2004; Fallon and Loughlin, 1982; Loughlin and Fallon, 1984).

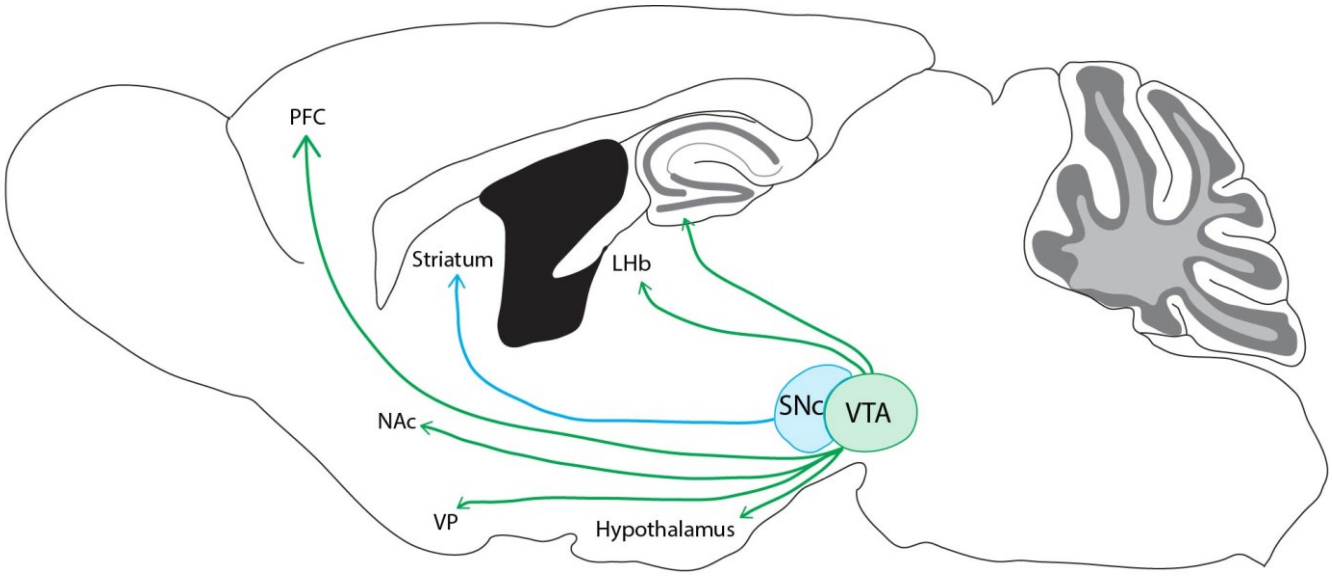


Figure 6: Schematic showing some of the projections of dopamine neurons from the VTA and SNc. The major mesolimbic and mesocortical projections (mesocorticolimbic) are shown in green and the nigrostriatal pathway is shown in blue. *Adapted from (Bjorklund and Dunnett, 2007) outlines adapted from (Franklin and Paxinos, 2008).*

1.3.2 GABA neuron projections

GABA neurons provide both long range inhibition and local inhibition of dopamine neurons. It has been shown in both rats and mice that GABA neurons in the VTA form local synapses (Omelchenko and Sesack, 2009) and project in parallel with dopamine neurons to different parts of the limbic system (Carr and Sesack, 2000a; Swanson, 1982; Van Bockstaele and Pickel, 1995). Although widely assumed to be the case, it is unknown whether distinct populations of GABA interneurons and projection neurons exist. This is because they are currently no way of distinguishing GABA interneurons from GABA projection neurons in this region.

A comprehensive tracing study used both a GAD2Cre driver line and a VGATCre driver line to map the projections of GABA neurons from the VTA using stereotaxic injections of a Cre-dependant virus (Taylor *et al.,* 2014). Data from both mouse lines revealed that GABA neurons primarily innervate structures of the limbic system. Such areas include the dorsal raphe, the VP, the LHb, the central amygdala, the BNST and the preoptic areas (LPO/MCPO). There is also smaller levels of innervation in the NAc and PFC **(Figure 7)** (Taylor *et al*., 2014). In addition to tracing GABA neuron efferents the authors of this study also traced the projections of glutamate neurons using VGLUT2Cre mice. They noted that apart from those originating from dopamine neurons, the majority of efferents from the VTA appeared to be originating from glutamate neurons rather than GABA neurons. As the GABA neurons are the second largest population, this suggests that either GABA neurons have more sparse axonal arborisations, or a larger proportion of these neurons form only local connections (Taylor *et al.,* 2014). Although this study provides anatomical evidence that VTA GABA neurons provide wide, long-range connections, few target areas have been confirmed by other methods (Morales and Margolis, 2017; Taylor *et al*., 2014). Thus far, the only functional connections of VTA GABA neurons observed by electrophysiology or electron microscopy are onto glutamate neurons of the LHb (Root *et al.,* 2014b), or onto cholinergic interneurons of the NAc (Brown *et al*., 2012; van Zessen *et al*., 2012). No studies are yet to investigate the specific projection of SNc GABA neurons.

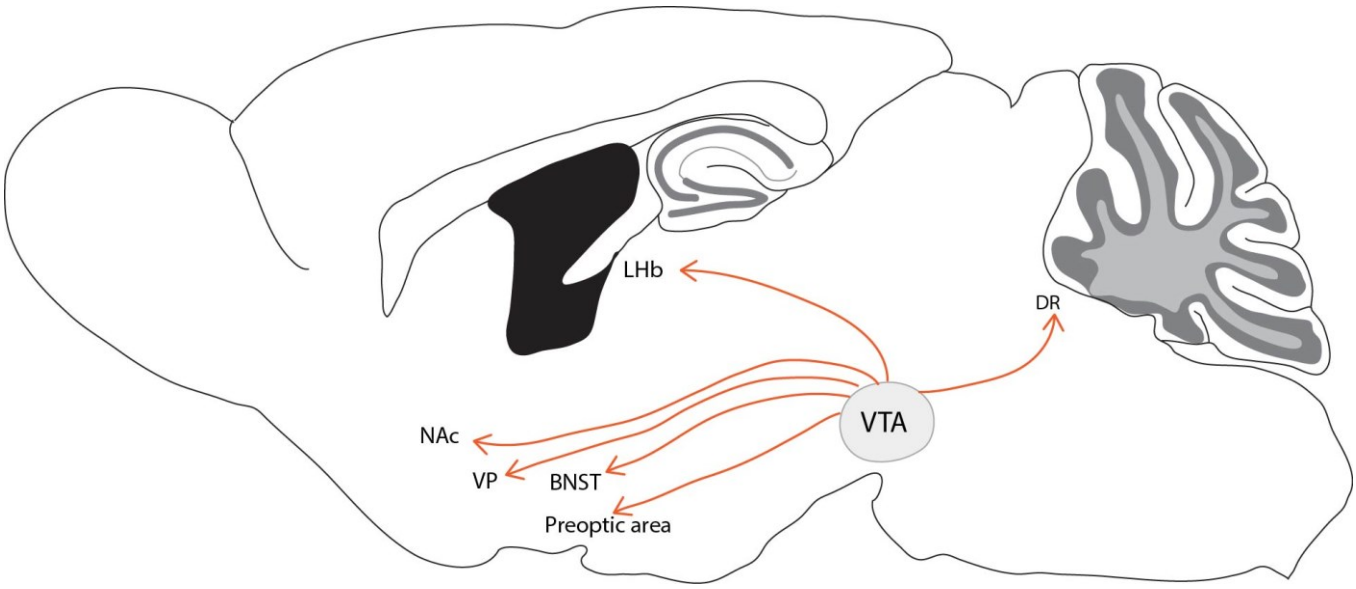


Figure 7: Schematic illustrating some of the established (anatomical) projections from GABA neurons in the VTA. *Adapted from (Taylor et al., 2014), Outlines adapted from (Franklin and Paxinos, 2008).*

1.3.3 Local GABA neuron connections of the VTA and SNc

Local GABAergic connections were first identified in early anatomical tracing studies that combined TH immunostaining with anterograde tracers injected directly into the VTA. Local synapses were then visualised with electron microscopy combined with immunogold-silver labelling for GABA - and for TH - to determine cell phenotype (Omelchenko and Sesack, 2009). Researchers are beginning to take advantage of transgenic mouse lines to target midbrain GABA neurons. Optogenetic stimulation of VTA GABA neurons after AAV-ChR2-eyfp injection into the midbrain of GAD2Cre mice results in the inhibition of dopamine neurons suggesting local synapses (Tan *et al.,* 2012; van Zessen *et al.,* 2012). It is widely accepted that a large majority of dopamine neurons are inhibited by aversive stimuli (Hong *et al.,* 2011; Ungless *et al.,* 2004). Using a foot shock paradigm in freely moving mice, it has been shown that VTA GABA neurons mediate this inhibitory response of dopamine neurons (Tan *et al.,* 2012; van Zessen *et al.,* 2012). Optogenetic activation of GABA neurons in the VTA, in the absence of the aversive stimuli, is also enough to produce conditioned place aversion (Tan *et al.,* 2012; van Zessen *et al.,* 2012). It has been suggested that inhibition of dopamine neurons can be mediated through dopamine acting on D2 autoreceptors, after somatodendritic release. D2 autoreceptors activation activates G-protein inwardly rectifying potassium (GIRK) which leads to hyperpolarisation (Beckstead *et al.,* 2004). Injection of the dopamine receptor antagonist haloperidol before and after foot shock fails to alter dopamine neuron inhibition. In contrast, infusion of bicuculline (a competitive GABAA receptor antagonist) blocks dopamine neuron response to the foot shock. This suggests that the dopamine neuron inhibition is mediated through GABA and not dopamine (Tan *et al.,* 2012).

1.3.4 Glutamate neuron projections

Like VTA GABA neurons, it has been shown that midbrain glutamate neurons can regulate the activity of the dopamine system through either local connections onto TH+ and TH- neurons (Dobi *et al.,* 2010; Wang *et al.,* 2015b), or via long range connections to dopamine neuron target areas (Hnasko *et al*., 2012; Root *et al*., 2014a; Taylor *et al*., 2014; Yamaguchi *et al*., 2011; Zhang *et al*., 2015). VTA glutamate neurons innervate many of the same regions as VTA GABA neurons (Hnasko *et al.,* 2012; Taylor *et al.,* 2014). Tracing studies have shown that VGLUT2 expressing neurons from the VTA send projections to the LHb, PFC and NAc (shell and core), the amygdala, the preoptic area, the stria terminalis and the VP (Root *et al.,* 2014a; Taylor *et al.,* 2014; Yamaguchi *et al.,* 2011). These are regions that also receive innervation from TH+ axons. A comparative study that examined the projections of both GABA and glutamate neurons concluded that glutamate projections are much more prominent than GABA projections in most of these regions. This suggests that the majority of TH- axons deriving from the VTA express VGLUT2, and are excitatory rather than inhibitory (Taylor *et al.,* 2014) (**Figure 8).**

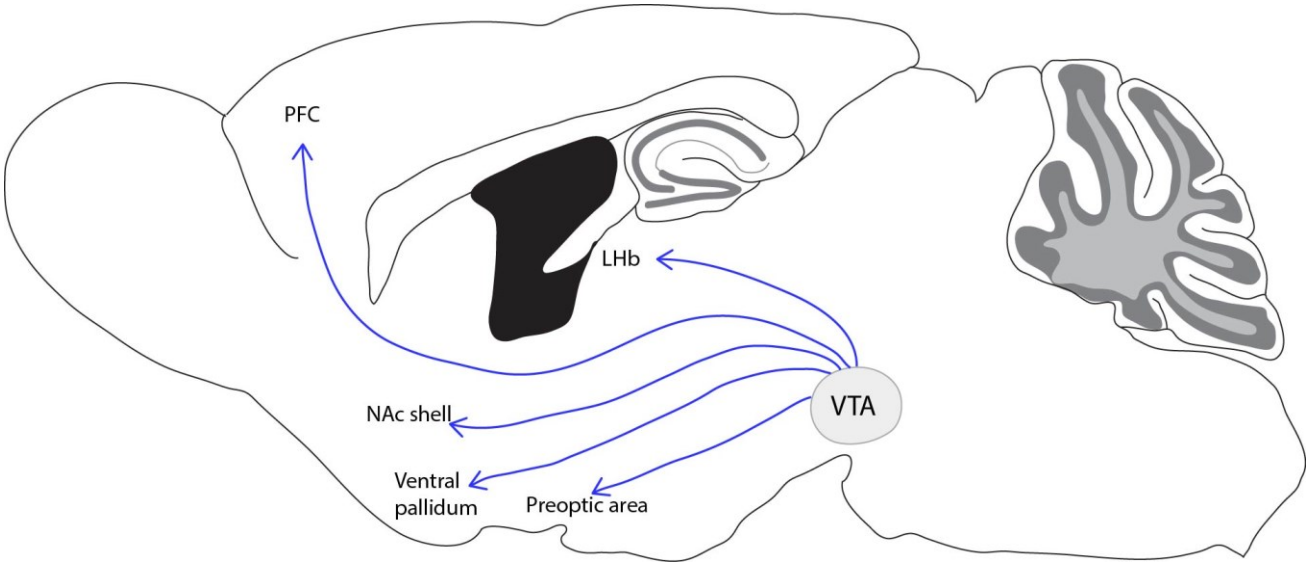


Figure 8: Schematic illustrating some of the established (anatomical) projections from glutamate neurons in the VTA. *Adapted from (Taylor et al., 2014), Outlines adapted from (Franklin and Paxinos, 2008).*

1.3.5 Local glutamate neuron connections

The presence of local glutamatergic synapses was first investigated in 2010 (Dobi *et al.,* 2010). Anterograde tracers *phaseolus vulgaris* leucoagglutinin (PHA-L) and wheat germ agglutinin (WAG) were injected into the VTA. Dual-immunolabelling and electron microscopy were used to determine whether PHA-L or WAG positive axon terminals contain glutamate. This was combined with TH immunostaining to show that local glutamatergic synapses are present on both dopaminergic and non-dopaminergic neurons (Dobi *et al.,* 2010). Consistent with this anatomical data, whole cell recordings of VTA neurons have shown that glutamate release from these terminals evokes EPSCs on VTA dopamine and non-dopamine neurons. Therefore, blocking action potential activity significantly decreases the frequency of excitatory events in dopamine and non-dopamine neurons (Dobi *et al.,* 2010). Further work again highlighted local glutamatergic synapses in the VTA in VGLUT2Cre mice expressing cre-dependant viral vector channel rhodopsin (ChR2) tethered to mCherry. Electron microscopy revealed varicosities co-expressing mCherry and VGLUT2, these corresponded to axon terminals establishing asymmetric synapses onto local neurons (TH+ and TH-) (Wang *et al.,* 2015b). The glutamate release from local VTA VGLUT2 neurons onto dopaminergic neurons is suggested by the detection of VGLUT2 protein, which is required for the packaging of glutamate into synaptic vesicles (Wang *et al.,* 2015b). Optogenetic activation of VTA glutamate neurons in V*GluT2*-ChR2-mCherry mice induced AMPA/NMDA receptor-dependent firing of dopamine neurons (Wang *et al.,* 2015b).

1.3.6 Co-releasing projections

The strongest glutamatergic connections from dopamine neurons have been observed in the NAc, OT and the entorhinal cortex. There is also co-release in the central amygdala and cingulate cortex (Mingote *et al.,* 2015). Optical activation of ChR2 expressing dopamine neuron axon terminals in the NAc shell results in robust glutamate-mediated EPSCs in medium spiny neurons (MSNs) (Stuber *et al.,* 2010; Tecuapetla *et al.,* 2010) and cholinergic interneurons (Chuhma *et al.,* 2014; Mingote *et al.,* 2015). In the PFC, glutamate release from midbrain dopamine neurons exclusively targets GABAergic

interneurons, with a particular bias towards fast-spiking parvalbumin interneurons (Kabanova *et al.,* 2015) **(Figure 9).** TH expressing axons release GABA through re-uptake form the synaptic cleft (Berrios *et al.,* 2016; Kim *et al.,* 2015; Tritsch *et al.,* 2014). In addition, dopamine neurons have been shown to release GABA in the dorsal striatum after non-canonical GABA synthesis via ALDH1A1 (Kim *et al.,* 2015) **(Figure 9).** GABA and glutamate co-releasing neurons project to the LHb where they form both asymmetric (excitatory) and symmetric (inhibitory) synapses onto glutamate neurons (Root *et al.,* 2014b) **(Figure 9).**

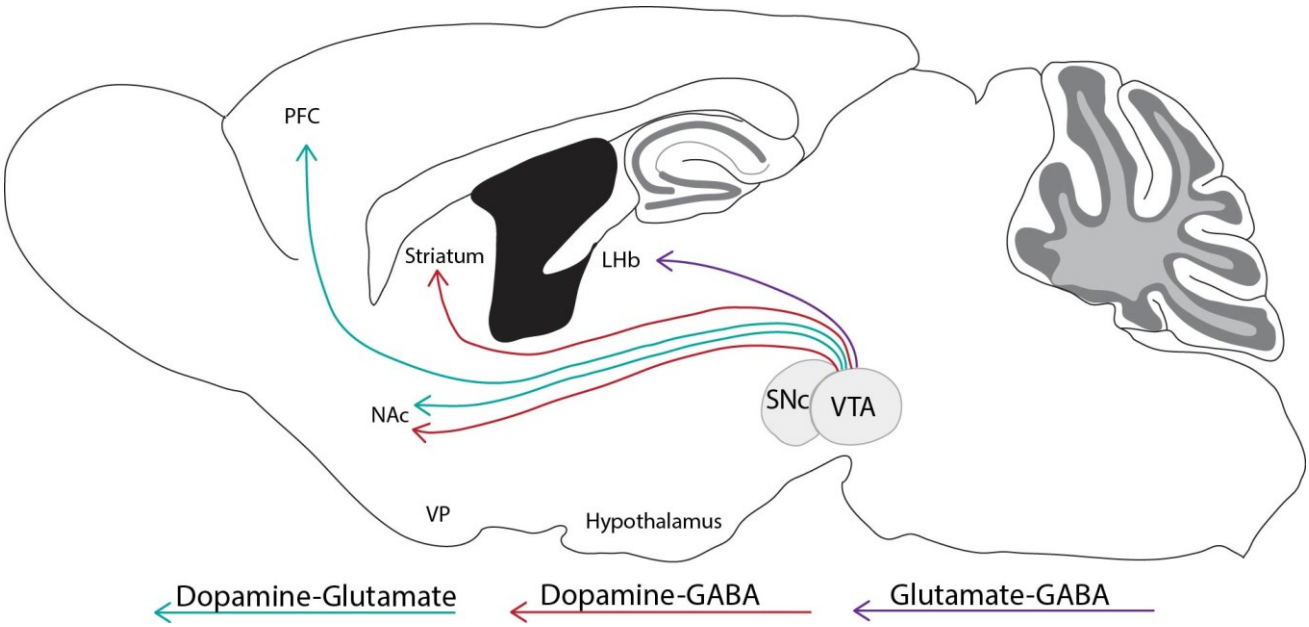


Figure 9: Schematic showing the long-range projections of different co-releasing neurons of the VTA and SNc. *Outlines adapted from (Franklin and Paxinos, 2008)*

1.4 Inputs into the VTA and SNc

Monosynaptic rabies based viruses have been instrumental in tracing and mapping input to the VTA and SNc (Beier *et al.,* 2015; Faget *et al.,* 2016; Ogawa *et al.,* 2014; Watabe-Uchida *et al.,* 2012). These technologies combined electron microscopy for the anatomical identification of synapses and selective stimulation (via optogenetics) and electrophysiology for their functional characterisation has enabled the identification of specific inputs to dopamine and GABA neurons of the VTA and SNc. So far no studies have sought to characterise specific inputs onto glutamate or co-releasing neurons in the VTA or SNc (Morales and Margolis, 2017). The VTA and SNc receives innervation from diverse brain structures. In addition input from local GABA and glutamate neurons, dopamine neurons in both the VTA and SNc receive innervation from diverse areas that include autonomic, motor and somatosensory regions (Beier *et al.,* 2015; Faget *et al.,* 2016; Ogawa *et al.,* 2014; Watabe-Uchida *et al.,* 2012). They receive inhibitory inputs from the VP (Hjelmstad *et al.,* 2013), LH (Nieh *et al.,* 2015) and the rostro-medial tegmental nucleus (RMTg), also referred to as the tail of the VTA (Jhou *et al.,* 2009; Kaufling *et al.,* 2010). They receive both excitatory and inhibitory from the DR (Beier *et al.,* 2015) and PAG (Omelchenko and Sesack, 2010). They receive excitatory glutamate inputs from the mPFC (Backman et al., 2006; Carr and Sesack, 2000c), pedunculopontine tegmentum (PPTg) (Charara *et al.,* 1996), laterodorsal tegmentum nucleus (LDTg) (Omelchenko and Sesack, 2005), LHb (Omelchenko *et al.,* 2009) and the BNST (Georges and Aston-Jones, 2001). As observed in their projections, dopamine neurons in the VTA and SNc also receive relatively different inputs in terms of density of innervation, rather than region. For example, the largest innervation of VTA dopamine neurons is from the LH, whereas SNc dopamine neurons receive denser innervation from the somatosensory and motor cortices (Watabe-Uchida *et al*., 2012). GABA neurons receive inhibitory input from a subgroups of medium spiny neurons of the nucleus accumbens (Bocklisch et al., 2013a). They receive Glutamate and GABA input form the BNST (Kudo *et al*., 2012) DR (Beier *et al*., 2015) PAG (Omelchenko and Sesack, 2010) and LH (Nieh *et al*., 2015), and they receive glutamate input from LHb (Omelchenko *et al*., 2009) and mPFC .

1.5 VTA and SNc circuits and behaviour

1.5.1 VTA and SNc dopamine neurons and behaviour

Dopamine neurons of the VTA and SNc have been extensively studied. Recent developments in the investigative tools available in neuroscience have resulted in vital advances that have changed the way we view this system. Far from being a homogenous population of cells, viral tracing along with optogenetic and chemogenetic approaches in transgenic animals have revealed discrete subpopulations of dopamine neurons that play distinct roles in the behavioural output of the system (Bariselli *et al*., 2016; Gunaydin *et al*., 2014; Ikemoto, 2007; Lammel *et al*., 2008; Lammel *et al*., 2011; Lammel *et al*., 2012; Lammel *et al*., 2014b; Margolis *et al*., 2006b; Margolis *et al*., 2008; Roeper, 2013; Saunders *et al*., 2015; Stamatakis and Stuber, 2012; Tye *et al*., 2013). 'Putative' midbrain dopamine neurons can be activated in response to rewarding and aversive stimuli (Cohen *et al*., 2012; Eshel *et al*., 2016; Matsumoto and Hikosaka, 2009; Schultz, 1986, 2007; Schultz *et al*., 1997). They are activated following an unexpected rewarding stimuli following learning and they shift their responses to cues that predict reward. At the same time, they decrease their firing when an expected reward is omitted. They encode reward prediction error (Cohen *et al*., 2012; Eshel *et al*., 2016; Matsumoto and Hikosaka, 2009; Schultz, 1986, 2007; Schultz *et al*., 1997). Paradoxically, it has also been demonstrated that some dopamine neurons can also be excited or inhibited by cues predicting an aversive outcome

It has been established that functional subpopulations of dopamine neurons can be distinguished by their electrophysiological activity and their projection targets (Lammel *et al*., 2008; Lammel *et al*., 2011; Roeper, 2013). For example, *in vitro* recordings from dopamine neurons labelled by retrograde fluorescent beads injected into either the ventral striatum or the prefrontal cortex, revealed two different populations that exhibited different electrophysiological activity. One population that lay in the SNc and projected to the lateral shell of the NAc exhibited the classical 'functional fingerprint' associated with dopamine neuron activity. In contrast, a population of dopamine neurons whose cell

bodies lie in the ventro-medial VTA and sent projections to the mPFC, core and medial shell of the NAc and the BLA exhibited a persistently higher firing rate with action potentials that generally had smaller afterhyperpolarisations (Lammel *et al*., 2008). As well as electrophysiological differences, dopamine neurons have also been shown to elicit responses to different stimuli in a projection specific manner. For example unconditioned or unexpected rewarding stimuli causes dopamine release in the nucleus accumbens (NAc) medial shell, but not in other striatal regions (Aragona *et al*., 2008; Bassareo *et al*., 2002; Goto *et al*., 2007; Stuber *et al*., 2005) It has been shown that synapses onto those dopamine neurons projecting the medial shell of the NAc are selectively modified (as indicated by an increase in AMPAR/NMDAR receptor ratios) by a rewarding stimulus (e.g. cocaine) (Lammel *et al.,* 2011). In contrast, synapses on dopamine neurons projecting to mPFC were modified only by an aversive stimulus (e.g. injection of formalin into the hind paw to cause irritation). However, synapses onto some dopamine neurons, for example sending projections to the lateral shell of the NAc can be modified by both types of stimuli, rewarding and aversive. This suggests that this projecting population encodes salient stimuli rather than rewarding or aversive (Lammel *et al.,* 2011). In addition to dopamine neuron activity being projection specific, it has also been shown to be input specific. Laterodorsal tegmentum neurons preferentially innervate those dopamine neurons that project to the nucleus accumbens lateral shell, optogenetic activation of these VTA afferents elicits aversive behaviours in mice. Whereas lateral habenula neurons synapse primarily on dopamine neurons projecting to the mPFC and optogenetic activation of these neurons elicits reward (Lammel *et al*., 2012). In a review paper published in 2013, at least seven functional subgroups of dopamine neurons were proposed. These have different cell body positions within the VTA and SNc, different projection targets, synaptic inputs and electrophysiological properties. All of which result in different behaviours (Roeper, 2013).

1.5.2 VTA and SNc GABA neurons and behaviour

Whilst dopamine neurons have been intensely studied in terms of their responses to stimuli and contribution to behaviour, only a handful of studies have investigated the functional contribution of GABA neurons to this system. In terms of their activity, *in vivo* recordings have shown that VTA GABA neurons increase their firing rate during exposure to reward predicting cues and maintain the increased firing rate during the receipt of the reward. In contrast to the majority of midbrain dopamine neurons, their activity also increases transiently in response to aversive stimuli (Cohen *et al.,* 2012; Tan *et al.,* 2012). It has been suggested that the inhibition of dopamine neurons in response to aversive stimuli is mediated through local connections from these GABA neurons. In a foot shock paradigm GABA neurons increase their firing rate and local inhibition of dopamine neurons inducing conditioned place aversion. Optogenetic stimulation of VTA GABA neurons is sufficient to drive this conditioned place aversion. This behaviour is blocked by an infusion of bicuculline, a competitive GABAA receptor antagonist, suggesting that the inhibition of dopamine neurons is mediated through GABA binding to GABAA receptors (Tan *et al*., 2012). Investigators have also studied the effect of optogenetic activation of VTA GABA neurons in reward seeking behaviour. Activation of the GABA neurons during the cues predicting reward did not alter reward seeking or anticipatory behaviour of the mice However, activation following reward delivery significantly decreased reward consumption. These results indicated that VTA GABA neuron activation is sufficient to disrupt reward consumption following reward presentation (van Zessen *et al*., 2012). Stimulation also reduces reward consumption in a free reward paradigm (where sucrose is readily available). These observed behaviours were again blocked by application of a GABAA receptor antagonist into the VTA, suggesting the behaviour is mediated through local connections (van Zessen *et al.,* 2012).

The most well studied of the VTA/SNc GABA projection is the VTA-NAc (Brown *et al*., 2012). Although the NAc and its afferents clearly play important roles in mediating motivated behavioural responses, it has been shown that stimulation of the entire VTA GABA neuron population reduces dopamine release in the NAc, and disrupts reward consumption (Tan *et al*., 2012). However, activation of this VTA-NAc GABAergic population alone through the optogenetic stimulation of VTA-NAc GABA terminals the NAc is not sufficient to induce the disruption in reward consumption. These projections selectively innervate cholinergic interneurons. Optogenetic stimulation of these terminals leads to inhibition of this interneuron population which enhances stimulus outcome learning. This suggests that VTA-NAc GABA projections are involved in encoding salience (Brown *et al*., 2009). In contrast, stimulation of VTA GABA terminals in the DR and PAG elicits a cardiovascular depressor response, which is blocked by infusion of a GABA-blocking agent, picrotoxin (Kirouac *et al.,* 2004) These examples of differentially evoked responses suggests that like dopamine neurons, GABA neurons also form discrete functional subpopulations; some of which are almost certainly projection specific. (Brown *et al*., 2012; Carr and Sesack, 2000a; Kirouac *et al*., 2004; Margolis *et al*., 2006a; Stamatakis *et al*., 2013; Steffensen *et al*., 1998; Van Bockstaele and Pickel, 1995; van Zessen *et al*., 2012). The main limitation to optogenetic approaches targeting the whole population of GABA neurons is that responses illicited could be due to local connections or projecting neurons. Whilst specific projections can be targeted via optogenetic stimulation of terminals, there is no way of selectively studying the local connections.

In addition to these observed contributions to behavioural output, GABA neurons in the VTA are known to be a major target for drugs of abuse. These substances increase the levels of dopamine release in different brain regions. This is mediated via the drastic alteration of GABA transmission in the VTA which results in disinhibition of dopamine neurons (Bonci and Williams, 1997; Johnson and North, 1992b; Madhavan *et al*., 2010; Mansvelder and McGehee, 2000; Nugent *et al*., 2007; Szabo *et al*., 2002; Tan *et al*., 2010). This results in increased and aberrant activity in dopamine neurons and promotes drug seeking behaviour. Repeated exposure to cocaine reduces the activity of VTA GABA

neurons through inhibitory long-term potentiation of NAc-VTA connections. This reduction in activity of GABA neurons in the VTA results in dis-inhibition of dopamine neurons. Similarly, the activation of mu opioid receptors by opioids in the VTA produces reward by disinhibiting midbrain VTA dopamine neurons. This is via inhibition of GABAergic inputs, which either arise from local GABA neurons or from afferents to the VTA (Chieng *et al*., 2011).

1.5.3 VTA and SNC glutamate neurons and behaviour

Optogenetic stimulation of glutamatergic terminals selectively in both the NAc and LHb (Qi *et al.,* 2016; Root *et al.,* 2014a). VTA glutamatergic neurons projecting to the NAc (primarily the medial shell) form asymmetric synapses. Selective activation of VTA glutamate neuron terminals in the NAc results in mice acquiring conditioned place aversion. This stimulation also disrupts the positive reinforcement of a positive reward. It is thought that this behaviour is mediated through the excitation of parvalbumin expressing GABA interneurons in the NAc. Activation of these interneurons drives the inhibition of NAc MSNs that is likely to contribute to the aversive behaviour (Qi et al., 2016; Root et al., 2014a; Wang et al., 2015b) . In contrast, optogenetic stimulation of glutamate neurons in the VTA of mice induces conditions place preference, a response that is mediated by activation of post-synaptic glutamate receptors on VTA dopamine neurons (Wang *et al*., 2015b). In a similar problem to the targeting of GABA neurons, stimulation of the entire population of glutamate neurons will result in target area release of glutamate as well as local release. This can make results more difficult to interpret.

1.6 Molecular diversity of neurons in the VTA and SNc

Molecular techniques such as microarray, single cell qPCR and more recently, RNA-sequencing, have uncovered considerable differences in the gene expression of dopamine neurons in the VTA and SNc but also of the neurons within each region. Dopamine neurons exhibit differential expression of dopamine neuron marker genes. In addition to this, other molecular differences between dopamine neurons have been identified. The majority of studies that examined the diversity of dopamine neurons focused on the comparison of the broad dopaminergic populations by comparing gene expression profiles in the VTA and SNc (Greene et al., 2005b; Grimm et al., 2004b). This comparison is of particular clinical importance due to the selective vulnerability of SNc dopamine neurons in Parkinson's disease. The first two studies (published in quick succession) performed separate microarrays on pooled RNA from laser dissected, TH stained, dopamine neurons from the VTA and the SNc (Greene et al., 2005b; Grimm et al., 2004b). Both reported that the substantial majority of genes analysed showed no difference in expression between SNc and VTA dopamine neurons. This is most probably due to their similar developmental origin and dopaminergic phenotype. However, they found that approximately 150 genes were expressed in a differential manner. Among these transcripts were: transcription factors, proteins involved in vesicle trafficking and axon guidance, ion channels and receptors, neuropeptides and genes related to energy metabolism (Greene et al., 2005b; Grimm et al., 2004b). A further study comparing the dopamine neurons in these two nuclei took a high through-put approach by utilising translating affinity ribosome purification (TRAP), a method that allows for the selective isolation of ribosome bound mRNA from a genetically defined cell population. They isolated dopamine RNA from tissue punches of the VTA and of the SNc for RNA-sequencing. They then compared the transcriptomes from the two nuclei (Brichta *et al.,* 2015).

The first study to take a single cell approach conducted single cell qPCRs of FACs sorted dopamine neurons from DATCre:Ai9 mice that express tomato under the control of the DAT promoter. They analysed the expression of 96 genes selected from the previous studies on dopamine neurons. The list

included: transcription factors, channels and receptors, PD related genes, neuropeptides and secretary factors. Although a large proportion of the genes appeared to be uniformly expressed across all the cells examined, they also concluded that several genes were differentially expressed between individual neurons. They were able to group the neurons based on the pattern of expression of 18 key genes, thus allowing the classification of subtypes in a polythetic manner. Based on the gene expression pattern, they clustered the neurons into six different sub groups. Some of which seemed to have regional specificity within the midbrain. For example, one subgroup that was defined by co-expression of ALDH1A1, Sncg, and Sox6 was largely localised to the SNc. They later went on to show that this subgroup was selectively vulnerable to the MPTP Parkinsons disease model (Poulin *et al.,* 2014). No such studies have been conducted to investigate gene expression or molecular diversity in GABA or glutamate neurons of the VTA and SNc.

1.7 Selectively targeting neuronal populations

Throughout this introductory chapter I have tried to build a picture of the functional and molecular heterogeneity that is observed in neurons of the VTA and SNc. This increasing level of complexity highlights some issues with the current methods available for studying neurons in the VTA and SNc. Due to its behavioural importance and clinical relevance, understanding the organisation and functional connectivity of subpopulations of neurons within the VTA and SNc is an important goal in neuroscience. Many of the tools available for selectively targeting and manipulating populations require a genetic entry point. Generally, the most commonly used are related to neurotransmitter synthesis and release (Backman *et al*., 2006; Borgius *et al*., 2010; Lammel *et al*., 2015; Lindeberg *et al*., 2004; Taniguchi *et al*., 2011; Vong *et al*., 2011). For this reason, most studies in the VTA and SNc target the entire population of neurons defined by genetic markers for a single neurotransmitter. The cre lines used most often in the VTA and SNc are TH/DAT-Cre for dopamine neurons, VGAT/GAD2-cre for GABA neurons and VGLUT2-Cre for glutamate neurons. With our increasing understanding of neuronal diversity, it is becoming more apparent that this approach does not provide a high enough resolution for a complex system. Not only is there overlap in expression between some of these neuronal markers, but there is also populations of co-releasing neurons. There is no doubt that co-releasing cells would have been inadvertently stimulated in studies targeting specific cell types. Upon stimulation, researchers could be evoking the release of more than one - or of a conversely acting – neurotransmitter. This could have a profound effect on the resulting behavioural responses observed. It is possible that this could have led to erroneous interpretation of results. There are novel tools available to target cells based on the expression of both cre and flp recombinases, which are controlled by two different promoters, such as INTERSECT (Fenno *et al*., 2014). In a lot of cases, and particularly with GABA neurons in the VTA and SNc, we lack an understanding of their molecular diversity which makes it difficult to selectively target subpopulations. This is why we require novel genetic entry points and by extension, why uncovering the molecular diversity of neurons within the VTA and SNc has become of increasing importance.

1.8 Project outline

Dopamine neurons have so far been the main focus of study in the VTA and SNc, which is of no surprise considering their clinical importance. Dopamine neurons make up just under 70% of the neurons in the VTA and SNc. They lie intermingled with GABA neurons, which comprise around 30%, and a small population of glutamate neurons (Nair-Roberts *et al*., 2008). Despite them being the second largest population of neurons in the VTA and SNc, GABA neurons in this region have been somewhat neglected in the literature. We know that these GABA neurons are functionally important, they are the main target of drugs of abuse (Bonci and Williams, 1997; Johnson and North, 1992b; Madhavan *et al*., 2010; Mansvelder and McGehee, 2000; Nugent *et al*., 2007; Szabo *et al*., 2002; Tan *et al*., 2010), their selective activation drives conditioned place aversion (Tan *et al*., 2012) and a subpopulation has been implicated in salient learning (Brown *et al*., 2012). It is known that they provide local inhibition of dopamine neurons within the VTA and SNc (Omelchenko and Sesack, 2009; van Zessen *et al*., 2012). It is also known that they send long range projections to many target regions that are often also innervated by dopamine neurons (Brown *et al*., 2012; Taylor *et al*., 2014). A fundamental piece of information missing from the literature is whether these GABA neurons form distinct populations of GABA projection neurons and GABA interneurons. This is widely assumed to be the case (e.g., see discussion of GABA 'interneurons' of the VTA in (Gantz *et al*., 2018)). This idea has been difficult to test because it is challenging to selectively label interneurons. There are currently no molecular markers for subpopulations of GABA neurons in the VTA and SNc. In neuronal networks where GABA neurons have been well studied (e.g., the cortex, hippocampus, striatum, and spinal cord) it has been shown that GABA neurons, in particular GABA interneurons, exhibit huge amounts of diversity (Bikoff *et al*., 2016; Kepecs and Fishell, 2014; Tepper *et al*., 2010; Tremblay *et al*., 2016; Tricoire *et al*., 2011). We hypothesised, that GABA neurons in the VTA and SNc exhibit similar levels of diversity.

The aim of my PhD was to investigate the molecular diversity of neurons within the dopaminergic nuclei of the midbrain, with a particular focus on the GABA neuron population. The overall goal was to uncover molecular markers of subpopulations of GABA neurons in order to provide novel genetic entry points for the investigation of their function. To achieve this aim, I took two complimentary approaches. The first, was a biased approach where I selected candidates for investigation based on current literature. I selected candidates from genes that are commonly used as markers for GABA interneuron subpopulations in other brain regions. The second, was an unbiased approach where I isolated and sequenced RNA specifically from GABA and dopamine neurons in the midbrain. Candidates for investigation were then based on the direct comparison of the transcriptomes of GABA and dopamine neurons.

In **chapter 2** and **chapter 3** I discuss the biased approach. After preliminary immunostaining, I selected two potential candidates for further experimentation. The first candidate from this approach, neuronal nitric oxide synthase (nNOS), is discussed in **chapter 2**. Using a combination of immunostaining and viral tracing in NOS1Cre mice, I have identified 3 distinct populations of nNOS positive neurons in the VTA and SNc. The first, whose cell bodies are found in the RLI nucleus, which appears to be glutamatergic, sends long-range projections out of the midbrain. The second, whose cell bodies are found in the PBP and SNc, appears to be a population of GABA interneurons. The third, whose cell bodies are found in the SNc, appears to be a population of interneurons that expresses TH. The second candidate from the biased approach, parvalbumin, is discussed in **chapter 3**. Using a combination of immunostaining and viral tracing in PVCre mice, I found that there is a subpopulation parvalbumin expressing GABA neurons in the VTA and SNc. The data presented in regards to PV+ projections is in its preliminary stages. However, these PV+ neurons appear to be another population of GABA interneurons.

The unbiased approach, is discussed in **chapter 4**. I used a polysome profiling technique that involved the selective expression of tagged polyribosomes in GABA and dopamine neurons. RNA was then isolated specifically from GABA neurons and dopamine neurons via immunoprecipitation of tagged polysomes and sent for sequencing. I directly compared the transcriptomes from these two libraries. Using the PANTHER gene ontology database and a novel approach that we developed that compared expression data from the Allen Brain Atlas to my transcriptome database. This led to the identification of 12 novel GABA neuron markers. I went on to investigate 7 of these candidates via immunostaining. Using this biased approach, I have identified novel genetic entry points for the future study of subpopulations of GABA neurons in the VTA and SNc.

Chapter 2 – A biased approach: Investigating the expression of neuronal nitric oxide synthase in the VTA and SNc

2.1 Introduction

2.1.1 The diversity of GABAergic interneurons

GABAergic interneurons represent a minority neuronal population in the brain and yet they serve a crucial function. They provide essential inhibition to complex brain circuits by controlling the activity level of principal neurons. Without this vital inhibitory input excitation can become out of control, leading to seizures and failure of higher brain functions. In addition to controlling levels of excitation, interneurons also contribute to the coordination and temporal control of neural circuits (Kandel, 2013; Kepecs and Fishell, 2014; Klausberger and Somogyi, 2008b; Wamsley and Fishell, 2017). A hallmark of GABAergic interneurons is their structural and functional diversity, a characteristic that contributes to their intricate control over neuronal networks. They exhibit distinct morphology, synaptic specificity, and physiological and biochemical characteristics.

Whilst GABAergic interneurons have not been extensively studied in the VTA and SNc, they have been in other brain regions. This is particularly true for the hippocampus (Somogyi and Klausberger, 2005), cortex (Kepecs and Fishell, 2014; Sugino *et al*., 2006; Tremblay *et al*., 2016), spinal cord (Bikoff *et al*., 2016) and striatum (Tepper *et al*., 2010). There are currently eight cardinal interneuron markers that

are used to identify and selectively target subpopulations of interneurons in the brain. These consist of neuropeptides: somatostatin (SOM) cholecystokinin (CCK), vasoactive intestinal peptide (VIP) and neuropeptide Y (NPY); calcium binding proteins: parvalbumin (PV) and calretinin (CALB2); Reelin (RELN); and nitric oxide synthase (nNOS) (Kepecs and Fishell, 2014; Wamsley and Fishell, 2017). Defining subpopulations of interneurons is not straightforward. For example, in the cortex virtually all interneurons express one of four core molecular markers: PV, SOM, VIP or RELN. These subclasses can then be broken down further based on cell morphology, axon targeting bias, intrinsic and synaptic physiology, embryonic origin and expression of additional interneuron markers. Consequently, there is overlap of multiple different properties between populations. nNOS+ interneurons in the cortex can be either SOM+ or RELN+/SOM- and PV+ cells can either be basket cells or chandelier in shape, to name just a few of the possible variations (Kepecs and Fishell, 2014; Taniguchi *et al*., 2013; Tremblay *et al*., 2016; Wamsley and Fishell, 2017).

The different possible combinations of properties provides a huge breadth of potential subpopulations of interneurons, each with the ability to modulate neural circuits. So far, twenty-one distinct subgroups have been distinguished in the CA1 region of the hippocampus, and it is likely that even more exist in the cortex (Klausberger and Somogyi, 2008b). The extreme diversity of the cells that are responsible for the inhibitory and temporal control of a circuit exponentially increases the signalling complexity of that circuit. We already know that there is a substantial population of GABA neurons in the VTA and SNc (Nair-Roberts *et al*., 2008). We also know that these GABA neurons provide inhibitory control of dopamine neurons (Omelchenko and Sesack, 2009) in the VTA and SNc, and that this inhibition leads to changes in behaviour (Tan *et al*., 2012; van Zessen *et al*., 2012). It is therefore rational to hypothesise that diverse interneuron populations will be present in the VTA and SNc, the core nuclei of the complex and diverse dopamine system.

2.1.2 The expression of GABAergic interneuron markers in the VTA and SNc

When selecting candidates for this biased approach, I began by examining Allen Brain Atlas *in situ* hybridisation (ISH) images of the midbrain for each of the eight interneuron molecular markers (Lein *et al.,* 2007) and by exploring the published literature **(Figure 10)**. However, many of the molecular markers are either thought to be expressed in subpopulations of dopamine neurons, or they were undetectable in the VTA and SNc. Although there is evidence of expression in VTA GABA neurons, the expression of CALB2 and CCK in dopamine neurons is well established and uncontested in the literature (Gonzalez-Hernandez and Rodriguez, 2000; Hokfelt *et al*., 1980; Isaacs and Jacobowitz, 1994; Klink *et al*., 2001; Liang *et al*., 1996; Merrill *et al*., 2015; Rogers, 1992; Seroogy *et al*., 1988; Seroogy *et al*., 1989). In contrast, there is no evidence of expression of VIP in either GABA or dopamine neurons in the VTA and SNc (Dougalis *et al*., 2012; Poulin *et al*., 2014). For this reason, CALB2, CCK and VIP were ruled out as candidates. Whilst the majority of candidates showed some level of detection in the VTA and SNc in the Allen Brain Atlas ISH images, NPY did not, thus suggesting it is not expressed in the VTA and SNc (Lein *et al*., 2007). There is no evidence in the literature surrounding the expression of SOM or RELN in the VTA and SNc. Despite this the Allen Brain ISH data suggests that there may be a few cells expressing these candidates. Some preliminary immunostaining in wild-type (WT) tissue was conducted with antibodies for both SOM and RELN. This was conducted by Katlyn Green, a technician in our lab. This immunostaining was unable to detect SOM or RELN immunoreactive cells in the VTA or SNc. I therefore decided not to pursue them as candidates. The literature surrounding the expression nNOS and PV in the VTA and SNc is less clear than that of CALB2 and CCK and VIP. Whilst there is indication of the expression of both nNOS and PV in the VTA and SNc (Backes and Hemby, 2003; Gonzalez-Hernandez and Rodriguez, 2000; Klejbor *et al.,* 2004; Klink *et al.,* 2001; Merrill *et al.,* 2015; Mitkovski *et al.,* 2012; Olson and Nestler, 2007; Poulin *et al.,* 2014), evidence surrounding which neuronal population expresses these markers is contradictory. Taking into account the ISH data from the Allen Brain Atlas and the inconclusive literature, nNOS and PV seemed like promising candidates

and were selected for investigation in the VTA and SNc. For the remainder of this chapter I will focus on nNOS, firstly by introducing nNOS and its use as a molecular marker before moving on to detail the evidence surrounding nNOS expression in the VTA and SNc. PV is discussed in **chapter 3**.

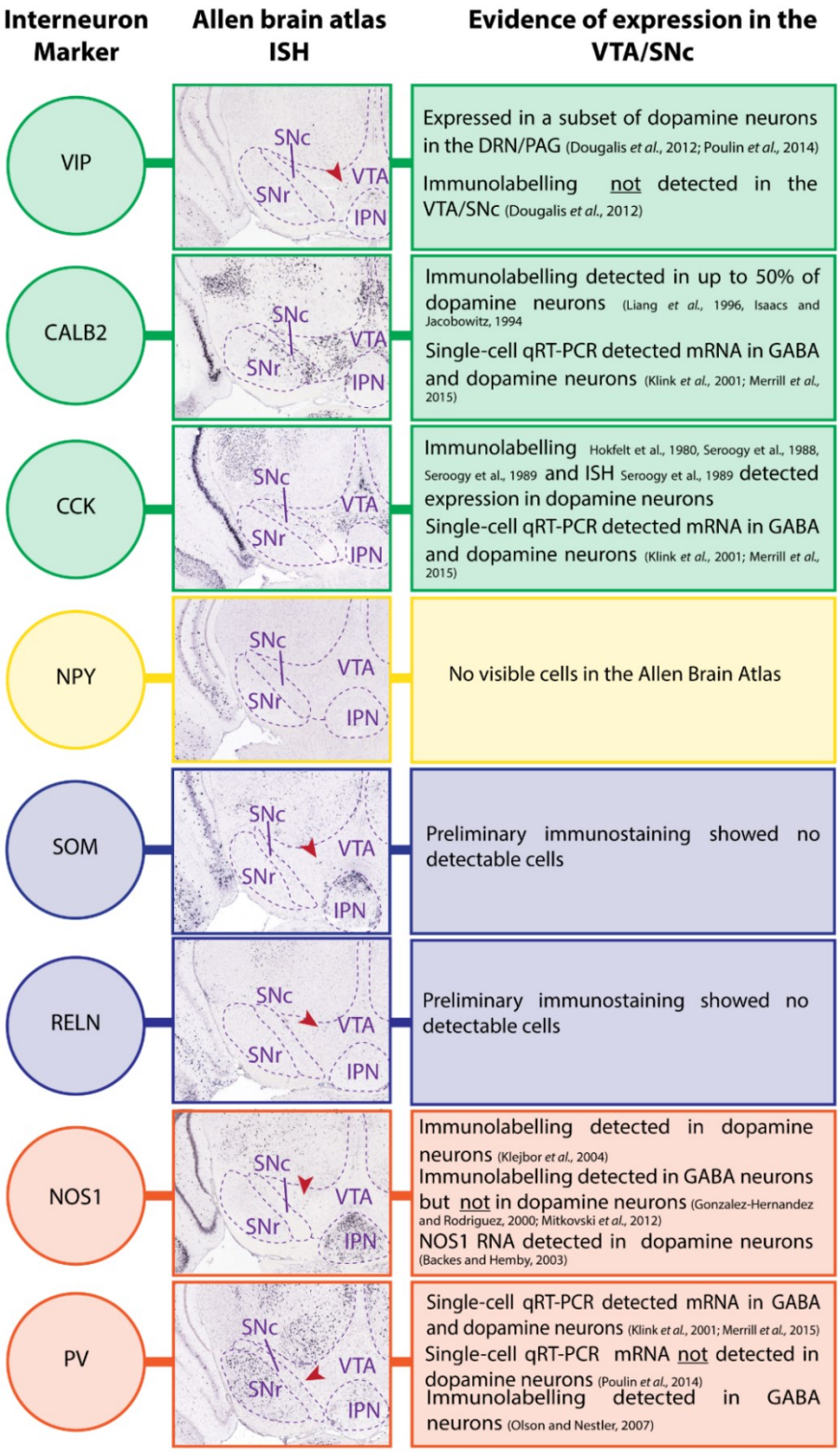


Figure 10: Molecular markers of GABA interneurons and evidence of their expression in the VTA and SNc. Green: candidates expressed in dopamine neurons, yellow: no evidence of expression in the VTA and SNc, blue: preliminary immunostaining revealed no detectable cells, orange: inconclusive and contradicting expression data. *ISH images from the Allen brain atlas* © 2004 Allen Institute for Brain Science. Available from: http://mouse.brain-map.org/ *(Lein et al., 2007)*

2.1.3 Introduction to neuronal nitric oxide synthase

nNOS, also called NOS1, is a member of the nitric oxide synthase family of enzymes that catalyse the synthesis of nitric oxide (NO) from L-arginine (Garthwaite, 1991; Knowles *et al.,* 1989). NO is an important signalling molecule in the body that is crucial for many physiological processes in the nervous system, cardiovascular system and immune system (Furchgott, 1983; Furchgott and Zawadzki, 1980; Huang *et al.,* 1993; Huang *et al.,* 1995; Xie *et al.,* 1992). nNOS which is expressed in neurons and smooth muscle, endothelial NOS (eNOS) which synthesises NO in endothelial cells in the vasculature, and iNOS which is expressed in macrophages (Cho *et al.,* 1992; Hibbs *et al.,* 1987; Knowles *et al.,* 1989; Lamas *et al.,* 1992; Moncada *et al.,* 1991; Nishida *et al.,* 1992; Xie *et al.,* 1992). Under physiological conditions the constitutively expressed nNOS is the principal source of NO in the brain (Demas *et al.,* 1999; Huang *et al.,* 1993). Its activity is Ca^{2+} dependent. NO synthesis is stimulated by the rapid Ca^{2+} influx induced after that activation of NMDA receptors by glutamate (Garthwaite *et al.,* 1988). NO is a gaseous transmitter that can move rapidly across plasma membranes in anterograde and retrograde directions to act presynaptically, postsynaptically or within the cell that has produced it. Its diffusive nature means it can influence many different cells and structures in its vicinity, making it well suited to its role as a neuromodulator (J Garthwaite and Boulton, 1995; Wang and Marsden, 1995). Since its discovery as a messenger molecule within the central nervous system, NO and nNOS expressing cells have been shown to play a role in a huge variety of processes. For example, they play essential roles in hippocampal long term potentiation and synaptic plasticity (Hardingham *et al.,* 2013), and are involved in the regulation of sleep and wake cycles (Kilduff *et al.,* 2011), appetite, body temperature, neurovascular coupling to control neocortical blood flow (Cauli and Hamel, 2010; Cauli *et al*., 2004; Perrenoud *et al*., 2012b), and synaptic integration of adult born neurons (Overstreet and Westbrook, 2003). Although vital for many normal functions, when synthesised in excess NO becomes cytotoxic and has been closely associated with brain ageing and neurodegenerative diseases such as Alzheimer's Disease, Parkinson's Disease and Huntington's Disease. It also plays a role in depression,

stroke, sleep apnoea, and epilepsy (Gautier-Sauvigne *et al.,* 2005; Gholipour *et al.,* 2010; Guix *et al.,* 2005; Lu *et al.,* 2015; Morris *et al.,* 2016).

2.1.4 nNOS as a molecular marker in the brain

nNOS immunoreactive cells have been detected throughout the adult rodent brain (Rodrigo *et al*., 1994; Vincent and Kimura, 1992). They are well characterised in the cortex and hippocampus, brain regions where nNOS expression is used as an identifier for a subpopulation of GABAergic interneurons (Tremblay *et al*., 2016; Tricoire and Vitalis, 2012). It has been shown that nNOS expressing neurons, like most interneurons, are extremely heterogeneous. For example, in the hippocampus where nNOS+ interneurons represent the most abundant interneuron subpopulation (Fuentealba *et al*., 2008) they can be further divided into five subpopulations. This is based on their morphology and their co-expression of other interneuron markers such as VIP, NPY, CB2, and SOM (Freund and Buzsaki, 1996; Fuentealba *et al*., 2008; Jaglin *et al*., 2012; Price *et al*., 2005; Somogyi *et al*., 2012; Tricoire *et al*., 2010; Tricoire and Vitalis, 2012; Zsiros and Maccaferri, 2005). In the neocortex nNOS neurons can be split into two crude nNOS+ populations. nNOS-type (i) cells are highly immunoreactive for nNOS and are primarily projection neurons (Higo *et al*., 2009; Tomioka *et al*., 2005; Tricoire and Vitalis, 2012). These nNOS+ neurons are sparsely distributed in the cortex and co-express additional interneuron markers, including SOM and NPY (Jaglin *et al*., 2012; Kubota *et al*., 2011; Magno *et al*., 2012; Perrenoud *et al*., 2012a; Perrenoud *et al*., 2012b). nNOS-type (i) cells have been shown to be selectively activated during sleep (Gerashchenko *et al*., 2008; Tricoire and Vitalis, 2012). nNOS-type (ii) neurons exhibit lower levels of nNOS immunoreactivity (Kubota, 2014; Magno *et al*., 2012; Perrenoud *et al*., 2012a; Smiley *et al*., 2000; Tricoire and Vitalis, 2012; Yan *et al*., 1996). They are more abundant than type (i) neurons and can be further broken down into three subpopulations based on morphology and co-expression of PV, SOM, VIP and CLB2 (Karagiannis *et al*., 2009; Kubota, 2014; Tricoire and Vitalis, 2012; Vruwink *et al*., 2001). nNOS interneurons have also been characterised in the striatum (Hope *et al*., 1991; Smith *et al*., 2016; Tepper *et al*., 2010), amygdala (Joo *et al*., 2004; Wang *et al*., 2017) and the olfactory bulb

(Crespo *et al*., 2003). Apart from some weak nNOS immunoreactivity in the dendritic spines of CA1 pyramidal neurons in the hippocampus (Burette *et al*., 2002), the majority of nNOS immunoreactivity is observed in GABA neurons. This is true for the hippocampus, neocortex (Tricoire and Vitalis, 2012) olfactory bulb (Crespo *et al*., 2003) amygdala (Joo *et al*., 2004; Wang *et al*., 2017)and striatum (Hope *et al*., 1991; Smith *et al*., 2016; Tepper *et al*., 2010). In stark contrast to these regions nNOS expression in the nucleus tractus solitairii (NTS) (Lin, 2009; Lin *et al*., 2004) and hypothalamus (Chachlaki *et al*., 2017) are largely associated with glutamate neurons.

2.1.5 nNOS expression in the VTA and SNc

NO signalling may play a role in multiple behaviours closely linked to the midbrain dopamine system. These include normal behaviours such as feeding and drinking, and pathological behaviours such as the development of dependence on substances of abuse, in particular morphine and cocaine (Byrnes *et al*., 2000; Calapai *et al*., 1992; Gholami *et al*., 2003; Morley and Flood, 1991; Motahari *et al*., 2016; Tayfun Uzbay and Oglesby, 2001). In addition, several studies have suggested an involvement of NO in the selective degeneration of SNc dopamine neurons in Parkinson's disease (Jackson-Lewis and Smeyne, 2005; Przedborski *et al*., 1996). NO activity has also been linked to the regulation of dopamine transmission in the striatum of the rats and the facilitation of NMDA-induced burst firing in the VTA *in vitro* (Cox and Johnson, 1998; Lonart and Johnson, 1994; Stewart *et al*., 1996). Despite this, the information surrounding the expression of its synthesising enzyme - nNOS- in the VTA and SNc is inconsistent **(Table 1).**

The expression of nNOS in the VTA and SNc was first eluded to in two immunostaining studies in the rat brain (Rodrigo *et al*., 1994; Vincent and Kimura, 1992), though the results were contradictory from the offset. Both studies reported a scattering of nNOS+ cells in the VTA however one reported immunoreactivity throughout multiple sub-regions (IF, PN and PBP) (Rodrigo *et al*., 1994) and the other reported that the nNOS immunoreactive cells were localised only to VTAR (Vincent and Kimura,

1992). Almost a decade later, there was still disagreement in the literature. Two studies of the rat VTA reported co-expression of nNOS and TH (Backes and Hemby, 2003; Klejbor *et al*., 2004). A macroarray reported the presence of NOS1 transcripts in RNA extracted from LCM isolated TH+ dopamine neurons, the level of which decreased after acute cocaine administration (Backes and Hemby, 2003). Similarly, an immunostaining study in the VTA reported significantly higher levels of nNOS/TH co-localisation in certain sub-regions, with up to 97.1% of NOS+ cells in the RLi co-localising with TH, over half of the total number of dopamine neurons. nNOS immunoreactivity was also reported in the PBP with much less (0.4%) co-localisation with TH (Klejbor *et al*., 2004). Two further immunostaining studies reported no, or virtually no, co-localisation with TH in the SNc (Gonzalez-Hernandez and Rodriguez, 2000; Mitkovski *et al*., 2012). To date, there has been fewer studies of nNOS expression conducted in the mouse brain. There are two conflicting immunostaining publications. The first fails to detect nNOS+ cell bodies in the VTA and SNc, reporting only the presence of nNOS fibres in the SNc (Gotti *et al*., 2005). The second reports nNOS+ cells in the VTA and SNc, none of which co-localise with TH (Cavalcanti-Kwiatkoski *et al*., 2010). A summary of reported nNOS expression is shown in **Table 1.**

Data surrounding nNOS expression in the VTA and SNc has so far been inconclusive. Results have been inconsistent in regard to the cell localisation within the nuclei, but also with regards to which neuronal population is expressing the enzyme. One reason for this inconsistency could be the use of different and un-validated antibodies. Despite this discrepancy in the literature, the fact remains that there is some evidence of nNOS expression in the VTA and SNc (both from the literature and in the Allen Brain Atlas). This finding, paired with the evidence of NO interactions in the midbrain dopamine system makes nNOS one of the best candidates from the list of interneuron markers. In this chapter, I describe how I set out to thoroughly investigate the presence of nNOS expressing cells within the VTA and SNc. My aim was to determine whether nNOS, as in other brain regions, can be used as a molecular marker for subpopulations of GABA neurons in the VTA and SNc.

Publication	Experiment	Species	VTA	SNc	GAD +	TH +
(Vincent and Kimura, 1992)	Immunohistochemistry	Rat	VTAR only	Yes	-	-
(Rodrigo *et al*., 1994)	Immunohistochemistry	Rat	IF/PN/PBP	Yes	-	-
(Gonzalez-Hernandez and Rodriguez, 2000)	Immunohistochemistry	Rat	-	Yes	Yes	<1%
(Backes and Hemby, 2003)	RNA from single dopamine neurons	Rat	Yes	-	-	Yes
(Klejbor *et al*., 2004)	Immunohistochemistry	Rat	RLi/IF/PBP	-	-	Yes
(Gotti *et al*., 2005)	Immunohistochemistry	Mouse	No	Fibres	-	-
(Cavalcanti-Kwiatkoski *et al*., 2010)	Immunohistochemistry	Mouse	Yes	Yes	-	no
(Mitkovski *et al*., 2012)	Immunohistochemistry	Rat	VTAR only	Yes	-	Virtually none

Table 1: Summary of the publications investigating the presence of nNOS in the VTA and SNc (- indicates that the region or co-expression that was not investigated).

2.2 Experimental Procedures

2.2.1 Animals

All breeding and experimental procedures were conducted in accordance with the Animals (Scientific Procedures) Act of 1986 (UK). All mice were maintained in social groups of 2-4, where possible, with appropriate environmental enrichment (e.g. bedding and tunnels). They were kept in rooms at a constant temperature and maintained on a 12 h light/dark cycle. They were fed on standard rodent chow and water *ad libitum*. Details of the mice strains used in this chapter are shown in **Table 2**.

Mouse line	Strain nomenclature	Supplier (#Stock No.)
C57Bl/6	C57Bl/6NCrl	Charles River (#027)
NOS1 KO	B6.129S4-*Nos1*^{tm1Plh}/J	The Jackson laboratory (#002986)
NOS1Cre	B6.129-*Nos1*$^{tm1(cre)Mgmj}$/J	The Jackson laboratory (#017526)
RiboTag	B6N.129-*Rpl22*$^{tm1.1Psam}$/J	The Jackson laboratory (#011029)
VGATCre	*Slc32a1*$^{tm2(cre)Lowl}$/J	The Jackson laboratory (#016962)

Table 2: Mouse strain information

2.2.2 DNA extraction

Upon weaning of litters ear notches were taken both for identification purposes and for genotyping. Tissue notches were placed in a 1.5 ml eppendorf tube and 100 µl of deoxyribonucleic acid (DNA) extraction buffer (25 mM NaOH, 200 mM ethylenediaminetetraacetic acid (EDTA) (pH 8.0)) was added, with the mixture then incubated at 85°C for 2 hours. 100 µl of 40 mM Tris-HCl (pH 5.0) was added, the solution was then mixed well with a vortex mixer before being centrifuged at 13,000 rpm for 3 minutes. The supernatant was used for polymerase chain reaction (PCR) amplification and subsequent genotyping. The extracted DNA was stored at 4°C.

Strain/Transgene	Primers	PCR cycles	Product weight
NOS1 KO	**Mutant F** - CTTGGGTGGAGAGGCTATTC **Mutant R** - AGGTGAGATGACAGGAGATC **WT F** - TCAGATCTGATCCGAGGAGG **WT R** - TTCCAGAGCGCTGTCATAGC	94°C 2min 94°C 20 secs 65°C 50 secs x10 68°C 10 secs 94°C 15 secs 60°C 15 secs x28 72°C 10 secs 72°C 2mins 10°C ∞	Mutant protein = 280 bp Wild type = 117 bp
NOS1Cre	**F -** TGGAGAGTTAGGGGCAGTTG **Mutant R** - CCAAAAGACGGCAATATGGT **WT R**- AGCCACTGCAGGGTAACAAG	94°C 2min 94°C 20 secs 65°C 15 secs x10 68°C 10 secs 94°C 15 secs 60°C 15 secs x28 72°C 10 secs 72°C 2mins 10°C ∞	Mutant = ~400 bp Wild type = ~483 bp
RiboTag	**F -** GGGAGGCTTGCTGGATATG **R –** TTTCCAGACACAGGCTAAGTACAC	94°C 2min 94°C 20 secs 65°C 15 secs x10 68°C 10 secs 94°C 15 secs 60°C 15 secs x28 72°C 10 secs 72°C 2mins 10°C ∞	Mutant = ~290 bp Wild type = 243 bp

Table 3: Genotyping information

2.2.3 Genotyping

1µl of extracted DNA was added to a commercially available PCR mix - ReddyMix (Thermo Fisher, USA) - with both forward and reverse primers (0.5 µM) **(Table 3).** PCR amplification was performed using a BIO-RAD PTC-200 DNA Engine Peltier Thermal Cycler. PCR products were separated by gel electrophoresis on a 2% agarose gel prepared with TAE buffer (40 mM Tris acetate (pH 8.3), 1 mM EDTA). SYBR Safe DNA Gel Stain (ThermoFisher) was included for visualisation under ultra-violet (UV) light. The PCR cycles and product weights for each transgene can be seen in Table 2. VGAT-ires-Cre mice do not require genotyping. In these mice the targeted Slc32a1 gene is located ~3.5kbp from the non-agouti locus. C57BL/6 Vgat-ires-Cre mice have agouti coat colour, whereas offspring that are negative for ires-Cre have black coats.

2.2.4 Perfusion fixation and tissue preparation

Mice were anaesthetised under isoflurane (4%) and were given a lethal intraperitoneal (IP) injection of pentobarbital (100mg/ml; Euthatal). They were transcardiallly perfused with 50ml of ice cold phosphate buffered saline (PBS) followed by 50-100ml of 4% paraformaldehyde (PFA; Sigma Aldrich) in PBS. When fixed, the brains were removed and placed in 10ml of 4% PFA for 1 hour post-fixation at room temperature. After 3 washes in PBS the brains were then placed in 30% sucrose (Sigma - Aldrich) dissolved in PBS - for cryo-protection - and then kept at 4°C for 24-48hrs. Subsequently, all brains were embedded in optimal cutting temperature (OCT) medium and snap frozen in isopentane (2-methlybutane) at -55°C. All tissue was then stored at -80°C until sectioning.

2.2.5 Immunocytochemistry

Unless otherwise stated, all immunostaining studies were conducted on adult mice aged 8-12 weeks old. Brains were sectioned using a Leica CM1800 cryostat (Leica Microsystems, Germany). Coronal sections (30 µm) were taken from brain regions of interest. Free floating sections were washed in PBS for 10mins at room temperature. Following this they were blocked in 6% normal donkey serum (NDS) in 0.2% Triton-x in PBS (PBSTx) for 60mins at room temperature. Primary antibodies **(Table 4)** were diluted in 2% donkey serum in PBSTx and sections were incubated in the primary antibody solutions overnight at 4°C. Sections were washed (3 x 10mins) in PBS at room temperature. Secondary antibodies **(Table 5)** were diluted in 2% donkey serum 0.2% PBSTx. Sections were incubated in secondary antibody solution for a minimum of 1.5hrs at room temperature. They were then washed (3 x 10 mins) in PBS. Stained sections were mounted onto glass microscope slides and when dry were cover-slipped using VectaShield mounting medium (Vector Laboratories).

Antibody	Host species	Manufacturer/Product No.	Concentration
Anti-TH	Chicken	Abcam (#ab76442)	1:1000
Anti-nNOS	Mouse	Sigma Aldrich (#N2280)	1:500
Anti-nNOS	Rabbit	Cell signalling (#4234)	1:500
Anti-nNOS	Rabbit	Sigma Aldrich (#N7155)	1:500
Anti-HA	Mouse	Sigma Aldrich (#H3663)	1:1000
Anti-HA	Rabbit	Abcam (#ab9110)	1:500
Anti-GABAARα1	Rabbit	Alomone (#AGA-001)	1:500
Anti-5HT	Rabbit	ImmunoStar (#20080)	1:2000
Anti-VGLUT2	Rabbit	Alomone (#AGC036)	1:500
Anti-VGAT	Rabbit	SYSY (#131003)	1:500
Anti-Substance P	Guinea Pig	Abcam (#ab10353)	1:500

Table 4: Primary antibody information

Antibody	Conjugation	Host species	Manufacturer (#Product No.)	Concentration
Anti-Chicken	Alexa-488	Goat	Invitrogen (#A11039)	1:1000
Anti-Chicken	Cy3	Donkey	Jackson (#703-165-155)	1:1000
Anti-Mouse	Cy3	Donkey	Jackson (#715-165-150)	1:1000
Anti-Mouse	Cy5	Donkey	Jackson (#715-175-151)	1:1000
Anti-Rabbit	Alexa-633	Goat	Invitrogen (#A21070)	1:1000
Anti-Rabbit	Cy3	Donkey	Jackson (#711-165-152)	1:1000
Anti-Goat	Alexa-488	Donkey	Invitrogen (#A11055)	1:1000
Anti-Guinea Pig	Alexa-488	Goat	Invitrogen (#A11073)	1:1000

Table 5: Secondary antibody information

2.2.6 Viral vectors

The virus used in this tracing experiment was AAV1-Ef1a-DIO-ChR2-mCherry. The DIO-ChR2-mCherry construct was kindly gifted by the Deisseroth Lab and was commercially packaged in AAV serotype 2/1 1 vector consisting of the AAV2 ITR genomes and the AAV1 serotype capsid gene (Vector Biolab, Philadelphia). The titres of purchased viruses vary with Lot. Number, for these tracing experiments all viruses were diluted in sterile PBS and 5% glycerol (pH 7.2) to a concentration of $2.7x10^{13}$ genome copies/ml.

2.2.7 Stereotaxic surgery for circuit tracing

Unless otherwise stated, all viral tracing experiments were conducted on adult (11-13 weeks) NOS1Cre (-/+) mice. Mice were briefly anaesthetised in an induction chamber with isoflurane and placed in a stereotaxic frame (David Kopf Instruments, California) with continued isoflurane administration. The eyes were protected with Lacri-lube, the scalp was shaved, and the skin disinfected with chlorheximide. All mice received a subcutaneous injection of carprofen (Rimadyl; 5mg/kg) for post-operative anaesthesia. An incision (<1cm) was made along the midline and bupivacaine (2.5mg/ml) was delivered directly to the incision site for local anaesthesia. A small hole was drilled in the scalp based on co-ordinates from bregma. Using a 33-gauge metal needle (11530332 RN NEEDLE (33/12/3) S) and Hamilton syringe (11530072 85 RN 5uL SYR) the virus solution was injected unilaterally. 0.1-0.3µl was injected at a flow rate of 0.3µl/min. The flow rate was controlled by a programmable pump Harvard Apparatus (704507 Elite Nanomite Infusion/Withdrawal Programmable Pump 11). After injection, the needle was left in place for 5mins to allow for the spread of the virus. The incision was then sutured using blue, nylon monofilament, non-absorbable sutures (VWR, 2-0, catalogue number: 95060-062). Mice were allowed to recover in a heated chamber (30°C) before being placed back into their home cage with littermates. All mice were monitored for five days after surgery, during this time they had access to carprofen (Rimadyl; 50mg/ml) in their drinking water. Two weeks after surgery the mice underwent transcardial perfusion and the brains were removed for circuit tracing.

2.2.8 Confocal Imaging, image processing and analysis

Confocal images were acquired using a Leica SP5 confocal microscope with the pinhole set at 1 Airy unit. Multi-channel images were acquired sequentially. All images were processed with Fiji software.

(i) Wild type Vs NOS1-KO

To compare nNOS antibody staining in wild type and NOS1-KO mice, I was blind to the strain of the mouse from the stage of immunolabelling until after image analysis. Mice for each experimental group

were stained in parallel to control for differences between staining experiments. All images in this section were obtained with matched confocal settings and a step size of 1µm Each anti-nNOS antibody was tested in a total of three male WT and three male nNOS-deficient mice. The concentration of nNOS antibody was optimised through staining and imaging at three concentrations (1:250, 179 1:500, 1:1000). Stacked images from the optimum concentration of 1:500 are shown. 5-z-planes were stacked for example images and brightness and contrast was adjusted equally across all images to enable a direct comparison.

(ii) Quantification of nNOS expressing neurons

For the quantification of nNOS expressing neurons triple immunolabelling for nNOS, HA, and TH was conducted in three male VGATCre:RiboTag mice. To obtain estimates of the numbers of nNOS neurons, and their neurotransmitter phenotype, every fourth midbrain section was selected for staining and imaging. Tilescans were taken of the entire VTA and SNc visible on the right-hand side of the brain section. Merged tilescan images were processed using Fiji (ImageJ) and VTA and SNc sub-region anatomy was defined based on TH expression. HA+ cells, nNOS+ cells and HA+/nNOS+ were counted in each sub-region using the ImageJ cell counter plugin. Images of cell bodies were acquired with z-stacks of 1 µm. To determine co-localisation, channels were viewed both individually and in composite. Co-localisation was determined if the cell body was visible in multiple channels through its entire thickness (multiple z planes). Representative examples of stacked images are shown.

(iii) Comparison of ChR2-mCherry axon terminals

Images of axon terminals in nNOS+ neuron target areas were acquired with z-stacks of 0.5 µm. 10 Z-planes were stacked and brightness and contrast was adjusted equally across all axonal projection images for comparison.

(iv) Determining the degree of co-localisation between ChR2-mCherry and nNOS

Images focused on mCherry-Chr2 cell bodies were acquired with z-stacks of 1 µm. For quantification 20x images were acquired from the middle of each sub-region, 1 image per mouse, in 3-5 mice (depending on sub-region). To determine co-localisation with nNOS and TH, channels were viewed both individually and in composite. Co-localisation was determined if the cell body was visible in multiple channels through its entire thickness (multiple z planes). Cells were counted using the Fiji cell counter plugin. Representative examples of stacked images are shown for each sub-region.

(v) Imaging synaptic boutons

Images of synaptic terminals were acquired with z-stacks of 0.25 µm. ChR2-mCherry+ synaptic boutons were located in single z-planes, which were extracted from the stack to determine co-localisation with VGAT or VGluT2. Synaptic terminals were examined in three different mice.

2.3 Results

2.3.1 Neurons in the VTA and SNc express nNOS

(i) Verification of nNOS antibodies

Some preliminary nNOS immunostaining was conducted in our lab by a previous MPhil student (Eliza Kalk), in which various nNOS antibodies were tested (Kalk, 2015). Eliza optimised the staining protocol for two different anti-nNOS antibodies: Cell Signalling (#4234), raised in rabbit and Sigma-Aldrich (#N7155), raised in rabbit **(see Table 2).** The results suggested that there is an nNOS expressing population of neurons in the VTA and SNc, and that these neurons are TH-. Despite this, there was variability between antibodies. These results are reported in Eliza's MPhil thesis (Kalk, 2015). Due to this variability, and the inconsistent expression data currently available for nNOS in the midbrain nuclei, I first wanted to verify and further optimise the nNOS antibodies. In addition to the two antibodies already tested I also investigated a third anti-nNOS antibody, Sigma-Aldrich (#N2280). In order to thoroughly verify their specificity, each antibody was used to stain midbrain sections from both wild type mice (n=3) and nNOS KO mice (Huang *et al.,* 1993) (n=3), using the nNOS KO tissue as a negative staining control. It has consistently been stated that there is a large population of nNOS expressing neurons in the IPN (Ascoli *et al*., 2008; Rodrigo *et al*., 1994; Vincent and Kimura, 1992). Therefore, this region is suitable as a positive immunostaining control. Each antibody was tested at three different concentrations for optimisation (1:250, 1:500, 1:1000). Preliminary staining suggested that 1:500 was the optimum dilution for all three anti-nNOS antibodies. To ensure that any differences between staining observed was down to knocking out nNOS and not an experimental artefact, wild type and KO tissue sections were stained in parallel - whilst I was blinded to the genotype. In order to identify midbrain anatomy and sub-regions of the VTA and SNc the sections were also stained for TH, a marker for dopamine neurons.

All three antibodies exhibited immunoreactivity in the IPN and in regions of the VTA and SNc in wildtype mice **(Fig. 11 A-C).** The Cell Signalling antibody displays the least immunoreactivity within the VTA and SNc **(Figure 11A)**. There appears to be multiple immunoreactive spots -which could be cells- in and around the RLi nucleus. These are also present in the NOS1 KO mice. The Sigma-Aldrich (#N7155) antibody failed to detect cell bodies and instead a large majority of immunoreactive processes are visible **(Figure 11B)**, this appears to be non-specific staining. For this antibody there appears to be no difference in immunoreactivity between the WT and KO tissue in the VTA and SNc. This is noteworthy as this particular antibody was used in a study that had previously investigated the expression of nNOS in the VTA and SNc in the mouse brain (Klejbor *et al*., 2004). The final antibody - Sigma-Aldrich (#N2280)- exhibits clear immunoreactive cell bodies in the WT which are completely absent in the KO tissue **(Figure 11C)**. Based on these three comparisons I was able to conclude that the third antibody (Sigma-Aldrich (#N2280)) gives the most reliable immunostaining result for nNOS in the VTA and SNc. This was confirmed by looking throughout the cortex and hippocampus to ensure that nNOS+ neurons that were present in the WT were absent in the KO mice. From this point forward, all nNOS staining was conducted using the #N2280 antibody.

(ii) nNOS+ neurons are scattered throughout the VTA and SNc and are TH-

Having established the most reliable antibody for nNOS I next wanted to take a closer look at the localisation of nNOS expressing cells within the midbrain nuclei, and investigate their presence in relation to dopamine neurons. To this end, I took tile scans of the entire midbrain region to get a complete picture of the location of the nNOS+ neurons. This was once again repeated in KO tissue to ensure reliable detection of nNOS **(Figure 12).** These sections were co-stained for nNOS and TH with the IPN again used as a positive immunostaining control. Importantly, the dense nNOS+ neurons observed in the IPN of the WT tissue are absent in the KO mouse. In the WT mouse brain nNOS+ neurons can be seen in the RLi, PBP and SNc. These are in close proximity to TH+ neurons but there is no co-localisation between nNOS and TH **(Figure 12).** This result is in contrast to the previous nNOS

immunostaining paper conducted in mice that showed striking co-localisation of nNOS and TH, particularly in the RLi (Klejbor *et al*., 2004). In addition to those cells within the dopaminergic nuclei, nNOS+ neurons are also observed in the SNr and lateral substantia nigra (SNL) which is in agreement with previous publications (Gonzalez-Hernandez and Rodriguez, 2000; Rodrigo *et al*., 1994). These results suggest that nNOS expressing neurons are present in multiple regions of the midbrain and that they are not dopamine neurons.

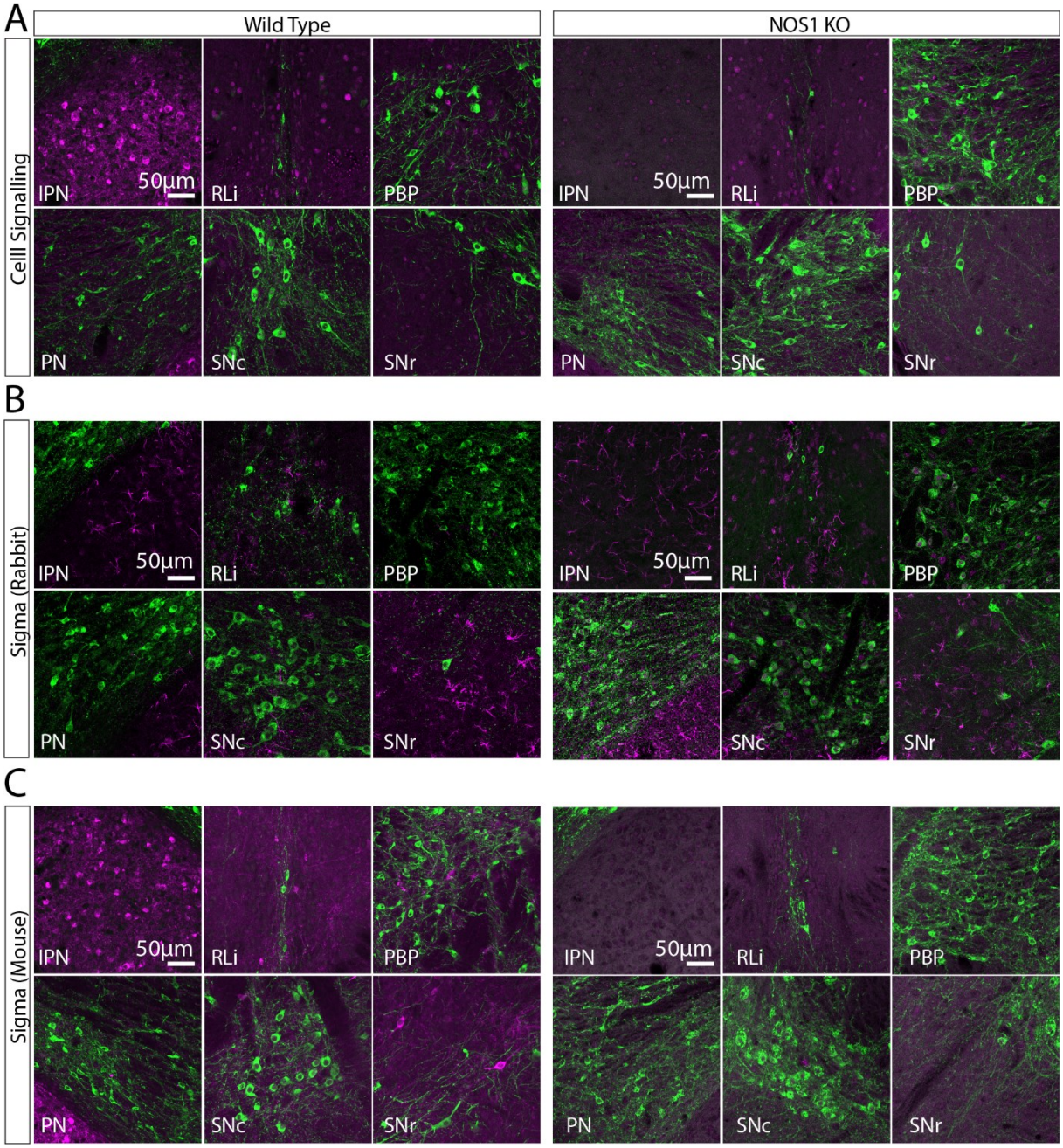


Figure 11: A comparison of three anti-nNOS antibodies in the midbrain of WT and NOS1-KO mice. Double immunostaining for nNOS (magenta) and TH (green) **A:** Anti-nNOS, Cell signalling (Rabbit; #4234), 1:500 dilution. B: Anti-nNOS, Sigma-Aldrich (Rabbit; #N7155) 1:500 dilution. C: Anti-nNOS, Sigma-Aldrich (Mouse; #N2280) 1:500 dilution.

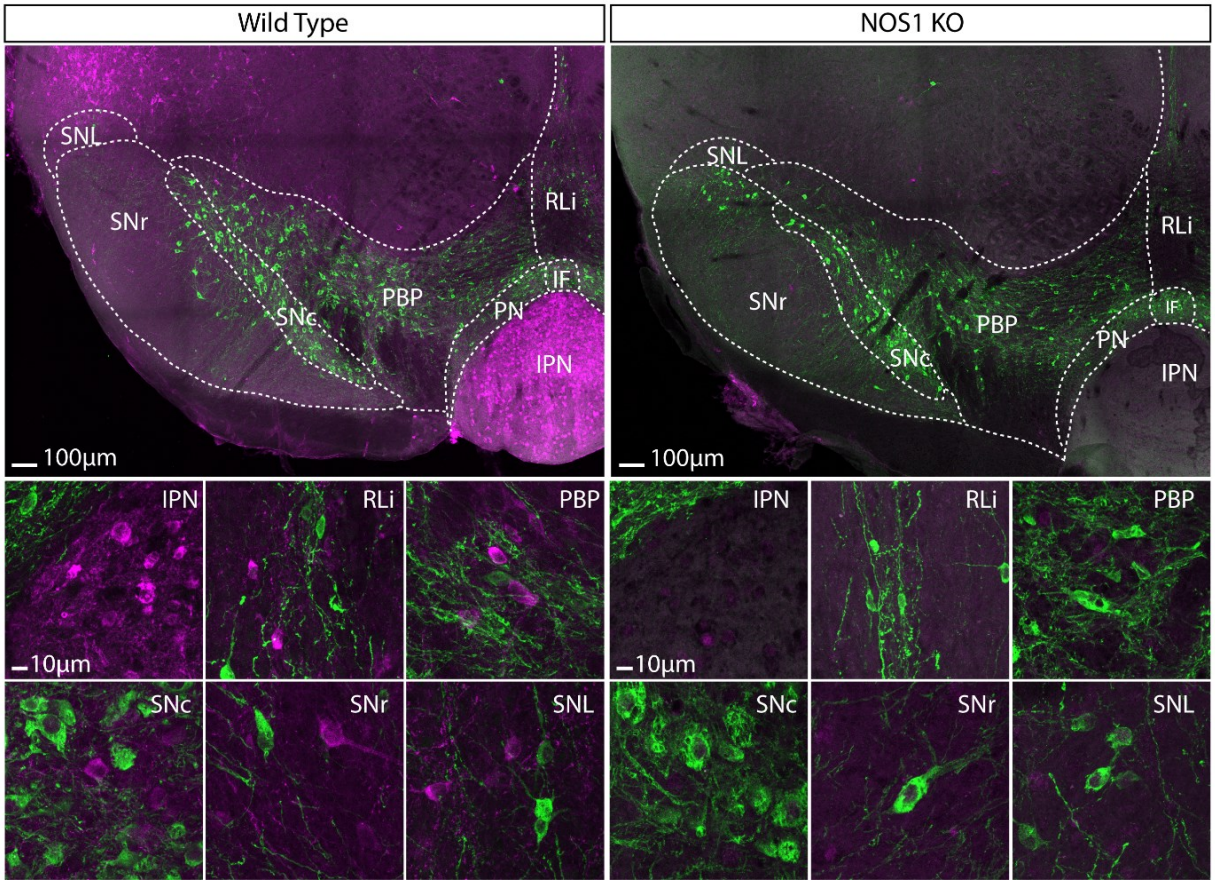


Figure 12: Dual immunostaing for nNOS (magenta) and TH (green) in the VTA and SNc. In wild type tissue nNOS+ cells can be observed in the IPN, RLi, PBP, SNc, SNr and SNL. All of which were completely absent in the KO tissue. There is no co-localisation between nNOS and TH.

(iii) Subpopulations of both GABA and glutamate neurons in the VTA and SNc express nNOS

I next wanted to determine the neurochemical identity of the nNOS+ neurons. Since they are TH- the most likely scenario is that the nNOS+ neurons are GABA neurons. To investigate this, I conducted immunostaining in VGATCre:RiboTag tissue. The VGATCre mouse line (Vong *et al*., 2011), where cre-recombinase is under the control of the promoter for VGAT, is crossed with the RiboTag mouse line (Sanz et al., 2009b) which contains a floxed hemagglutinin (HA)-tagged exon in the RLp22 gene (the RiboTag mouse is described in more detail in **chapter 4**. The resulting offspring (VGATCre:RiboTag) exhibits HA expression specific for VGAT expressing (GABA) neurons. We have found that the RiboTag mouse is an effective tool for immunostaining. GFP (Z/EG) and tdTomato reporter lines to target GABA neurons have proved less effective in the VTA and SNc. Antibodies for HA work very well in the VTA and SNc, making the RiboTag mouse an ideal reporter line.

Triple immunostaining for nNOS, HA and TH was carried out in midbrain sections from VGATCre:RiboTag mice (n=3). I wanted to conduct an unbiased and systematic count of nNOS immunoreactive cells. To that end, I took unilateral midbrain tile scans of every fourth brain section in each of the mice. Nuclei sub-regions were defined using TH immunostaining and images from a mouse brain atlas (Franklin and Paxinos, 2008). All nNOS+ and HA+ neurons within each sub-region were counted. A total of 1420 nNOS+ neurons (473 neurons per mouse; ±49%) were counted across the three mice. The number of nNOS+ cells vary in different sub-regions, with the largest population lying in the PBP of the VTA. 41.8% (±3.3%) of the total number of nNOS+ cells are located in the PBP, 28.8% (±2.8%) are located in the RLi nucleus, and two smaller populations are present in the VTAR (11.5% ±2.4%) and SNc (17.9% ± 0.9%) **(Figure 13A).** nNOS+ neurons were virtually absent in the PN and IF. In agreement with the nNOS immunostaining I observed in the WT mice, there is no co-localisation between TH+ and nNOS+ cells. Co-localisation between nNOS and HA+ cells is observed. However, the degree of co-localisation between nNOS and HA varies in different sub-regions. In the PBP and SNc, the nNOS staining co-localises with HA in the large majority of detected nNOS+ neurons,

suggesting that the nNOS+ cells in these regions are mostly GABAergic. However, in the more rostral sub-regions - the VTAR and the RLi - the degree of co-localisation is less. In order to quantify this, I counted the number of cells showing nNOS/HA co-localisation and calculated the percentage of nNOS expressing cells that were HA+. Throughout the entire midbrain, 54.8% (±3.0%) of nNOS+ cells are HA+. The PBP shows the highest degree of co-localisation where 78.1% (±2.8%) of nNOS+ cells are HA+. In contrast, only 23.2% (±6.0%) of nNOS+ neurons in the RLi are HA+ **(Figure 13B)**. In the VTAR an average of 38% of nNOS+ neurons are HA+, indicating a more varied population. These VTAR cells make up a very small nNOS population, an average of 69 cells per mouse. The total proportion of GABA neurons that express nNOS is 9.3% (±1.0%). This proportion is similarly small across all regions ranging from an average of 6.3% (±0.4%) in the SNc to 14.0% (±5.4%) in the RLi **(Figure 13C).** Broadly speaking, the midbrain dopaminergic nuclei contain three types of neuron: dopaminergic, GABAergic and glutamatergic. We know from the literature that the RLi and VTAR contain lower numbers of GABA neurons than the other midbrain regions, and instead have a larger proportion of glutamate neurons (Nair-Roberts *et al.,* 2008). It is therefore reasonable to assume that the nNOS+ HA- TH- neurons observed in these regions are likely to be glutamatergic. Representative images from each of these sub-regions is shown in **Figure 13D-G.**

These data suggest that there are not only regional differences in the numbers of nNOS expressing neurons in different subregions, but also differences in their neurochemical identiy. The largest population of nNOS+ neurons is in the PBP, most of which are GABA neurons. In contrast, the second largest nNOS+ population lies in the RLi nucleus and mostly consists of glutamate neurons. There is a small population of nNOS+ neurons in the SNc, most of which are GABA neurons. Finally, the VTAR contains a small number of nNOS+ that are made up of both GABA and glutamate neurons. A schematic summarising these results is shown in **Figure 14.**

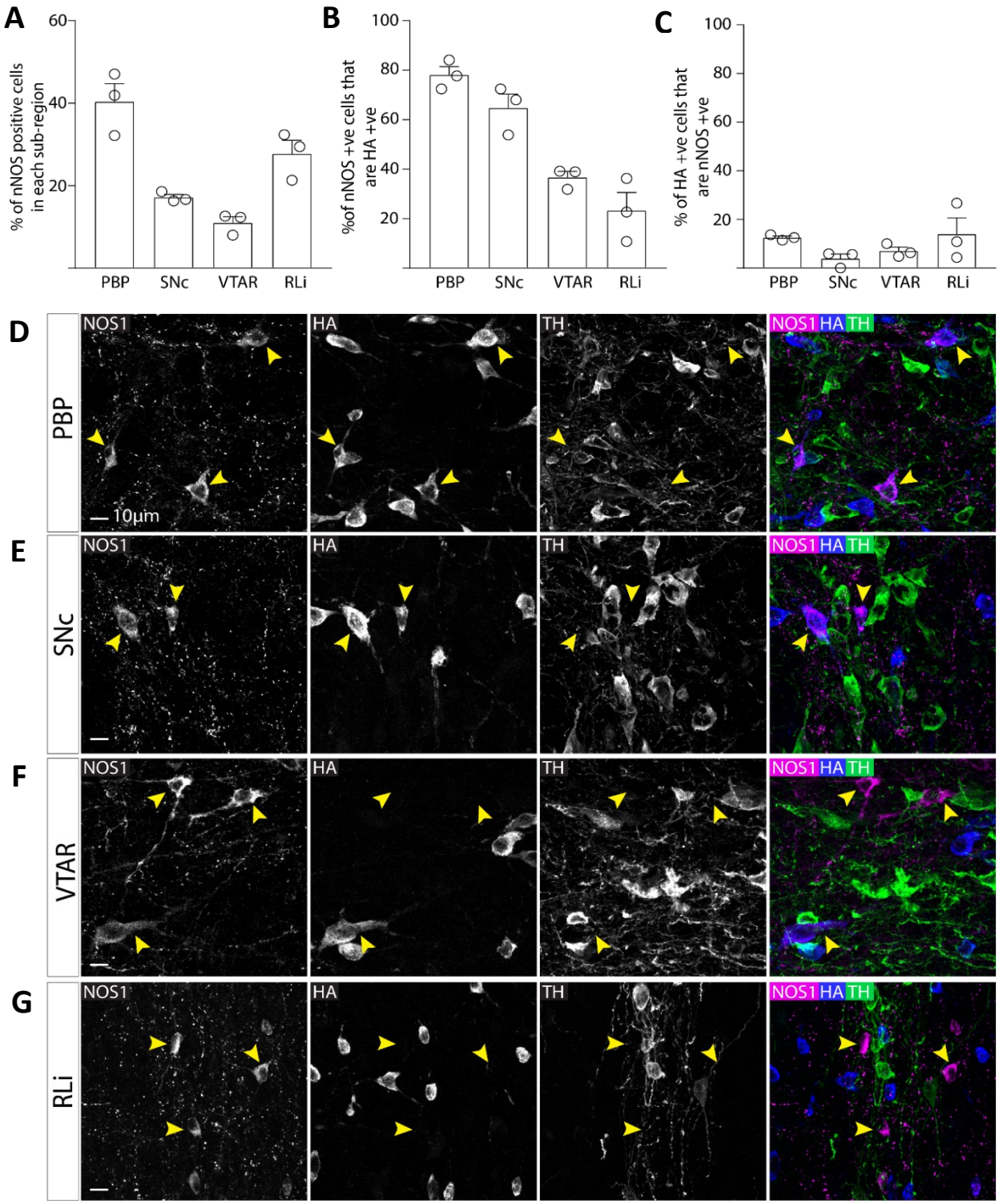


Figure 13: Triple immunostaining for nNOS, HA and TH in VGATCre:RiboTag tissue (continued on next page)

Figure 13: Triple immunostaining for nNOS, HA and TH in VGATCre:RiboTag tissue (continued)

A: The average percentage of nNOS+ cells localised to the PBP, SNc, VTAR and RLi (mean/standard error of the mean;SEM; n=3). **B:** The average percentage of nNOS+ cells that co-localised with HA in the PBP, SNc, VTAR and RLi (mean/SEM; n=3). **C:** The average percentage of HA+ cells that were nNOS+ (mean/SEM; n=3). **D-G:** Representative images taken from the PBP, SNc, VTAR and RLi illustrating the degree of co-expression between nNOS, HA and TH in the PBP, SNc, VTAR and RLi. Yellow arrows highlight the location of nNOS+ neurons.

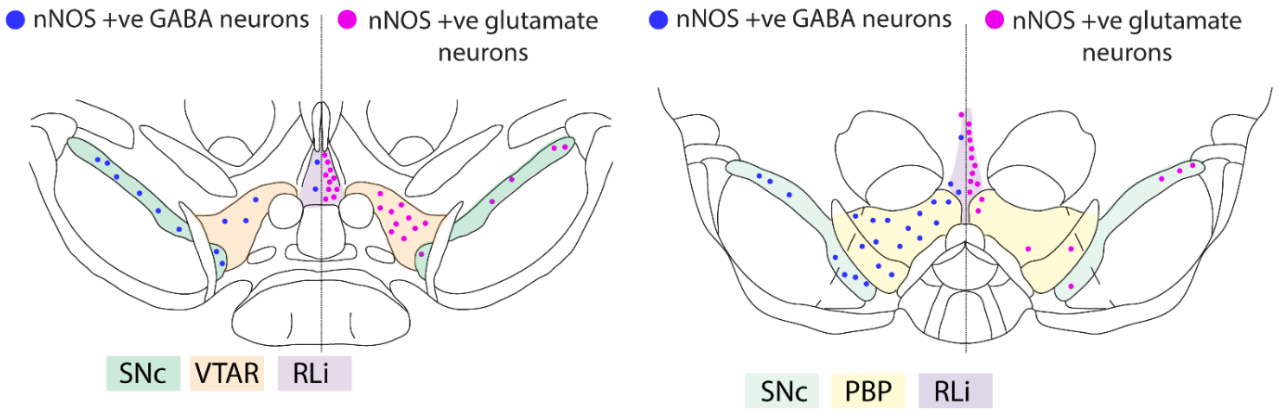


Figure 14: Schematic illustrating localisation of nNOS+ GABA (blue) and nNOS+ glutamate (magenta) in sub regions of the VTA and the SNc. *Brain outlines were traced from (Franklin and Paxinos, 2008)*

2.3.2 nNOS expressing neurons in the midbrain contain projecting and non-projecting populations

Having established that there is an nNOS expressing population of neurons in the VTA and SNc, some of which are GABA neurons and some of which are glutamate neurons, we next wanted to trace the circuitry of these nNOS+ cells. The aim was to establish whether these neurons send long range projections or whether they act locally as interneurons. In order to trace their axonal projections a Cre-dependant AAV containing ChR2-mCherry was injected into the midbrain of NOS1Cre mice. In these mice Cre-recombinase expression is heterozygously expressed under the control of the NOS1 promoter.

A total of 18 NOS1Cre mice (10 females, 8 males) received stereotaxic injections of AAV1-Ef1a-DIO-ChR2-mCherry into the midbrain. Based on the immunostaining data, there are distinct populations of nNOS expressing neurons in close proximity within the midbrain dopaminergic nuclei. We also know that there are large populations of nNOS expressing neurons in surrounding areas, in particular, the IPN and the supramamillary nucleus (SUM) (Gonzalez-Hernandez and Rodriguez, 2000; Rodrigo *et al*., 1994). In order to establish the circuitry of the nNOS+ populations in the VTA/SNc, it was important to try and limit the spread of the virus to these surrounding populations. To do this, I systematically varied the injection co-ordinates (anterior-posterior; AP -3.00-3.40mm, medial-lateral; ML +0.4-0.9mm, dorsal-ventral; DV 4.3-4.8mm) and volumes (0.1-0.3 µl) for the 18 mice **(Table 6).** The ChR2-mCherry expression was examined throughout the entire brain of every injected mouse. The observed expression is summarised in **(Table 6).** In brains that exhibited similar cell body expression patterns of the virus consistent axon terminal expression is also observed. Based on the overall expression patterns recorded, the injected brains are clustered into five groups **(Table 7).** Example images of these expression patterns can be seen in **Figures 15** and **16.**

	Group 1						Group 2				Group 3		Group 4			Group 5		
Mouse #	**1**	**2**	**3**	**4**	**5**	**6**	**7**	**8**	**9**	**10**	**11**	**12**	**13**	**14**	**15**	**16**	**17**	**18**
♂/♀	♀	♂	♂	♀	♀	♂	♂	♀	♀	♀	♀	♀	♂	♀	♀	♂	♂	♂
Coordinates	**Surgery details**																	
AP (-)	3.0	3.0	3.0	3.0	3.0	3.0	3.4	3.4	3.4	3.0	3.0	3.0	3.3	3.0	3.0	3.0	3.3	3.3
ML (+)	0.4	0.4	0.4	0.4	0.4	0.4	0.4	0.4	0.4	0.4	0.4	0.4	0.7	0.7	0.7	0.9	0.7	0.7
DV (-)	4.8	4.8	4.8	4.8	4.8	4.6	4.3	4.3	4.3	4.8	4.8	4.8	4.6	4.8	4.8	4.8	4.8	4.8
Inj. Vol. (µl)	0.3	0.3	0.3	0.2	0.2	0.1	0.1	0.1	0.1	0.1	0.1	01	0.1	0.1	0.1	0.1	0.1	0.1
Region	**Cell bodies**																	
SUM	+++	+++	+++	++	++	++	-	-	-	-	+	+	-	-	-	-	-	-
VTAR	+++	+++	+++	++	++	+	+	++	++	+++	++	+	+++	+++	+++	-	+	+
RLi	+++	+++	+++	+++	+++	++	+++	+++	+++	+++	-	-	-	-	-	-	-	-
PBP	+++	+++	+++	+++	+++	+++	+++	+++	+++	+++	+++	+++	+++	+++	+++	++	+++	++
SNc	+++	+++	+++	+++	+++	+++	+++	+++	+++	+++	+++	+++	+++	+++	+++	++	+++	+
IPN	-	-	-	-	-	-	-	-	-	-	-	-	-	-	-	-	-	-
Region	**Axon terminals**																	
Cortex																		
Endopiriform	+	-	-	-	-	-	-	-	-	-	-	-	-	-	-	-	-	-
Septum																		
MS	++	++	++	++	++	++	++	++	++	++	-	-	-	-	-	-	-	-
DB	+	++	++	+	+	++	+	+	+	+	-	-	-	-	-	-	-	-
LS	+	+	+	+	+	+	+	+	+	+	-	-	-	-	-	-	-	-
ST	+	+	+	-	-	+	+	+	+	+	-	-	-	-	-	-	-	-
Striatum																		
NAc (shell)	+	+	+	+	+	+	+	+	+	+	-	-	-	-	-	-	-	-
VP	+++	+++	+++	+++	+++	+++	+++	+++	+++	+++	-	-	-	-	-	-	-	-
NAc (core)	-	+	-	-	-	+	-	-	-	+	-	-	-	-	-	-	-	-
SI	+	+	+	-	-	+	-	-	-	-	-	-	-	-	-	-	-	-
GP	+	+	-	-	-	+	-	-	-	-	-	-	-	-	-	-	-	-
Hypothalamus																		
LH	+++	+++	+++	+++	+++	+++	+++	+++	+++	+++	-	-	+	+	+	-	-	-
PH	+	+	+	+	+	+	-	-	-	-	-	-	-	-	-	-	-	-
DM	+	+	+	+	+	+	+	+	+	+	-	-	-	-	+	-	-	-
PO	++	++	++	++	++	++	+	+	+	+	-	-	-	-	-	-	-	-
ZI	+	+	+	+	+	+	+	+	+	+	-	-	-	-	-	-	-	-
Thalamus																		
LHb	+	+	+	+	+	+	+	+	+	+	-	-	-	-	-	-	-	-
PF	+	+	+	+	+	-	-	-	-	-	-	-	-	-	-	-	-	-
MD	+	+	+	+	+	+	-	-	-	+	-	-	-	-	-	-	-	-
LD	++	++	++	+	-	-	-	-	-	-	-	-	-	-	-	-	-	-
VM	+	+	+	-	-	-	+	+	+	+	-	-	-	-	-	-	-	-
Fimbria	+	+	+	-	-	-	-	-	-	-	-	-	-	-	-	-	-	-
Amygdala																		
medial	+	+	+	-	-	-	-	-	-	+	-	-	-	-	-	-	-	-
AA	+	+	+	-	-	-	-	-	-	+	-	-	-	-	-	-	-	-
Midbrain																		
IPN	+++	+++	+++	++	++	++	-	-	-	-	+	+	-	-	-	-	-	-
SNr	+	+	+	+	+	+	+	+	+	+	+	+	+	+	+	+	+	+
Mammillary	+	+	+	+	+	+	+	-	-	-	-	-	-	-	-	-	-	-
Pons/medulla																		
DR	++	++	++	++	+	+	+	+	+	++	-	-	-	-	-	-	-	-
PMnR	++	++	++	+	+	+	+	+	+	++	-	-	-	-	-	-	-	-
RMg	+	+	+	-	-	-	-	-	-	-	-	-	-	-	-	-	-	-
MnR	++	++	++	++	++	++	++	++	+	++	-	-	-	-	-	-	-	-
LDTg	+	+	+	-	+	+	-	-	-	-	-	-	-	-	-	-	-	-
DMTg	+	+	+	-	-	-	-	-	-	-	-	-	-	-	-	-	-	-
ATg	+	+	+	-	-	++	-	-	-	-	-	-	-	-	-	-	-	-
Tz	+	+	-	-	-	+	-	-	-	-	-	-	-	-	-	-	-	-
PAG	+	+	+	+	+	+	+	+	+	+	-	-	-	-	-	-	-	-
CLi	+	+	+	+	+	+	+	+	+	+	-	-	-	-	-	-	-	-
Pn	+	+	+	+	+	+	-	-	-	-	-	-	-	-	-	-	-	-
NRO	+	+	+	+	+	+	+	+	+	+	-	-	-	-	-	-	-	-
Mrt	+	+	+	+	-	+	-	-	-	-	-	-	-	-	-	-	-	-

Table 6: Injections details, cell body detection and axon terminal detection in all injected mice. The degree of ChR2-mCherry detection is depicted with -/+

	Group 1 (Mice 1-6)	Group 2 (Mice 7-10)	Group 3 (Mice 11 &12)	Group 4 (Mice 13-15)	Group 5 (Mice 16-18)
Region	**Cell Bodies**				
SUM					
VTAR					
RLi					
PBP					
SNc					
Region	**Axon terminals**				
VP					
PO					
AV					
MD					
LH					
IPN					
PMnr/MnR					
DR					
PNc/RIP					

Table 7: A summary of five groups of expression patterns observed in the injected mice

The brains in group 1 received the largest injection volume and therefore exhibited the most cell body expression of ChR2-mCherry. ChR2-mCherry+ cells were observed throughout the dopaminergic nuclei: in the PBP, SNc, VTAR and RLi. In these brains the virus also spreads to the SUM, where it is expressed in a fairly large population of neurons. Many axon terminals can also be seen throughout multiple brain regions in the group 1 brains **(Tables 6 and 7).** The brains in group 2 exhibit robust ChR2-mCherry cell body expression in the same midbrain regions: the PBP, SNc, VTAR and RLi. However, in these cases the virus does not spread to the SUM. The most striking difference between the projections observed in group 1 and group 2 brains is the presence of ChR2-mCherry+ terminals in the anterior ventral thalamus (AV) and in the IPN. In group 1 brains there is dense innervation of ChR2-mCherry+ axons in both regions, but this is completely absent in group 2 brains. This suggests that the

terminals seen in the AV and IPN are likely to be arising from those ChR2-mCherry+ in the SUM nucleus. The remaining axon terminals are observed in both group 1 and group 2 brains suggesting these are coming from ChR2-mCherry+ neurons other than those in the SUM. F

The brains in group 3 again exhibit robust ChR2-mCherry expression in cell bodies of the PBP and SNc. There is however, a slightly smaller number of cells expressing the virus in the VTAR and none at all in the RLi. In these brains there is also a very small number of SUM cell bodies expressing ChR2-mCherry, although much fewer than observed in group 1. In the two brains of this group, the only ChR2-mCherry+ terminal present outside of the midbrain are in the IPN -this being less than that observed for those in group 1. This small amount of IPN innervation is likely originating from the small amount of ChR2-mCherry+ neurons in the SUM. No additional axon terminals are observed, suggesting that the ChR2-mCherry+ neurons present in the PBP/SNc/VTAR are not sending long-range projections. It also suggests that the ChR2-mCherry+ axon terminals observed in group 1 and 2 mice are originating from the neurons in the RLi and not the other sub-regions.

The brains in group 4 exhibit robust expression of ChR2-mCherry in cell bodies of the PBP and SNc in these brains there is also a much larger population of ChR2-mCherry+ cells in the more dorsolateral part of the VTAR. In these brains there are no ChR2-mCherry+ cell bodies in the RLi or SUM. Apart from a very small presence of ChR2-mCherry+ fibres in the LH, there are no ChR2-mCherry+ axon terminals outside the midbrain nuclei. As these fibres in the LH are not present in group 2, it is likely they are arising from the neurons in the lateral-dorsal VTAR. The distance between the sections containing cell bodies in the dorsolateral VTAR and the fibres in the LH is very small; meaning it is possible that these particular fibres are dendrites rather than projections. Consistent with those brains in group 3, the ChR2-mCherry neurons in the PBP and SNc appear to not be sending long range projections. This is confirmed by the brains in group 5. As in all other groups, the mice in group 5 exhibit ChR2-mCherry+ neurons in the PBP and SNc. In contrast to group 4, there is very little or no cell body expression present in the VTAR. In these brains, there is absolutely no nNOS+ fibres outside

of the VTA or SN suggesting there is no long-range projections. Representative example images of ChR2-mCherry+ cell body expression and of ChR2-mCherry+ axon terminals are shown in **Figure 15** and **Figure 16,** respectively.

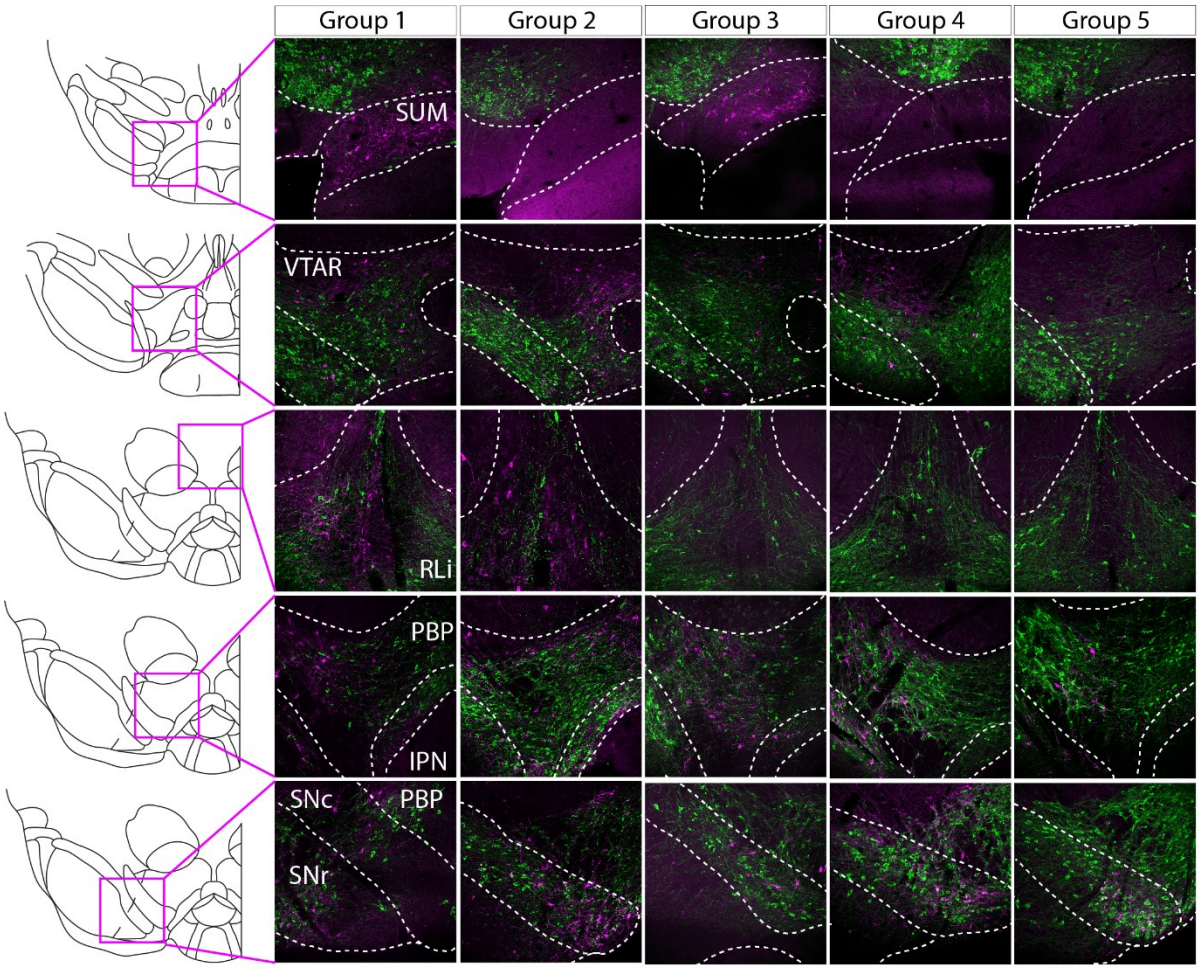


Figure 15: Representative images showing the ChR2-mCherry (magenta) cell body expression exhibited by each injected group. Images are shown of the SUM, RLI, VTAR, PBP and SNc. Sections are stained for TH ((green) as a means to determine the VTA sub-regions, and VTA and SNc boundaries. *Brain outlines were traced from (Franklin and Paxinos, 2008)*

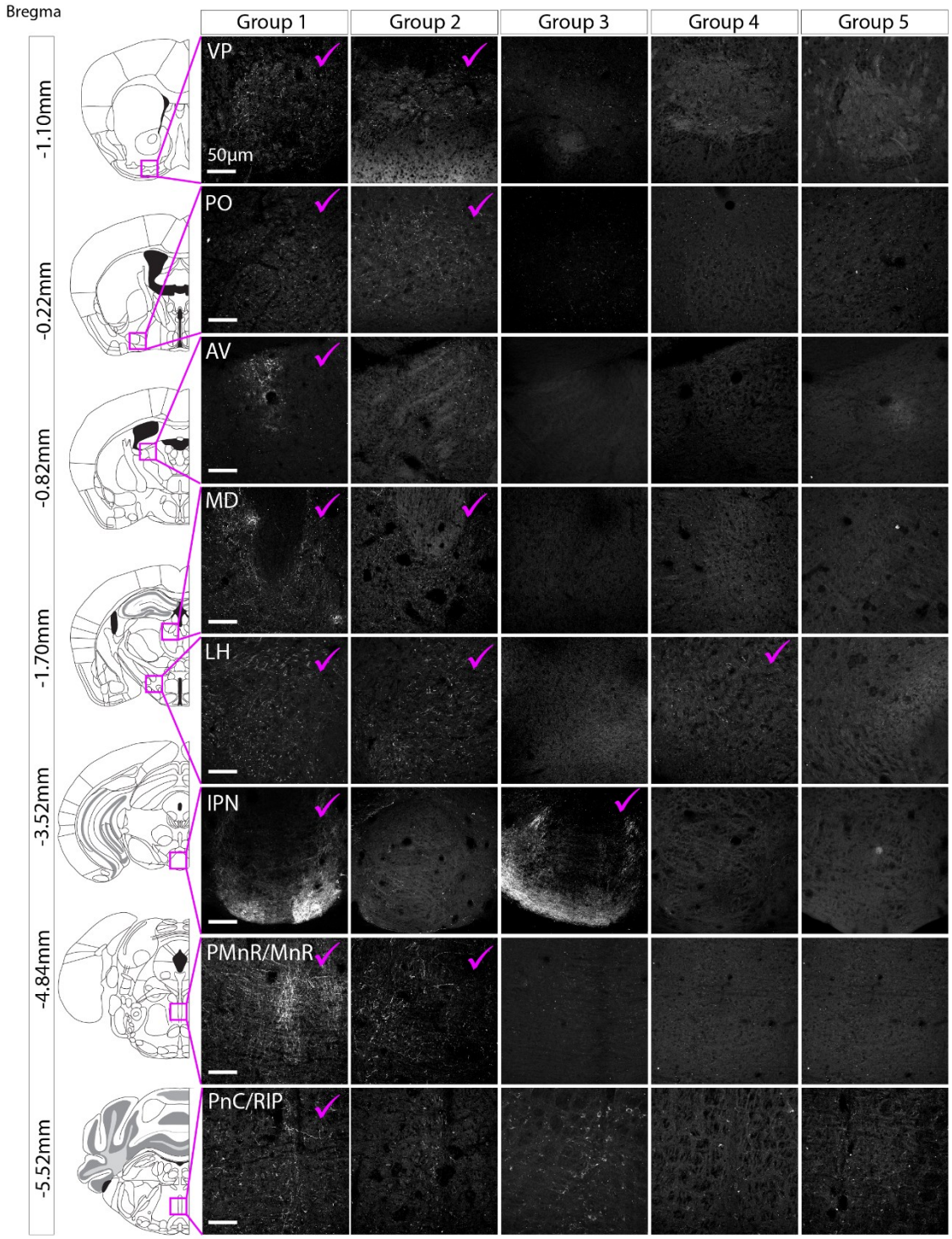


Figure 16: Representative images showing the presence or absence of ChR2-mCherry+ axon terminals in different brain regions of each injected group. Images are shown for the VP, PO, AV, MD, LH, IPN, PMnR/MnR and PNc/RIP. A pink tick represents the presence of axon terminals. *Brain outlines were traced from (Franklin and Paxinos, 2008)*

Based on the pattern of ChR2-mCherry+ cell bodies and ChR2-mCherry+ axon terminals observed in each injected brain, we are able to determine information about which ChR2-mCherry+ neurons are which projections **(Table 7).** A comparison of these 5 different groups has led us to deduce that of the VTA and SNC nNOS+ neurons those in the RLi send long range projections, whereas those in the PBP and SNc do not project outside the VTA and SN. When the virus expression is contained within the dopaminergic nuclei and spreads as far as the nNOS+ neurons in the RLi nucleus (group 2), ChR2-mCherry+ axon terminals are present in multiple brain regions. Brain areas appearing to receive the most innervation from these RLi neurons are the VP, the preoptic area (PO), the lateral hypothalamus (LH) and the paramedian, median and dorsal raphe (PMnR, MnR and DR). These observed target regions are consistent with a study that traced axon projections of RLi neurons in the rat brain using PHAL-L (Del-Fava *et al*., 2007). When the virus is contained to the VTA and SNc but does not spread into the RLi nucleus, no axon terminals are observed outside of the VTA and SN. This is consistently seen across 3 groups (8 mice). Combining these with the data from the VGATCre:RiboTag immunostaining tells us two things. Firstly, it appears to be the nNOS+ glutamate neuron population of the RLi that is sending long-range projections. Secondly, the nNOS+ GABA population in the PBP and SNc appears to be interneurons.

2.3.3 The degree of ChR2-mCherry and nNOS co-localisation is region specific

To verify the NOS1Cre mouse line and to confirm that ChR2-mCherry+ cells are nNOS+, midbrain sections from injected mice were co-stained for nNOS and TH. ChR2-mCherry+ cells were counted in each sub-region and the percentage of nNOS staining co-localisation was calculated. In the PBP (n=5 mice, 230 cells), VTAR (n=4 mice, 40 cells), and RLi (n=3 mice, 155 cells) nucleus, the vast majority of ChR2 labelled cells are immunoreactive for nNOS **(Figure 17A, C and D)**: 88.3% (±2.4%), 78.5% (±4.8%) and 91.5% (±3.5%), respectively. There is very little ectopic expression. Consistent with the immunostaining data, there is only minimal or no (in the case of the RLi) ChR2-mCherry co-localisation

with TH (5.7%; ±2.5%, 14.4%; ±6.0% and 0% in the PBP, VTAR and RLi, respectively). In contrast, in the SNc (n=3 mice, 129 cells), 72.1% (±7.9%) of the ChR2-mCherry+ cells are not immunoreactive for nNOS **(Figure 17B).** In addition to this, a total of 47.7% (±6.2%) of the ChR2-mCherry+ neurons in the SNc are TH+. As observed in both the WT and VGATCre: RiboTag mice none of the nNOS antibody staining co-localised with TH antibody staining in the SNc. The regional specificity of these ChR2-mCherry+ TH+ cells suggests that this is unlikely to simply be ectopic expression of the AAV. We hypothesised that these neurons appear nNOS- because they are either expressing very low levels of the enzyme (so that it is not detectable with the nNOS antibody), or that nNOS mRNA is being transcribed but the protein is not being synthesised. This suggests that the number of SNc nNOS1 expressing neurons was previously underestimated. In any case, these results suggest the presence of a third population of nNOS expressing cells in the midbrain nuclei, a TH+ subpopulation that is predominantly found in the SNc.

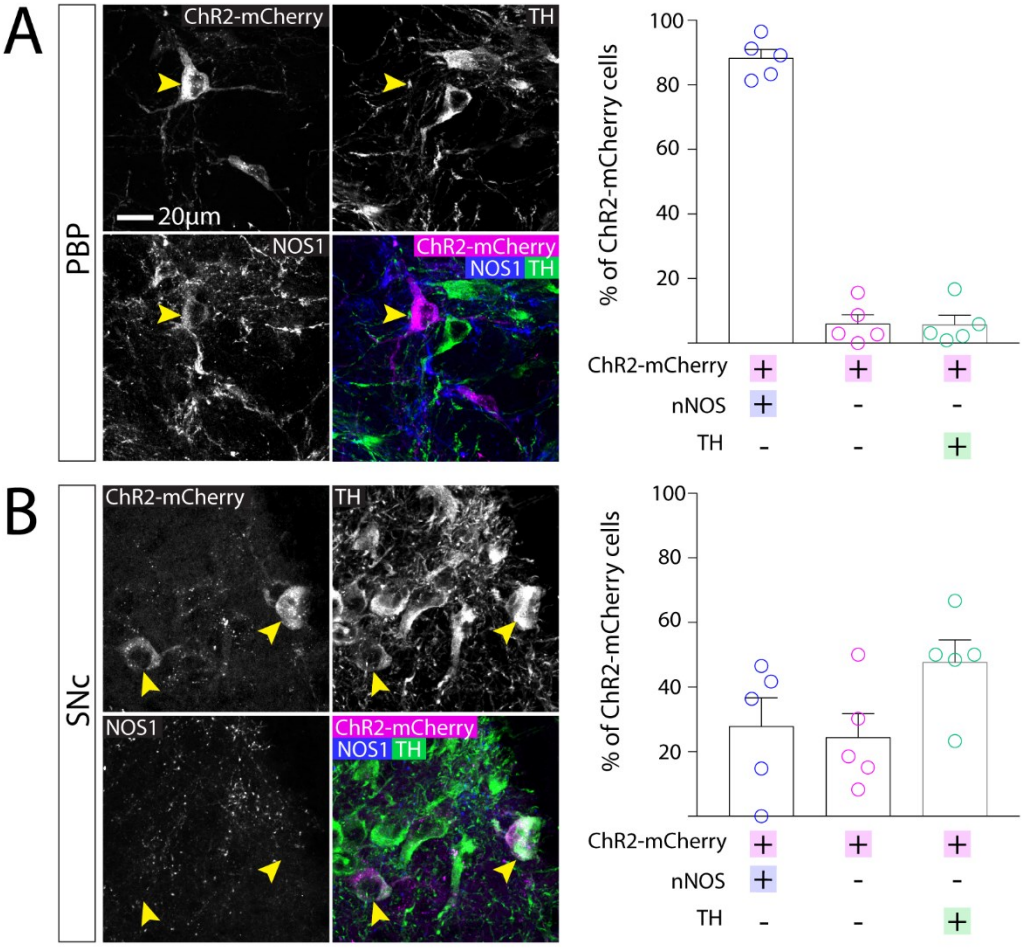


Figure 17: The degree of co-localisation between ChR2-mCherry+ and nNOS+ neurons in each sub-region ***(continued next page)***

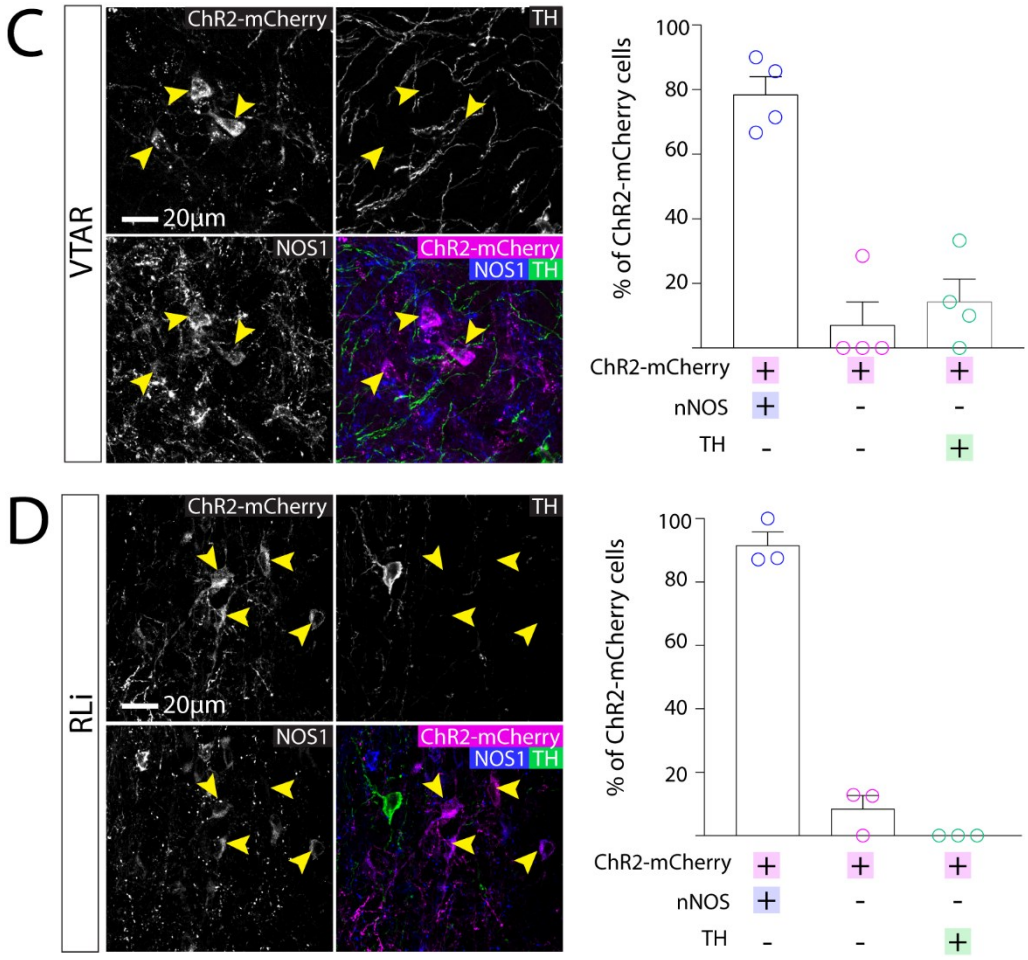


Figure 17: The degree of co-localisation between ChR2-mCherry+ and nNOS+ neurons in each sub-region. Left panels show representative images of immunostaining in each sub-region, PBP**(A),** SNc**(B),** VTAR**(C),** RLi**(D).** ChR2-mCherry (magenta), nNOS (blue), TH (green) **A:** Graph showing the average % co-localisation between ChR2-mCherry, TH and nNOS (mean/SEM) in the PBP. Individual data points from each mouse shown on the graph (230 ChR2-mCherry+ cells counted across 5 mice). **B:** The average % co-localisation between ChR2-mCherry, TH and nNOS (mean/SEM) in the SNc. Individual data points from each mouse shown on the graph (129 ChR2-mCherry+ cells counted across 5 mice). **C:** The average % co-localisation between ChR2-mCherry, TH and nNOS (mean/SEM) in the VTAR. Individual data points from each mouse shown on the graph (40 ChR2-mCherry+ cells were counted across 4 mice) **D:** The average % co-localisation between ChR2-mCherry, TH and nNOS (mean/SEM) in the RLi. Individual data points from each mouse shown on the graph (155 ChR2-mCherry+ cells were counted across 3 mice).

2.3.4 nNOS neurons are GABAARα1+

GABA A receptor alpha 1 (GABAARα1) subunit is thought to be expressed exclusively in GABA neurons in the PBP of the VTA (Tan *et al*., 2010). It can therefore be considered a molecular marker for GABA neurons in this region. In contrast to other GABA neuron markers, GAD67/65 and VGAT antibodies for GABAARα1+ work well in the VTA and SNc. A few midbrain sections from each of the injected brains were co-stained for TH and GABAARα1. It was found that all ChR2-mCherry expressing neurons are immunoreactive for GABAARα1, except for those that also express TH - which were GABAARα1- **(Figure 18).** This result agrees with previous suggestions that there is little or no overlap between TH and GABAARα1. Not all nNOS+ neurons in the RLi and VTAR are VGAT+, this suggest that GABAARα1 expression does not always co-localise with VGAT in these regions.

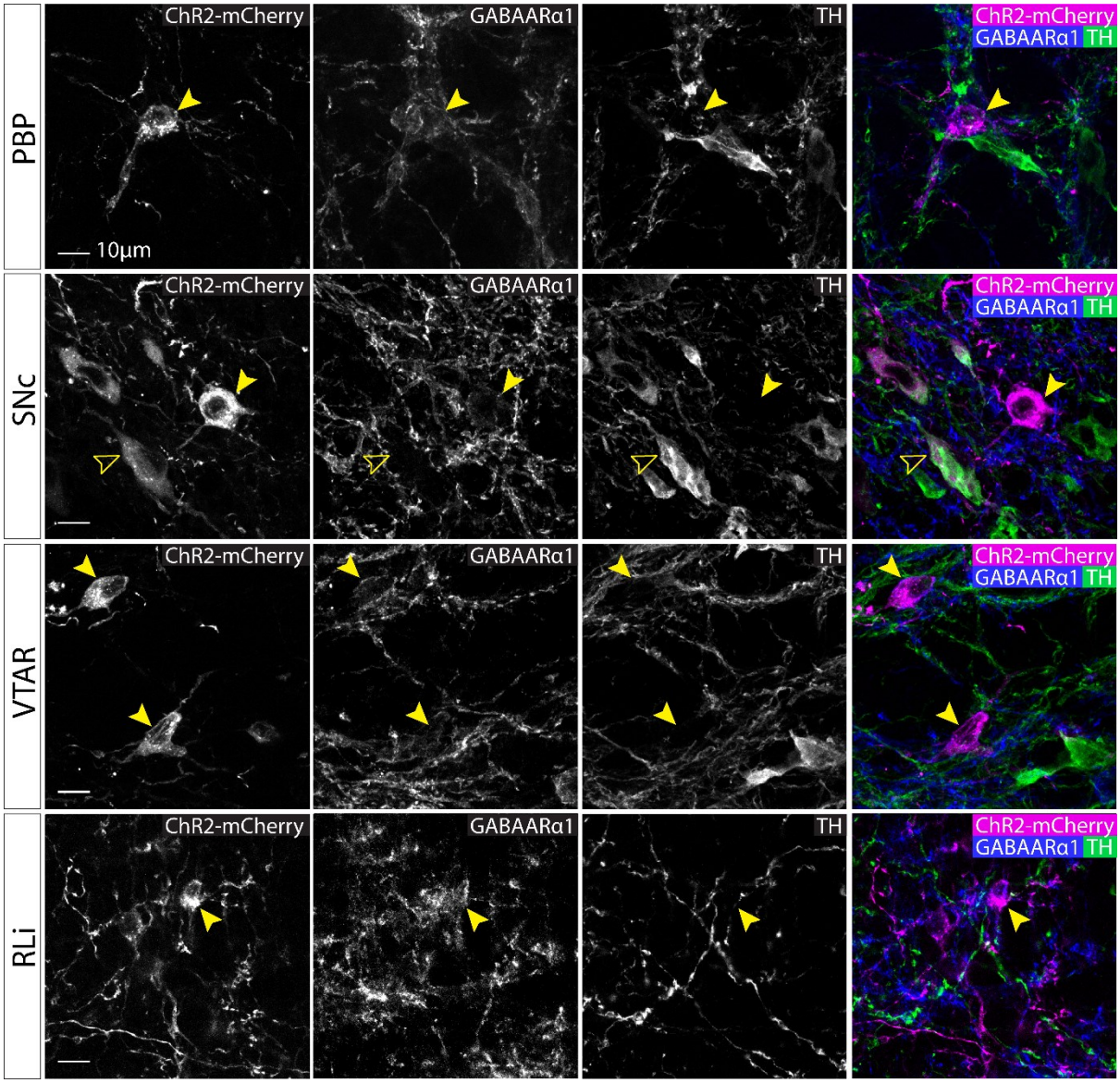


Figure 18: ChR2-mCherry+ neurons are GABAARα1+. ChR2-mCherry co-localises with immunostaining for GABAARα1 (solid yellow arrows) except in TH+ neurons (empty yellow arrow).

2.3.5 Neurochemical identity of nNOS+ interneurons in the VTA and SNc

Based on the nNOS immunostaining in the VGATCre:RiboTag tissue and GABAARα1 staining in the injected brains, we expect that the ChR2-mCherry+ interneurons in the VTA and SNc are GABA neurons. Most of the nNOS+ neurons in the PBP and SNc were HA+, this means that they express VGAT - a key marker gene for GABA neurons. In addition to this ChR2-mCherry+ (TH-) neurons co-localise with GABAARα1, which also suggests a GABA neuron phenotype. The neurochemical identity of the ChR2-mCherry+ TH+ population that lies mainly in the SNc is less clear. This is because this population has so far not been detected with nNOS immunostaining. I wanted to further examine the neurochemical identity of these non-projecting nNOS neurons while also attempting to confirm that they make local synapses in the midbrain nuclei. I did this with immunostaining for VGAT and VGLUT2, presynaptic markers for GABAergic and glutamatergic synapses respectively.

In this section all images were obtained from the brains of mice in group 5 – the non-projecting nNOS neurons.

(i) There is co-localisation between ChR2-mCherry and VGAT in the PBP

Single z-plane images of sections stained for VGAT and TH revealed co-localisation between VGAT and ChR2-mCherry **(Figure 19A).** These appear to be pre-synaptic terminals, some of which lie in close proximity to, but not co-localising with, TH+ processes. This suggests that nNOS+ interneurons form inhibitory synapses onto dopamine neurons. Not all VGAT+ terminals are close to TH processes which means nNOS neurons could also innervate processes from non-dopaminergic neurons **(Figure 19A).**

(ii) There is co-localisation between ChR2-mCherry and VGLUT2 in the PBP

Interestingly, single z-plane images stained for VGLUT2 and TH suggest the possibility that some nNOS+ neurons also form local glutamatergic synapses. These VGLUT2+ terminals are few and far between when compared to the VGAT+ terminals **(Figure 19B).** Surprisingly, the VGLUT2 antibody staining allowed us to visualise some VGLUT2+ cell bodies **(Figure 20A).** In the PBP we observe an

occasional mCherry-Chr2+ VGlut2+ cell body. This is a very small proportion of the total number of ChR2-mCherry+ neurons. Most of the ChR2-mCherry+ neurons are VGLUT2- **(Figure 20B).** These VGLUT2+ cell bodies tend to lie in the more medial part of the PBP, an area known to have a higher density of glutamate neurons than the more lateral regions. This data suggests that in addition to the GABA interneurons, there may be a very small number of glutamate nNOS+ neurons in the PBP that do not send long range projections and instead form local synapses.

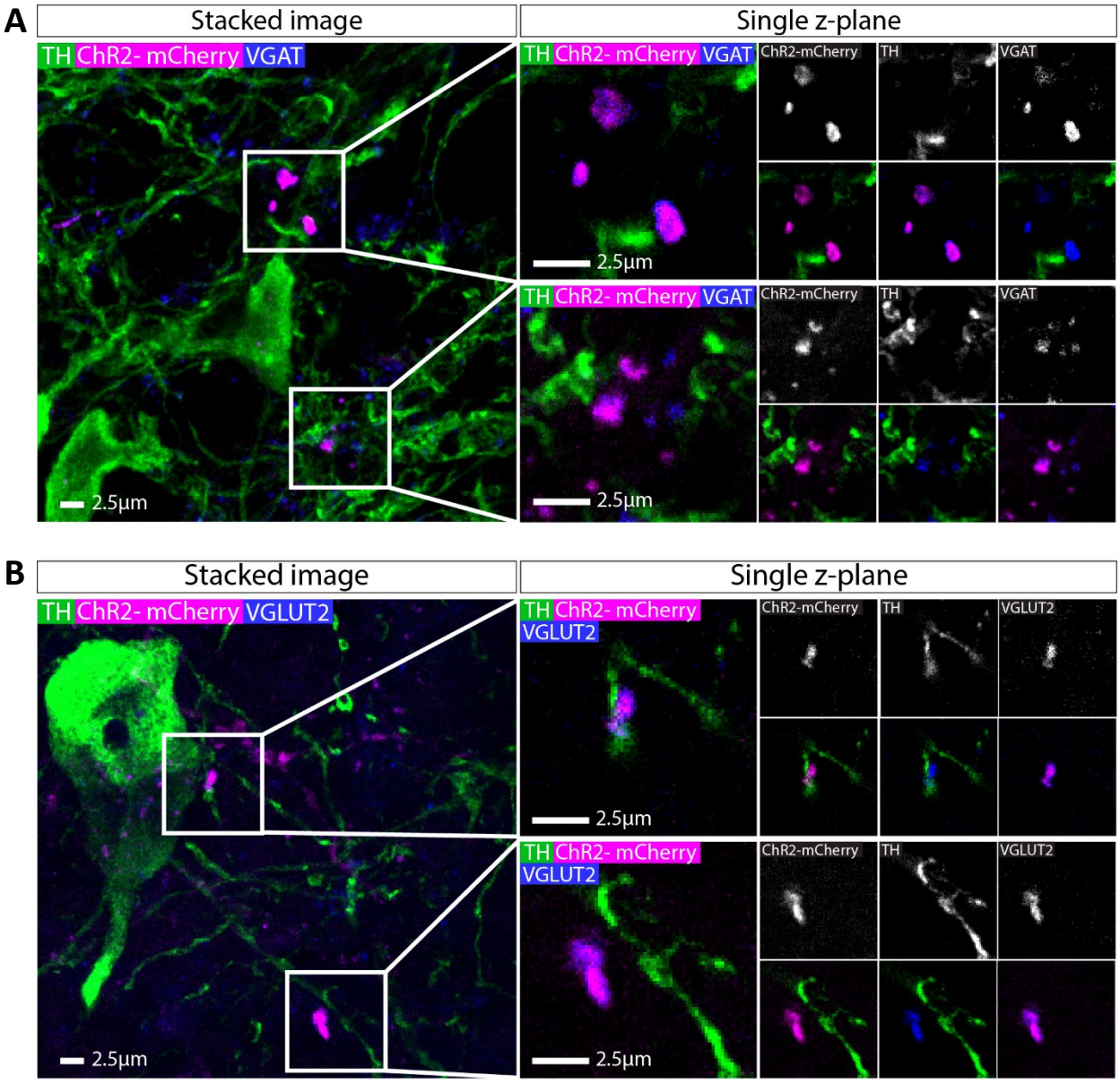


Figure 19: **ChR2-mCherry+ neurons form synapses in the VTA**. **A:** ChR2-mCherry co-localises with VGAT in a single z-plane image suggesting the presence of GABAergic synapses. **B:** ChR2-mCherry co-localises with VGLUT2 in a single z-plane image suggesting the presence of glutamatergic synapses.

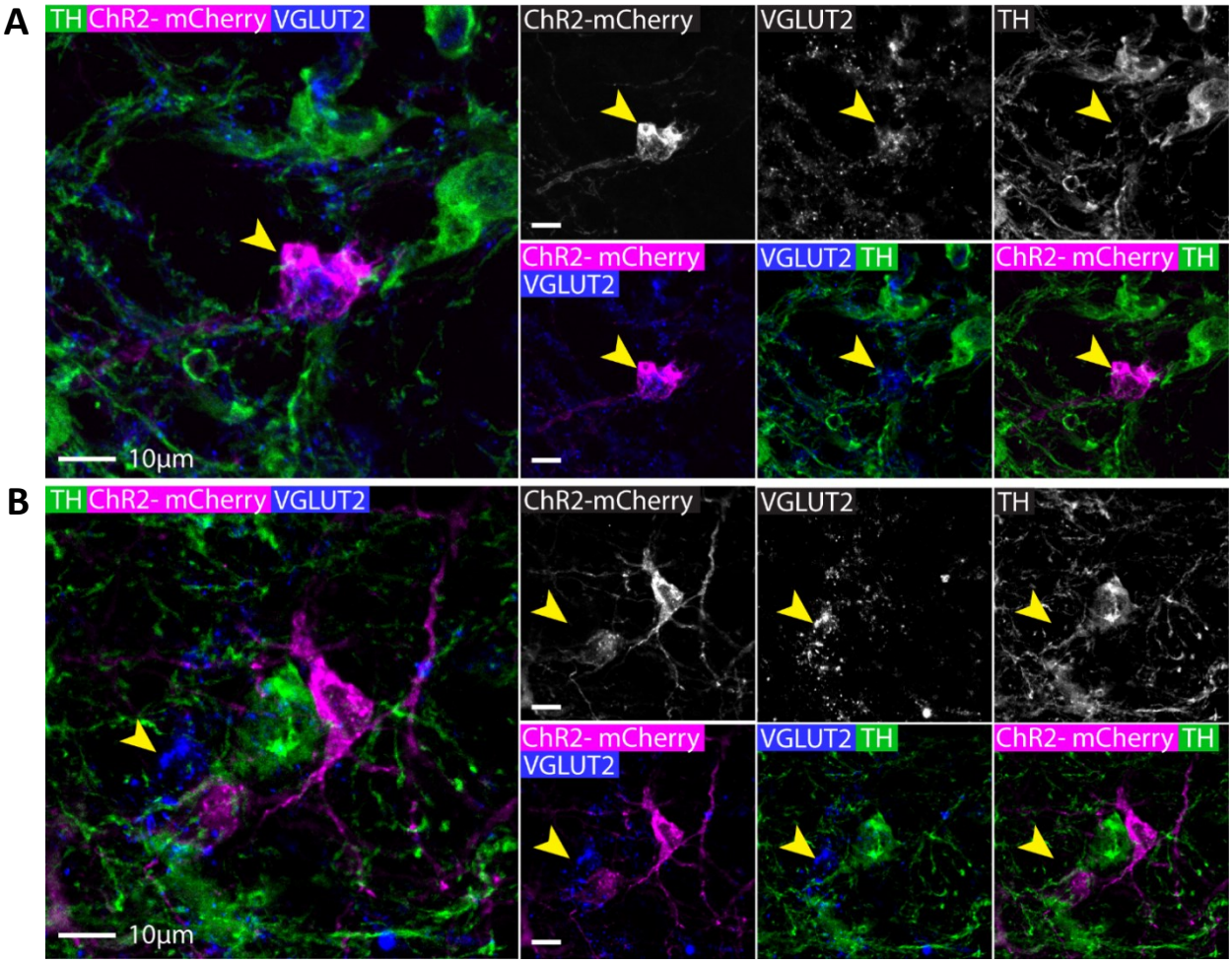


Figure 20: There is some co-localisation between ChR2-mCherry+ (magenta) cell bodies and VGLUT2 (blue) immunostaining in the PBP. This occurs in some **(A),** but not all **(B)** ChR2-mCherry+ neurons in the medial PBP. Yellow arrows point to VGLUT2 cell bodies.

(ii) TH+ interneurons may form VGAT+ synapses

The phenotype of the TH+ population is less clear, but is of great interest. Dopamine releasing axon terminals are not thought to be present within the midbrain nuclei. It has long been accepted that all dopamine neurons send long-range projections. However, outside of the midbrain there is evidence of TH+ GABAergic interneurons. TH+ interneurons are known to exist in the striatum of mice , rats (Meredith et al., 1999), non-human primates (Dubach et al., 1987; Robinson et al., 2002a) and humans (Cossette *et al*., 2005a; Cossette *et al*., 2005b; Cossette *et al*., 2004; Petroske *et al*., 2001; Porritt *et al*., 2000). These TH+ interneurons express no other markers for dopamine neurons and release GABA as their neurotransmitter (Xenias et al., 2015b). The major question here is whether these TH+ interneurons are dopamine neurons or GABA neurons. I was interested in determining whether there was any co-localisation between TH+ ChR2-mCherry+ axon terminals and VGAT. Single z-plane images of VGAT terminal staining shows some co-localisation between ChR2-mCherry, VGAT and TH **(Figure 21).** This suggests that these ChR2-mCherry+ TH+ nNOS neurons may form GABAergic synapses.

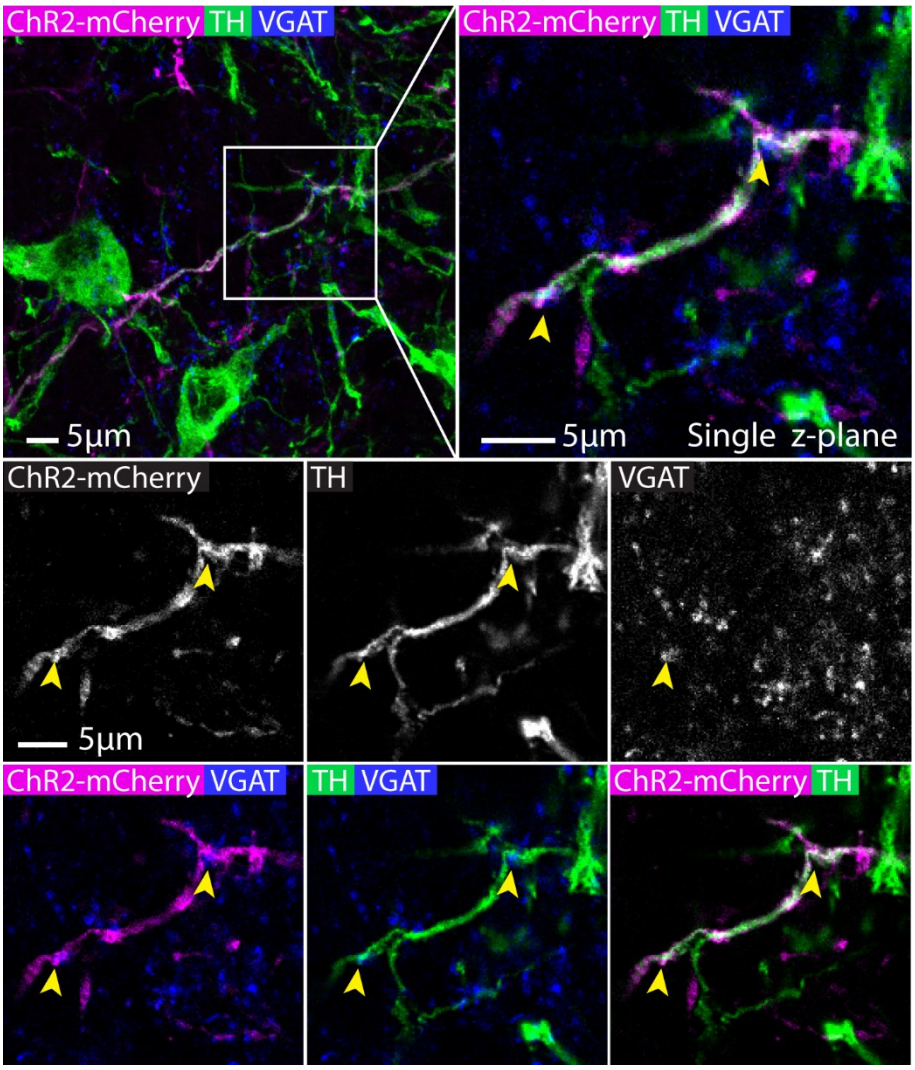


Figure 21: ChR2-mCherry+ (magenta) TH+ (green) and VGAT+ (blue) co-localisation in the PBP.

Yellow arrows point to regions of co-localisation.

2.3.6 Neuronal phenotype of nNOS+ projection neurons in the VTA

Based on the circuit tracing analysis, it is clear the axon terminals seen throughout the brain are largely originating from a midline population of nNOS expressing cells, in the RLi nucleus. The immunostaining in the VGATCre:RiboTag tissue suggests that the majority of nNOS expressing neurons in the RLi are HA- VGAT- and TH-, suggesting a glutamatergic phenotype. To confirm this, I again conducted immunostaining with antibodies for VGLUT2 and VGAT.

In this section all images were obtained from the brains of mice in group 2.

(i) The ChR2-mCherry neurons in the RLi are largely VGLUT2 +

The glutamatergic phenotype of these projecting neurons was confirmed with VGLUT2 cell body immunoreactivity. A large number of the ChR2-mCherry + cells in the RLi co-localised with VGLUT2 **(Figure 22).** There is a much larger amount of co-localisation between ChR2-mCherry+ and VGLUT+ cells in the RLi, when compared to the PBP.

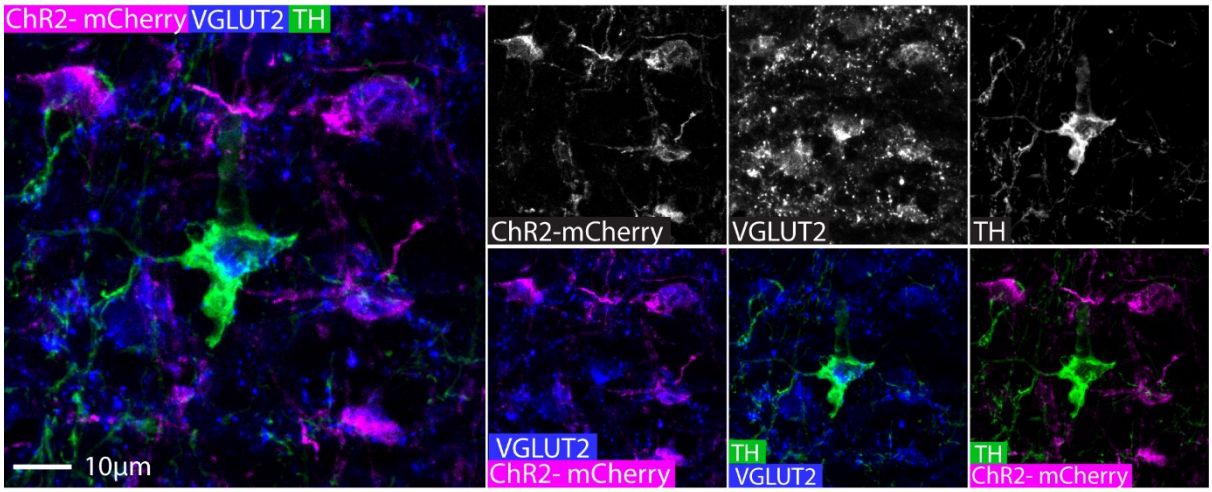


Figure 22: There is co-localisation between all imaged ChR2-mCherry+ (magenta) cell bodies and VGLUT2 (blue) immunostaining in the RLi.

Next, I conducted terminal staining in target regions of these nNOS projection neurons. Not only did this allow me to determine whether these nNOS projection neurons are forming glutamatergic or GABAergic synapses, but it also distinguished axon terminals from fibres of passage. I chose to further investigate the axon terminals in the VP and the raphe nuclei.

(ii) nNOS+ neurons from the RLi heavily innervate the VP

The VP is the area that appears to receive the most prominent input from the nNOS+ neurons in the RLi nucleus. This is consistent with a previous RLi neuronal tracing paper (Del-Fava *et al*., 2007). The VP can be defined by substance P immunoreactivity (Marksteiner et al., 1992; Napier et al., 1995; Zahm and Heimer, 1988). VP containing sections were stained for substance P and VGLUT2, and substance P and VGAT **(Figure 23).** Tile scans were taken in order to visualise the ChR2-mCherry+ axon terminals in the anatomy of the ventral striatum. ChR2-mCherry+ terminals are more prevalent in the VP (substance P+ region) compared to the horizontal limb of the diagonal band of Broca (HDB) and shell of the NAc; areas that receive sparse innervation. This innervation is present throughout the extent of the VP. ChR2-mCherry terminals can be clearly visualised amongst substance P terminals **(Figure 23A).** VGLUT2 terminal staining reveals co-localisation between VGLUT2 and ChR2-mCherry+ axon terminals in the VP suggesting glutamatergic synapses **(Figure 23B).** Terminal staining for VGAT shows that ChR2-mCherry+ terminals also co-localise with VGAT suggesting there could also be GABAergic synapses present **(Figure 23C).** These VGAT+ ChR2-mCherry+ terminals are much less frequent than the VGLUT2+ ChR2-mCherry+ terminals suggesting that most of the VP innervation from the RLi nNOS+ neurons is excitatory.

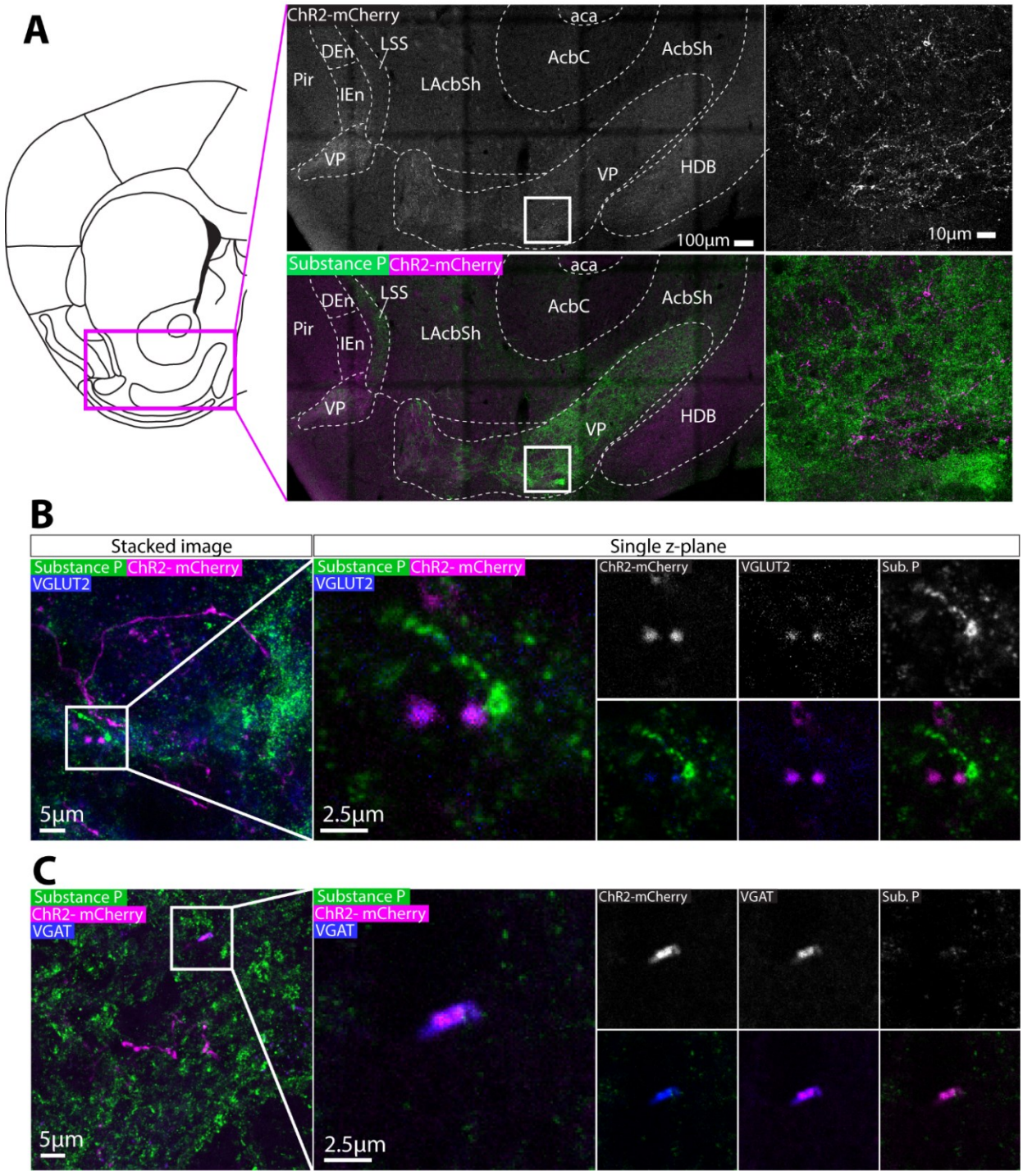


Figure 23: ChR2-mcherry+ axon terminals in the VP. A: Tile-scans of the ventral striatum show that ChR2-mCherry+ axon terminals (magenta) are more prevalent in the VP compared to nearby regions. Substance P immunostaining (green) highlights the VP region**. B:** Co-localisation between ChR2-mCherry (magenta) and VGLUT2 (blue) can be seen in single z-plane images in the VP. **C:** Co-localisation between ChR2-mCherry (magenta) and VGAT (blue) can be seen in single z-plane images in the VP. *Brain outlines were traced from (Franklin and Paxinos, 2008)*

(iii) nNOS+ neurons from the RLi innervate the PMnR, MnR and the DR.

Three sub-regions of the raphe nuclei also receive input from the nNOS+ RLi neurons: the paramedian raphe (PMnR), the median raphe (MnR) **(Figure 24 A)** and the dorsal raphe (DR) **(Figure 24 B).** Immunostaining for TH and serotonin (5-HT) revealed ChR2-mCherry+ terminals in these regions, are in close proximity to - and potentially innervating - 5-HT+ neurons. Interestingly, TH+ fibres seemingly innervate the same 5-HT+ neurons **(Figure 24 C).** Similar to the VP, VGLUT2 **(Figure 24 D)** and VGAT **(Figure 24E)** staining both co-localises with ChR2-mCherry terminals in single z-plane images. Although there appears to be a greater number of VGLUT2+ terminals, these data suggest that input to the raphe from these neurons could be both excitatory and inhibitory.

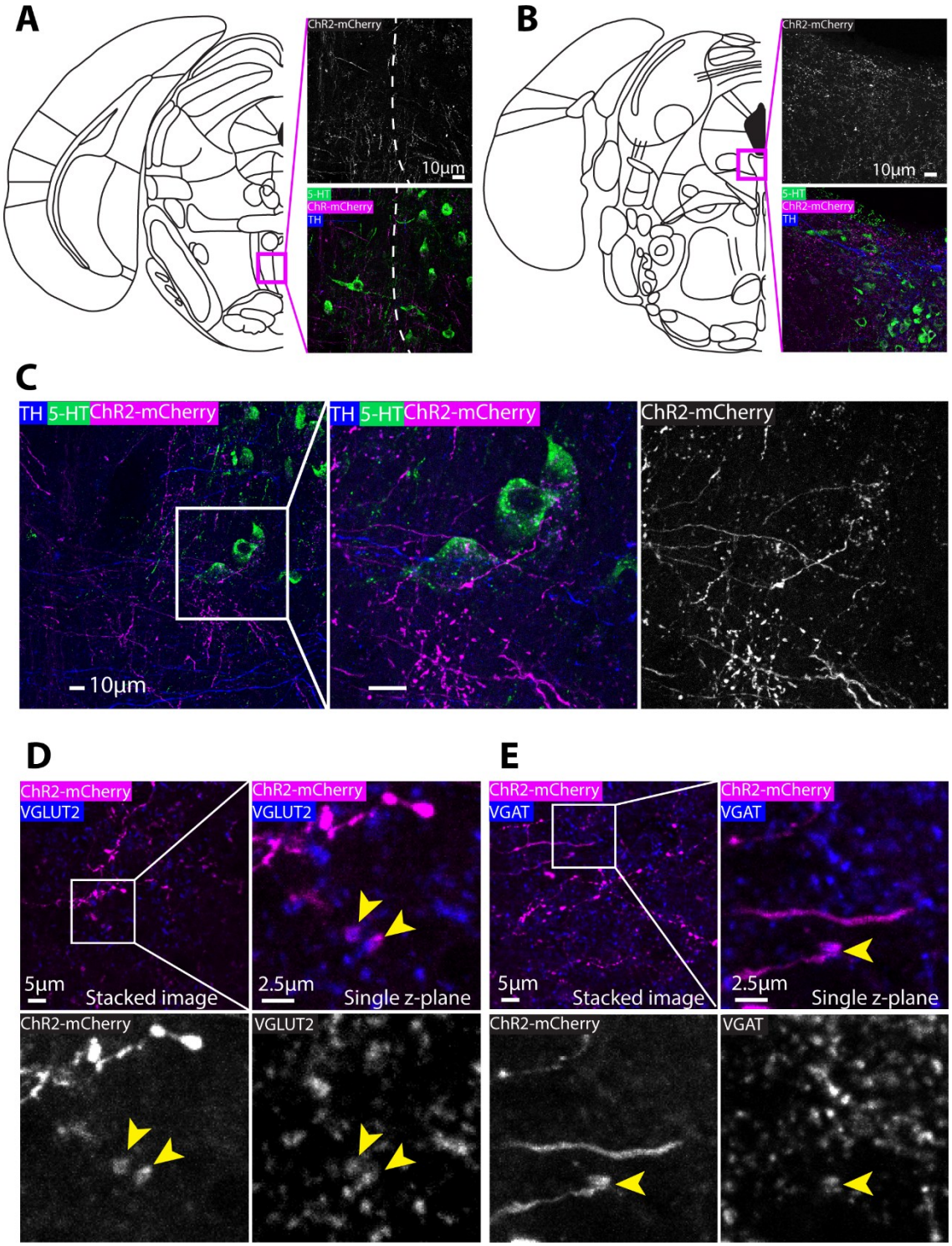


Figure 24: ChR2-mcherry+ axon terminals in the raphe. *Continued on next page.*

Figure 24: ChR2-mcherry+ axon terminals in the raphe *(continued).* A: ChR2-mCherry+ fibres are present in the PMnR/MnR **(A)** and DR **(B). C:** ChR2-mCherry+ (magenta) fibres are in very close proximity to 5-HT+ neurons (green) that also appear to be receiving innervation from TH+ axons (blue). Example image taken from the MnR. **D:** Co-localisation between ChR2-mCherry (magenta) and VGLUT2 (blue) can be seen in single z-plane images in the DR. **E:** Co-localisation between ChR2-mCherry (magenta) and VGAT (blue) can be seen in single z-plane images in the DR. *Brain outlines traced from (Franklin and Paxinos, 2008)*

2.4 Discussion

2.4.1 Validation of anti-nNOS antibodies in the VTA and SNC

Whilst there had been some investigation into the expression of nNOS in the VTA and SNc, the resulting data were inconsistent. This includes conflicting results in seven immunohistochemistry papers in the rat and mouse brain **(see Table 1)** (Cavalcanti-Kwiatkoski *et al*., 2010; Gonzalez-Hernandez and Rodriguez, 2000; Gotti *et al*., 2005; Klejbor *et al*., 2004; Mitkovski *et al*., 2012; Rodrigo *et al*., 1994; Vincent and Kimura, 1992). We hypothesised that this variation in the literature was in part due to the use of different and un-validated antibodies. For this reason, the initial task I undertook was the validation of three different nNOS antibodies by immunostaining in both WT and nNOS KO mice. Out of the three antibodies tested, only one (#N2280) exhibited no immunoreactivity in the nNOS KO mice in the VTA and SNc. Having established this as the most reliable antibody, I was able to comprehensively examine the expression pattern of nNOS in the VTA and SNc, the sub-regional localisation of nNOS+ neurons, and their molecular phenotype.

2.4.2 There are at least three distinct populations of nNOS+ neurons in the VTA and SNc

(i) nNOS immunostaining revealed two distinct nNOS+ populations

Initial immunostaining in WT tissue revealed that nNOS+ are present in multiple sub-regions of the VTA and SNc. Additionally, nNOS+ cells were always TH- indicating that nNOS is not expressed in dopamine neurons. Immunostaining in VGATCre:RiboTag tissue revealed a regional specificity to the nNOS+ cells. nNOS+ neurons in the PBP and SNc were HA+ (GABA neurons), but co-localisation was less apparent in the more rostral parts of the VTA. The VTAR contained a mixed population of HA+ and HA- nNOS cells, but cells in this region were only a very small proportion of the total number of nNOS+ cells. The RLi, which contained 28% of the total population of nNOS cells and contained mostly HA- cells.

It is well established that in the VTA and SNc all neurons express markers for at least one of three cell populations: dopamine, GABA, or glutamate. The HA-TH- nNOS+ neurons, that appeared most prevalently in the RLi nucleus, were therefore classed as glutamate. There was a small degree of overlap in neuronal phenotype in that small number of nNOS+ neurons in the PBP and SNc were HA- (glutamate) and small a number in the RLi were HA+ (GABA). However, this immunostaining showed a distinct regional specificity in terms of neuronal phenotype.

(ii) nNOS circuit tracing revealed projecting and non-projecting populations of nNOS+ neurons

To trace axonal projections of nNOS+ neurons I injected a Cre-dependant AAV expressing ChR2-mCherry into the midbrain of NOS1Cre mice. In order to target the different nNOS neuron populations and avoid those nNOS+ neurons in surrounding areas, I systematically varied both the volume of virus injected and the stereotaxic co-ordinates. It was clear that brains that exhibited a similar pattern of ChR2-mCherry expression in cell bodies in the midbrain also exhibited a similar pattern of expression in axon terminals. Based on these patterns, I was able to deduce which nNOS+ populations were sending which projections. In those mice where virus expression was confined to the VTA and SNc, ChR2-mCherry+ axon terminals (outside the VTA and SNc) were only present when the virus spread into the RLi nucleus. When the virus was confined only to the PBP, SNc and VTAR, no ChR2-mCherry terminals were observed outside the midbrain. This indicates that the nNOS+ neurons in the RLi, that consists mainly of glutamate neurons are sending long-range projections. It also suggests that nNOS+ GABA neurons in the PBP, SNc and VTAR are interneurons.

(iii) nNOS immunostaining in virus injected NOS1Cre mice revealed a TH+ nNOS population in the SNc

Having previously validated the nNOS antibody in the NOS1 KO mouse, I used nNOS immunostaining to validate the NOS1Cre mouse line. Whilst near perfect co-localisation occurred between nNOS+ and ChR2-mcherry+ cells in the PBP, RLi and VTAR, the result in the SNc was more mixed. Around 28% of ChR2-mCherry+ cells co-localised with nNOS. Surprisingly, almost 50% were TH+. Consistent with the

immunostaining results I had observed in the WT and VGATCre:RiboTag mice, no nNOS immunoreactive cells were TH+. A possible reason for not detecting this TH+ population is that these cells in the SNc are expressing such low levels of the enzyme that the antibody is unable to detect it. Alternatively, they could be transcribing nNOS mRNA and not synthesizing the protein. There is a sub-population of nNOS expressing interneurons in the cortex, broadly termed nNOS-type (ii) interneurons, whose numbers are thought to often be underestimated. These express lower levels of nNOS than nNOS-type (i) cells, they are therefore more difficult to detect via immunohistochemical methods (Perrenoud *et al*., 2012a; Tricoire and Vitalis, 2012). It is possible that these TH+ neurons in the SNc are exhibiting similarly low levels of nNOS. This data suggested to us a third sub-population of nNOS+ neurons in the dopaminergic nuclei. A TH+ population of interneurons that lies primarily in the SNc. Whether these TH+ neurons are really nNOS+ or not, the existence of a TH+ non-projecting population is extremely interesting.

(iv) Summary of three nNOS+ neuronal populations

Whilst there is a small degree of overlap between their properties, I have found that nNOS+ neurons in the VTA and SNc form at least three subpopulations. The first is a projecting population that consists mainly of glutamate neurons whose cell bodies are confined to the RLi nucleus. The second is an interneuron population consisting mainly of GABA neurons whose cell bodies lie throughout the PBP, SNc and VTAR. The third is an interneuron population whose cell bodies mostly lie within the SNc. These three populations are summarised **Figure 25.**

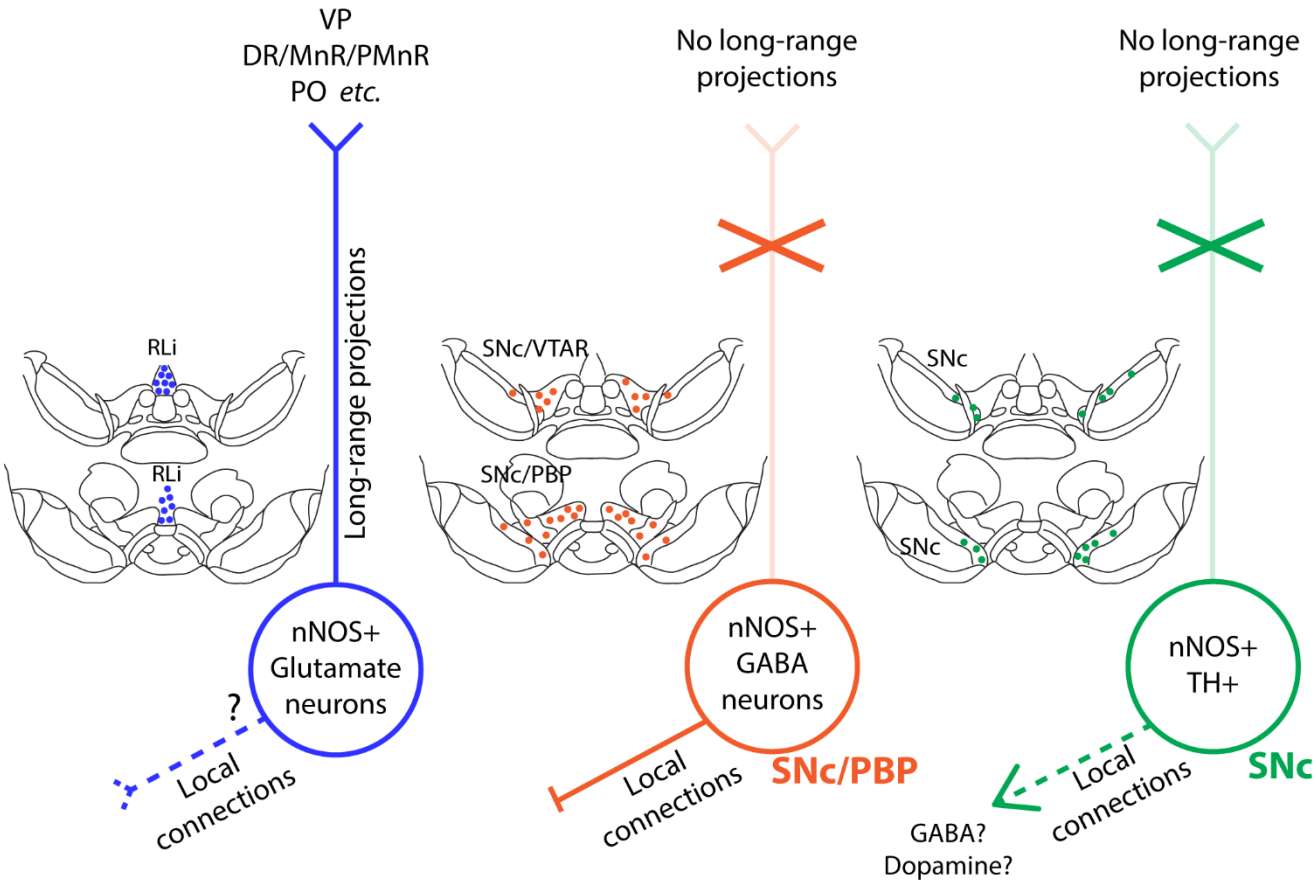


Figure 25: A summary of the three types of nNOS+ neurons discovered in the VTA and SNc. *Midbrain outlines were traced from (Franklin and Paxinos, 2008)*

2.4.3nNOS+ glutamate projection neurons

These neurons lie in the RLi nucleus. They are TH- and largely VGAT- suggesting that most have a glutamatergic phenotype. This was later confirmed with VGLUT2 and ChR2-mCherry cell body co-localisation. These neurons send long-range projections to multiple brain regions, many of which have previously been reported as target areas of RLi neurons (Del-Fava *et al.,* 2007). Using PHAL-L tracing, it has previously been shown that RLi neurons heavily target the ventromedial part of the VP, largely avoiding the NAc (Del-Fava *et al*., 2007). This pattern of innervation is replicated here. I also observed dense innervation in the DR, MnR, LH and preoptic area, with sparse fibres observed in other regions such as the medio-dorsal part of the thalamus the LHb and NAc. These areas are not only consistent

with what we know about RLi projections but also with what we currently know about glutamate projections (Del-Fava *et al*., 2007; Hnasko *et al*., 2012; Taylor *et al*., 2014). Despite anatomical tracing experiments of VTA glutamate neurons (Hnasko *et al*., 2012; Taylor *et al*., 2014) confirmation of their synaptic and electrophysiological activity has so far been limited to the LHb and the medial NAcc (Qi *et al*., 2016; Root *et al*., 2014a). I have shown here that in single stack images ChR2-mCherry+ axon terminalis co-localise with VGLUT, a pre-synaptic marker of glutamatergic synapses. Although this indicates the presence of glutamatergic synapses, functional connectivity will need to be confirmed by photo-activation of terminals to stimulate glutamate release and evoke EPSCs.

Immunostaining in VGATCre:RiboTag mice revealed that RLi nNOS+ neurons are TH- and largely VGAT- (~80%). 20% of the nNOS+ RLi neurons express VGAT and some - but not many -VGAT+/ChR2 mCherry+ axon terminals were also observed in the VP and DR. It is possible that in addition to the large population of nNOS+ glutamate neurons, there is also an intermingled population of nNOS+ GABA projection neurons. We do not yet know if these neurons express VGLUT2 in addition to VGAT, and therefore could also be a subpopulation of GABA and glutamate co-releasing neurons. Also, we are not yet sure what proportion of glutamate neurons are nNOS+. It is likely that nNOS+ neurons form a sub-population of glutamate neurons. It has previously been shown that VGLUT2+ cells send a dense innervation to the medial shell of the NAc. This is an area which does not receive the same level of innervation from nNOS+ neurons, suggesting the terminals in the medial shell of the NAc are arising from nNOS- glutamate neurons. The easiest way to determine what proportion of glutamate neurons are nNOS+ would be through nNOS immunostaining in a VGLUT2-reporter line.

Dual-immunolabelling and electron microscopy combined with anterograde tracers injected into the VTA has shown that local glutamatergic synapses are present on both dopaminergic and non-dopaminergic neurons (Dobi *et al*., 2010; Wang *et al*., 2015b). Consistent with this anatomical data, whole cell recordings of VTA neurons have shown that glutamate release from these terminals evokes EPSCs on VTA dopamine and non-dopamine neurons. Blocking action potential activity significantly

decreased the frequency of excitatory events in dopamine and non-dopamine neurons (Dobi *et al.,* 2010). Another question that remains to be answered is whether any of these nNOS+ neurons in the RLi nucleus are also innervating neurons locally within the VTA and SNc. In order to distinguish the RLi terminals from terminals of nNOS+ neurons in the VTA or SNc, the RLi neurons will need to be selectively targeted. This may be possible by simply adjusting the coordinates of the stereotaxic injections to obtain a more medial spread of the virus. Alternatively, it may be necessary to make use of the newly created VGLUT2-flp (B6;129S-*Slc17a6*$^{tm1.1(flpo)Hze}$/J) mouse line in combination with NOS1Cre, and the INTERSECT AAV that requires co-expression of both cre and flp-recombinase for its activation. This can then be combined with electron microscopy to establish the presence of asymmetric synapses. Or, with optogenetic activation of nNOS+ RLi neurons combined with *in vitro* electrophysiology recordings to see if their activation evokes EPSCs in neighbouring cells.

2.4.3 nNOS+ GABA interneurons

Although widely assumed to be the case in the field, there has been no direct evidence for the presence of distinct populations of GABA interneurons in the PBP, VTAR and SNc. Across these three regions nNOS+ neurons interneurons make up less than 10% of the total GABA neuron population. Here I provide evidence of a population of nNOS+ neurons that do not send long-range projections outside of the VTA and SNc. Just under 80% of these neurons express VGAT, a marker for GABA neurons. Dual-immunolabelling and electron microscopy combine with anterograde tracers injected into the VTA has indicated the presence of local GABAergic synapses (Omelchenko and Sesack, 2009). In addition to this optogenetic stimulation of VTA GABA neurons after AAV-ChR2-eyfp injection into the midbrain of GAD2Cre mice results in the inhibition of dopamine neurons suggesting the presence of local GABAergic synapses (Tan *et al.,* 2012; van Zessen *et al.,* 2012). That being said, without the use of a selective interneuron marker it has been impossible to establish whether the GABA neurons providing local innervation are interneurons or whether they also send long-range collaterals. My data

suggests that there is a subpopulation of nNOS+ GABA neurons in the PBP, SNc and VTAR that do not send any long-range projections outside of the VTA and SNc. I have therefor provided the first evidence of a distinct interneuron population in the VTA and SNc. Through a combination of AAV-Chr2-mCherry injections into nNOS1cre mice and immunostaining for VGAT, a pre-synaptic maker for GABAergic synapses, I have provided preliminary evidence for the presence of local GABAergic synapses from these nNOS+ interneurons. Optogenetic stimulation of nNOS+ neurons in the VTA and in brain slices, in combination with electrophysiological recordings from dopamine neurons could give an indication as to whether nNOS+ GABA interneurons directly inhibit the activity of dopamine neurons.

2.4.4 nNOS+ TH+ interneurons

Of the nNOS+ interneurons there is a small population that is TH+. These TH+ interneurons are confined to the SNc. The idea that there is a group of TH+ neurons in the midbrain that does not send long range projections is controversial so these neurons will be of particular interest to those in the field. Due to the difficulty faced in identifying this subpopulation through immunostaining methods the molecular phenotype of these neurons has been much harder to define. A series of experiments would be required to establish whether these neurons are dopamine, GABA, or glutamate neurons.

I have worked under the assumption that ChR2-mCherry expression in these neurons is not ectopic. My assumption being that these TH+ neurons had not been detected earlier due to them expressing lower levels of the enzyme, or not translating the RNA. This could be confirmed in multiple ways. ISH for NOS1 in combination with TH and HA immunostaining in VGATCre:RiboTag tissue would confirm the nNOS expression in TH+ neurons, and determine whether they express VGAT. Based on the fact that in the SNc TH+ neurons rarely express VGLUT2 (Yamaguchi *et al*., 2013), I expect that a glutamtergic phenotype is unikely. This can be tested, via nNOS ISH and TH immunostaining in a VGLUT2 reporter line or, via VGLUT ISH. Whether or not these TH+ neurons are nNOS+ or nNOS-, I have shown that there is a subpopulation of TH+ neurons that don't send long range projections. This

is controversial and could have negative impliactions for the use of TH-Cre driver lines to target dopamine neurons. The use of these mice to target and activate dopamine neurons would have almost certainly resulted in the activation of these interneurons, which could have had profound effects on behavioural output, and may have lead to erroneous interpretation of results.

Although these neurons are TH+ this does not necessarily mean that they are synthesising and releasing dopamine. It is widely accepted in the field that all dopamine neurons send long range projections and that dopamine released in the VTA and SNc is released from dendrites of projecting dopamine neurons (Beckstead *et al.,* 2004; Pucak and Grace, 1994; Santiago and Westerink, 1991; Zhou *et al.,* 2009). TH+ GABAegic interneurons have been indentified in the striatum (Dubach et al., 1987; Ibanez-Sandoval et al., 2010; Mao et al., 2001; Meredith et al., 1999; O'Byrne et al., 2000; Petroske et al., 2001; Tashiro et al., 1989; Unal et al., 2011; Unal et al., 2015; Xenias et al., 2015b). It is possible that the TH+ NOS+ neurons seen here are a subpopulation of GABA interneurons. Optogenetinc stimulation of these TH+ neurons in the striatum fails to elicit any detectable release of dopamine (Ibanez-Sandoval et al., 2010; Xenias et al., 2015b). In agreement with this, it has been shown that these TH+ positive interneurons do not express any of the three additional markers for dopamine neurons; AADC, dopamine or DAT (Xenias et al., 2015b) . Instead, optogentic activation of these neurons elicited GABA-mediated IPSCs in median spiny neurons, resulting in widespread inhibiton of medium spiny neurons in the striatum (Ibanez-Sandoval et al., 2010; Xenias et al., 2015b). Co-localistation with both GABA synthesising enzymes GAD65 and GAD67 has also been reported (Betarbet *et al*., 1997; Cossette *et al*., 2005a; Mazloom and Smith, 2006; San Sebastián *et al*., 2007; Tandé *et al*., 2006). It Is important to note that this interneuron population is considered to be distinct from the nNOS+ interneurons in the striatum (Ibanez-Sandoval *et al*., 2010; Tepper *et al*., 2010). The simplest way of establishing whether these TH+ nNOS+ neurons are synthesizing dopamine would be to conduct immunostaining for AADC. This enyme - along with TH - is essential for dopamine synthesis. Alternatively, it could be possible to use fast-scan cyclic voltammetry in VTA or SNc slices to determine if dopmaine is released in the VTA/SNc after optogenetic stimulation of SNc nNOS+ neurons.

Before further investigation it would be important to determine whether or not these TH+ interneurons are not an artefact of the Cre-Driver line. To do this, it would be important to conclude if if they are present in other mouse lines. For example, the inducible NOS Cre line. Because they are not detectable through nNOS immunostaining, and because there are currently no TH-flp or nNOS-flp mouse lines, we are currently unable to distinguish them from other TH+ neurons in WT mice. In order to study this population further we would need to identify some other markers. One way of doing this would be to dissect virus expressing TH+ cell bodies via laser capture microdissection (LCM), and then perform single cell qRT-PCR or RNA-sequncing of RNA extracted from this population.

Chapter 3 – A biased approach: Investigating the expression of parvalbumin in the VTA and SNc

3.1 Introduction

3.1.1 Parvalbumin as a molecular marker in the brain

PV is a calcium binding albumin protein. It is an important modulator of intracellular calcium dynamics. PV acts as a slow Ca^{2+} buffer and is thought to affect the time course of Ca^{2+} transients in terminals after an action potential (Baimbridge *et al*., 1992; Chard *et al*., 1993). This indicates a role in the regulation of synaptic plasticity. In GABA neurons it has been suggested PV may be related to controlling their excitability and therefore the effectiveness of their inhibition (Bischop *et al*., 2012; Caillard *et al*., 2000). Despite it being used widely as a molecular marker, the general role of PV in the nervous system remains poorly understood.

PV+ interneurons are considered the largest population of interneurons in the cortex, where they make up 40% of the interneuron population (Tremblay *et al*., 2016); in the hippocampus they make up 24% of the population (Bezaire and Soltesz, 2013). PV+ interneurons are also prevalent in the striatum (Gerfen *et al*., 1985; Kita *et al*., 1990; Mura *et al*., 2000; Tepper *et al*., 2010). They are perhaps the most well characterised of the interneuron populations, partly due to their distinctive electrophysiological firing properties. They exhibit a fast-spiking action potential phenotype which makes them easily identifiable (Hu *et al*., 2014; Kawaguchi *et al*., 1987; McCormick *et al*., 1985; Tremblay *et al*., 2016). PV+ interneurons contribute to the generation of network oscillations in the

hippocampus and cortex (Cardin *et al*., 2009; Hu *et al*., 2014; Sohal *et al*., 2009; Stark *et al*., 2013), the regulation of plasticity and learning (Donato *et al*., 2013; Hu *et al*., 2014; Kuhlman *et al*., 2013; Letzkus *et al*., 2011; Wolff *et al*., 2014) and they are essential for working spatial memory (Murray *et al*., 2011). Along with these normal brain functions, dis-regulation in PV interneuron networks have been implicated in numerous neurological disorders. For, example a reduced number of PV immunoreactive cells have been reported in the cortex of post-mortem brains from schizophrenic patients (Beasley and Reynolds, 1997; Hashimoto *et al*., 2003; Hu *et al*., 2014). On top of this, multiple schizophrenia 'risk' genes have been implicated in the circuit integration and normal function of PV+ interneurons (e.g. NGR1, ERGB4, DISC1) . Disruption in PV interneuron circuitry is also thought to occur in epilepsy, depression, autism and Alzheimer's disease (Marin, 2012).

The PV+ interneuron populations scan be spilt into further subpopulations based on their morphology and their synaptic targeting bias. They can either be basket or chandelier (also called axo-axonic) cells (Kepecs and Fishell, 2014; Tremblay *et al*., 2016). The PV+ basket cells appear more abundantly in the cortex than the chandelier cells. They specifically target the primary dendrites or soma of principal cells or of other PV+ interneurons (Beierlein *et al*., 2000; Gibson *et al*., 1999; Jiang *et al*., 2015; Kawaguchi and Kubota, 1997; Kubota *et al*., 1994; Pfeffer *et al*., 2013; Tremblay *et al*., 2016). They can also be identified by the expression of Tac1, the gene that encodes four products of the tachykinin peptide hormone family, substance P and neurokinin A,, neuropeptide K and neuropeptide gamma (Zeisel *et al*., 2015). The chandelier cells specifically innervate the axon initial segment of principal cells (Ascoli *et al*., 2008; Jiang *et al*., 2015; Kawaguchi and Kubota, 1997), a single chandelier cell can innervate a few hundred principal cells in a clustered manner (Blazquez-Llorca *et al*., 2015) . Though both basket and chandelier cells potentials, the chandelier cells fire at a slightly slower frequency than the basket cells (Goldberg *et al*., 2011; Reyes *et al*., 1998; Taniguchi *et al*., 2013; Woodruff *et al*., 2011)

3.1.2 Evidence of parvalbumin expression in the VTA and SNc

The evidence surrounding the expression of PV in the in the VTA is inconclusive. To date, four studies have reported the presence of PV in the VTA and SNc (Klink *et al*., 2001; Merrill *et al*., 2015; Olson and Nestler, 2007; Poulin *et al*., 2014), and two studies have reported its absence (Celio, 1990; Poulin *et al*., 2014) **(Table 6).** Many more have investigated PV+ neurons in the SNr (Abe *et al*., 2010; Cebrián *et al*., 2005; Hontanilla *et al*., 1997; Lee and Tepper, 2007; Rajakumar *et al*., 1994; Reiner and Anderson, 1993; Rodríguez and González-Hernández, 1999). Two single-cell qRT-PCR studies reported the presence of PV mRNA in both GAD+ and TH+ neurons (Klink *et al*., 2001; Merrill *et al*., 2015). One of these reported wide spread expression of PV, with PV mRNA being detected in over half of all GABA neurons and just under 20% of dopamine neurons, this is a much higher proportion of PV+ cells in the VTA than reported elsewhere (Merrill *et al*., 2015) in both of these studies a very small number of cells were investigated. In contrast, a separate study that performed single cell qRT-PCR on dopamine neurons specifically, failed to detect PV mRNA in any of the cells (Poulin *et al*., 2014). To date, only two studies has investigated the presence of PV in the VTA (Celio, 1990; Olson and Nestler, 2007) or SNc (Celio, 1990) at the protein level. The first failed to detect any PV+ cells in the VTA and SNc but did the report the presence of PV+ fibres. Immunostaining in the VTA of rats revealed PV+ neurons in the VTAR 75% of which co-localised with GAD. Much fewer, only one or two per section, PV+ neurons were reported in more caudal regions of the VTA (Olson and Nestler, 2007). These studies are summarised in **Table8.**

Publication	Experiment	Species	VTA	SNc	GAD +	TH +
(Klink *et al*., 2001)	Single-cell qRT-PCR	Rat	Yes	Yes	Yes	Yes
(Olson and Nestler, 2007)	Immunohistochemistry	Rat	Mostly VTAR	No	Yes (75%)	-
(Poulin *et al*., 2014)	Single-cell qRT-PCR	Mouse	No	No	NA	No
(Merrill *et al*., 2015)	Single-cell qRT-PCR	Rat	Yes	-	Yes (58.3%)	Yes (18.8%)
(Celio, 1990)	Immunohistochemistry	Rat	No	No	-	-

Table 8: Summary of the publications investigating the presence of PV in the VTA and SNc (- indicates region or co-expression that was not investigated).

Similar to that of nNOS, the evidence surrounding PV expression in the VTA and SNc is unclear. Results have been inconsistent in regard to cell localisation within the nuclei, but also in regards to which neuronal population is expressing PV. PV expression in these nuclei has not been studied extensively. In fact, in most of the studies mentioned here, PV expression was not the core interest of the research. In this chapter, I describe how I set out to comprehensively investigate the presence of PV+ neurons in the VTA and SNc. My aim was to determine whether PV, as in other brain regions, can be used as a marker for GABA neurons in the VTA and SNC.

3.2 Experimental procedures

3.2.1 Animals

See section **2.2.1.**

Details of the mice strains used in this chapter are shown in **Table 9**.

Mouse line	Strain nomenclature	Supplier (#Stock No.)
C57Bl/6	C57Bl/6NCrl	Charles River (#027)
RiboTag	B6N.129-*Rpl22*$^{tm1.1Psam}$/J	The Jackson laboratory (#011029)
PV-Cre	B6;129P2-*Pvalb*$^{tm1(cre)Arbr}$/J	The Jackson laboratory (#008069)
VGATCre	*Slc32a1*$^{tm2(cre)Lowl}$/J	The Jackson laboratory (#016962)

Table 9: Mouse strain information

3.2.2 DNA extraction

Protocol described in **2.2.2.**

3.2.3 Genotyping

Protocol described in **2.2.3**

Primer and PCR information for relevant mice can be seen in **Table10.**

Strain/Transgene	Primers	PCR cycles	Product weight
RiboTag	**F -** GGGAGGCTTGCTGGATATG **R –** TTTCCAGACACAGGCTAAGTACAC	94°C 2min 94°C 20 secs 65°C 15 secs x10 68°C 10 secs 94°C 15 secs 60°C 15 secs x28 72°C 10 secs 72°C 2mins 10°C ∞	Mutant =~290 bp Wild type =243 bp
PV-Cre	Mutant F - GCGGTCTGGCAGTAAAAA CTATC Mutant R - GTGAAACAGCATTGCTGTCAC TT WT F - CAG AGC AGG CAT GGT GAC TA WT R - AGT ACC AAG CAG GCA GGA GA	94°C 2min 94°C 20 secs 65°C 15 secs x10 68°C 10 secs 94°C 15 secs 60°C 15 secs x28 72°C 10 secs 72°C 2mins 10°C ∞	Mutant = ~100 bp Wild type = 500 bp

Table 10: Genotyping information

3.2.4 Perfusion fixation and tissue preparation

Protocol described in **2.2.4**

3.2.5 Immunocytochemistry

Protocol described in **2.2.5**. Antibodies used in this chapter are shown in **Tables 11 and 12**

Antibody	Host species	Manufacturer/Product No.	Concentration
Anti-TH	Chicken	Abcam (#ab76442)	1:1000
Anti-PV	Rabbit	Abcam (#ab11427)	1:500
Anti-nNOS	Mouse	Sigma (#N2280)	1:500
Anti-HA	Mouse	Sigma (#H3663)	1:1000
Anti-GABAARα1	Rabbit	Alomone (#AGA-001)	1:500
Anti-VGLUT2	Rabbit	Alomone (#AGC036)	1:500
Anti-VGAT	Rabbit	SYSY (#131003)	1:500

Table 11: Primary antibody information

Antibody	Conjugation	Host species	Manufacturer (#Product No.)	Concentration
Anti-Chicken	Alexa-488	Goat	Invitrogen (#A11039)	1:1000
Anti-Mouse	Cy3	Donkey	Jackson (#715-165-150)	1:1000
Anti-Mouse	Cy5	Donkey	Jackson (#715-175-151)	1:1000
Anti-Rabbit	Alexa-633	Goat	Invitrogen (#A21070)	1:1000
Anti-Rabbit	Cy3	Donkey	Jackson (#711-165-152)	1:1000

Table 12: Secondary antibody information

3.2.6 Viral vectors

Viral vectors as described in **2.2.6**

3.2.7 Stereotaxic surgery for circuit tracing

Protocol described on **2.2.7**

3.2.8 Confocal Imaging, image processing and analysis

All images used in this thesis were via laser scanning microscopy using a Leica SP confocal microscope (Leica Microsystems), with the pinhole set at 1 Airy unit. Images of cell bodies were acquired with a z-step size of 1 µm, images of processes were acquired with a step size of 0.5 µm, and images of synaptic boutons were acquired with a step size of 0.25 µm. All images were processed with Fiji software and stacked example images are shown. To determine co-localisation of PV and HA/TH/nNOS, channels were viewed both individually and in composite. Co-localisation was determined if the cell body was visible in multiple channels through its entire thickness (multiple z planes).

3.3 Results

3.3.1 Neurons in the VTA and SNc that express PV

Dual immunostaining in the midbrain of WT tissue (n=3) revealed PV immunoreactive neurons in the VTA and SNc. No extensive immunostaining investigation has previously been conducted for PV in the mouse brain. However, distribution observed here is similar to that observed in the rat brain (Olson and Nestler, 2007). The distribution of PV+ cells was as expected throughout the rest of the brain e.g. the cortex and hippocampus exhibited robust PV expression. In addition, the well characterised PV+ neurons in the SNr (Abe *et al*., 2010; Cebrián *et al*., 2005; Hontanilla *et al*., 1997; Lee and Tepper, 2007; Rajakumar *et al*., 1994; Reiner and Anderson, 1993; Rodríguez and González-Hernández, 1999), red nucleus (Celio, 1990; Hontanilla *et al*., 1995), and IPN (Celio, 1990) were clearly visible surrounding the VTA and SNc **(Figure 26)**. All this suggests that the antibody used produces reliable staining.

Tile scans were taken at different rostro-caudal levels throughout the midbrain nuclei **(Figure 26).** Consistent with the observations in the rat brain, PV+ neurons were more abundant in the VTAR and there is a cluster in the more rostral medial part of the PBP. PV immunoreactive cells appear at all levels in the SNc **(Figure 26).** Unlike nNOS+ neurons, PV+ neurons are present in the PBP and RLi in very small numbers, in some sections they were not present in these sub-regions at all. Unlike nNOS PV+ cells are present in the PN and IF. This data is preliminary and exploratory, the PV+ cells were not quantified. Preliminary images suggest the highest density of PV+ neurons can be found in the VTAR and SNc. In general, PV+ neurons are harder to find than the nNOS+ population seen previously **(Figure 26).** Higher resolution images of PV+ neurons in these regions is shown in **(Figure 27).** In no region did PV+ cells co-localise with TH immunostaining, suggesting PV is not expressed in dopamine neurons. In addition to PV+ cell bodies, PV+ fibres can also clearly be seen. These are particularly prominent in the medial regions of the VTA, the IF and PN and also the PBP **(Figure 27).**

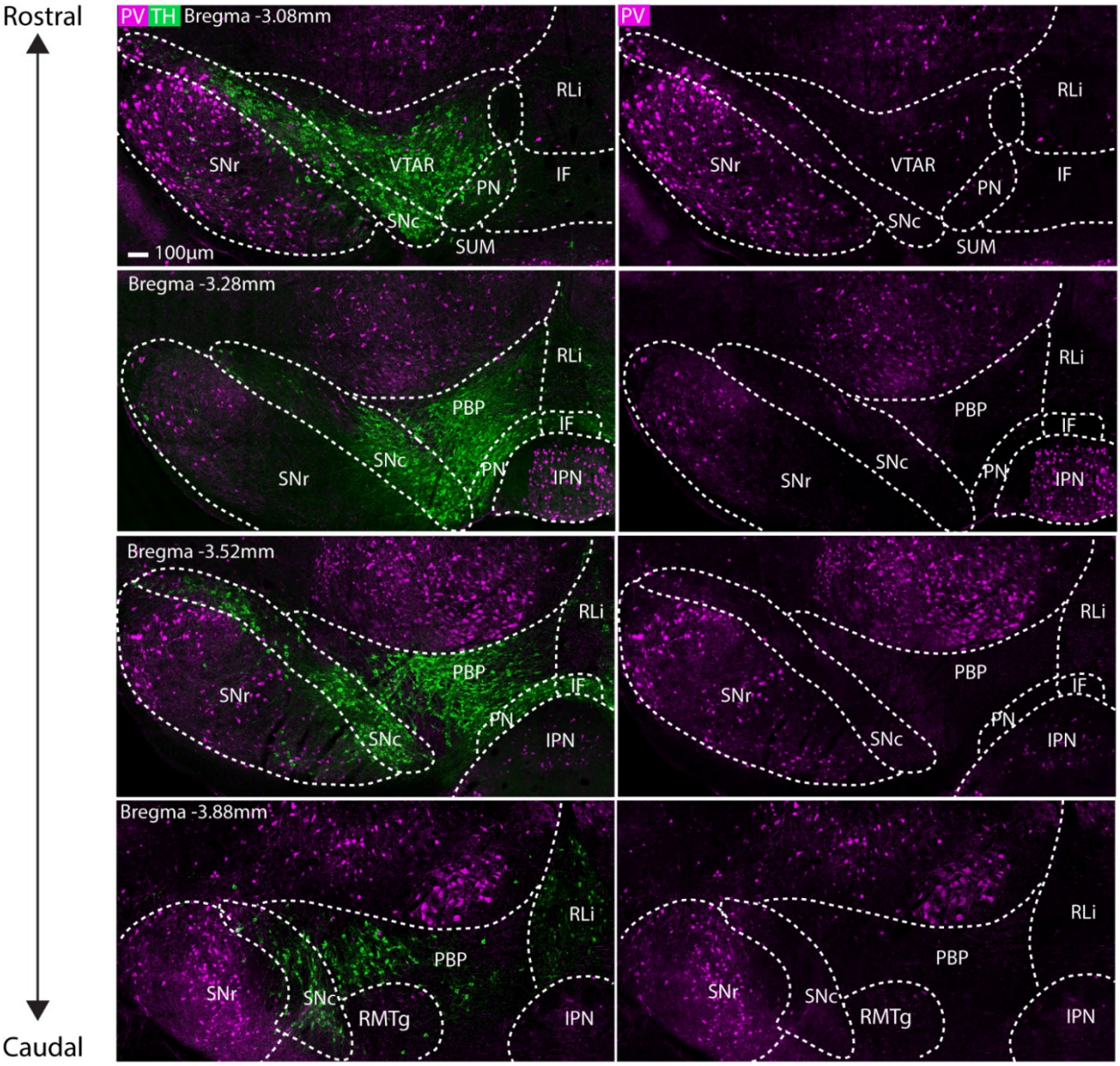


Figure 26: Tile-scans from different rostro-caudal levels of the VTA and SNc showing the distribution of PV+ neurons. Left panels show a merged image of TH (green) and PV (magenta) immunostaining. Right panels show the same image with PV immunostaining alone. PV+ neurons are visible in s in areas surrounding the VTA. PV+ neurons a present in greater numbers in the more rostral regions if the VTAR. There is a small cluster of PV+ neurons in the rostro-medial PBP but other than that they are largely absent for this region. A few PV+ neurons can be seen in the SNc at all levels. There is small number of PV+ neurons in the RMTg and the most caudal regions of the VTA.

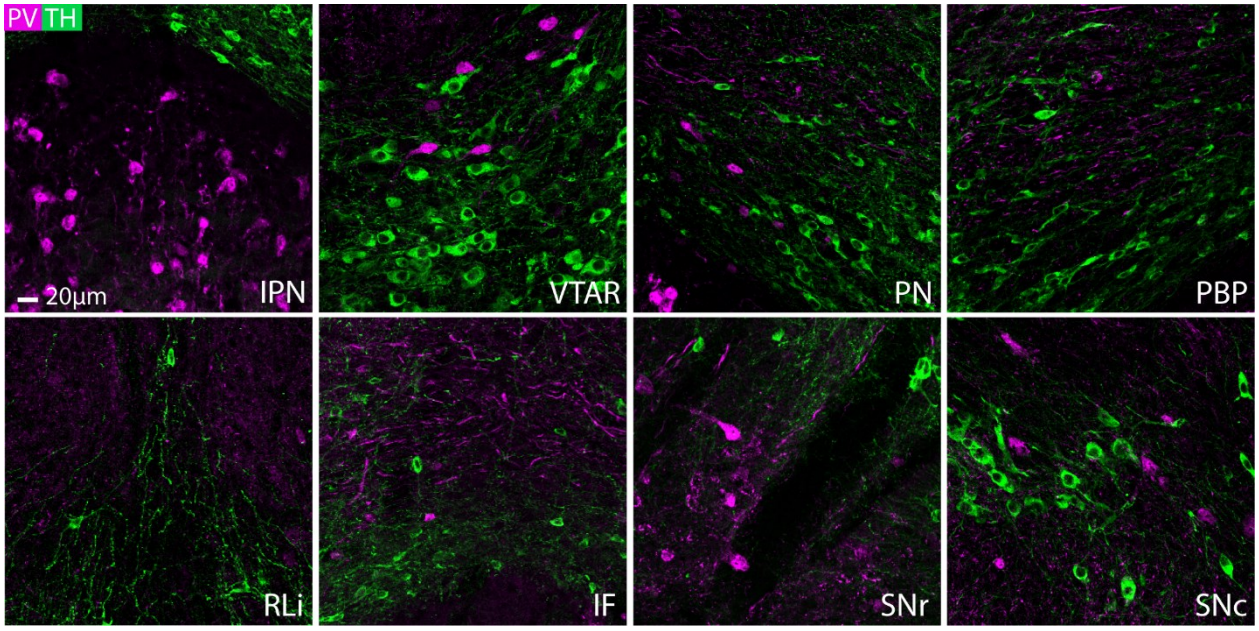


Figure 27: Double immunostaining for PV (magenta) and TH (green) in sub-regions of the VTA and SNc. As expected, PV+ neurons are prominent in the IPN and SNr. In regions of the VTA and SNc PV+ neurons lie intermingled with TH+ neurons but never co-localise. In stark contrast to nNOS, PV+ neurons were rarely observed in the PBP and RLi. Many immunoreactive PV+ fibres were observed, these were particularly abundant in the IF and PN and PBP.

3.3.2 PV+ neurons are GABA neurons

I next wanted to determine the neurochemical identity of the PV+ neurons. Since they are TH- the next most likely scenario is that they are GABA neurons. In a similar approach to that taken with nNOS, I used the VGATCre:RiboTag mouse line as a GABAergic reporter line. The distribution of PV+ neurons in VGATCre:RiboTag tissue (n=3) was the same as that observed in the WT brains **(Figure 28).** There was once again no localisation between PV+ neurons and TH+ neurons. Almost every PV+ neuron imaged was HA+. This suggests that they are GABA neurons. The distribution of PV+ neurons consistently observed across all mice is summarised in **(Figure 29).** Preliminary, exploratory data suggests one difference between the distribution of PV+ and nNOS+ cells in the VTA and SNc is that instead of being equally dispersed throughout sub-regions, PV+ neurons appear to form dense clusters. PV+ neurons appear to be more prevalent in the rostral regions of the VTA and SNc, they appear most abundant in the VTAR although this has not been quantified. Moving caudally the number of PV+ neurons in the VTA appears to decrease. Except for a cluster of cells in the rostro-medial PBP, PV+ cells seem almost non-existent in this region. There is also a small cluster of cells in the rostro-medial tegmental nucleus (RMTg), also known as the tail of the VTA which lies ventrally to the caudal PBP.

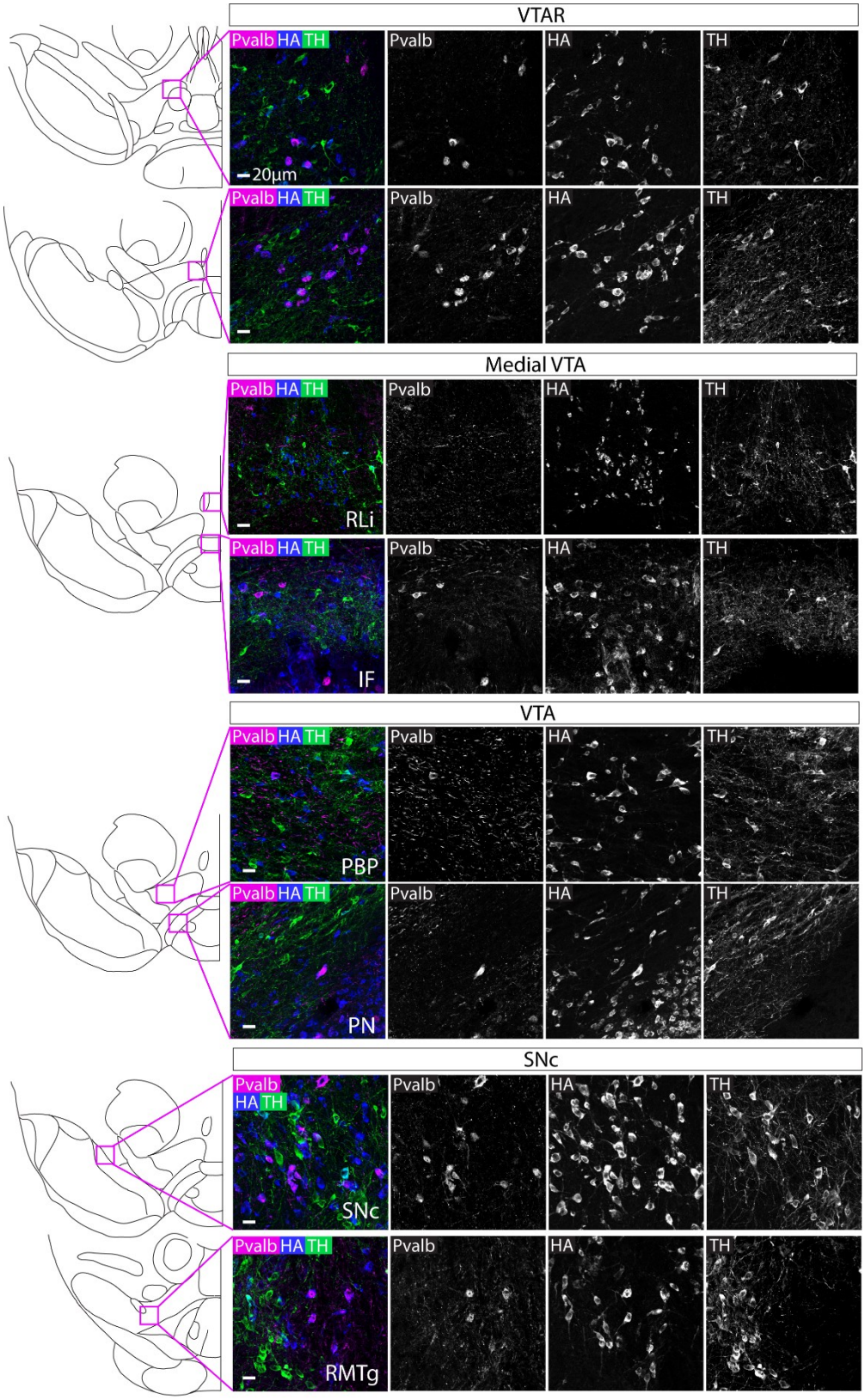


Figure 28: Triple immunostaining for PV (magenta), HA (blue) and TH (green) in VGATCre:RiboTag mice. A-D = Rostral – caudal. A distribution of PV+ neurons similar to that of WT was observed. All PV+ neurons in the VTA regions are HA+ except for just two neurons in the VTAR. *Midbrain outlines were traced from (Franklin and Paxinos, 2008)*

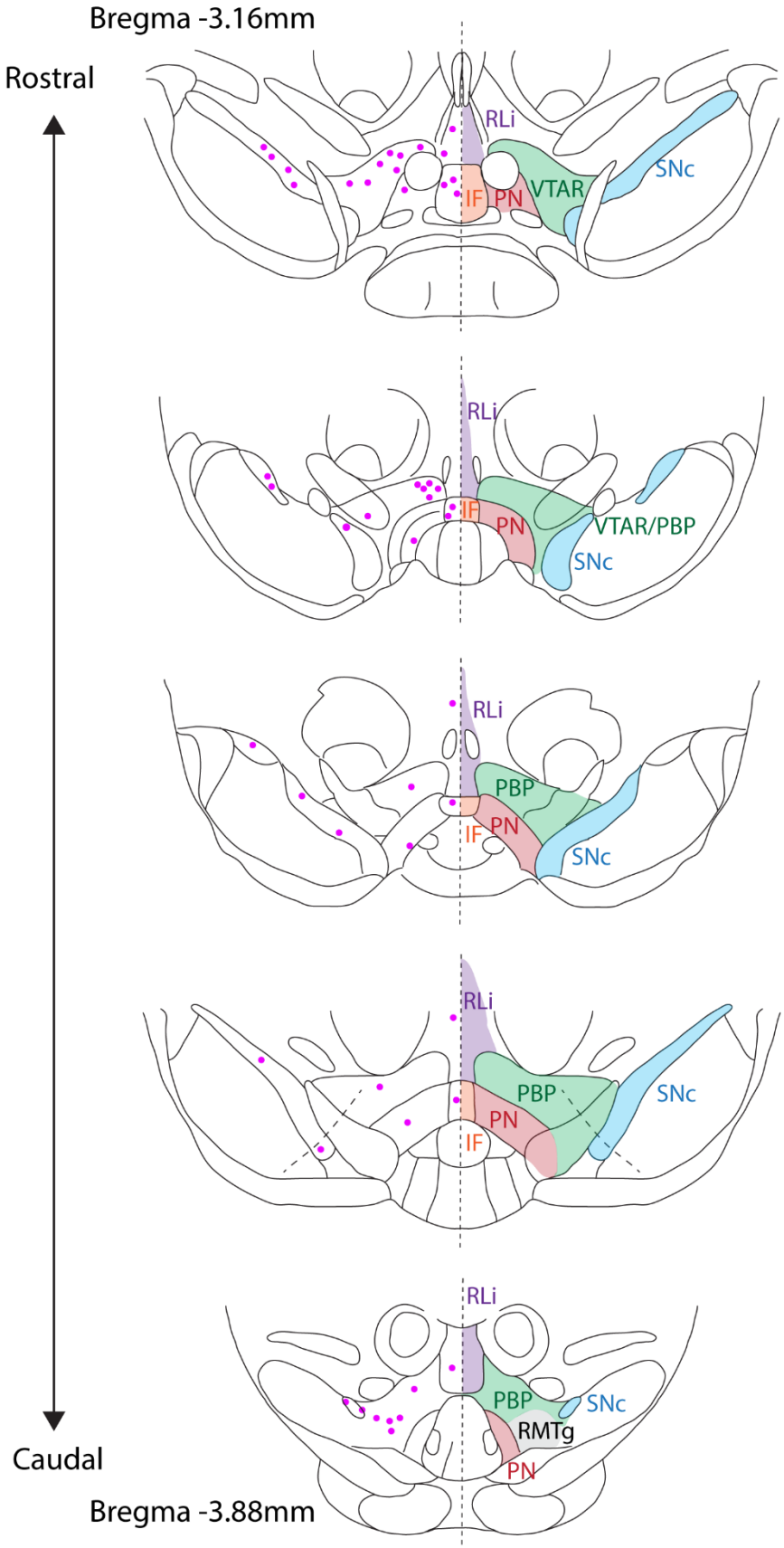


Figure 29: Schematic illustrating the distribution of parvalbumin+ cells (magenta dots) observed throughout the VTA and SNc. *Midbrain outlines were traced from (Franklin and Paxinos, 2008)*

3.3.3 Parvalbumin expressing neurons and nNOS expressing neurons are distinct populations in the VTA and SNc

Having established that in the VTA and SNc there is a subpopulation of GABA neurons that express PV, I was curious to see whether this population overlaps with the nNOS expressing GABA neurons I described in **chapter 2**. To investigate this, I conducted triple immunostaining for PV, nNOS and TH in WT tissue (n=1). This has so far only been conducted in one brain but this was investigated thoroughly in all regions. There was no co-localisation between PV and nNOS in the VTA and SNc **(Figure 30).** This preliminary data suggests that the PV expressing GABA neurons and the nNOS expressing GABA neurons are separate populations in the VTA and SNc.

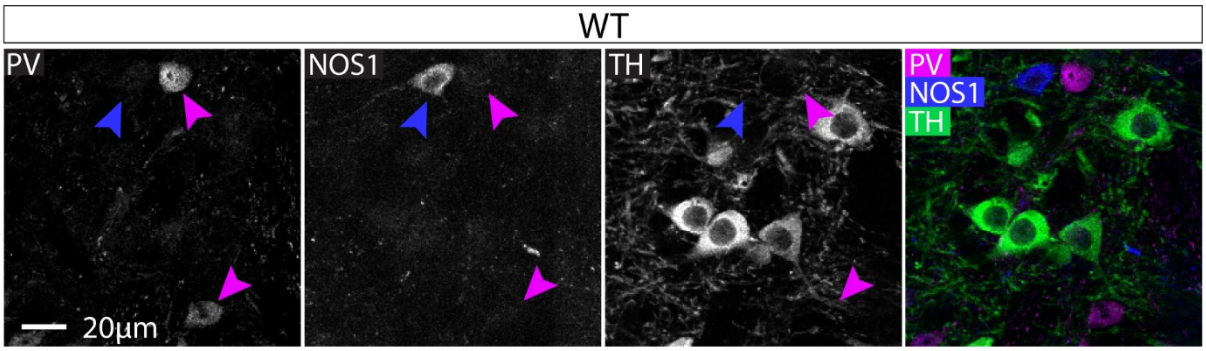


Figure 30: Triple immunostaining for PV (magenta), NOS1 (blue) and TH (green) in the VTA. There is no co-localisation between PV (location indicated by pink arrow) and PV (blue arrows). Example image shown were taken from the PBP.

3.3.4 PV+ neurons of the VTA and SNc do not send long-range projections

My next aim was to determine whether these PV+ GABA neurons send projections outside of the VTA and SNc. To this end, PV-Cre mice (Hippenmeyer *et al*., 2005) were injected with a Cre-dependant AAV expressing ChR2-mCherry. Four female PV-Cre mice received preliminary injections of systematically varied volumes (0.2-0.3µl) and coordinates (AP -3.3 to 3.5mm, ML +0.4 to 0.6mm, DV -4.6 to 5.5mm), in an attempt to avoid virus expression in the substantial populations of PV+ neurons in the areas surrounding the VTA and SNc, particularly the SNr. Two weeks after surgery injected mice underwent

transcardial perfusion with 4% PFA and the brains were removed. The entire brains were sectioned and examined for ChR2-mCherry expression, systematically in a manner such as nNOS.

The ChR2-mCherry expression pattern observed was consistent across the four mice. Cell body expression in the VTA and SNc was minimal, a smaller number ChR2-mCherry+ neurons were observed compared to the numbers seen in the PV immunohistochemistry experiments. A summary of the location of ChR2-mCherry+ cell bodies is shown in **figure 31**. I was unable to detect any axon terminals outside of the midbrain in any of the four mice examined, suggesting all ChR2-mCherry expressing neurons were interneurons.

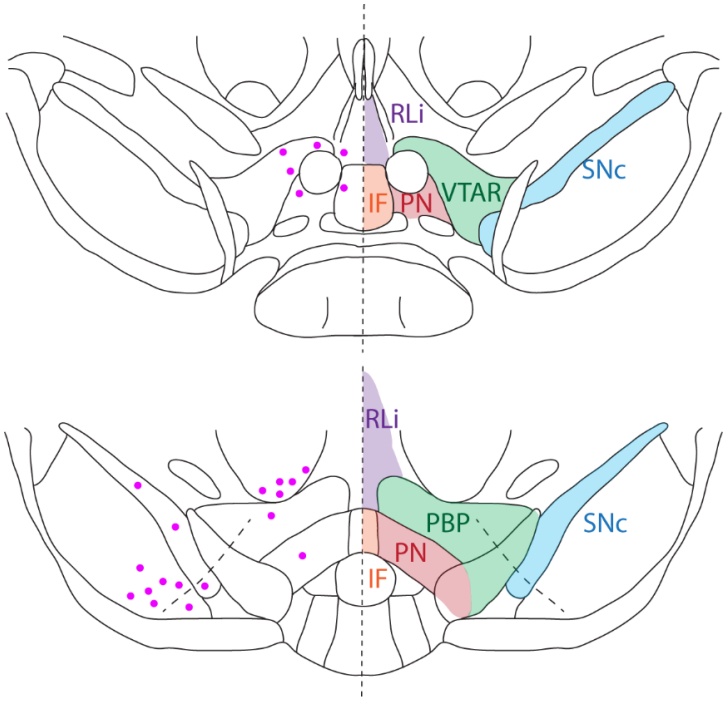


Figure 31: Schematic illustraiting the precence of ChR2-mCherry+ cells (magenta dots) in the midbrian of injected mice. *Midbrain outlines were traced from (Franklin and Paxinos, 2008)*

3.3.5 Most ChR2-mCherry + neurons are PV+ and GABAARα1+

To verify that expression of the virus was specific to PV+ neurons, midbrain sections from injected mice were co-stained for TH and PV. The majority, though not all, ChR2-mCherry+ cells appear to be PV+ **(Figure 32)**. There was also some Chr2-mCherry+ PV- neurons observed in the VTAR and SNc. These degree of co-localisation has not been quantified. Some of the midbrain sections from each mouse were also stained for GABAARα1, a GABA A receptor subunit that it specific to GABA neurons in the VTA (Tan *et al*., 2010). All ChR2-mCherry+ neurons imaged were GABAAα1+, this provides further confirmation of their GABAergic phenotype **(Figure 33).**

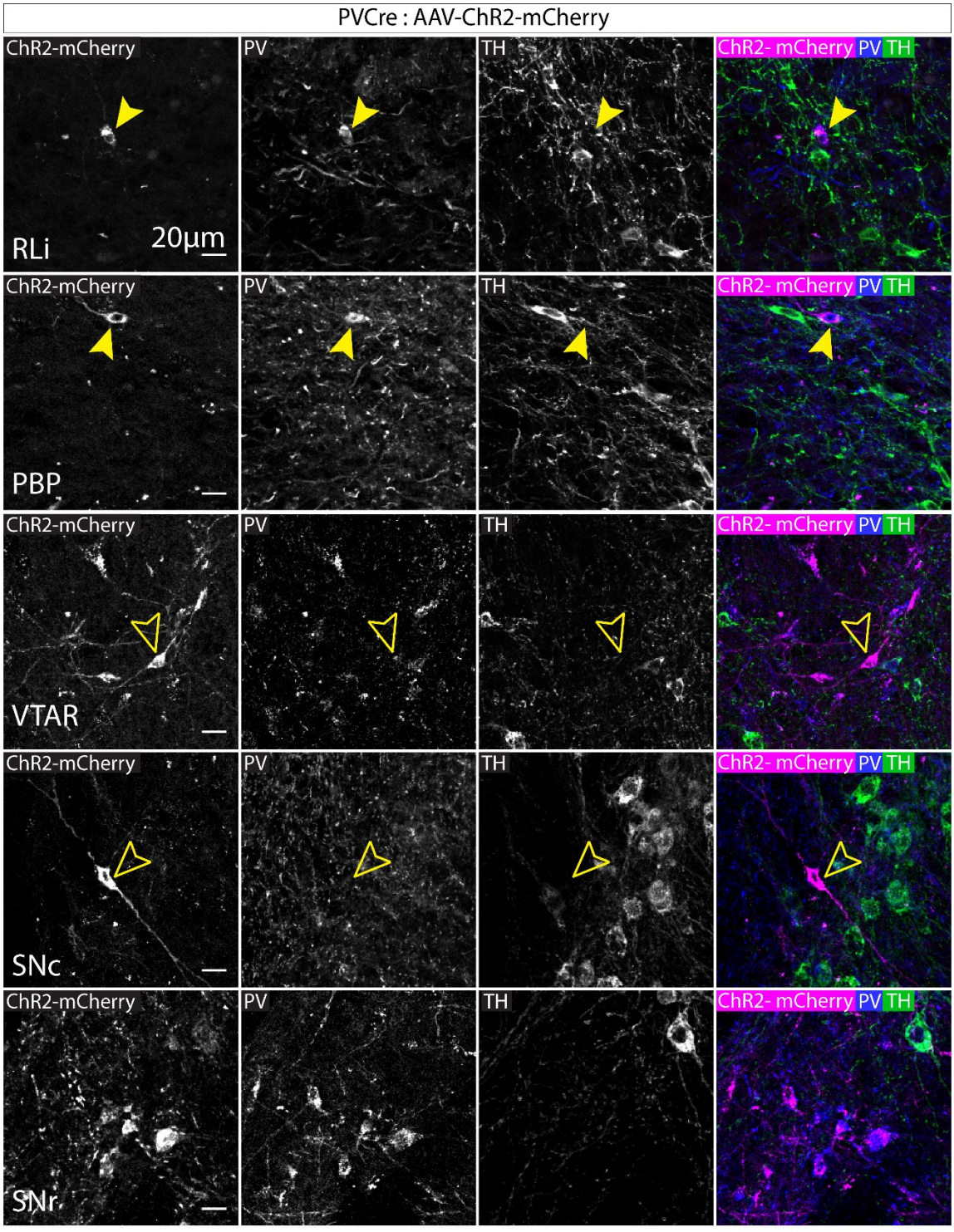


Figure 32: Triple immunostaining for PV (magenta), NOS1 (blue) and TH (green) in the VTA. ChR2-mCherry expression co-localises with PV in cells in the RLi, PBP and SNr (solid yellow arrows). Some cells in the VTAR and SNc appear to be PV- (empty yellow arrows).

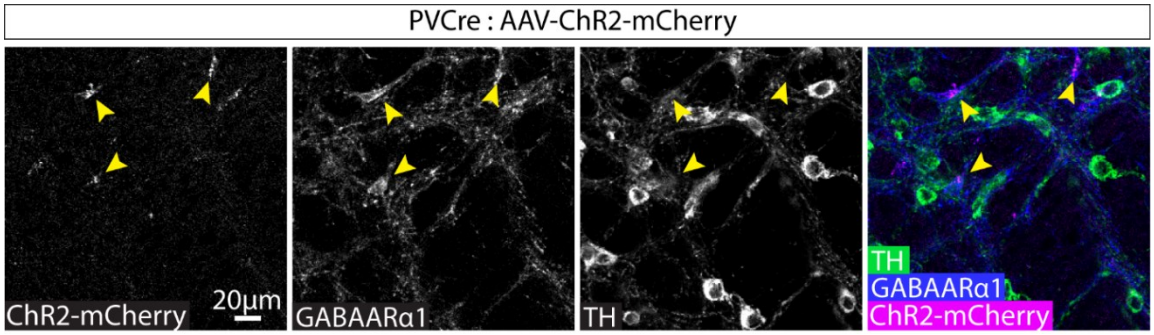


Figure 33: ChR2-mCherry+ neurons co-localise with GABAARα1. Example images shown were taken from the VTAR.

3.3.6 ChR2-mCherry+ neurons fibres and axon terminals are present in the VTA and SNc

ChR2-mCherry processes and axon terminals can be observed throughout the VTA **(Figure 34).** These can be observed in areas where no ChR2-mCherry+ neurons are present. Due to the expression of ChR2-mcherry cells in the SNr we are unable to determine if these terminals are originating from neurons in the VTA and SNc or the SNr. To confirm these are ChR2-mcherry terminals sections from injected mice were stained for TH and VGAT, the presynaptic marker for GABAergic synapses. This revealed co-localisation between ChR2-mCherry and VGAT, suggesting all axon terminals observed are GABAergic **(Figure 35).** This is consistent with the immunostaining data that suggests all PV+ cells are VGAT+.

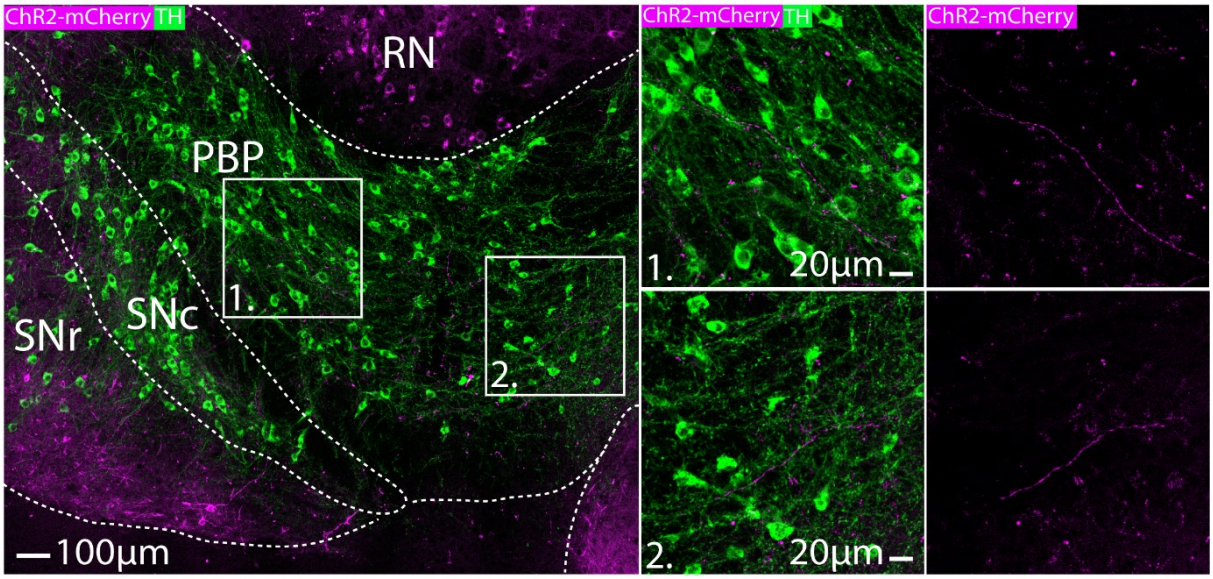


Figure 34: Examples of ChR2-mCherry+ processes and terminals within the VTA and SNc. Right hand image is a tile scan of the VTA/SNc and surrounding area. White boxes illustrate area of zoom for images on the left. ChR2-mCherry+ processes and terminals are present amongst TH+ neurons.

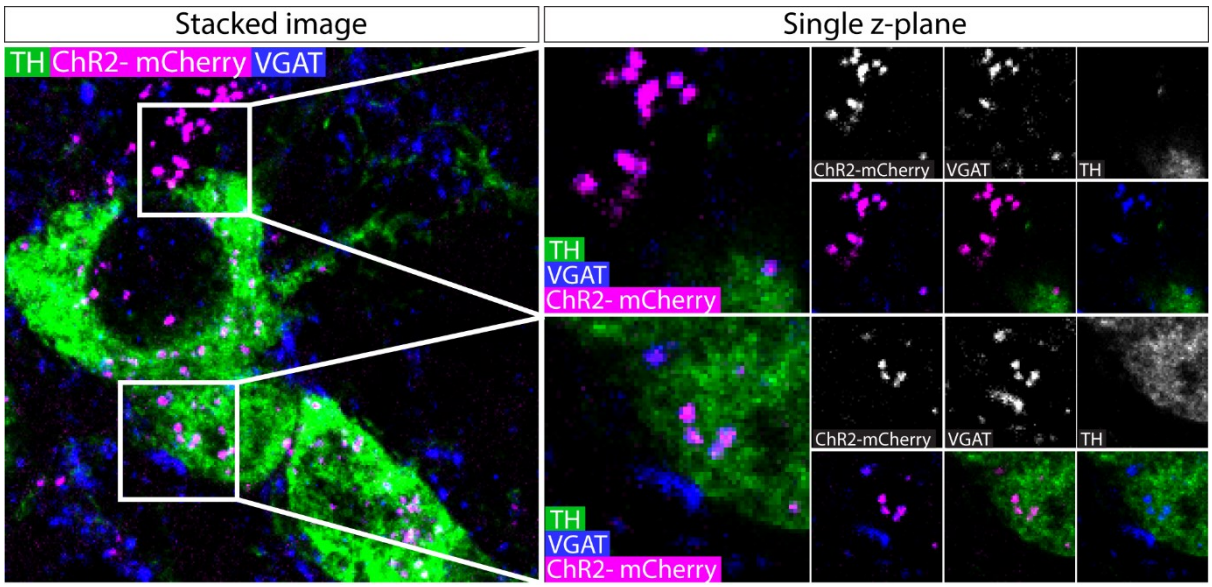


Figure 35: CHR2-mCherry+ terminals co-localise with VGAT. In a single z-plane image, all ChR2-mCherry+ axon terminals appear to co-localise with VGAT. White box illustrates are of zoom.

3.4 Discussion

3.4.1 There are PV+ GABA neurons in the VTA and SNc

This is the first time PV expression in the VTA and SNc has been investigated using immunostaining in the mouse brain. Through immunostaining in both WT and VGATCre:RiboTag mouse tissue I have identified a subpopulation of PV expressing GABA neurons within the VTA and SNc. Although it has not been quantified there appeared to less PV+ cells in the VTA and SNc than there were nNOS+ cell. In contrast to nNOS+ which appeared fairly evenly dispersed throughout the PBP, RLi and SNc. PV+ neurons appeared in clusters. They were most abundant in the VTAR and SNc although a dense cluster was consistently present in the rostro-medial PBP. It is possible that this cluster of cells is continuous with those observed in the VTAR. PV+ cells were also seen through all levels of the SNc and in the more rostral parts of the IF and PN and rarely seen in the rest of the PBP or RLi. The overall distribution of PV+ cells observed in VTA is similar to that previously reported in the rat brain (Olson and Nestler, 2007).

No PV+ neurons in either WT tissue or VGATCre:RiboTag tissue were TH+ and almost all of the PV immunoreactive neurons in the VGATCre:RiboTag tissue were HA+. These data suggest that in the VTA and SNc, PV is expressed in GABA neurons and not dopamine or glutamate neurons. Olson and Nestler (2007) have previously reported that all PV+ cells in the VTAR are GAD+ but the few cells observed in more caudal VTA regions were GAD- (Olson and Nestler, 2007). The difference in degree of co-localisation observed is likely down to the use of GAD antibodies. Antibodies for the GAD enzymes are thought to be unreliable in the VTA and SNc, this is believed by most to be the case by most researchers in the field. For this reason ISH for GAD1/GAD2/VGAT or the use of transgenic reporter lines are the methods of choice to identify GABA neurons in this brain region (Margolis *et al*., 2012; Nair-Roberts *et al*., 2008; Tan *et al*., 2012; van Zessen *et al*., 2012). Another possibility is that it good be a difference between species. An additional immunostaining study in the rat reported no visible

PV+ cells in the VTA and SNc. This study was investigating the presence of PV+ cells throughout the entire rat brain (Celio, 1990). My conjecture here would be that the authors did not look through all rostro-caudal levels of the VTA and SNc. Focusing in the more caudal sections where barely any PV+ cells are present could have led to a falsely negative result. PV+ fibres throughout the VTA and SNc were reported in both studies and were also observed in my own data (Celio, 1990). Both my own observations and the two previous immunohistochemistry studies reported PV+ fibres in both the VTA and SNc. This consistent with reports investigating inputs to the VTA and SNc, PV+ GABA neurons in the globus pallidus (GP) innervate the SNc (Oh *et al*., 2017) and PV+ GABA neurons in the VP send substantial projection to the VTA (Faget *et al*., 2016).

Though in agreement with immunostaining data, this result is in disagreement with two out of three single-cell RNA-seq studies. One of these reported as much PV mRNA in as many as 18.8% of dopamine neurons (Merrill *et al*., 2015). This does not seem to be the case at the protein level. This same study also reported PV mRNA is as many as 58.3% of GABA neurons in the VTA(Merrill *et al*., 2015), this is a much larger proportion than observed here.

3.4.2 Preliminary tracing experiments suggests PV+ neurons in the VTA and SNc are interneurons

To date four PV-Cre mice have undergone AAV injections in to the VTA and SNc. In order to specifically target the neurons in the VTA and SNc only, the injection protocol still needs to be adapted. So far, I have been unable to restrict the expression of the virus to the VTA and SNc resulting in a small amount of expression in the SNr and red nucleus. Despite this, ChR2-mCherry+ cell bodies were observed in the VTA and SNc and no ChR2-mCherry+ axon terminals were observed outside of the VTA and SN. The ChR2-mCherry+ cell bodies exhibited a similar distribution to those observed in the immunostaining experiment. However, there appeared to be a decreased number of ChR-mCherry+ cells in these PV-Cre mice compared to the numbers of PV+ neurons observed in both the WT and the VGATCre:RiboTag mice. In addition, not all ChR2-mCherry+ cells were PV+. There could be a number of reasons for this. Firstly, ChR2-mcherry+ cells that appear PV- could either be transcribing PV mRNA

but not synthesising the protein or they could be synthesising the PV protein in such low levels that is not being detected by the antibody. This could be confirmed by ISH for PV. In addition, this could be mis-expression of the virus in these cells. This could be ruled out by crossing the PV-mouse line with either a fluorescent reporter mouse, or with the RiboTag mouse combined with immunostaining for PV. I have presented preliminary data suggesting ChR2-mCherry+ axon terminals in the VTA and SNc co-localise with VGAT in single z-plane images suggesting they form GABA synapses, a functional connection will need to be confirmed using optogenetic stimulation combined with electrophysiological recordings. Furthermore, we currently do not know whether these axon terminals are originating from the ChR2-mcherry + cells in the VTA and SNc, or from those in the SNr. The circuit tracing of these PV+ neurons is still in its preliminary stages and more injections will need to be conducted in order to confirm that these are interneurons.

Chapter 4 – An unbiased approach: A comparison of the transcriptomes from GABA and dopamine neurons

4.1 Introduction

In a second approach to identify novel molecular markers of subpopulations of GABA neurons in the VTA and SNc. I set out compare the transcriptomes of GABA neurons and dopamine neurons in the midbrain. Whilst some effort has been made to determine patterns of gene expression in midbrain dopamine neurons the gene expression profile of GABA neurons in the VTA and SNc has yet to be investigated.

4.1.1 The isolation of ribosome associated mRNA from complex tissues

One of the major challenges in transcriptome profiling of cell populations from the brain or indeed other complex tissues, is that cell populations lie intermingled. This means that the isolation of RNA from specific cell types, without unwanted contamination is particularly difficult. Some of this issue has been met my taking advantage of transgenic techniques, in particular fluorescent reporter lines, to identify genetically defined cell populations. Target cell types can then be isolated with enzymatic dissociation and fluorescence activated cell sorting (FACs) or laser capture microdissection (LCM). These cellular isolation procedures have some limitations. For both enzymatic association and manual dissection, the three-dimensional relationship of a cells in a complex tissue must be completely

disrupted which could lead to stress induced changes in gene and protein expression. In addition to this, in LCM cell bodies are isolated from tissue section meaning in cells with very complex anatomy such as neurons are astrocytes, some dendritic or axonal mRNA will be left behind. All proteins are translated from mRNAs that are bound to a ribosome or polysome. Two research groups have taken advantage of this fact and have engineered technologies for the isolation of ribosome-associated mRNA from genetically defined cell types (Heiman et al., 2008; Sanz et al., 2009b). The RiboTag and translating ribosome affinity purification (TRAP) tools both provide a means of isolating cell specific mRNA via the immunoprecipitation of tagged polyribosomes. They achieve this by expressing a tagged ribosomal protein specifically in the target cell type - HA-Rpl22 for RiboTag and GFP-Rpl10 for TRAP (Heiman *et al.*, 2008).

The RiboTag mouse makes use of the Cre-LoxP recombination system meaning that it can be crossed with any available cre-drive line to drive cell specific expression of the tagged ribosomal protein. In contrast, when it was first introduced the TRAP methodology requires the creation of a bacTRAP mouse line for the targeting of a specific neuronal population. The fact that it could be crossed with any available Cre-driver line meant that RiboTag technique was more versatile (Heiman et al., 2008; Sanz et al., 2009b). It is for this reason that we decided to use the RiboTag technology to isolate mRNA from GABA and dopamine neurons in the midbrain.

4.1.2 RiboTag technology

The RiboTag mouse carries an epitope tagged ribosomal protein allele that can be activated in specific cell types by crossing with a Cre-Recombinase driver line. This makes the technology especially versatile as it can be used to selectively target any cell population that can be defined by a genetic marker. RiboTag mice have a hemagglutinin tagged exon in the Rlp22 gene, a gene that encodes for a core ribosomal subunit. The tagged exon lies downstream of the WT exon which is floxed by LoxP sites. Under normal conditions the WT exon is expressed. However in the presence of Cre-recombinase, recombination occurs and the wild type exon is excised resulting in expression of the

HA-tagged exon **(Figure 36)** (Sanz et al., 2009b). HA-tagged ribosomal protein is incorporated into polyribosomes and these polyribosomes and any associated mRNA can then be immunoprecipitated out of a mixed cell homogenate using antibodies for the HA-tag (Sanz et al., 2009b).

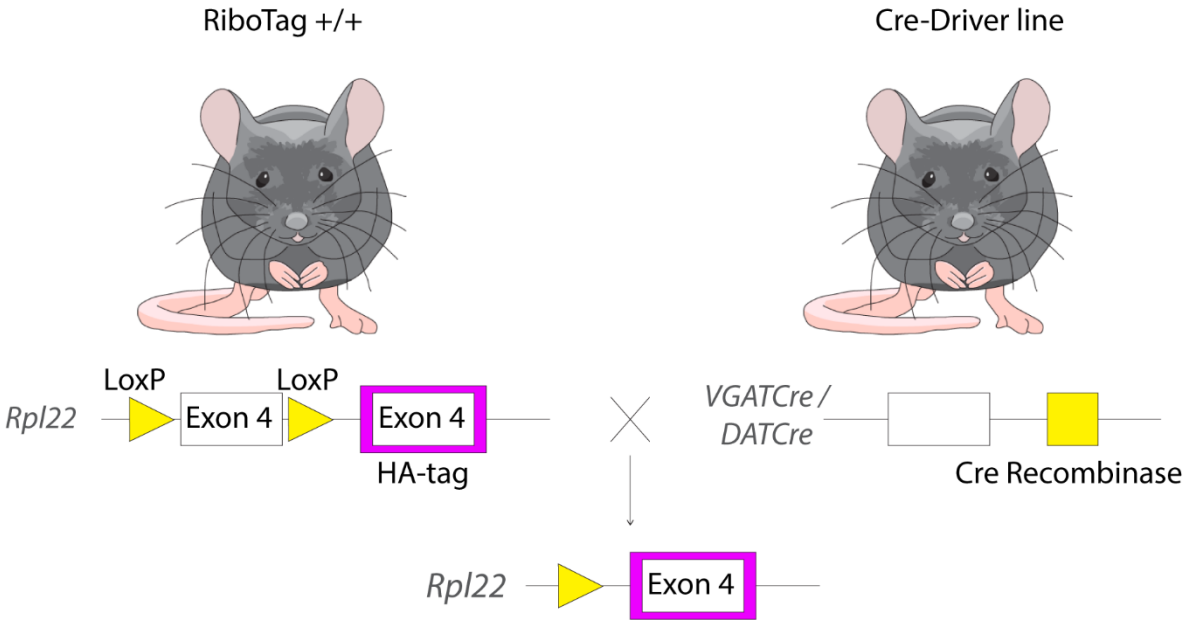


Figure 36: Schematic illustrating the RiboTag and Cre-Driver line cross. Crossing the RiboTag mouse with a Cre-recombinase expressing mouse results in the deletion of the WT exon 4 in the target cell population and replacement with the HA-tagged exon 4.

4.2 Experimental procedure

4.2.1 Animals

All breeding and experimental procedures were conducted in accordance with the Animals (Scientific Procedures) Act of 1986 (UK) (see section **2.2.1)**. Details of the mouse strains used in this chapter are shown in **Table 13.**

Mice homozygous for RiboTag were crossed with either mice heterozygous for DATCre or VGATCre. DATCre:RiboTag offspring were genotyped for the iCre. The expression of Cre in VGATCre:RiboTag offspring was observed via coat colour **(2.2.1).**

Mouse line	Strain nomenclature	Supplier (#Stock No.)
RiboTag	B6N.129-*Rpl22*$^{tm1.1Psam}$/J	The Jackson laboratory (#011029)
DATCre	Tg(Slc6a3-icre)1Fto (Turiault *et al.,* 2007)	Gifted from Prof. Francois Tronche
VGATCre	*Slc32a1*$^{tm2(cre)Lowl}$/J	The Jackson laboratory (#016962)

Table 13: Details of mice strains used in this chapter

4.2.2 DNA extraction

Protocol as described in **2.2.2**

4.2.3 Genotyping

Protocol as described in **2.2.3.** Genotyping information for this chapter is in **Table 14**

Strain/Transgene	Primers	PCR cycles	Product weight
RiboTag	**F –** GGGAGGCTTGCTGGATATG **R –** TTTCCAGACACAGGCTAAGTACAC	94°C 2min 94°C 20 secs 65°C 15 secs x10 68°C 10 secs 94°C 15 secs 60°C 15 secs x28 72°C 10 secs 72°C 2mins 10°C ∞	Mutant = ~290 bp Wild type = 243 bp
DATCre	F – TGGCTGTTGGTGTAAAGTGG Mutant R –CCAAAAGACGGCAATATGGT WT R – GGACAGGGACATGGTTGACT	94°C 2min 94°C 20 secs 65°C 15 secs x10 68°C 10 secs 94°C 15 secs 60°C 15 secs x28 72°C 10 secs 72°C 2mins 10°C ∞	Mutant = ~152 bp Wild type = 264 bp

Table 14: Genotyping information for mouse strains used in this chapter

4.2.4 Perfusion fixation and tissue preparation

Protocol as described in **2.2.4**

4.2.5 Immunostaining

Protocol as described in **2.2.5**. For information about the antibodies used in this chapter please see Tables 15 and 16.

Antibody	Host species	Manufacturer/Product No.	Concentration
Anti-TH	Chicken	Abcam (#ab76442)	1:1000
Anti-HA	Mouse	Sigma (#H3663)	1:1000
Anti-HA	Rabbit	Abcam (#ab9110)	1:500
Anti-GABAARα1	Rabbit	Alomone (#AGA-001)	1:500
Anti-GPR101	Rabbit	Sigma (#SAB4503289)	1:500
Anti-NRP2	Rabbit	Cell Signalling (#D39A5)	1:200
Anti-CBLN4	Rabbit	Invitrogen (#PA5-36472)	1:500
Anti-RORA	Rabbit	Sigma (#AV45628)	1:100
Anti-TRH	Rabbit	Abcam (#ab185658)	1:100
Anti-RXFP3	Goat	Santa Cruz (#sc47004)	1:100
Anti-S100B	Rabbit	Dako (#Z0311)	1:500

Table 15: Primary antibody information

Antibody	Conjugation	Host species	Manufacturer (#Product No.)	Concentration
Anti-Chicken	Alexa-488	Goat	Invitrogen (#A11039)	1:1000
Anti-Chicken	Cy3	Donkey	Jackson (#703-165-155)	1:1000
Anti-Mouse	Cy3	Donkey	Jackson (#715-165-150)	1:1000
Anti-Mouse	Cy5	Donkey	Jackson (#715-175-151)	1:1000
Anti-Rabbit	Alexa-633	Goat	Invitrogen (#A21070)	1:1000
Anti-Rabbit	Cy3	Donkey	Jackson (#711-165-152)	1:1000
Anti-Goat	Alexa-488	Donkey	Invitrogen (#A11055)	1:1000
Anti-Guinea Pig	Alexa-488	Goat	Invitrogen (#A11073)	1:1000

Table 16: Secondary antibody information

4.2.6 Preparation of fresh tissue for immunoprecipitation

10-14 week old mice were anaesthetised with isoflurane then decapitated. Their brains were removed and rapidly washed in ice cold PBS. The brains were placed on filter paper and excess tissue was trimmed away with a razor blade leaving a block of tissue containing the midbrain **(Figure 37A).** The midbrain was then snap frozen in isopentane at -55°C. Tissue was stored at -80°C until use.

4.2.7 Immunoprecipitation of tagged polyribosomes

100µl of protein G magnetic beads were pipetted into a 1.2 ml Eppendorf tube and placed on a magnet. The storage fluid was removed and the beads were washed in 1ml of citrate-phosphate buffer, pH 5.0 at 4°C for 5mins. After washing, the beads were incubated with 10µl of anti-HA antibody (Sigma Aldrich #H6908), the solution was mixed by pipetting and placed on a rotator at 4°C for 45mins. After coupling, the beads were washed once in fresh citrate-phosphate buffer, then twice in immunoprecipitation buffer (50mM Tris, pH 7.5, 100mM KCL, 12mM $MgCl_2$, 1% IGEPAL) (Sanz et al., 2009b).

Midbrain tissue was cryosectioned at 50µm, sections were collected with chilled forceps and placed in chilled 1.2ml Eppendorf tubes before being moved onto dry ice until homogenisation. 500ml of polysome buffer (50mM Tris, pH 7.5, 100mM KCL, 12mM $MgCl_2$, 1% IGEPAL, 1mM DTT, 200U/ml Promega RNAsin, 1mg/ml heparin, 100mg/ml cyclohexamide (Sigma Aldrich), 1x protease inhibitor cocktail (Sigma-Aldrich) was added to each tube of sections. Sections were homogenised on ice using a motorised pestle mixer (Kimble® Kontes). Following homogenisation an additional 500ml of polysome buffer was added. Samples were centrifuged at 10,000g for 10mins at 4°C to create a post-mitochondrial supernatant (Sanz et al., 2009b).

Following the final wash of the antibody-coupled beads the tubes were placed on a magnet, and the immunoprecipitation buffer was removed. 800ml of supernatants were then added directly to the

antibody-coupled Protein G magnetic beads and rotated overnight on a SB2 fixed speed rotator (Techne) at 4 °C. 50µl homogenate was placed in a fresh Eppendorf tube and placed on dry ice for later analysis. The following day, the samples were placed on the magnet and the supernatant was removed and collected. The beads were then washed three times in 1ml of high salt buffer (50mM Tris, pH 7.5, 300mM KCl, 12mM MgCl2, 1% IGEPAL, 1 mM DTT 100 µg/mL cycloheximide). Each time the solutions were mixed by gentle pipetting and placed on a rotator at 4°C for 5mins. After the final wash, polysomes were eluted from the beads by adding 350µl of lysis buffer (RLT buffer, Qiagen RNAeasy mini kit and β-mecaptethanol) and vortex mixing for 30 seconds. The eluted polysomes were removed from the beads and placed in a fresh 1.2ml Eppendorf tube on ice (Sanz et al., 2009b) **(Figure 37B).**

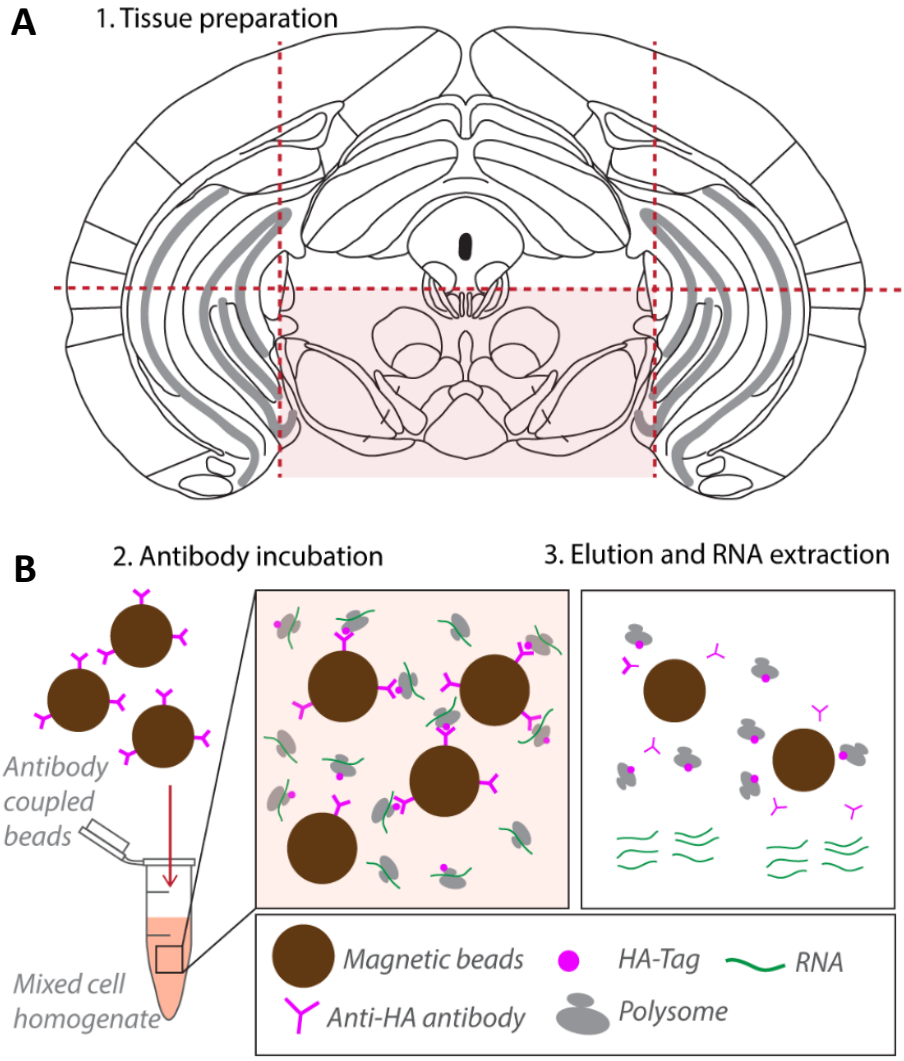


Figure 37: Schematic illustrating the protocol for the isolation of ribosomal associated mRNA from neurons in the midbrain. A: Schematic illustrating how the mouse brains were trimmed to leave a block of tissue containing the midbrain (red box). Red-dotted line illustrates where the tissue was cut. **B:** Schematic illustrating the immunoprecipitation protocol. Left panel shows the incubation of HA-antibody coupled magnetic beads with a mixed cell homogenate. Right panel shows the elution of tagged HA-tagged polysomes from the beads *(adapted from (Sanz et al., 2009b)). Brain outline as traced from (Franklin and Paxinos, 2008)*

4.2.8 RNA extraction

350µl of lysis buffer was added to 50ul of the input and unbound samples. The solutions were vortexed for 30 seconds then centrifuged for 3mins at 13,000rpm. 350µl of 70% ethanol was added to the input, the unbound and the IP samples. The solutions were mixed by gentle pipetting and transferred to RNAmini columns (QIAGEN). From this point RNA was extracted using RNAmini extraction kit (QIAGEN) according to the manufacturer's instructions. Extracted RNA was eluted from the columns in 30µl of RNase and nuclease free H_2O. RNA was then reverse-transcribed for qPCR analysis, taken for total RNA analysis on the bioanalyser or placed in dry-ice and stored at -80°C for later use.

4.2.9 Assessment of RNA quality and quantity

The quality of RNA samples was assessed using an RNA integrity number (RIN), obtained through capillary gel electrophoresis with an Agilent Bioanalyser and generated via an electropherogram using Agilent 2100 software. The RNA samples were loaded in an RNA-Pico Chip based on manufacturer's instructions. The RIN algorithm assigns an electropherogram a value of 1 to 10, with 10 being the least degraded. The RIN value is calculated based on several aspects of the electropherogram trace including: the ratio of the area under the 18S and 28S rRNA peaks to the total area under the graph, the height of the 28S peak, the area between the 18S and 5S rRNA peaks and the height of the marker peak (Schroeder *et al*., 2006). The bioanalyser also gives a quantification of total RNA in the loaded sample. Input and unbound samples contain amounts of RNA much larger that the IP samples. Therefore, in order to run them on the same RNA-Pico chip as the IP sample, they were diluted 1:20 in RNase free H_2O.

4.2.10 Reverse transcription

Total RNA from input and IP samples were quantified using a NanoDrop 1,000 spectrophotometer. Equal amounts of RNA from input and IP samples were used in the reverse transcription assay which was performed using PrimeScript™ RT reagent Kit with genomic DNA (gDNA) Eraser (Clonetech) according to manufacturer's instructions. A control RNA sample with the PCR mixture minus reverse transcriptase was included.

4.2.11 Quantitative-RT-PCR

Transcript levels of various genes were assessed by one-step qRT-PCR assays using the MESA Blue PCR Master mix (Eurpgentec). Each reaction used 0.5µl of primer, 10µl of MESA Blue 2xPCR Master Mix, 8.5µl of H_2O and 1µl of cDNA for a final volume of 20µl. The gene target and oligo sequences used are shown in **Table 14.** All oligos were sourced from Sigma Aldrich. Fold-enrichment of each gene in the IP sample was calculated using the ΔΔCt method with normalisation to beta-actin and comparison to the input sample.

Gene target	Sequence	Publication
Actin	F – AGTGTGACGTTGACATCCGTA R – GCCAGAGCAGTAATCTCCTTCT	
Th	F – CAGAGTTGGATAAGTGTCACCAC R – GGGTAGCATAGAGGCCCTTCA	
Slc6a3	F – CGGGCAGTTCAACAGAGAAGG R – GCCCACGTAGAAAGAGATGAGG	
Slc32a1	F – TCACGACAAACCCAAGATCAC R – GTCTTCGTTCTCCTCGTACAG	(Sgadò *et al.,* 2013)
Gad1	F – TCCAAGAACCTGCTTTCCTG R – GAGTATGTCTACCACTTCCAGC	(Sgadò *et al.,* 2013)
Gfap	F – GAACAACCTGGCTGCGTATAG R – GCGATTCAACCTTTCTCTCCAA	(Honsa *et al.,* 2014)
Cnp	F – ACGAGTGCAAGACGCTATTC R – CCGCTCGTGGTTGGTATC	

Table 17: Oligonucleotides used in quantitative RT-PCR experiments

4.2.12 Statistical comparisons

In these thesis statistical comparisons were performed in order to compare various aspects of the RNA extracted from VGATCre:RiboTag mice and DATCre:RiboTag mice and their Cre-negative controls. In all cases statistical analyses was conducted using GraphPad Prism 7. Unpaired student T-tests were used when data exhibited normal distribution. Man-Whitney tests were used when data was not normally distributed. Details of the test used in each comparison can be seen in the figure legend.

4.2.13 RNA-library preparation and sequencing

RNA samples with a RIN higher than 7 were used in RNA-seq libraries. Samples were first enriched for poly(A) containing transcripts using NEBNext Poly(A) mRNA Magnetic Isolation Module. Libraries were synthesised using NEBNext® Ultra™ Directional RNA Library Prep Kit for Illumina® and NEBNext® Multiplex Oligos for Illumina® (Index Primers Set 1). The library preparation protocol requires a minimum of 100ng of total RNA, because of this RNA samples were pooled where necessary. The same amount total RNA for IP and unbound were used to create each library. Libraries were synthesised based on manufacturer's instructions with the only difference being the volume of the total RNA sample and of the beads at the beginning of the process. Instead of 20 µl of NEBNext Oligo $d(T)_{25}$ beads and 50 µl of diluted RNA sample, 40 µl of beads and 100 µl of diluted RNA sample were used in the mRNA isolation step. The quality of the fragmented cDNA library was assessed on the Agilent bioanalsyser using a high sensitivity-DNA chip. Libraries were diluted to equal molarity and sequenced (in triplicate) using an illumina HiSeq 2500 system.

4.2.14 RNA-Seq Analysis

Analysis of the raw RNA-seq data was performed by Sanjay Khadayate of the MRC LMS bioinformatics facility.

(i) Alignment of RNA-Seq data

Raw RNA-seq reads were aligned against Ensembl Mouse genome reference sequence assembly (mm9) and transcript annotations using Tophat splice junction mapper version 2.0.11 (Kim *et al*., 2013). All parameters were set to default except inner distance between mate pairs (r=100) and library type (fr-firststrand).

(ii) Differential Gene Expression Analysis

Gene based read counts were obtained using HTSeq count module (version 0.5.4p3) (Anders *et al*., 2015). This was run using parameters m=union, stranded=reverse. Differential expression analysis was performed using DESeq2 Bioconductor package (version 1.4.5) (Love *et al*., 2014).The DESeq2 package uses a negative binomial model to model read counts and then performs statistical tests for differentially expression of genes. Raw p values were then adjusted for multiple testing with the Benjamini-Hochberg procedure. Genes with adjusted p value (PAdj) of 0.05 or less were considered differentially expressed.

4.2.15 Confocal Imaging, image processing and analysis

All images were acquired via laser scanning microscopy using a Leica SP confocal microscope (Leica Microsystems), with the pinhole set at 1 Airy unit. Multi-channel images were acquired sequentially. Images of cell bodies were acquired with a z-step size of 1 µm, images of processes were acquired with a step size of 0.5 µm. All images were processed with Fiji software and stacked example images are shown. To determine co-localisation of each candidate with HA and TH, channels were viewed both individually and in composite. Co-localisation was determined if the cell body was visible in multiple channels through its entire thickness (multiple z planes).

4.3 Results

To identify novel candidates for markers of subpopulations of GABA neurons in the VTA and SNc we sought to find genes that are enriched in GABA neurons but not in dopamine neurons. In order to do this, we aimed to directly compare the transcriptomes of GABA and dopamine neurons. In order to selectively target GABA neurons we crossed the RiboTag mouse with the VGATCre reporter line, and to selectively target dopamine neurons we crossed the RiboTag mouse with a DATCre line. For the purpose of verifying the immunoprecipitation protocol, cre-negative littermates were used as a negative control.

4.3.1 Expression of $RPL22^{HA}$ in target neurons

Immunohistochemistry on 30µm sections from VGATCre:RiboTag and DATCre:RiboTag mice revealed robust expression of the HA-epitope in midbrain neurons of both mice **(Figure 38).** Triple immunostaining for HA, GABAARα1 and TH in VGATCre:RiboTag tissue revealed co-localisation between HA and GABAARα1 **(Figure 38A).** Most HA+ neurons were TH-, although there was a small degree of co-localisation that is consistent with previous reports of VGAT/TH co-expression (Poulin *et al.,* 2014). This suggests that in these mice HA expression is specific to GABA neurons. Double immunostaining for TH and HA in the DATCre:RiboTag tissue revealed near perfect co-localisation between TH and HA. This suggests that in these mice HA expression is specific to dopamine neurons **(Figure 38B).**

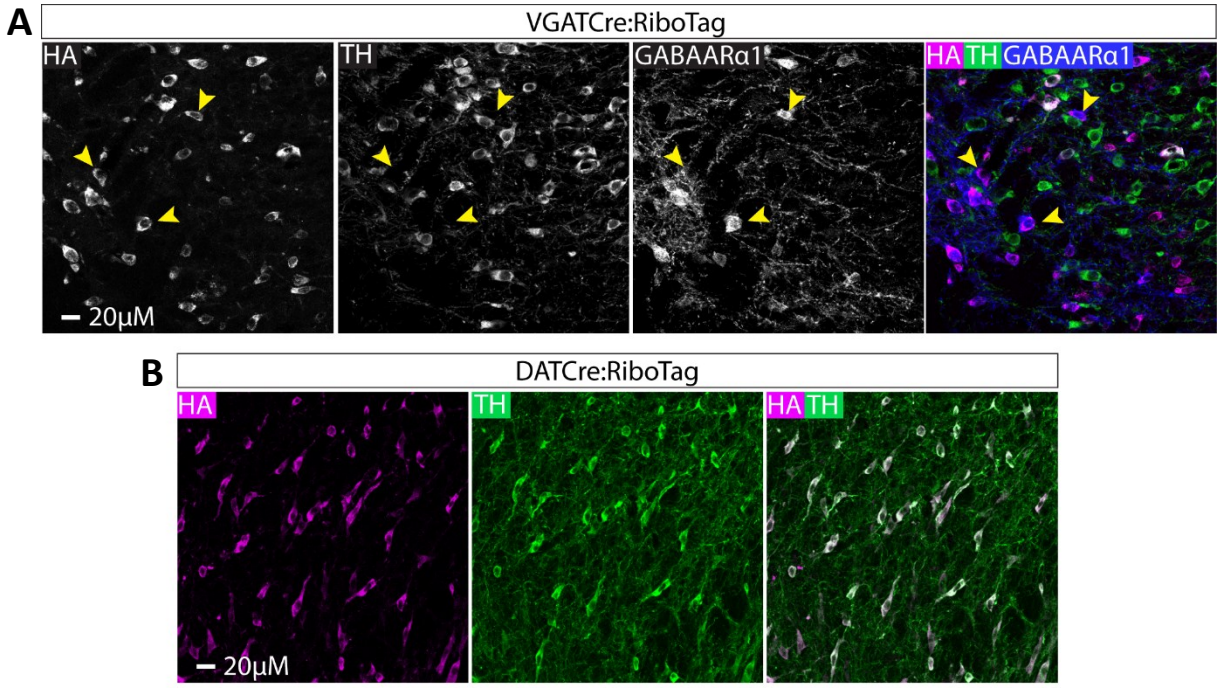


Figure 38. Immunohistochemistry for the HA-tag to verify expression in the target neuronal populations. A: Triple immunohistochemistry on VGATCre:RiboTag brain sections using anti-HA (magenta), anti-TH (green) to identify dopamine neurons and anti-GABAARα1 (blue) to mark GABA neurons. Merged images show co-localisation between HA and GABAARα1 (yellow arrows), with only a small degree of co-localisation between HA and TH (n=3) **B:** Double immunohistochemistry on DATCre:RiboTag brain sections using anti-HA (magenta) and anti-TH (green). Merged images reveal almost perfect co-localisation between TH and HA (n=3) *This DATCre:RiboTag image was taken by Kyoko Tossell*.

4.3.2 Assessment of purified RNA samples

Having confirmed cell type specific expression of the HA-tagged ribosomal protein in both mouse lines, I proceeded to isolate HA-tagged polysomes and associated mRNA from homogenised midbrain sections using immunoprecipitation. As a negative control, homogenised midbrain tissue from cre-negative littermates was also incubated with anti-HA coupled magnetic beads. An Agilent Technologies 2100 Bioanalyser was used to assess the both integrity and quantity of RNA samples obtained from eluted polysomes. RNA extracted from both the VGATCre:RiboTag and the DATCre:RiboTag tissue was assessed as well as cre-negative controls. The example electropherograms in **Figure 39 A and B** demonstrates intact 18S and 28S ribosomal RNA isolated from both GABA neurons (A) and dopamine neurons (B). The average RIN values, which reflect the quality of ribosomal RNA (rRNA) in the samples isolated from each neuronal type are shown in **figure 39 C and D.** This RIN value was also recorded for each input sample for comparison. The input is a sample of RNA taken directly from the mixed cell homogenate prior to the overnight incubation with antibody coupled beads. The RNA obtained from both GABA-IP and the dopamine-IP had an average RIN of >7. This indicated largely intact RNA of sufficient quality for downstream analyses, such as qRT-PCR and RNA-seq. The average RIN obtained from samples increased as I became more experienced and efficient.

An amount of background, non-specific RNA is obtained from the cre-negative controls. To confirm that it was not just background RNA observed in the GABA-IP and dopamine-IP I wanted to ensure that more RNA was being isolated from Cre+ tissues. The quantity of RNA input into each sample was variable **(Figure 40 A and C)**. To normalise this - and determine the difference between the Cre+ and Cre- mice - the quantity of RNA obtained from the IP experiment is shown as a percentage of the total RNA input (**Figure 40 B and D)**. In both mouse lines significantly more RNA is obtained from the VGATCre+ and DATCre+ littermates compared to the cre-negative controls.

4.3.3 Enrichment of cell type specific mRNAs

Next, I wanted to confirm that my GABA-IP and dopamine-IP samples were enriched for marker genes of the cell type of interest (GABA and Dopamine neurons). To determine this, RNA from both the IP and input samples were reversed transcribed and qRT-PCRs for GABA neuron specific genes (Vgat and Gad1) and dopamine neuron specific genes (Th and Dat) were performed on the copy DNA (cDNA). In addition to this, qRT-PCRs for genes that are expressed in neither neuronal population (glial markers Gfap and Cnp) were performed to act as a negative control. All cell specific marker genes and control genes were normalised to beta-actin (Actb) levels using the ΔΔCt method. In each case the IP sample was compared to the input sample. A comparison between the VGATCre+ and DATCre+ samples and Cre-negative controls are shown in **figure 41**. GABA neuron specific genes VGAT and GAD1 were significantly enriched in the VGATCre+ IP sample compared to the VGATCre control. In the VGATCre+ samples the average enrichment of VGAT is around 7-fold compared to the input sample, and the average enrichment of Gad1 is around 4-fold. There was no significant difference in the enrichment levels of CNPase and GFAP, glial cell markers, or DAT and TH, dopamine neuron specific genes. The dopamine neuron markers Dat and Th were both significantly more enriched in the DATCre+ sample compared to the cre-negative control. Both Dat and Th showed enrichment levels of around25-fold compared to the input samples. There was no significant difference between the enrichment levels of CNPase and GFAP (qRT-PCRs for the GABA neuron genes were not performed on these samples). These results showed that RNA specific to the target cell type was being obtained.

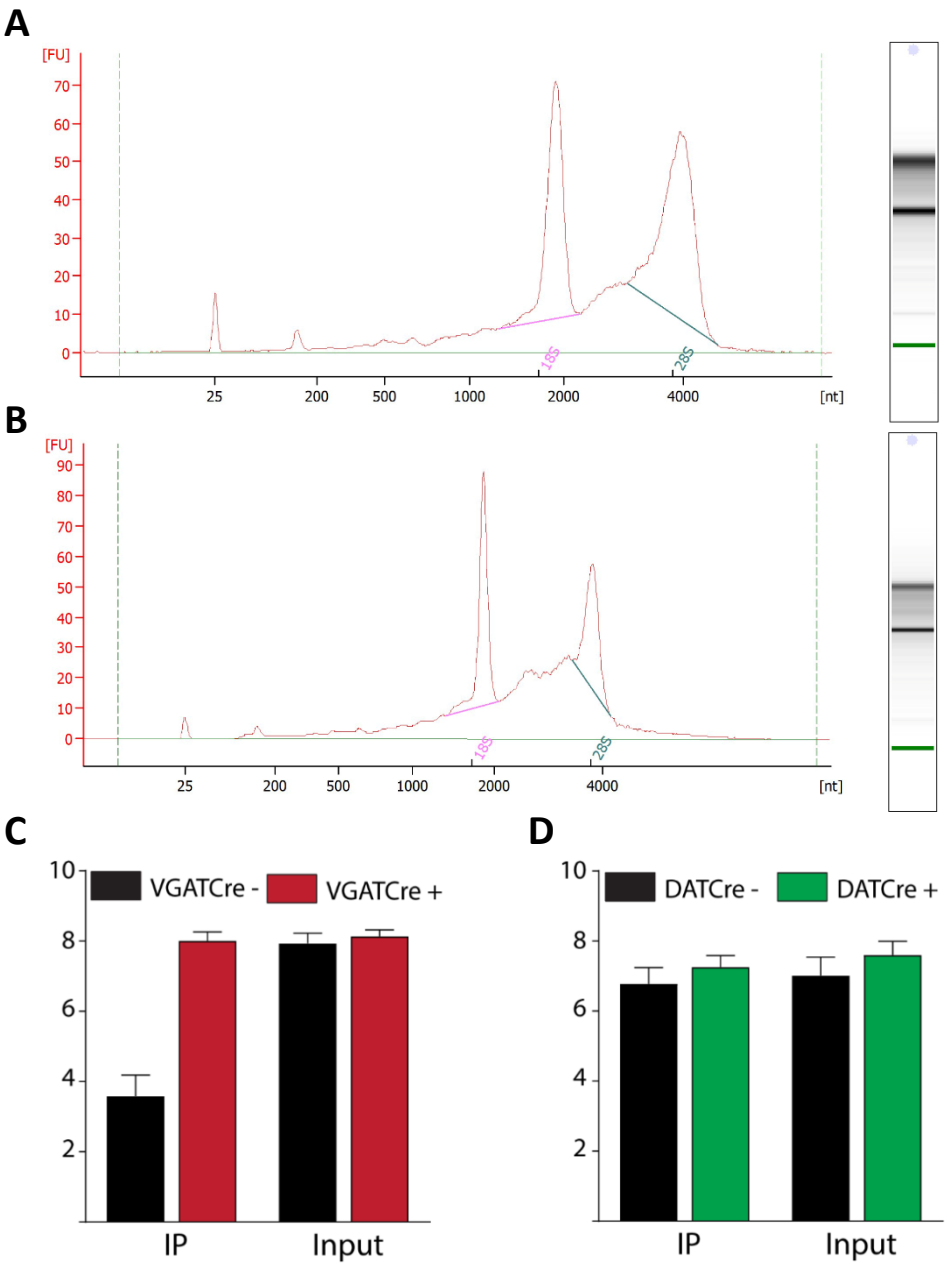


Figure 39: Assessment of RNA quality. Example electropherograms illustrating the quality of rRNA extracted from GABA-IP **(A)** and dopamine-IP **(B).** Graphs showing the average RIN of rRNA extracted from GABA-IP and input samples from VGATCre:RiboTag mice and their VGATCre- littermates (n=5) **(C)** and from DATCre:RiboTag mice and their DatCre- littermates **(D)** (n=5).

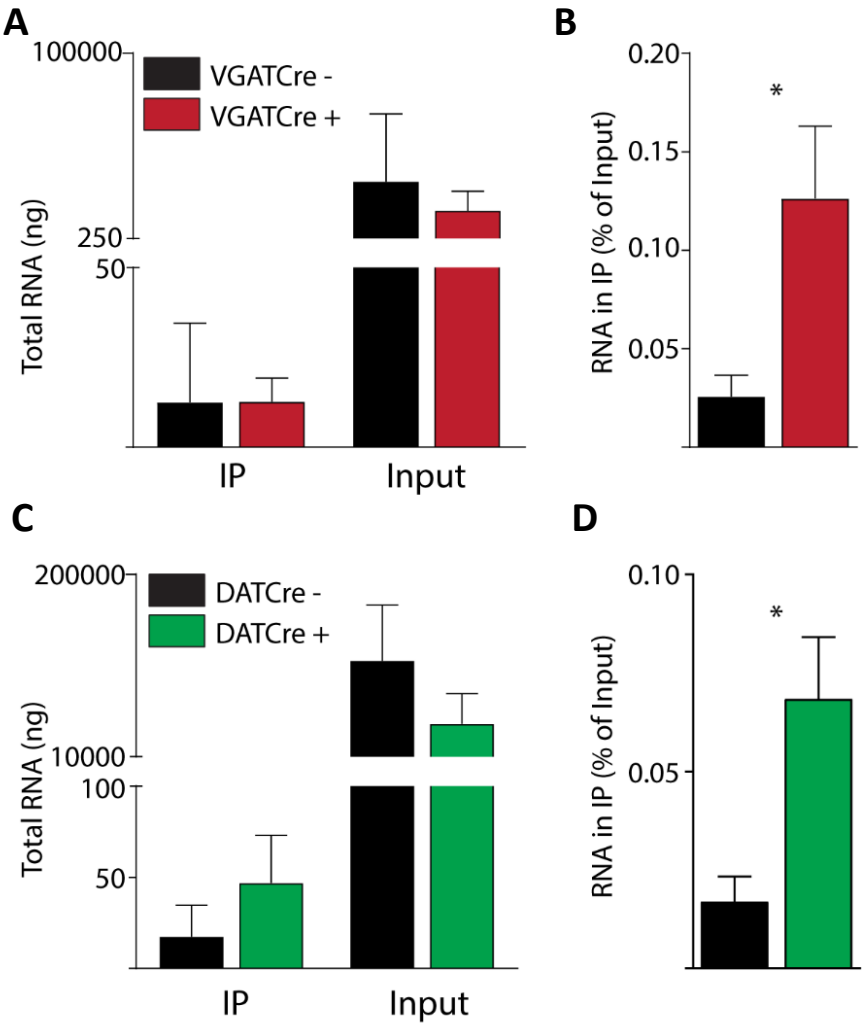


Figure 40: Assessment of RNA quantity. A: Graph showing the amount of total RNA isolated from both input and IP samples from VGATCre:RiboTag and VGATCre- littermates (n=5). **B:** The percentage of input RNA extracted from IP samples of VGATCre:RiboTag and VGATCre- littermates (n=5) (Unpaired T-test *=p<0.05) **C:** Graph showing the amount of total RNA isolated from both input and IP samples from DATCre:RiboTag and DATCre- littermates (n=5). **D:** The percentage of input RNA extracted from IP samples of VGATCre:RiboTag and VGATCre- littermates (n=5) (Man Whitney test *=p>0.05).

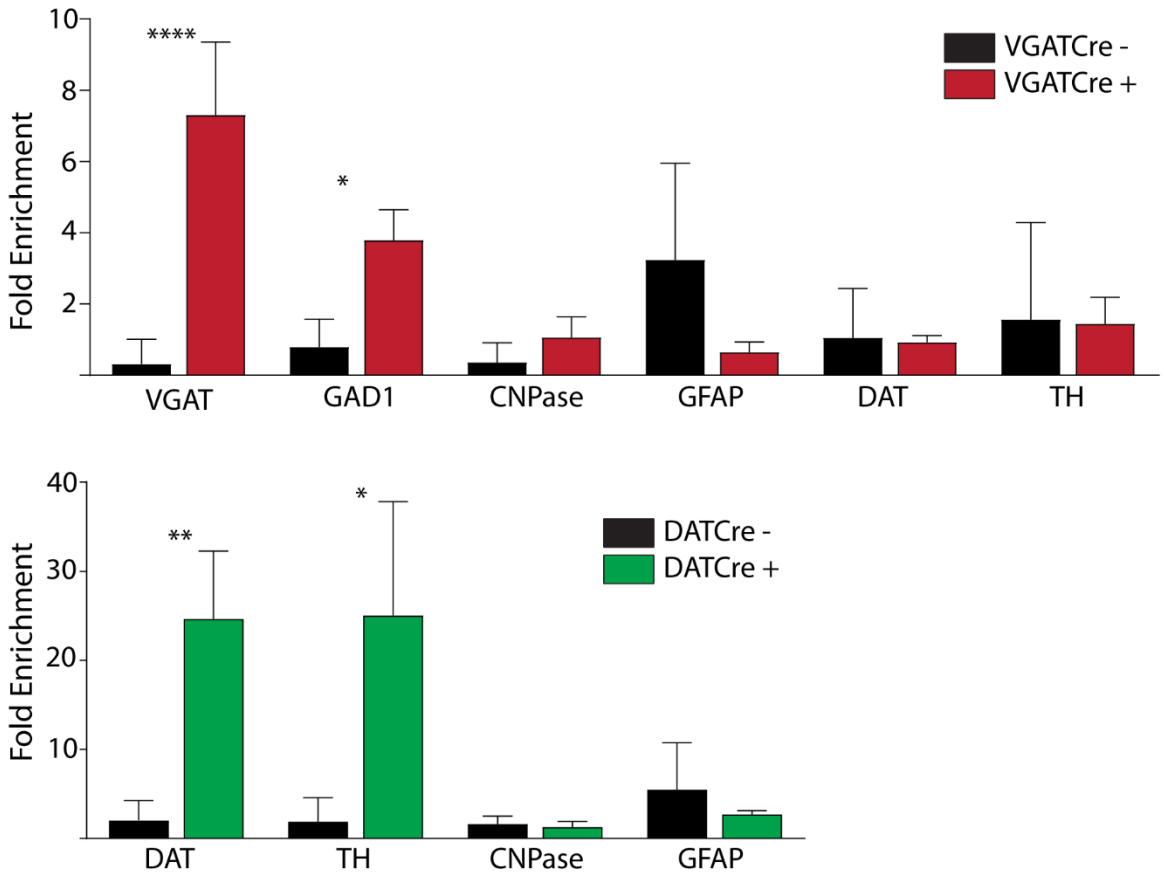


Figure 41: Enrichment of transcripts expressed in GABA and dopamine neurons. A: qRT-PCR of transcripts known to be expressed in GABA neurons, glial cells and dopamine neurons displayed a fold-enrichment of GABA neuron transcripts Vgat (Unpaired student t-test, ****=p<0.0001) and Gad1 (unpaired student t-test, *=p<0.05), with the VGATCre+ IP significantly higher than that in the VGATCre- IP. There was no significant difference in the enrichment levels of dopamine neuron transcripts and glial cell transcripts. **B:** qRT-PCR of transcripts expressed in dopamine neurons and glial cells showed a fold-enrichment of dopamine neuron transcripts DAT (Man-Whitney test ** = P<0.01) and TH (Man-Whitney test * = P<0.05), which is significantly higher in the DATCre+ IP sample compared to the DATCre- IP sample. There was no significant difference in the fold-enrichment of glial cell transcripts. The transcripts analysed by qPCR were *Vgat (Slc32a1); GAD1, 2'3'-cyclic nucleotide 3' phosphodiesterase (CNPase, Cnp); glial fibrillary acidic protein (GFAP)*; *Dat* and *Th.*

4.3.4 RNA-sequencing library preparation

As a way of confirming each IP sample sent for sequencing was successful we also harvested RNA from the unbound (UB) sample for each biological repeat. RNA-sequencing libraries were synthesised from both IP and UB RNA. Table 18 shows the details of RNA used in the libraries, the resulting cDNA and the index sequence used to identify each library.

Library No.	Sample type		Number of brains	Average RIN	Total RNA (ng)	Library index sequence
1	VGATCre:RiboTag	IP	6	8.5	115	ATCACG
2		Unbound		8.1	115	CGATGT
3	VGATCre:RiboTag	IP	4	9.1	150	TTAGGC
4		Unbound		9.3	150	TGACCA
5	VGATCre:RiboTag	IP	3	9.1	200	ACAGTG
6		Unbound		9.5	200	GCCAAT
7	DATCre:RiboTag	IP	3	7.4	150	CAGATC
8		Unbound		7.2	150	ACTTGA
9	DATCre:RiboTag	IP	3	7.9	125	GATCAG
10		Unbound		7.8	125	TAGCTT
11	DATCre:RiboTag	IP	3	7.3	120	GGCTAC
12		Unbound		7.8	120	CTTGTA

Table 18: Final RNA-sequencing library information.

The quality of the libraries was assessed using HS-DNA chip on the Agilent bioanalyser. The HS-DNA assay is used as a way of evaluating the RNA fragmentation process. The majority of RNA sequencing platforms provide relatively short sequencing reads (40-400 bp). RNA is therefore fragmented during library preparation. The NEBNext® Ultra™ Directional RNA Library Prep Kit for Illumina® protocol used here is optimised to produce RNA inserts for approximately 200 bp. From these RNA fragments cDNA is synthesised and adaptor and indexing sequences are added. The resulting cDNA library should

ideally be enriched for cDNA fragments of approximately 300bp. Example electropherograms obtained from GABA-IP (A) and dopamine-IP (B) are shown in **figure 42**. These electropherograms both show narrow distributions with a peak at approximately 300bp. This indicates the fragmentation process has worked well and the library is ready for sequencing.

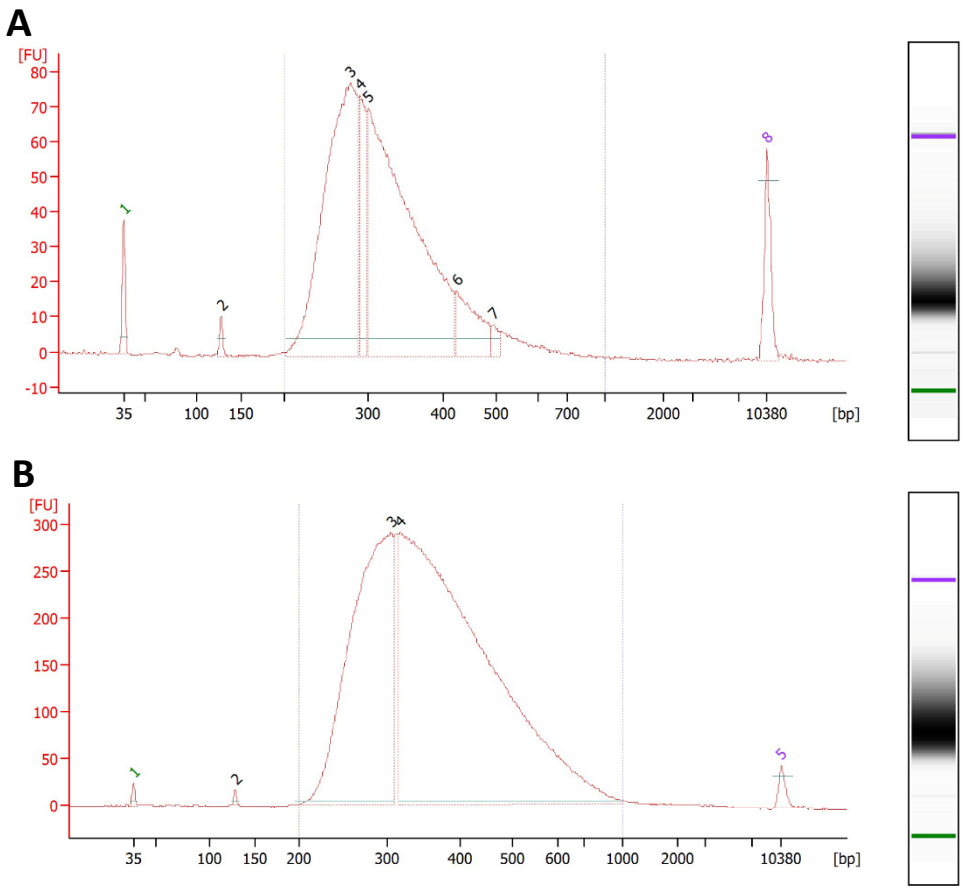


Figure 42: Examples of High sensitivity-DNA electropherograms of libraries prepared from IP-RNA.

A: Library prepared from GABA-IP. **B:** Library prepared from dopamine-IP

4.3.5 A direct comparison of the transcriptomes of GABA and dopamine neurons

Raw RNA-seq data was analysed by Sanjay Khadayate

To obtain a list of genes that are enriched in GABA neurons compared to dopamine a direct comparison of the libraries obtained from GABA-IP and dopamine-IP was performed. As a final verification of the RNA libraries, I first checked the fold enrichment levels of the control genes in GABA neurons, relative to dopamine neurons **(figure 43).** All GABA neuron specific transcripts examined were significantly enriched in GABA neurons compared to dopamine neurons. Parvalbumin was included here due to the large population of PV+ GABA neurons present in the SNr.

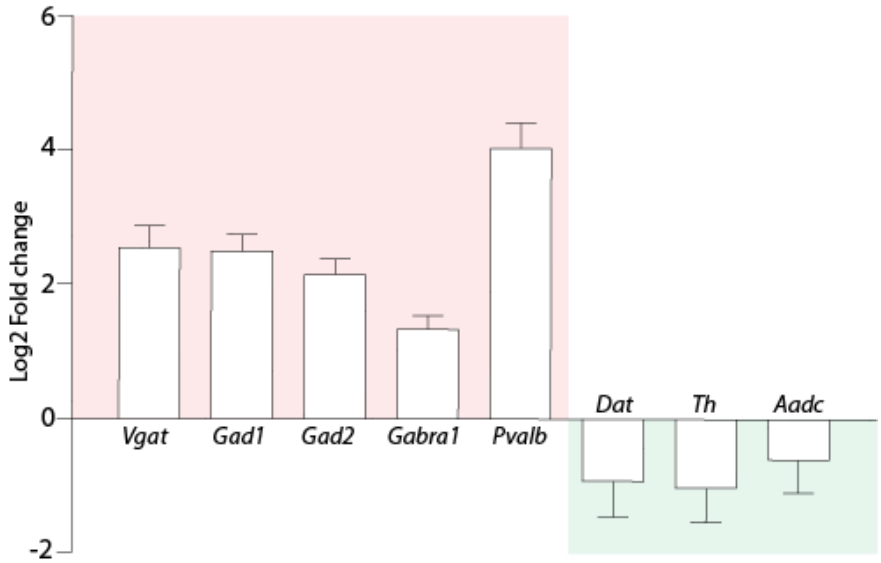


Figure 43: The fold enrichment in GABA-IP relative to dopamine-IP RNA subjected to RNA-seq for transcripts specific to GABA neurons and dopamine neurons. GABA neuron specific genes (red box) are all significantly enriched (P-Adj <0.05) in the GABA neuron database compared to the dopamine neuron database.

A total of 15,014 genes were differentially expressed (significantly enriched) in GABA neurons compared to dopamine neurons **(Figure 44)**. The RNA sequencing results obtained from both VGATCre:RiboTag mice and DATCre:RiboTag mice were consistent across all biological repeats, with slightly more genes appearing enriched in dopamine neuron than in GABA neurons **(Figure 44A).** 3364 genes were significantly enriched in GABA neurons compared to dopamine neurons **(Figure 44B)** (P-Adj > 0.05), in contrast, 3598 genes were significantly de-enriched.

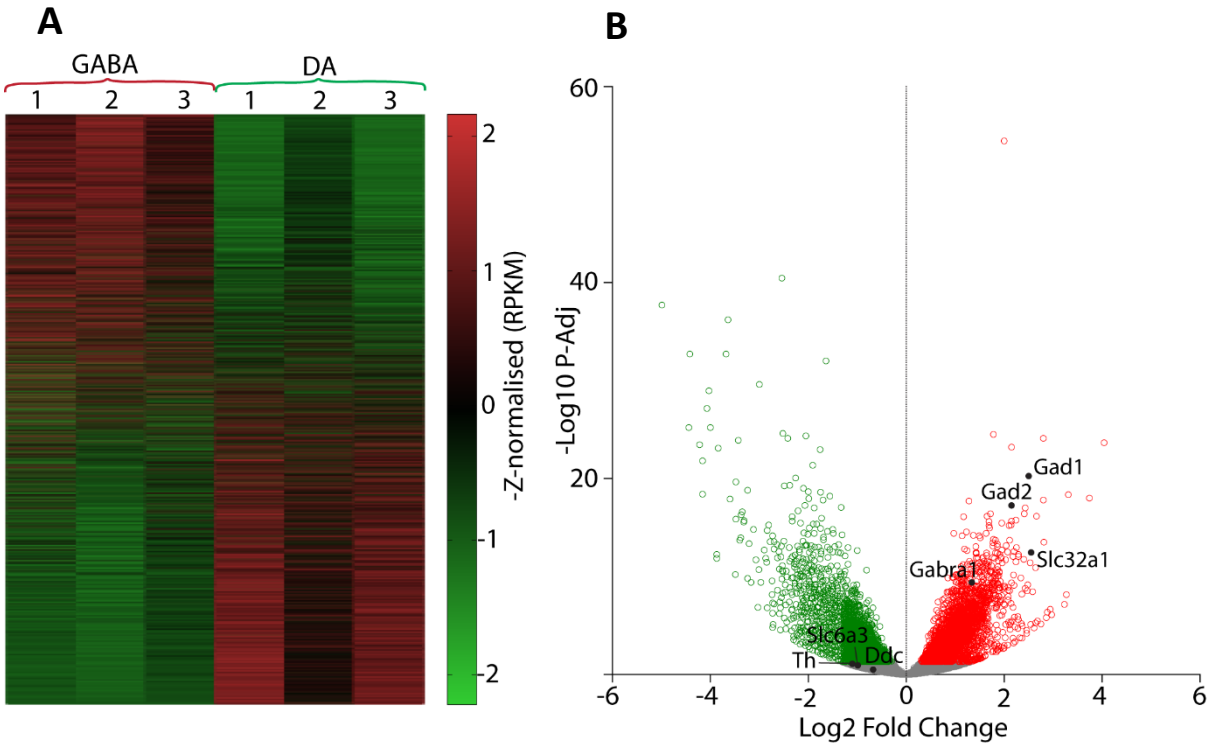


Figure 44: A direct comparison of the transcriptomes of GABA and dopamine neurons. A: Heatmap showing the genes differentially expressed in GABA and dopamine neurons (z-normalised (RPKM)), each column represents a distinct RNA-library (3 biological repeats for each neuronal population) and each row represents a different gene. Red-green scale illustrates level of enrichment (red = enriched, green = de-enriched). **B:** Volcano plot illustrating the proportion of differentially expressed genes that are significantly enriched (red) or de-enriched (green) in GABA neurons (grey = not significant) (Padj > 0.05).

4.3.6 The selection of candidate markers

We took a series of systematic steps to select the list of potential GABA neuron. The steps taken are described and summarised in **Figure 45.**

(i) PANTHER

The first step we took was to input the list of significantly enriched genes into the PANTHER database. PANTHER (**P**rotein **AN**alysis **TH**rough **E**volutionary **R**elationships) is a gene ontology database and classification system designed to classify proteins and their genes. Proteins are classified according to family and subfamily, molecular function, biological process or pathway (Mi *et al.,* 2017; Mi *et al.,* 2013). It is a useful tool for extracting sub-categories of genes from many potential candidates. Using PANTHER we wanted to not only reduce our list of genes to a more manageable figure, but to also extract categories that are likely to give us more usable candidates (i.e. genes/proteins that are studied in the brain and will therefore have available antibodies and Cre-lines).

Based on publications examining cell diversity via similar methods (Bikoff *et al*., 2016; Okaty *et al*., 2015) I extracted nine protein categories from PANTHER. We hypothesised that distinct subpopulations of neurons may be determined during development and therefore would exhibit differential expression of transcription factors. This has been shown to be correct for GABAergic interneurons of the dorsal horn (Bikoff *et al.,* 2016). PANTHER showed that 186 transcriptions factors were significantly enriched in GABA neurons. We were looking for genes that identify functionally distinct subpopulations of GABA neurons, it is therefore reasonable to predict that these genes will be related to cell communication and signalling. Based on this idea, the remaining eight categories extracted from PANTHER included cell communication, receptors, receptor activity and receptor binding, transporters, transporter activity, signal transducer activity and signalling molecules. These categories are similar to those shown to have those have distinct patterns of gene expression in different subpopulations of serotonin neurons (Okaty *et al.,* 2015). In total, 1102 genes were extracted from PANTHER. A complete list of these 1102 genes can be viewed in appendix 1.

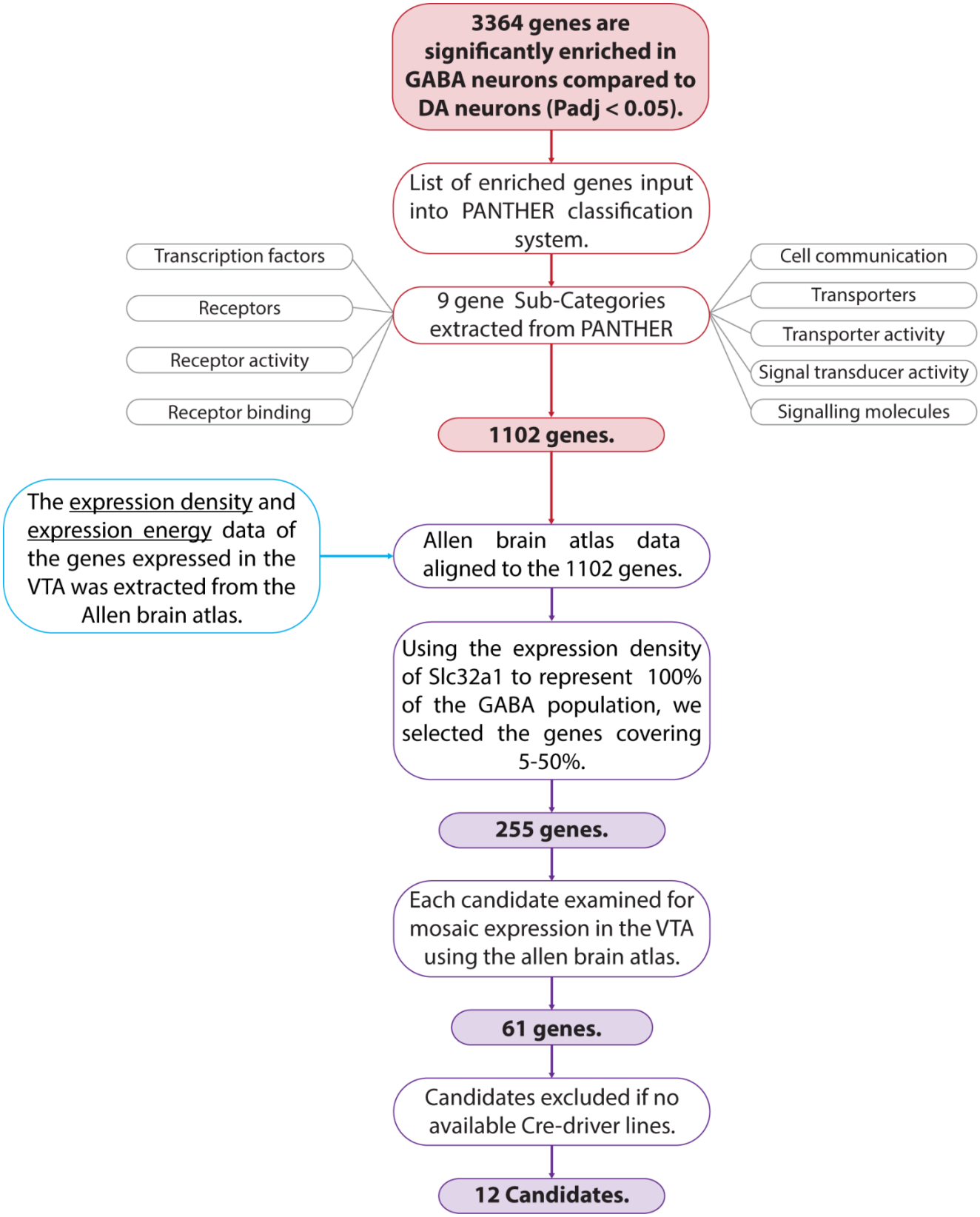


Figure 45: Flowchart summarising the steps taken in selecting novel candidates for markers of GABA neurons in the midbrain.

(ii) The Allen Brain Atlas

We wanted to further reduce our list of candidates using an unbiased approach. To this end, we downloaded the raw gene expression data from Allen brain atlas. The Allen Brain Atlas (ABA) brain explorer database contains a quantification of gene expression density and gene expression levels of genes found in different nuclei in the brain. These quantifications are calculated from the ISH images for each gene. We downl+oaded this data for all genes shown to be present in the VTA and aligned it to my sequencing data. The gene expression density values correspond to the amount of cells expressing each gene, and the gene expression level corresponds to the degree to which a gene is expressed by a given object (cell) (Lein *et al*., 2007). We plotted the ABA expression and intensity values for the 1102 genes extracted from PANTHER (**figure 46A).** For the purpose of identifying genes expressed in subpopulations of GABA neurons we were particularly interested in the gene expression density values. We took the gene expression density of a gene we know is expressed in all GABA neurons - *Vgat*- to signify 100% of the population GABA (i.e. all genes with an expression density value higher than that of *Vgat* are likely to be expressed in all GABA neurons, or multiple cell types within the midbrain). Our goal was to find markers for subpopulations of GABA neurons. Therefore, using the density of *Vgat* to represent 100% of GABA neurons, we extracted those genes expressed in between 5-50% of GABA neurons (based on ABA expression density values) **(Figure 46B)**. This left us with a list of 255 potential candidates. Those 255 genes extracted from this point are shown in appendix 1.

The ABA data was downloaded, sorted and aligned to my sequencing library using a custom written Python script by Max Ungless.

I then wanted to confirm that each of the genes in the list of candidates exhibited mosaic expression in the VTA and SNc in the ISH images in the Allen brain atlas, this left 61 genes remaining **(Figure 46B**). A complete list of those 61 genes exhibiting mosaic expression is shown in appendix 1.

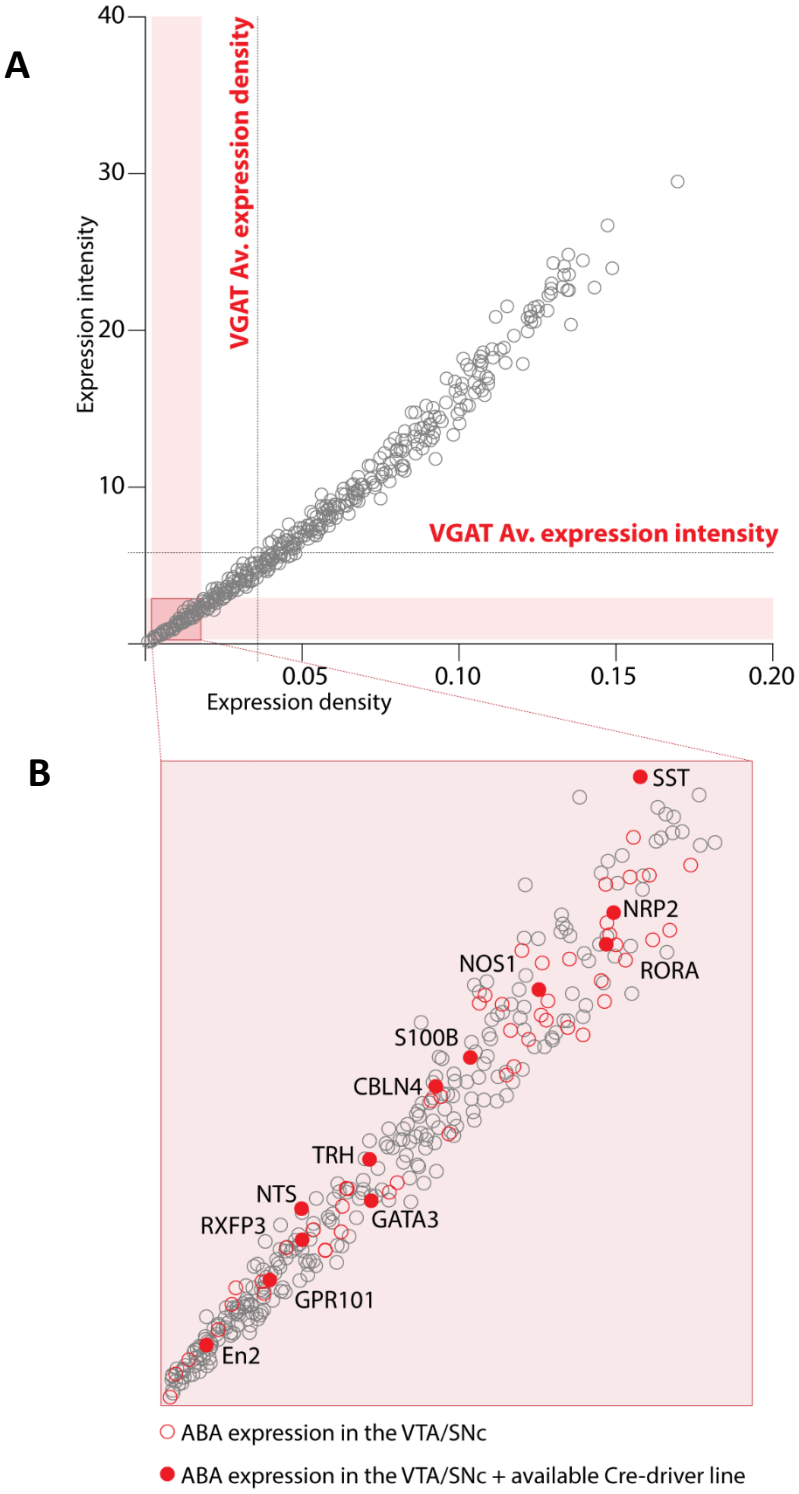


Figure 46: Quantitative data from the Allen Brain Atlas for 1102 genes extracted from PANTHER.

A: Scatter plot Expression density=no. expressing pixels/total number of pixels. B: 255 genes that are expressed in 5-50% of the GABA neuron population in the VTA. Empty red circles represent genes that exhibit mosaic expression in ISH images in the ABA. Solid red circles illustrate those genes with mosaic expression in the ABA and available Cre-Driver lines.

(iii) Final candidates

The overall aim of this research is to identify novel genetic markers for the identification and the selective targeting and manipulation of subpopulations of GABA neurons. For this reason, to obtain the final list of novel candidates I selected genes for which Cre-driver lines are already available. This left me with a final 12 candidates. A full list of the final candidates is shown in **Table 19.**

Gene Symbol	Gene description	Protein function	Log2Fold Change	P-Adj	Cre-Driver
Gata3	GATA binding protein 3	Transcription factor	2.44	9.03E-18	(Zhang *et al.,* 2014)
SOM	Somatostatin	Hormone	2.20	7.93E-10	JAX
Gpr101	G protein-coupled receptor 101	Orphan G protein-coupled receptor	1.24	4.25E-06	(Reinius *et al.,* 2015)
Cbln4	Cerebellin 4 Precursor	Small secreted protein	1.28	1.42E-05	MMRRC
Rxfp3	relaxin/insulin like family peptide receptor 3	G protein-coupled receptor/ receptor for neuropeptide relaxin3	1.71	4.59E-05	MMRRC
Nts	Pro-Neurotensin/ Neuromedin	Neurotransmitter/ neuromodulator	1.47	3.40E-04	JAX
Rora	RAR Related Orphan Receptor A	nuclear hormone receptor	1.10	4.95E-04	(Wu *et al.,* 2010)
Nos1	Neuronal nitric oxide synthase	NO synthesising enzyme	0.98	1.45E-03	JAX
Trh	Thyrotropin releasing hormone	Hormone	1.50	1.67E-03	(Sugrue *et al.,* 2010)
En2	Engrailed Homeobox 2	Transcription factor	1.14	2.21E-03	JAX
S100b	S100 Calcium Binding Protein B	Calcium binding protein	1.45	8.54E-03	(Tanaka *et al.,* 2008)
Nrp2	Neuropilin 2	Transmembrane receptor for semaphorin 3C	0.42	4.10E-02	(Wiszniak *et al.,* 2015)

Table 19: Details of the final 12 candidates identified as potential novel markers for subpopulations of midbrain GABA neurons. MMRRC - Mutant mouse resource and research centres, JAX - The Jackson Laboratory.

4.3.7 Validation of candidates

One of the final 12 candidates is nNOS. We already know that in the VTA and SNc a subpopulation (9.3%) of GABA neurons express nNOS **(See chapter 2).** This provides validation of the approach taken here to limit our list of potential candidates. At this stage I excluded the hormone somatostatin (SOM). As described in **Chapter 2,** SOM is used as a molecular marker for GABAergic interneurons in the hippocampus and cortex, and preliminary staining (conducted by Katlyn Green) in the VTA and SNc revealed no SOM+ neurons. I also excluded the neuromodulator *Nts* and transcription factor *Eng2* based on published literature surrounding their expression in the VTA and SNc. Neurotensin is expressed in a large population of TH+ neurons in the VTA and SNc (Hökfelt *et al.,* 1984; Seroogy *et al.,* 1988; Studler *et al.,* 1988). In adult mice the expression of Eng2 in the midbrain is thought to be confined to dopamine neurons (Simon *et al.,* 2001; Simon *et al.,* 2004). Considering the published literature, I also decided not to further investigate the expression of GATA3 in the VTA and SNc. It is already well established that GATA3 is expressed in all GABA neurons of the midbrain (Lahti *et al.,* 2013; Lahti *et al.,* 2016; Lakshmanan *et al.,* 1999; Nardelli *et al.,* 1999). The expression of the remaining 7 candidates was explored using immunohistochemistry in the VTA and SNc of VGATCre:RiboTag mice, using anti-HA to identify GABA neurons and anti-TH to identify dopamine neurons.

(i) G protein-coupled receptor 101 (GPR101)

GPR101 is s an orphan G protein-coupled receptor of unknown function. A role for GPR101 has been suggested in brain and pituitary development (Trivellin *et al.,* 2016) and gene mutations have been linked to acromegaly and gigantism (Trivellin *et al.,* 2014). Characterisation of a GPR101-Cre line revealed expression of the protein in D1 and D2 expressing medium spiny neurons of the striatum (Reinius *et al.,* 2015) but the expression pattern of the receptor in the VTA and SNc was not examined. ISH images of GPR101 expression in the VTA and SNc from the Allen brain revealed scattered populations of GPR101 expressing cells in the PBP and a slightly denser population in the rostral SNc (Lein *et al*., 2007) **(Figure 47).**

Triple immunostaining of GPR101, HA and TH in VGATCre:RiboTag mice (n=3) revealed co-localisation between GPR101 and HA **(Figure 48).** GPR101+ cells can be observed throughout the PBP and SNc most of which are HA+ and TH-. Also present GPR101+ cells that are TH+ and HA- **(Figure 48A).** The degree of co-localisation has not yet been quantified, but initial, exploratory images suggest GPR101+ TH+ neurons appear in lower numbers that GPR101+ HA+ neurons. GPR101+ cell bodies can be observed **(Figure 48C)**,immunoreactivity can also be seen in processes **(Figure 48B).** GPR101 appears to mark a sub-population of GABA neurons across the VTA and SNc and could be a useful genetic entry point to study these neurons.

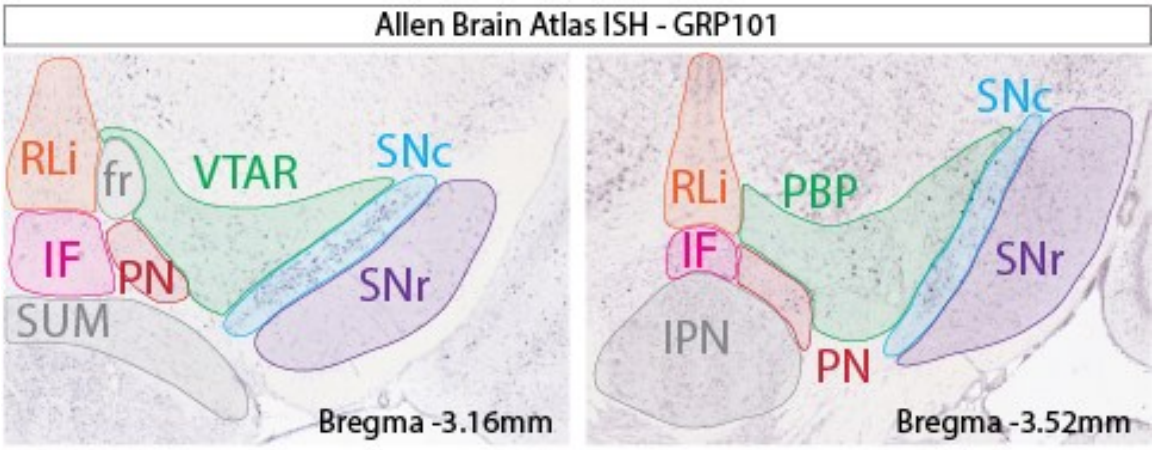


Figure 47: ISH data from the ABA showing the expression of GPR101 in the VTA and SNc (Lein *et al.*, 2007). © 2004 Allen Institute for Brain Science. Available from: http://mouse.brain-map.org/ *(Lein et al., 2007).* The right panel shows a coronal section through the rostral VTA and SNc, the image on the left is a more caudal cross section. Sub-regions were drawn on based on outlines in the mouse brain atlas (Franklin and Paxinos, 2008).

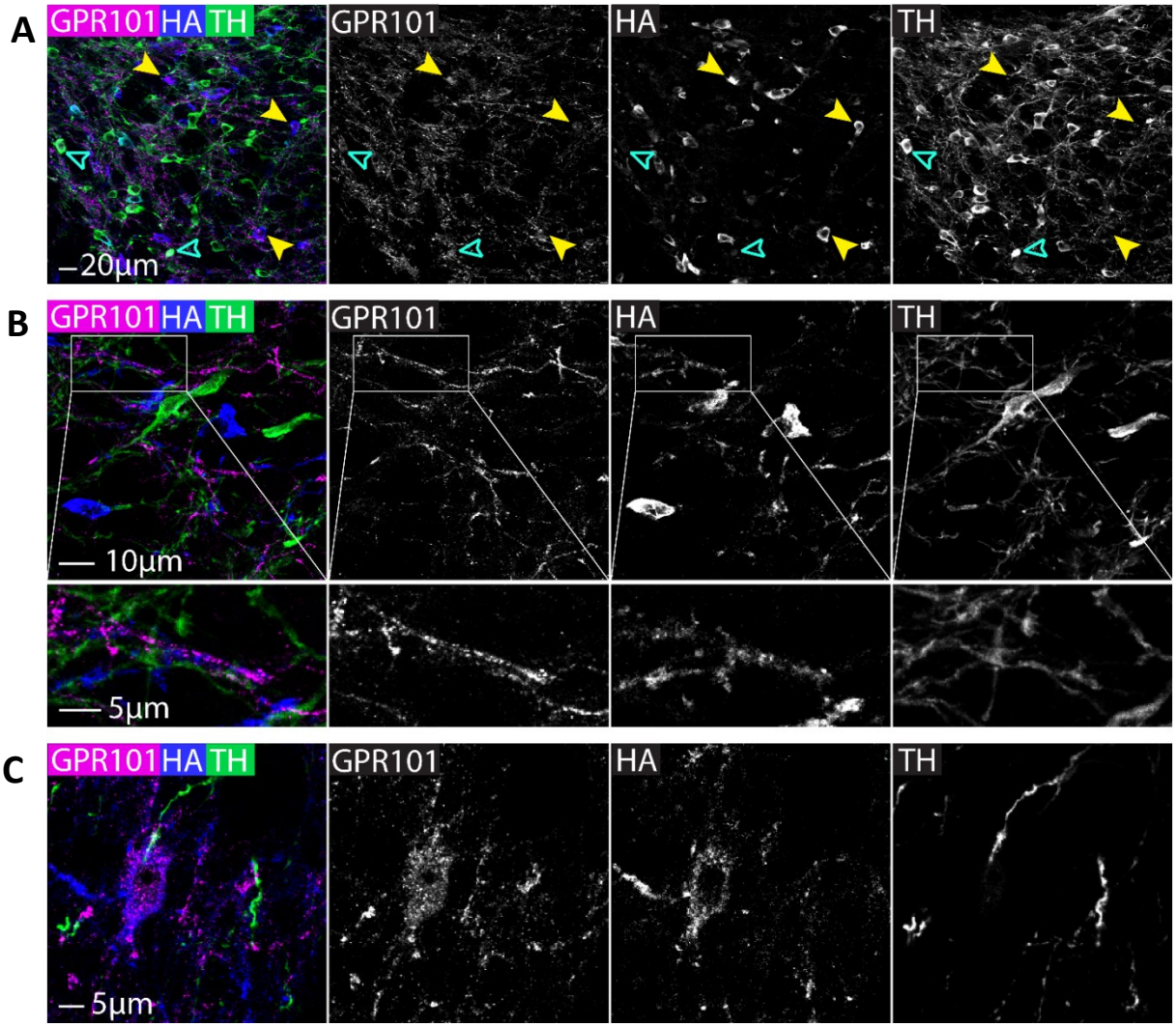


Figure 48: Immunohistochemistry showing the expression of GPR101 in relation to GABA neurons of the VTA and SNc. A: Triple immunostaining for GPR101 (magenta), HA (blue) and TH (green), revealed co-localisation between GPR101 and HA (yellow arrows). GPR101 immnoreactivity is observed in both the cell bodies and the processes of HA+ neurons in the midbrain. There is also some co-localisation between GPR101 and TH (empty cyan arrows). **B:** An example of GPR101+ process that co-localises with HA immnoreactivity in the VTA. **C:** A high resolution example GPR101 expression in a HA+ cell body in the VTA

(ii) Cerebellin 4 (Cbln4)

CBLN4 belongs to a small family of glycoproteins (cerebellins) that belong to the C1q/tumour necrosis factor superfamily. The family consists of four members CBLN1-4 with CBLN1 being the most studied prototypical family member (Chacón *et al*., 2015; Matsuda and Yuzaki, 2011; Wei *et al*., 2012). The cerebellin proteins are involved in the formation and maintenance of synapses in various brain regions (Matsuda and Yuzaki, 2011). CBLN4 binds strongly to presynaptic deleted in colorectal cancer (DDC), a transmembrane receptor that has a well-established role in axon guidance (Wei *et al*., 2012). In the hippocampus CBLN4 expression is localised to GABA interneurons where is plays a role in regulating synapses onto pyramidal neurons . For this reason it has been suggested that deficits in *Cbln4* expression may participate the onset of Alzheimer's Disease (Chacón *et al*., 2015).

Based on the Allen brain atlas ISH hybridisation images CBLN4 looks like the ideal candidate for a genetic marker of VTA neurons **(Figure 49).** There appears to be no expression in the SNc but there is strong signal in the PN and medial PBP. Triple immunostaining of CBLN4, HA and TH in VGATCre:RiboTag mice (n=3) revealed co-localisation between CBLN4 and HA **(Figure 50A).** The immunoreactivity observed appeared in a punctate like fashion, this has previously reported to be the case in other brain regions (Wei *et al*., 2012). A small amount of bright immunoreactivity is also visibe throughout the PBP in TH- HA- cells **(Figure 50B).** These were confirmed as cells using a DAPI stain. The degree of co-localisation between CBLN4 and HA has not yet been quantified. The need for higher resolution images to see the punctate like staining will make quantification a difficult task without the use of a reporter line. Despite this, CBLN4 appears to be expressed in GABA neurons of the VTA. It has the potential for use a novel genetic entry point to selectively target these GABA neurons.

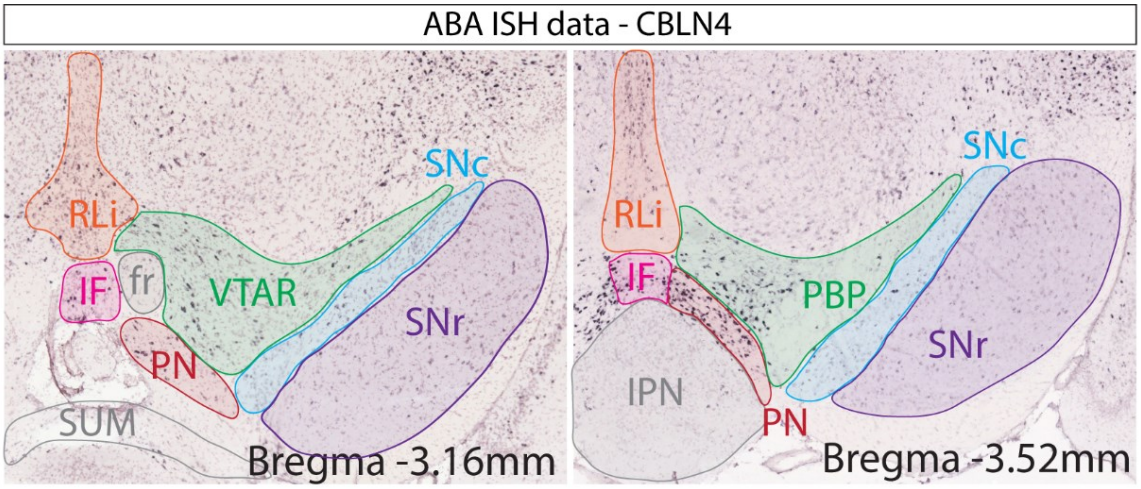


Figure: 49: ISH data from the ABA showing the expression of CBLN4 in the VTA and SNc (Lein *et al.*, 2007). © 2004 Allen Institute for Brain Science. Available from: http://mouse.brain-map.org/ *(Lein et al., 2007)* The right panel shows a coronal section through the rostral VTA and SNc, the image on the left is a more caudal cross section. Sub-regions were drawn on based on outlines in the mouse brain atlas (Franklin and Paxinos, 2008).

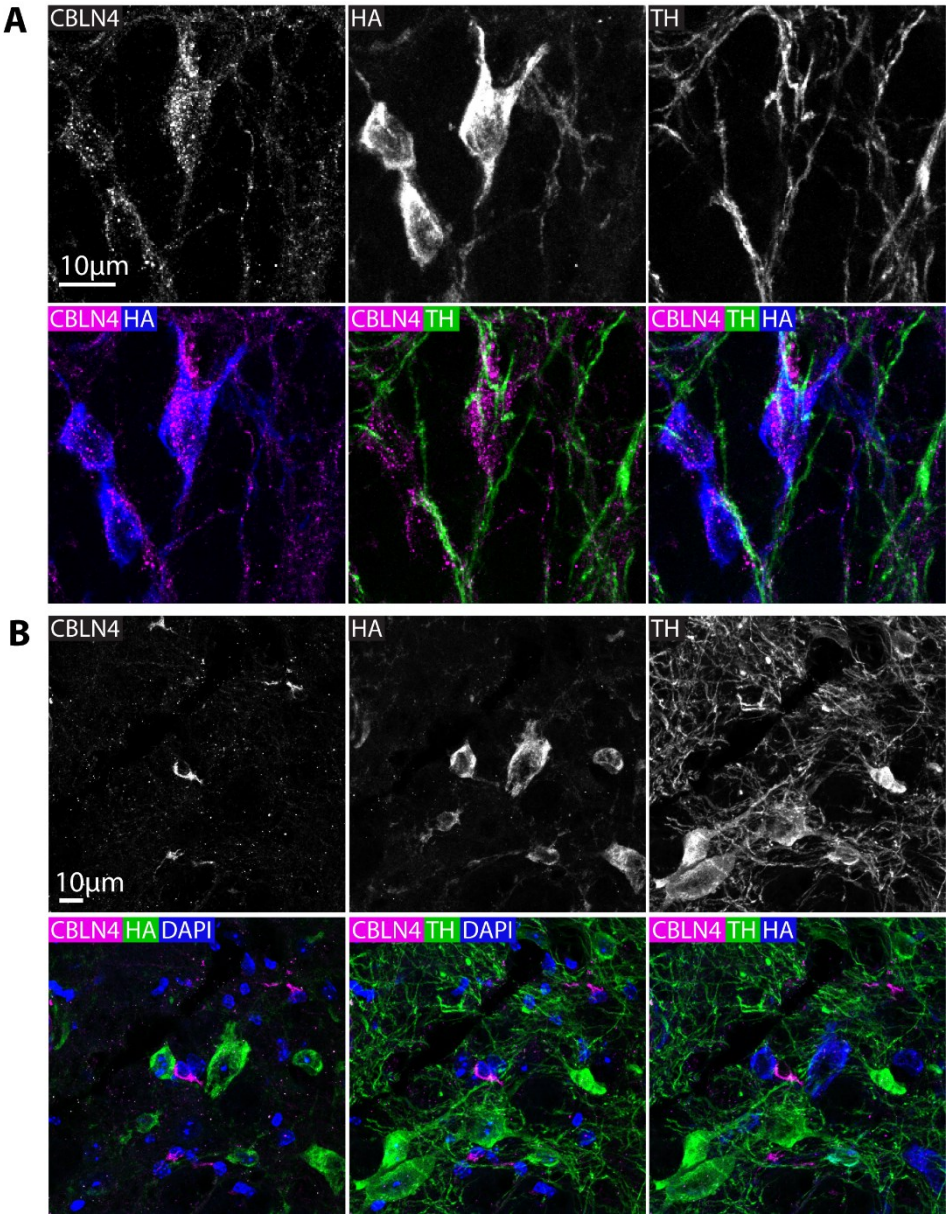


Figure 50: Immunohistochemistry showing the expression of CBLN4 in relation to GABA neurons of the VTA and SNc. A: Triple immunostaining for CBLN4 (magenta), HA (blue) and TH (green), revealed co-localisation between CBLN4 and HA. High resolution images were needed to visualise the punctate like immunoreactivity. **B:** At lower resolutions bright immunoreactivity was sparsely visible in HA- TH- cells (DAPI staining was used to confirm that these were cells).Example images taken for the PBP.

(iii) 4.3.10 Relaxin/insulin like family peptide receptor 3 (Rxfp3)

RxFP3 is a G-protein coupled receptor that is selectively activated by relaxin-3, a neuropeptide that is expressed in a small number of GABA neuron populations across the brain. Whilst the expression of RXFP3 and the activity of relaxin3- has not yet been investigated in the VTA, there is known to be a small population of neurons (~350) dorsal to the SNc that is known to express relaxin-3 (Ma *et al.,* 2007; Ma *et al.,* 2017; Smith *et al.,* 2010). Anatomical and pharmacological evidence so far suggests a role for relaxin-3/RXFP3 signalling in motivation, anxiety and stress related behaviours, circadian rhythms and learning and memory (Ma *et al.,* 2017). ISH images of the VTA and Signal for RXFP3 in the VTA and SNc of the Allen Brain Atlas is extremely sparse with only a few labelled cells in the more rostro medial regions of the VTA **(Figure 51).**

Triple immunohistochemistry for RXFP3, HA and TH in VGATCre:RiboTag mice revealed co-expression between the RXFP3 and HA. Whereas there is very little co-expression between RXFP3 and TH. Although the degree of co-expression has not been quantified, this exploratory data suggests that RXFP3 is predominantly expressed in GABA neurons (**Figure 52**). In the VTAR and the IF nucleus there is RXFP3+ neurons that are TH- and HA- suggesting that RXFP3 is also expressed in some glutamate neurons. These RXFP3+ glutamate neurons do not appear to be present in the RLi nucleus of the more lateral parts of the VTA, where there is significantly less glutamate neurons (Nair-Roberts et al., 2008). In the PN and PBP of the VTA, and in the SNc, there is also some co-localisation between RXFP3 and TH. Although many of these RXFP3+ TH+ cells also express HA+, this does suggest that RXFP3 could be expressed in a proportion of dopamine neurons. The degree of co-localisation between TH/RXFP3/HA has not yet been quantified but the immunostaining suggests that RXFP3 is expressed in a large population of GABA neurons within the VTA and SNc. It looks like a very good candidate as a novel genetic marker for a subpopulation of GABA neurons in these nuclei.

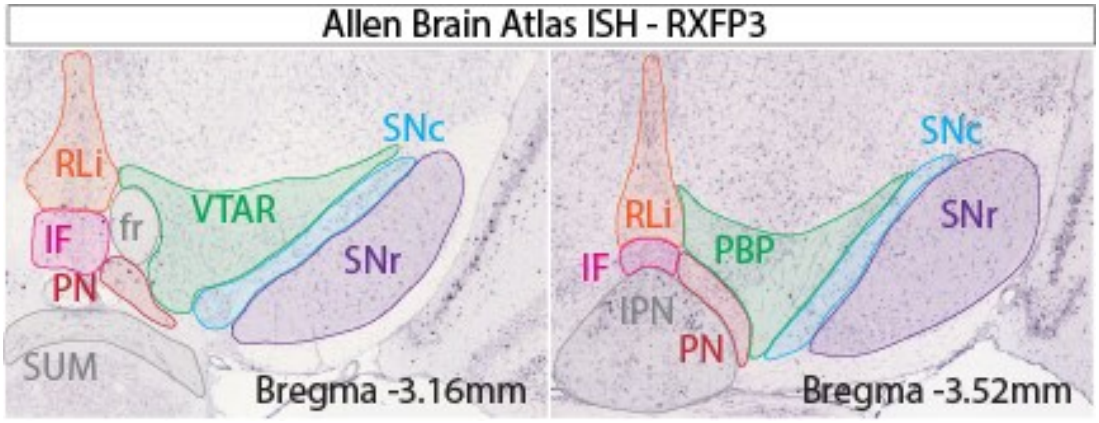


Figure 51: ISH data from the ABA showing the expression of RXFP3 in the VTA and SNc.
© 2004 Allen Institute for Brain Science. Available from: http://mouse.brain-map.org/ *(Lein et al., 2007)* The right panel shows a coronal section through the rostral VTA and SNc, the image on the left is a more caudal cross section. Sub-regions were drawn on based on outlines in the mouse brain atlas (Franklin and Paxinos, 2008).

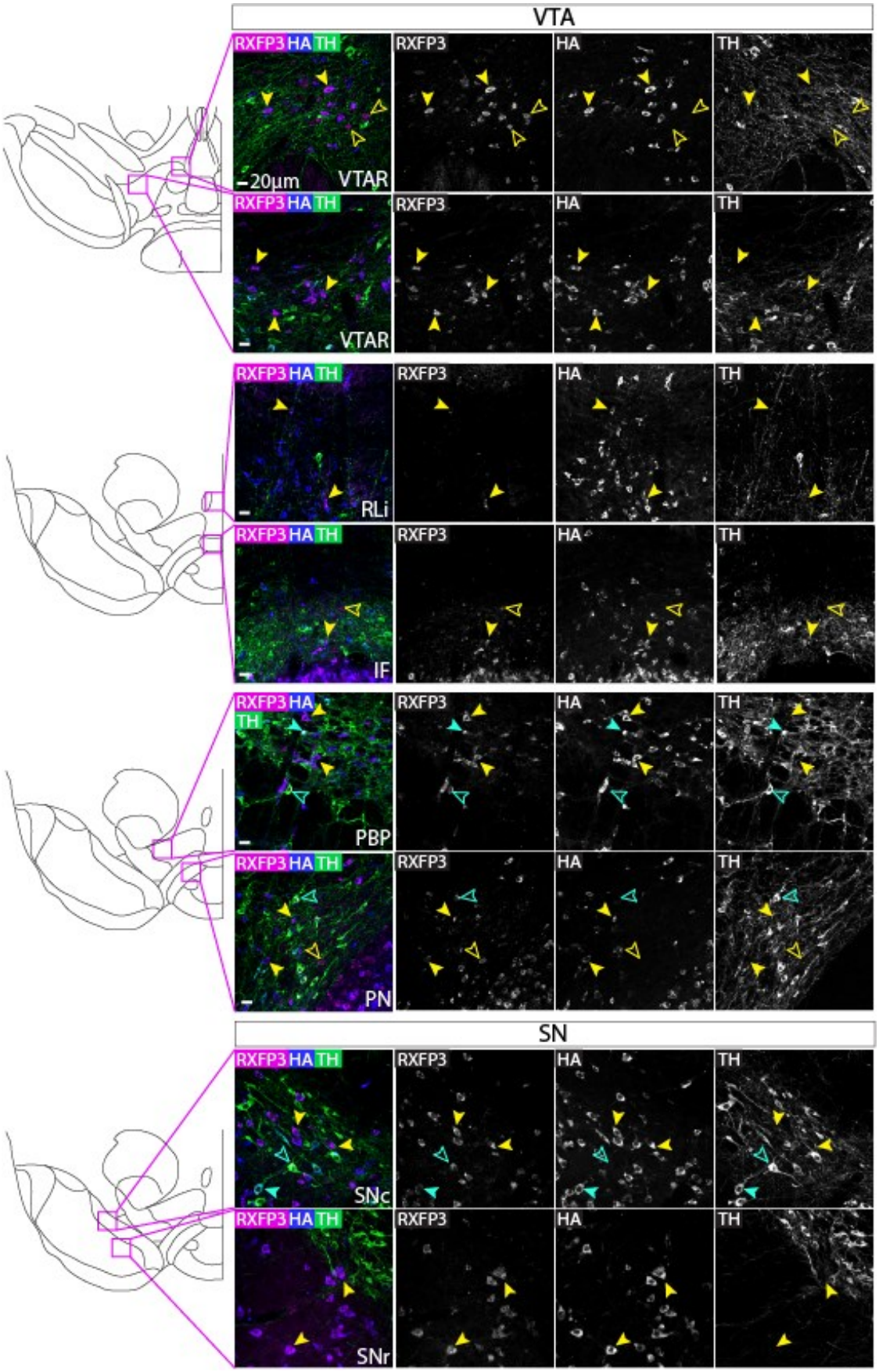


Figure 52: Immunohistochemistry showing the distribution of RXFP3 expressing cells in relation to GABA neurons in the VTA and SNc (legend continued)

Figure 52 continued: Immunohistochemistry showing the distribution of RXFP3 expressing cells in the VTA and SNc Triple immunostaing for RXFP3 (magenta), HA (blue) and TH (green) in different sub-regions of the VTA and SN. There is co-localisation between RXFP3 and HA, these RXFP3+ HA+ neurons are expressed throughout the VTA and SN, some of which are highlighted by solid yellow arrows heads. RXFP3+ cells that are HA- and TH- are present in in the VTAR and IF (empty yellow arrowheads). In the PBP, PN and SNc there is also occasional co-localisation between TH and RXFP3 (empty cyan arrowheads), although some of these TH+ RXFP3+ neurons also express HA. (n=3)

(iv) Retinoic acid related orphan receptor A (Rora)

Rora is a member of the NR1 subfamily of nuclear hormone receptors. It is expressed in abundance in the suprachiasmatic nucleus (SCN) and is known to be necessary for normal circadian rhythms in mice (Akashi and Takumi, 2005; Ko and Takahashi, 2006; Sato *et al*., 2004). RORA binds to bind retinoic acid-related orphan receptor response elements (ROREs) present in the promoter of *Bmal1,* and important circadian clock gene (Ko and Takahashi, 2006). It is also known to be critical for the development of the cerebellum (Dussault *et al.,* 1998) . Gene variants of RORA have been linked to Autism spectrum disorder (ASD)(Akashi and Takumi, 2005). ISH images of the VTA and SNc for RORA expression from the Allen brain atlas are shown in **Figure 53.**

Triple immunostaining for RORA, HA and TH in VGATCre:RiboTag mice revealed co-expression between RORA and HA in all regions of the VTA and SNc. Similar to the patterns observed with RXFP3 expression **(Figure 54).** There was also some co-localisation between RORA and TH. Although the RORA expressing cell shave not been quantified, this exploratory data suggests that the TH+ RORA+ neurons are more prevalent in the IF, PN and SNc. RORA+ HA+ and TH+ neurons and RORA+, HA- and TH- 'putative' glutamate neurons can also be observed. Immunoreactivity for RORA will need to be quantified to determine the proportion of co-expression with HA. So far it seems like a good candidate for use of a novel genetic entry point for targeting a sub-population of GABA neurons in the VTA and SNc.

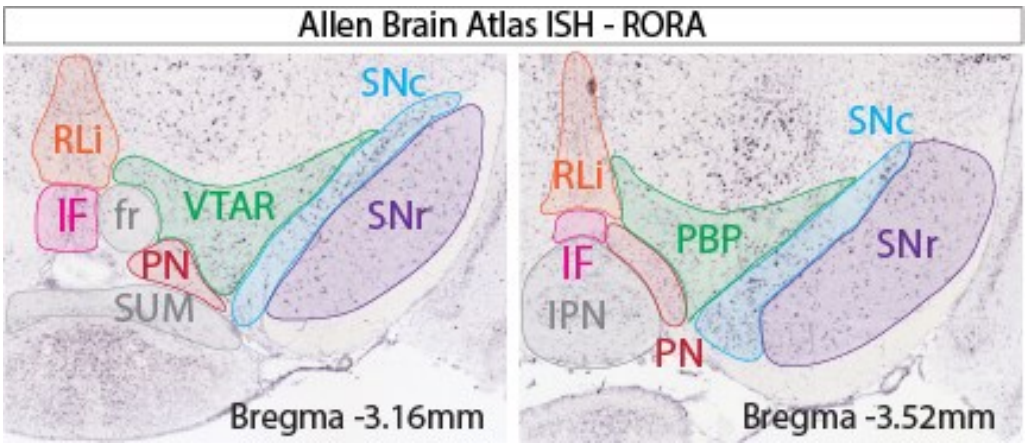


Figure 53: ISH data from the ABA showing the expression of RORA in the VTA and SNc. © 2004 Allen Institute for Brain Science. Available from: http://mouse.brain-map.org/ *(Lein et al., 2007)* The right panel shows a coronal section through the rostral VTA and SNc, the image on the left is a more caudal cross section. Sub-regions were drawn on based on outlines in the mouse brain atlas (Franklin and Paxinos, 2008).

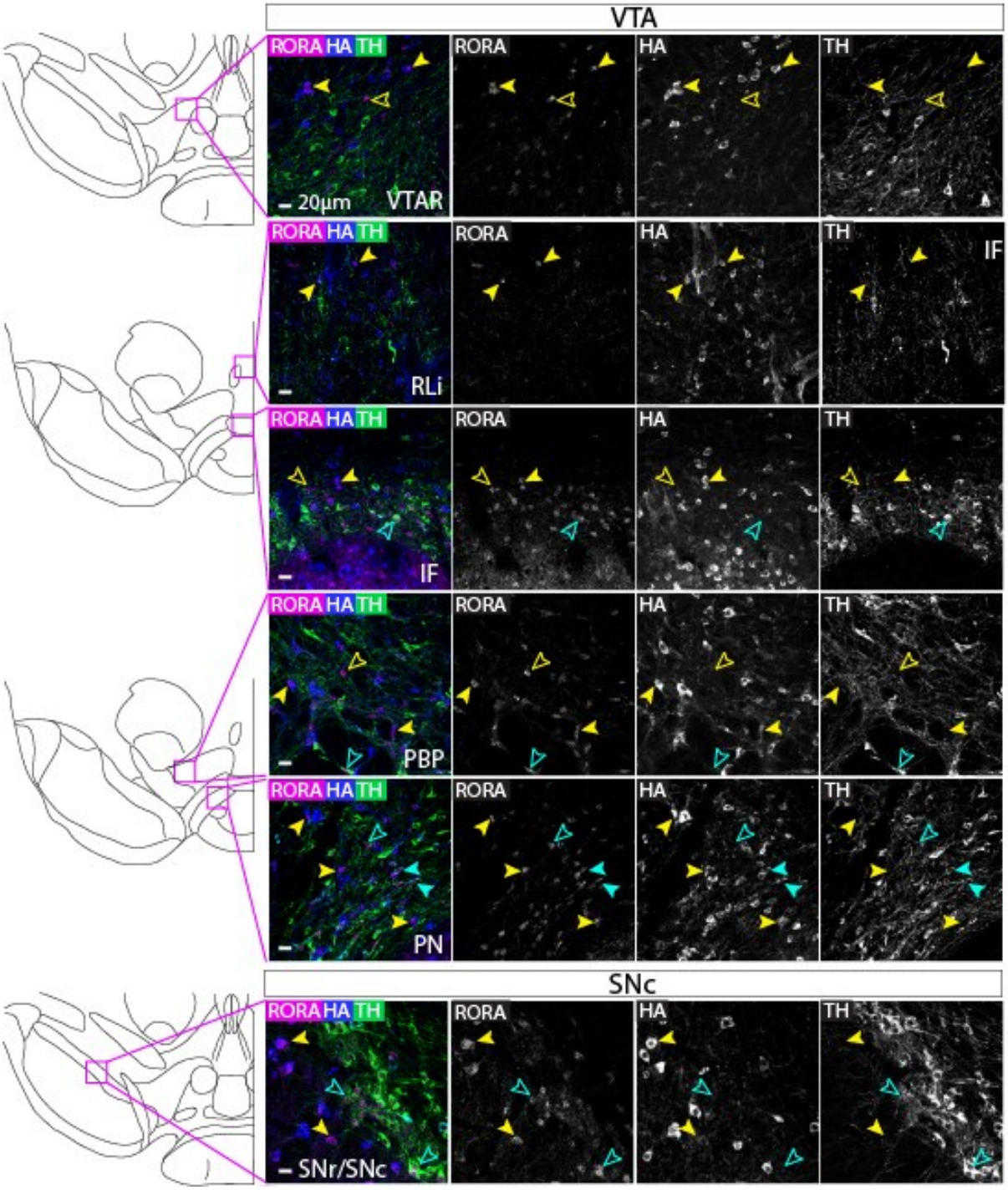


Figure 54: Immunohistochemistry showing the distribution of RORA expressing cells in relation to GABA neurons in the VTA and SNc. There are RORA expressing cells present throughout the VTA and SNc. A large proportion of these RORA expressing cells are HA+ (solid yellow arrows). There is also a population of RORA+ cells that so not co-localise with TH or HA (empty yellow arrows), co-localise with TH+ (empty cyan arrows) or co-localise with both TH and HA (solid cyan arrows) (n=3).

(v) Thyrotropin releasing hormone (TRH)

TRH is a neurotransmitter/neuromodulator that has an important role in the regulation of energy homeostasis, feeding behaviour, thermogenesis, and autonomic regulation (Joseph-Bravo *et al*., 2015, 2016). ISH images from the Allen brain atlas illustrating the expression of TRH in the VTA and SNc is shown in (**Figure** 55). Based on the ISH data only very small numbers of TRH+ neurons were present in the VTA and SNc. Initially immunohistochemistry for TRH in the VTA and SNc appeared unsuccessful. Based on TRH immunohistochemistry studies in the literature, TRH is present in the cytoplasm and therefore visualised in neuron cell bodies. In most cases these studies used homemade antibodies for TRH. In contrast, I observed TRH immnoreactivity in sparse processes throughout the VTA and SNc **(Figure 56).** These TRH+ processes were also observed in the hypothalamus, a region where TRH expressing cells are well characterised **(Figure 56 A).** Despite TRH immunoreactivity being observed in processes in the VTA, we are unable to establish whether these processes are dendrites or axon terminals, therefore, we do not know whether these processes are originating from neurons within the VTA and SNc or neurons from elsewhere in the brain. Although TRH could still be a potential marker for GABA neurons in the VTA or SNc, I feel that this will need to be confirmed with ISH or the use of a reporter line.

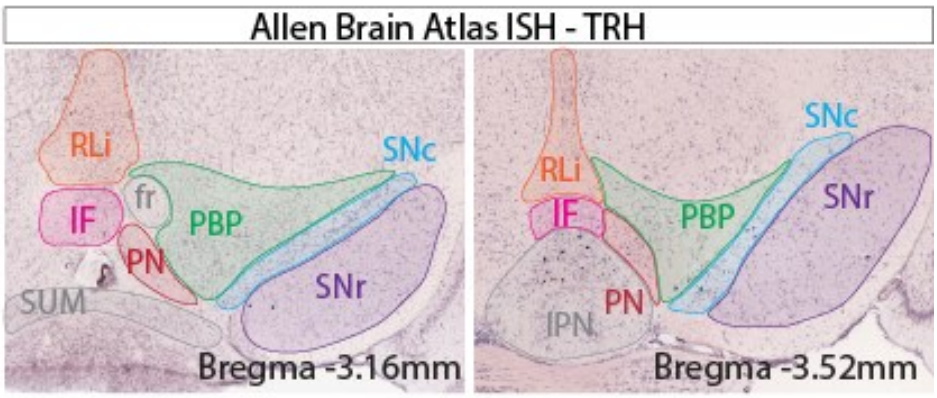


Figure 55: Immunohistochemistry showing the distribution of TRH expressing cells in the VTA and SNc. © 2004 Allen Institute for Brain Science. Available from: http://mouse.brain-map.org/ *(Lein et al., 2007)* The right panel shows a coronal section through the rostral VTA and SNc, the image on the left is a more caudal cross section. Sub-regions were drawn on based on outlines in the mouse brain atlas (Franklin and Paxinos, 2008)

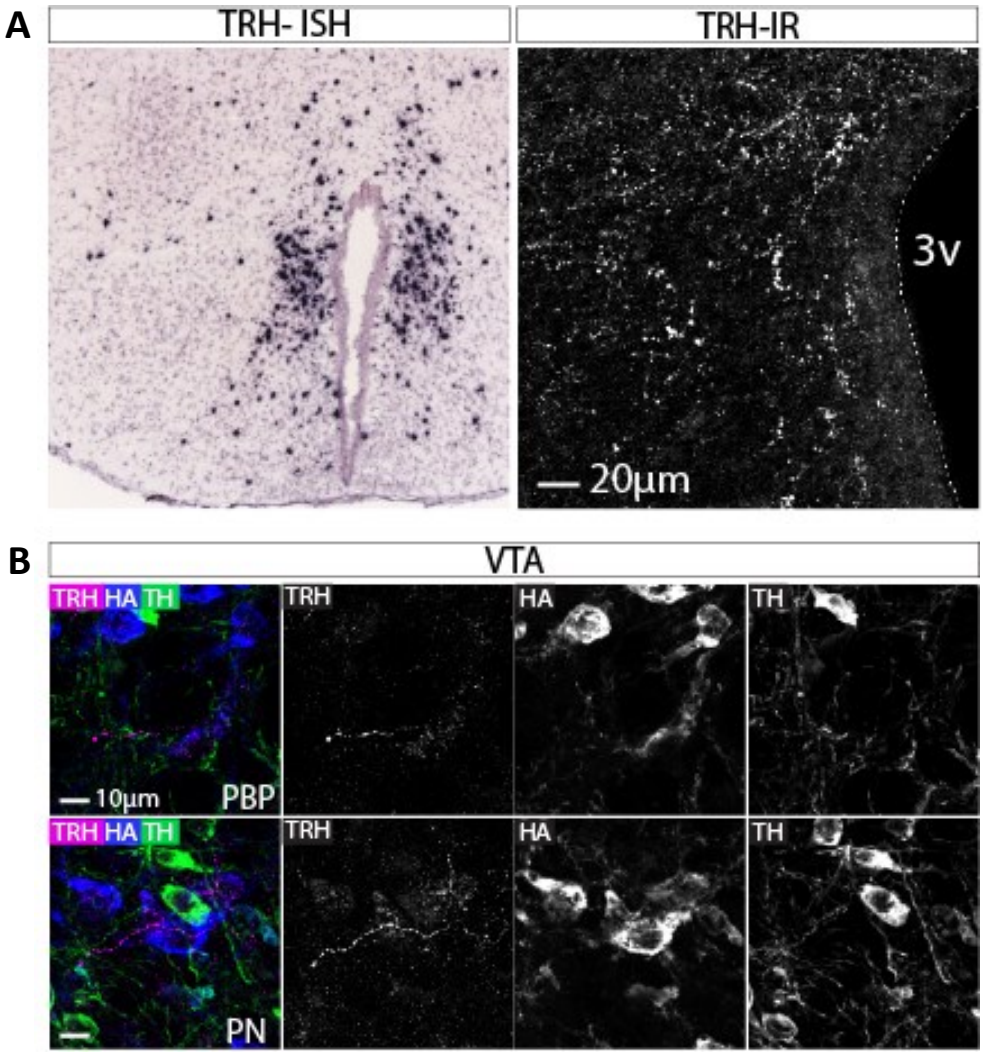


Figure 56: Immunohistochemistry showing the expression of TRH in the hypothalamus and in the VTA. A: A comparison of ISH for TRH from the Allen brain atlas and immunoreactivity observed with anti-TRH in hypothalamus. © 2004 Allen Institute for Brain Science. Available from: http://mouse.brain-map.org/ *(Lein et al., 2007)* **B:** Triple immunostaining of TRH (magenta), HA (blue) and TH (green) in the VTA of VGATCre:RiboTag mice (n=3), example image from the PBP.

(vi) S100 calcium binding protein (S100b)

S100B is a member of the S100 family of calcium binding proteins. It is primarily produced and released by astrocytes in the brain (Rothermundt *et al*., 2003; Yardan *et al*., 2011). Its astrocytic release can either be neurotrophic or neurotoxic depending on concentrations. Its levels in the brain have been shown to be increased in neurodegenerative and inflammatory diseases (Rothermundt *et al*., 2003). Despite being commonly used as an astrocytic marker; its expression is not glial specific. It has been shown to be expressed in neurons in multiple neocortical areas as well as the ventral pallidum and prerubral field (Vives *et al*., 2003).

ISH images from the Allen Brain Atlas revealed s100B expressing cells throughout the sub regions of the VTA and SNc **(Figure 57).** Triple immunostaining in VGATCre:RiboTag tissue showed some colocalistaion between HA+ and s100b+ neurons.. Preliminary images suggest that most HA+ cells were s100B-. In addition, there was S100B immunoreactivity visible throughout the VTA and SNc. This did not co-localise with HA or TH. Based on what we know about s100b expression in astrocytes, it is possible that these regions of immunoreactivity are glial cells. More staining is required to confirm this. It could be investigated with immunostaining for GFAP an astrocyte marker. There is also the possibility that this is background/non-specific staining from the primary antibody **(Figure 58).** Despite there being some co-localisation between HA and S100b, I think that more investigation is required here to determine whether s100B could be used as a molecular marker for GABA neurons in the VTA and SNc.

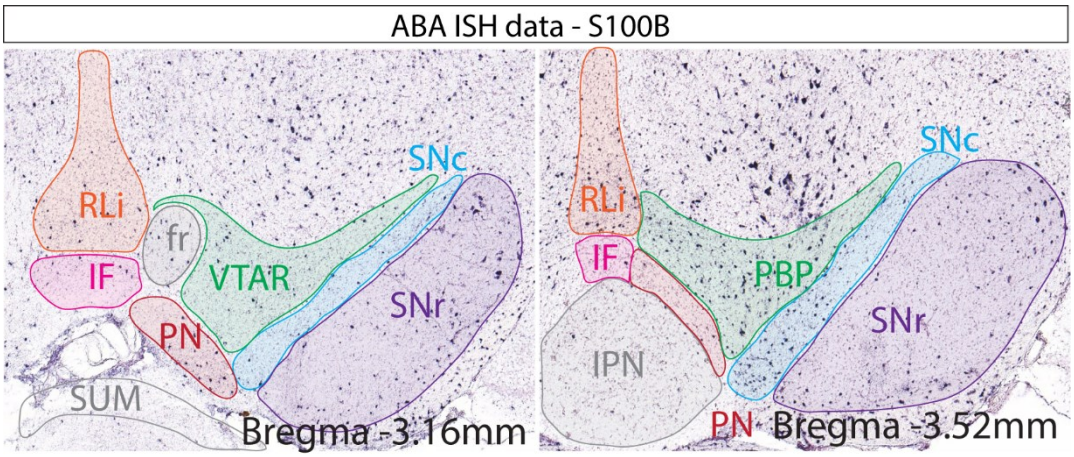


Figure 57: Immunohistochemistry showing the distribution of TRH expressing cells in the VTA and SNc. © 2004 Allen Institute for Brain Science. Available from: http://mouse.brain-map.org/ *(Lein et al., 2007)* The right panel shows a coronal section through the rostral VTA and SNc, the image on the left is a more caudal cross section. Sub-regions were drawn on based on outlines in the mouse brain atlas (Franklin and Paxinos, 2008)

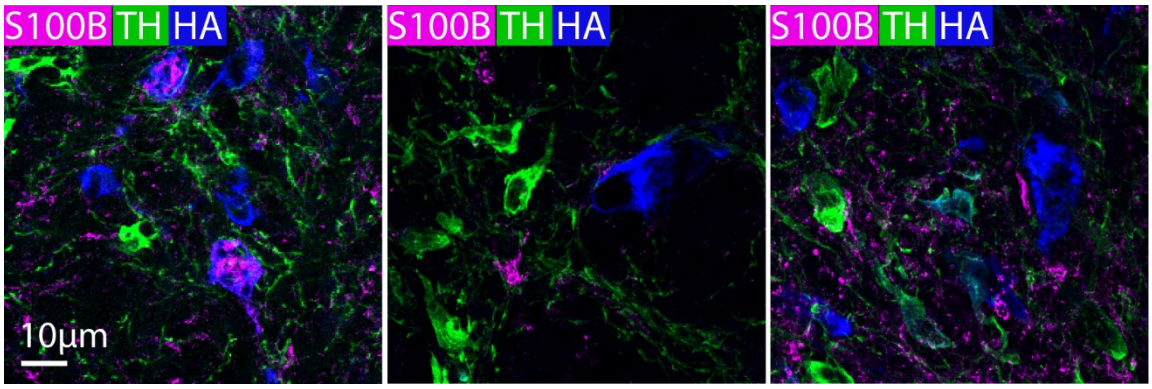


Figure 58: Immunohistochemistry showing the distribution of s100B in the VTA and SNc. There is a small degree of co-localisation between S100B and HA. However, the majority of immunoreactivity observed does not co-localise with HA or TH.

(vii) Neuropilin 2 (Nrp2)

NRP2 is a transmembrane receptor that binds semaphorins SEMA3C and SEMA3F (Chen *et al.,* 2000; Torigoe *et al.,* 2013). NRP2 and its ligand activity has been linked to the axon guidance of various neuronal populations during development, including dopamine neurons (Kolk *et al.,* 2009). Despite this, the expression of NRP2 in the VTA and SNc has not been examined.

ISH images of NRP2 expression in the VTA and SNc is shown in **figure 59**. ISH data from the Allen Brain Atlas (only available in sagittal sections) shows NRP2 expressing cells throughout the VTA sub regions. In agreement with NRP2 immunostaining in the cortex (Tran *et al.,* 2009), NRP2 expression in the VTA and SNc appears to be restricted to dendrites. Because of this, it is difficult to confirm which neuronal population is expressing NRP2. Triple immunostaining for NRP2, HA, and HA in VGATCre:RiboTag mice, revealed NRP2+ dendrites sparsely distributed throughout the VTA and SNc **figure 60.**There is no localisation between TH and NRP2 observed suggesting NRP2 is not expressed in dopamine neurons. Whether or not the NRP2+ dendrites are from GABA neurons or dopamine neurons will have to be established with an alternative method such as ISH or with the use of a reporter line.

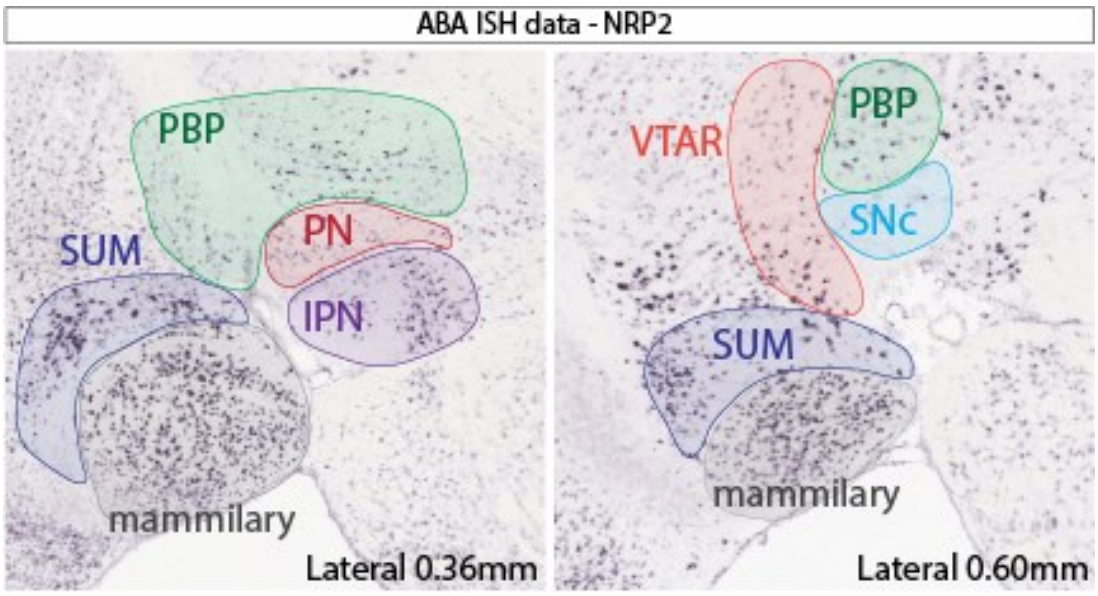


Figure 59: ISH images from the ABA showing the expression of NRP2 in the VTA and SNc (sagittal). © 2004 Allen Institute for Brain Science. Available from: http://mouse.brain-map.org/ *(Lein et al., 2007)*

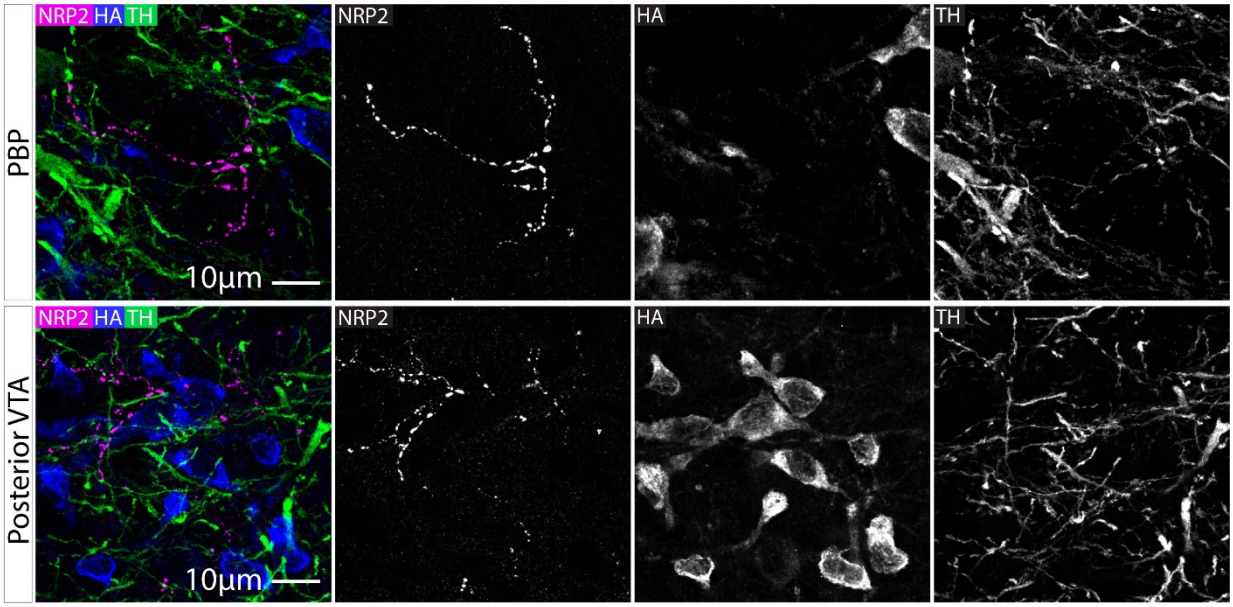


Figure 60: Immunohistochemistry showing examples of NRP2 expressing dendrites in the VTA. NRP2 immunoreactivity is localised to TH- dendrites.

4.4 Discussion

4.4.1 Verification of RNA isolated via immunoprecipitation

Prior to sequencing I took a number of steps to verify the RNA extracted from GABA and dopamine neurons. Using an Agilent Bioanalyser to examine the RNA and ensure that it was good enough quality for further experimentation (RIN <7). I also verified that the RNA was enriched for transcripts specific to the target cell type. I used qRT-PCR for GABA neuron specific transcripts (Vgat and Gad1), dopamine neuron specific transcripts (Dat and Th) and transcripts that are not expressed in either cell type (glial specific markers Gfap and Cnp). GABA-IP RNA exhibited a 7-fold and 4-fold enrichment of Vgat and Gad1 transcripts respectively. A significantly higher fold-enrichment that observed in the Cre-negative control. The dopamine-IP RNA exhibited 25-fold enrichment of both Dat and Th, significantly higher than the Cre-negative littermate. Hence showing that the RNA extracted from the immunoprecipitated polysomes was specific to the target cell type in both cases. When I was confident that the RNA was cell specific I made RNA libraries and sent them for sequencing. The GABA-IP database was directly compared to the dopamine-IP database, my first point of call and as a final verification step, was to check that GABA neuron specific transcripts were significantly enriched compared to dopamine neuron specific transcripts. This is the first gene expression database that is specific to GABA neurons in the midbrain.

4.4.2 Selection of candidate markers for GABA neuron subpopulations

I have presented a novel, systematic and unbiased approach for the selection of candidate markers. 3364 genes were significantly enriched in GABA neurons compared to dopamine neurons. First, we used PANTHER, a gene ontology database to extract sub categories of genes that were more likely to be differentially expressed in functionally different subpopulations. These included transcription factors and categories related to cell communication and signalling. We also hypothesised that many

genes in these categories would be more widely 'usable' candidates in that antibodies and Cre-driver lines would be more readily available.

Second we took the list of significantly enriched genes (reduced using PANTHER) and compared it to the raw expression data for the VTA. These data were extracted from the Allen Brain Atlas and represent quantification (expression density and expression intensity) of the ISH data of all genes detected in the VTA. This was aligned to my sequencing data. We took the average expression density of VGAT, a gene that we know is expressed in 100% of GABA neuron in the VTA and SNc. We were then able to select the genes that, based on the ISH Allen brain atlas data, were expressed in 2-50% of the GABA neuron population. From this reduced list of 255 genes candidates were selected based on mosaic VTA/SNc expression in the Allen brain atlas and the availability of Cre-driver lines. nNOS appearing in the list of final 12 candidates provides validation of the approach taken, since we already know that nNOS is expressed in a subpopulation of GABA neurons in the VTA and SNc **(Chapter 2).**

4.4.3 Limitations to the candidate selection process

The main limitation to the approach taken here was that the mixed cell homogenate used in the IP experiment also contained tissue from the IPN, SNr and red nucleus – all of which contain populations of GABA neurons. Therefore, my transcriptome database for GABA neurons contains genes expressed in these regions. Using the nuclei specific gene list from the Allen brain atlas would have helped to filter out those genes that are expressed more specifically in the surrounding regions. The sub-region boundaries in the Allen brain atlas and the genes within them are estimations based on the mouse brain atlas and the ISH data. In some cases, genes that are known to be expressed in high levels in areas surrounding the VTA and SNc, but in lower levels within the VTA and SNc, appeared to have high expression density and expression intensity values (one example being PV). This suggests that there is some degree of boundary overlap or error. By selecting those candidates that exhibited mosaic

expression in the VTA and SNc in the ISH in the Allen brain atlas would have helped filter out any genes that were erroneously attributed to the VTA.

4.4.4 Validation of candidates

In order to validate the final list of candidate, and determine if they are expressed in GABA neurons, I conducted triple immunostaining in the VTA and SNc of VGATCre:RiboTag mice. All seven candidates (GPR101, CBLN4, RFXP3, RORA, TRH, S100B and NRP2) exhibited some level of immunoreactivity in the VTA and SNc. GPR101, CBLN4, RFXP3, RORA and S100B displayed immunoreactivity in cell bodies and I was able to confirm co-localisation with HA. GPR101, RXFP3 and RORA also exhibited a small degree of co-localisation with TH. These have not yet been quantified, but in all cases TH colocalistaion appeared less abundant than HA co-localisation. This suggests that GPR101, RXFP3 and RORA are expressed more frequently in GABA neurons and, therefore, could make good candidates for molecular markers of GABA neurons in the VTA and SNc.

CBLN4 did not co-localise with TH. It exhibited the punctate immunoreactivity that has previously been observed in the thalamus and hippocampus (Chacón *et al*., 2015; Wei *et al*., 2012). This immunoreactivity can be observed in HA+ cell bodies and HA+ processes. There also appears to be some immunoreactivity in HA- TH- cells. This staining is not the punctate stain expected based on past literature and I am currently uncertain as to whether this is real expression or non-specific staining. CBLN4 is a particularly interesting candidate. In the hippocampus, CBLN4 is expressed in GABA interneurons and is believed to be important in the regulation of inhibitory synapse formation onto principle neurons . It would be interesting to establish whether CBLN4 is expressed in interneurons in the VTA and SNc. NRP2 and TRH exhibited immunoreactivity in processes only. For this reason, I have been unable to confirm co-localisation with HA, which is largely restricted to cell bodies. At no point did NRP2 or TRH immunoreactivity co-localise with TH staining, suggesting they are not expressed in dopamine neurons. The next most likely scenario is that they are expressed in GABA neurons, but this

requires further investigation. S100B exhibited immunoreactivity throughout the VTA and SNc. Although there was some co-localisation with HA, there appeared to be background staining present, and there was a large number or cells that appeared HA- and TH-. This staining combined with the knowledge that s100B is primarily expressed in glial cells in other brain regions suggests that it might not be a suitable candidate for further investigation.

4.4.5 Future directions

Based on my immunostaining data, GPR101, CBLN4, RFXP3, RORA, TRH and NRP2 all have the potential to be good candidates for genetic markers of subpopulations of GABA neurons in the VTA and SNc. A next important step would be to establish the proportion of GABA neurons expressing theses markers, or whether any sub-regional differences occur. In the case of NRP2 and TRH, where immunoreactivity is only seen in processes, this would need to be done with either ISH or by crossing NRP2-Cre and TRH-Cre driver lines with a reporter line. Indeed, all of these candidates have available Cre-driver lines available and crossing these lines with either fluorescent reporters or with RiboTag would be a valuable way of confirming expression of the candidate gene and validating the immunostaining data.

I have provided 6 possible new genetic entry points for the selective targeting of subpopulation of GABA neurons all with available Cre-driver lines. Having confirmed their expression in GABA neurons of the VTA and SNc, the next question to be addressed is whether neurons expressing each of these candidates are GABA projection neuron, interneurons or both. It would be possible to take a similar approach to that shown in Chapters 2 and 3 for nNOS+ and PV+ neurons respectively.

Finally, the overall goal here was to provide novel genetic entry points for subpopulations of GABA neurons in the VTA and SNc for the future study of their function. It was for this reason that we took a bias towards those candidates for which there were existing Cre-Driver lines. Optogenetic approaches could be used to determine the functional connectivity of these subpopulations and their

contribution to the regulation of the dopamine neuron system and ultimately to behavioural output. For those candidates that are also expressed in small populations of dopamine or glutamate neurons (RORA and RXFP3) the Cre-driver lines can be used in conjunction with the VGAT-Flp line and the INTERSECT virus in order to specifically target the GABA neurons.

Chapter 5 – Summary and future directions

Despite being the second largest neural population present in the VTA and SNC, we know remarkably little about the GABA neuron population. For example, we cannot yet answer the fundamental question as to whether the local GABA synapses arise from axon collaterals of GABA neurons that are projecting elsewhere. Or, whether there exists a distinct population of GABA interneurons. This is due to the fact there are no known molecular markers for subpopulations of GABA neurons in the VTA and SNc. Despite this, we know that GABA neurons are functionally important. They play a role in aversion and reward disruption, and have been implicated in associative learning (Brown *et al.,* 2012; Cohen *et al.,* 2012; Tan *et al.,* 2012; van Zessen *et al.,* 2012). They are also the target of many drugs of abuse which hijack the dopamine system by altering GABAergic transmission in the VTA . In other brain regions such as the cortex, hippocampus and striatum, the diversity of GABA neurons has been well studied. We know that GABA neurons - in particular, GABAergic interneurons - exhibit significant diversity (Ascoli *et al*., 2008; Bezaire and Soltesz, 2013; Bikoff *et al*., 2016; DeFelipe *et al*., 2013; Freund and Buzsaki, 1996; Kepecs and Fishell, 2014; Parra *et al*., 1998; Somogyi and Klausberger, 2005; Tepper *et al*., 2010; Tremblay *et al*., 2016). They differ in their electrophysiology, gene expression, morphology and area of target innervation. The occurrence of such diversity in cells that regulate the activity of a system increases the signalling complexity of a network of cells, thus driving complex and diverse behaviours (Kepecs and Fishell, 2014; Tremblay *et al*., 2016). Due to the complexity and broad functions of the midbrain dopamine system we hypothesised that the GABA neurons involved in regulating dopamine neuron activity will display similar levels of diversity.

Presented in this thesis are the results of my investigation into the molecular diversity of GABA neurons in the VTA and SNc. The overall aim of my PhD research was to uncover novel molecular

markers for sub-populations of GABA neurons in the VTA and SNc with the aim of providing genetic entry points for the future study of their function. To achieve this goal, I took two approaches. The first, as described in **chapters 2** and **3** was a 'biased approach' in which in which I selected two known interneuron markers from other brain regions and investigated their expression in the VTA and SNc. nNOS and parvalbumin were selected as candidates due to their being inconclusive literature surrounding their expression in this region. In **chapter 2,** I show through immunostaining and anatomical tracing experiments, that the VTA and SNc contains three distinct sub-populations of nNOS+ neurons. These sub-populations are sub-region specific. The RLI, which lies on the midline, contains projection neurons that are mostly nNOS+ glutamate neurons. The PBP and SNc contains nNOS+ interneurons that are a mostly GABA population. Additionally, the SNc contains a third population, TH+ interneurons, whose phenotype is currently unknown. In **chapter 3** I show through immunostaining and preliminary anatomical tracing studies that there is a small population of PV+ GABA neurons that lie in the SNc and VTAR and are likely to be interneurons. These data provide the first direct evidence that molecularly distinct populations of GABA interneurons exist in the VTA and SNc.

In the second 'unbiased approach', which is discussed in **chapter 4,** I aimed to uncover novel candidates for markers of subpopulation of GABA neurons by directly comparing the transcriptomes from midbrain and GABA and midbrain dopamine neurons. I isolated cell-type specific mRNA for sequencing using immunoprecipitation of tagged polyribosomes. Upon comparing the two transcriptomes I obtained a list of genes significantly enriched in GABA neurons compared to dopamine neurons in the VTA and SNc. As well as making use of the PANTHER gene ontology database to extract gene categories likely to provide usable candidates, I also developed a novel, unbiased approach. I compared the sequencing database to the raw data extracted from the Allen brain atlas. In doing this I established 12 candidates as potential molecular makers of GABA neuron in the VTA. 6 of which were then verified using immunostaining.

Overall my data show that GABA neurons in the VTA and SNc are molecularly diverse. I have provided the first direct evidence for the presence of a distinct population of GABA interneurons (nNOS+) and preliminary evidence for a second (PV+). These two proteins could both be used as genetic entry points for the specific study of GABA interneurons in the VTA and SNc. Until now, due to the lack of molecular markers for interneurons in these regions, there has been no way of distinguishing interneurons from projection neurons. For this reason, studies using optogenetics to investigate the role of GABA neurons in the VTA and SNc have targeted the entire population. Using PV and nNOS as novel genetic entry points would allow researchers to investigate the distinct role of these interneurons in the midbrain dopamine system.

I have also provided the first gene expression database for GABA neurons in the midbrain and the second gene expression database for dopamine neurons. I compared the GABA neuron database to the dopamine neuron database in order to establish genes that are significantly more enriched in GABA neurons. I then used a unique and systematic approach to identify novel markers for subpopulations. This new unbiased approach can be applied to databases for other nuclei in the brain. For example, the transcriptome database I have presented contains information about GABA neurons in the SNr. The quantified ISH data for the SNr could be downloaded and aligned to my database and it can be used to establish candidates for markers of GABA neurons in the SNr. In addition, by comparing the dopamine and GABA neuron databases, the same approach could be used to establish novel candidate for markers of subpopulations of dopamine neurons.

References

Abe, M., Kimoto, H., Eto, R., Sasaki, T., Kato, H., Kasahara, J., and Araki, T. (2010). Postnatal development of neurons, interneurons and glial cells in the substantia nigra of mice. Cellular and molecular neurobiology *30*, 917-928.

Adcock, R.A., Thangavel, A., Whitfield-Gabrieli, S., Knutson, B., and Gabrieli, J.D. (2006). Reward-motivated learning: mesolimbic activation precedes memory formation. Neuron *50*, 507-517.

Akashi, M., and Takumi, T. (2005). The orphan nuclear receptor ROR[alpha] regulates circadian transcription of the mammalian core-clock Bmal1. Nat Struct Mol Biol *12*, 441-448.

Anders, S., Pyl, P.T., and Huber, W. (2015). HTSeq--a Python framework to work with high-throughput sequencing data. Bioinformatics *31*, 166-169.

Aragona, B.J., Cleaveland, N.A., Stuber, G.D., Day, J.J., Carelli, R.M., and Wightman, R.M. (2008). Preferential enhancement of dopamine transmission within the nucleus accumbens shell by cocaine is attributable to a direct increase in phasic dopamine release events. J Neurosci *28*, 8821-8831.

Aransay, A., Rodriguez-Lopez, C., Garcia-Amado, M., Clasca, F., and Prensa, L. (2015). Long-range projection neurons of the mouse ventral tegmental area: a single-cell axon tracing analysis. Front Neuroanat *9*, 59.

Ascoli, G.A., Alonso-Nanclares, L., Anderson, S.A., Barrionuevo, G., Benavides-Piccione, R., Burkhalter, A., Buzsaki, G., Cauli, B., Defelipe, J., Fairen, A*., et al.* (2008). Petilla terminology: nomenclature of features of GABAergic interneurons of the cerebral cortex. Nat Rev Neurosci *9*, 557-568.

Backes, E., and Hemby, S.E. (2003). Discrete cell gene profiling of ventral tegmental dopamine neurons after acute and chronic cocaine self-administration. J Pharmacol Exp Ther *307*, 450-459.

Backman, C.M., Malik, N., Zhang, Y., Shan, L., Grinberg, A., Hoffer, B.J., Westphal, H., and Tomac, A.C. (2006). Characterization of a mouse strain expressing Cre recombinase from the 3' untranslated region of the dopamine transporter locus. Genesis *44*, 383-390.

Baimbridge, K.G., Celio, M.R., and Rogers, J.H. (1992). Calcium-binding proteins in the nervous system. Trends in Neurosciences *15*, 303-308.

Bao, S., Chan, V.T., and Merzenich, M.M. (2001). Cortical remodelling induced by activity of ventral tegmental dopamine neurons. Nature *412*, 79-83.

Bariselli, S., Glangetas, C., Tzanoulinou, S., and Bellone, C. (2016). Ventral tegmental area subcircuits process rewarding and aversive experiences. Journal of neurochemistry *139*, 1071-1080.

Bassareo, V., De Luca, M.A., and Di Chiara, G. (2002). Differential Expression of Motivational Stimulus Properties by Dopamine in Nucleus Accumbens Shell versus Core and Prefrontal Cortex. J Neurosci *22*, 4709-4719.

Beasley, C.L., and Reynolds, G.P. (1997). Parvalbumin-immunoreactive neurons are reduced in the prefrontal cortex of schizophrenics. Schizophrenia research *24*, 349-355.

Beaulieu, J.M., and Gainetdinov, R.R. (2011). The physiology, signaling, and pharmacology of dopamine receptors. Pharmacol Rev *63*, 182-217.

Beckstead, M.J., Grandy, D.K., Wickman, K., and Williams, J.T. (2004). Vesicular Dopamine Release Elicits an Inhibitory Postsynaptic Current in Midbrain Dopamine Neurons. Neuron *42*, 939-946.

Beier, K.T., Steinberg, E.E., DeLoach, K.E., Xie, S., Miyamichi, K., Schwarz, L., Gao, X.J., Kremer, E.J., Malenka, R.C., and Luo, L. (2015). Circuit Architecture of VTA Dopamine Neurons Revealed by Systematic Input-Output Mapping. Cell *162*, 622-634.

Beierlein, M., Gibson, J.R., and Connors, B.W. (2000). A network of electrically coupled interneurons drives synchronized inhibition in neocortex. Nat Neurosci *3*, 904-910.

Bentivoglio, M., and Morelli, M. (2005). Chapter I The organization and circuits of mesencephalic dopaminergic neurons and the distribution of dopamine receptors in the brain. In Handbook of Chemical Neuroanatomy, M.B.A.B. S.B. Dunnett, and T. Hökfelt, eds. (Elsevier), pp. 1-107.

Berrios, J., Stamatakis, A.M., Kantak, P.A., McElligott, Z.A., Judson, M.C., Aita, M., Rougie, M., Stuber, G.D., and Philpot, B.D. (2016). Loss of UBE3A from TH-expressing neurons suppresses GABA co-release and enhances VTA-NAc optical self-stimulation. Nat Commun *7*, 10702.

Betarbet, R., Turner., R., Chockkan, V., DeLong, M.R., Allers, K.A., Walters, J., Levey, A.I., and Greenamyre, J.T. (1997). Dopaminergic Neurons Intrinsic to the Primate Striatum. The Journal of Neuroscience *17*, 6761-6768.

Bezaire, M.J., and Soltesz, I. (2013). Quantitative assessment of CA1 local circuits: knowledge base for interneuron-pyramidal cell connectivity. Hippocampus *23*, 751-785.

Bikoff, J.B., Gabitto, M.I., Rivard, A.F., Drobac, E., Machado, T.A., Miri, A., Brenner-Morton, S., Famojure, E., Diaz, C., Alvarez, F.J.*, et al.* (2016). Spinal Inhibitory Interneuron Diversity Delineates Variant Motor Microcircuits. Cell *165*, 207-219.

Bischop, D.P., Orduz, D., Lambot, L., Schiffmann, S.N., and Gall, D. (2012). Control of Neuronal Excitability by Calcium Binding Proteins: A New Mathematical Model for Striatal Fast-Spiking Interneurons. Frontiers in Molecular Neuroscience *5*, 78.

Bjorklund, A., and Dunnett, S.B. (2007). Dopamine neuron systems in the brain: an update. Trends Neurosci *30*, 194-202.

Bjorklund, A., and Lindvall, O. (1975). Dopamine in dendrites of substantia nigra neurons: suggestions for a role in dendritic terminals. Brain Res *83*, 531-537.

Blazquez-Llorca, L., Woodruff, A., Inan, M., Anderson, S.A., Yuste, R., DeFelipe, J., and Merchan-Perez, A. (2015). Spatial distribution of neurons innervated by chandelier cells. Brain Struct Funct *220*, 2817-2834.

Bocklisch, C., Pascoli, V., Wong, J.C., House, D.R., Yvon, C., de Roo, M., Tan, K.R., and Luscher, C. (2013a). Cocaine disinhibits dopamine neurons by potentiation of GABA transmission in the ventral tegmental area. Science *341*, 1521-1525.

Bocklisch, C., Pascoli, V., Wong, J.C.Y., House, D.R.C., Yvon, C., de Roo, M., Tan, K.R., and Lüscher, C. (2013b). Cocaine Disinhibits Dopamine Neurons by Potentiation of GABA Transmission in the Ventral Tegmental Area. Science *341*, 1521-1525.

Bonci, A., and Williams, J.T. (1997). Increased probability of GABA release during withdrawal from morphine. J Neurosci *17*, 796-803.

Borgius, L., Restrepo, C.E., Leao, R.N., Saleh, N., and Kiehn, O. (2010). A transgenic mouse line for molecular genetic analysis of excitatory glutamatergic neurons. Molecular and cellular neurosciences *45*, 245-257.

Brichta, L., Shin, W., Jackson-Lewis, V., Blesa, J., Yap, E.L., Walker, Z., Zhang, J., Roussarie, J.P., Alvarez, M.J., Califano, A.*, et al.* (2015). Identification of neurodegenerative factors using translatome-regulatory network analysis. Nat Neurosci *18*, 1325-1333.

Brischoux, F., Chakraborty, S., Brierley, D.I., and Ungless, M.A. (2009a). Phasic excitation of dopamine neurons in ventral VTA by noxious stimuli. PNAS *106*, 4894-4899.

Brischoux, F., Chakraborty, S., Brierley, D.I., and Ungless, M.A. (2009b). Phasic excitation of dopamine neurons in ventral VTA by noxious stimuli. Proc Natl Acad Sci U S A *106*, 4894-4899.

Bromberg-Martin, E.S., Matsumoto, M., and Hikosaka, O. (2010). Dopamine in motivational control: rewarding, aversive, and alerting. Neuron *68*, 815-834.

Brown, M.T., Henny, P., Bolam, J.P., and Magill, P.J. (2009). Activity of neurochemically heterogeneous dopaminergic neurons in the substantia nigra during spontaneous and driven changes in brain state. J Neurosci *29*, 2915-2925.

Brown, M.T., Tan, K.R., O'Connor, E.C., Nikonenko, I., Muller, D., and Luscher, C. (2012). Ventral tegmental area GABA projections pause accumbal cholinergic interneurons to enhance associative learning. Nature *492*, 452-456.

Burette, A., Zabel, U., Weinberg, R.J., Schmidt, H.H.H.W., and Valtschanoff, J.G. (2002). Synaptic Localization of Nitric Oxide Synthase and Soluble Guanylyl Cyclase in the Hippocampus. The Journal of Neuroscience *22*, 8961-8970.

Buzsáki, G., and Chrobak, J.J. (1995). Temporal structure in spatially organized neuronal ensembles: a role for interneuronal networks. Current Opinion in Neurobiology *5*, 504-510.

Byrnes, J.J., Pantke, M.M., Onton, J.A., and Hammer, R.P., Jr. (2000). Inhibition of nitric oxide synthase in the ventral tegmental area attenuates cocaine sensitization in rats. Prog Neuropsychopharmacol Biol Psychiatry *24*, 261-273.

Caillard, O., Moreno, H., Schwaller, B., Llano, I., Celio, M.R., and Marty, A. (2000). Role of the calcium-binding protein parvalbumin in short-term synaptic plasticity. Proceedings of the National Academy of Sciences *97*, 13372-13377.

Calapai, G., Altavilla, D., Marciano, M.C., Mazzaglia, G., Cilia, M., Squadrito, F., and Caputi, A.P. (1992). Nitric oxide (NO) mediates antidipsogenic action of Escherichia coli endotoxin (LPS) and tumor necrosis factor (TNF-alpha) in the rat. Pharmacol Res *26 Suppl 2*, 166-167.

Cardin, J.A., Carlen, M., Meletis, K., Knoblich, U., Zhang, F., Deisseroth, K., Tsai, L.H., and Moore, C.I. (2009). Driving fast-spiking cells induces gamma rhythm and controls sensory responses. Nature *459*, 663-667.

Carlsson, A., Falck, B., and Hillarp, N.A. (1962). Cellular localization of brain monoamines. Acta Physiol Scand Suppl *56*, 1-28.

Carr, D.B., and Sesack, S.R. (2000a). GABA-containing neurons in the rat ventral tegmental area project to the prefrontal cortex. Synapse *38*, 114-123.

Carr, D.B., and Sesack, S.R. (2000b). Projections from the rat prefrontal cortex to the ventral tegmental area: target specificity in the synaptic associations with mesoaccumbens and mesocortical neurons. The Journal of neuroscience : the official journal of the Society for Neuroscience *20*, 3864-3873.

Carr, D.B., and Sesack, S.R. (2000c). Projections from the Rat Prefrontal Cortex to the Ventral Tegmental Area: Target Specificity in the Synaptic Associations with Mesoaccumbens and Mesocortical Neurons. The Journal of Neuroscience *20*, 3864-3873.

Carter, D.A. (2017). Molecular phenotyping of transient postnatal tyrosine hydroxylase neurons in the rat bed nucleus of the stria terminalis. J Chem Neuroanat *82*, 29-38.

Cauli, B., and Hamel, E. (2010). Revisiting the role of neurons in neurovascular coupling. Front Neuroenergetics *2*, 9.

Cauli, B., Tong, X.K., Rancillac, A., Serluca, N., Lambolez, B., Rossier, J., and Hamel, E. (2004). Cortical GABA interneurons in neurovascular coupling: relays for subcortical vasoactive pathways. J Neurosci *24*, 8940-8949.

Cavalcanti-Kwiatkoski, R., Raisman-Vozari, R., Ginestet, L., and Del Bel, E. (2010). Altered expression of neuronal nitric oxide synthase in weaver mutant mice. Brain Res *1326*, 40-50.

Cebrián, C., Parent, A., and Prensa, L. (2005). Patterns of axonal branching of neurons of the substantia nigra pars reticulata and pars lateralis in the rat. The Journal of Comparative Neurology *492*, 349-369.

Celio, M.R. (1990). Calbindin D-28k and parvalbumin in the rat nervous system. Neuroscience *35*, 375-475.

Chachlaki, K., Malone, S.A., Qualls-Creekmore, E., Hrabovszky, E., Münzberg, H., Giacobini, P., Ango, F., and Prevot, V. (2017). Phenotyping of nNOS neurons in the postnatal and adult female mouse hypothalamus. Journal of Comparative Neurology *525*, 3177-3189.

Chacón, P.J., del Marco, Á., Arévalo, Á., Domínguez-Giménez, P., García-Segura, L.M., and Rodríguez-Tébar, A. (2015). Cerebellin 4, a synaptic protein, enhances inhibitory activity and resistance of neurons to amyloid-β toxicity. Neurobiology of aging *36*, 1057-1071.

Charara, A., Smith, Y., and Parent, A. (1996). Glutamatergic inputs from the pedunculopontine nucleus to midbrain dopaminergic neurons in primates: Phaseolus vulgaris-leucoagglutinin

anterograde labeling combined with postembedding glutamate and GABA immunohistochemistry. J Comp Neurol *364*, 254-266.

Chard, P.S., Bleakman, D., Christakos, S., Fullmer, C.S., and Miller, R.J. (1993). Calcium buffering properties of calbindin D28k and parvalbumin in rat sensory neurones. The Journal of Physiology *472*, 341-357.

Chen, H., Bagri, A., Zupicich, J.A., Zou, Y., Stoeckli, E., Pleasure, S.J., Lowenstein, D.H., Skarnes, W.C., Chédotal, A., and Tessier-Lavigne, M. (2000). Neuropilin-2 Regulates the Development of Select Cranial and Sensory Nerves and Hippocampal Mossy Fiber Projections. Neuron *25*, 43-56.

Cheramy, A., Leviel, V., and Glowinski, J. (1981). Dendritic release of dopamine in the substantia nigra. Nature *289*, 537-542.

Chieng, B., Azriel, Y., Mohammadi, S., and Christie, M.J. (2011). Distinct cellular properties of identified dopaminergic and GABAergic neurons in the mouse ventral tegmental area. J Physiol *589*, 3775-3787.

Cho, H.J., Xie, Q.W., Calaycay, J., Mumford, R.A., Swiderek, K.M., Lee, T.D., and Nathan, C. (1992). Calmodulin is a subunit of nitric oxide synthase from macrophages. J Exp Med *176*, 599-604.

Chuhma, N., Mingote, S., Moore, H., and Rayport, S. (2014). Dopamine Neurons Control Striatal Cholinergic Neurons via Regionally Heterogeneous Dopamine and Glutamate Signaling. Neuron *81*, 901-912.

Cohen, J.Y., Haesler, S., Vong, L., Lowell, B.B., and Uchida, N. (2012). Neuron-type-specific signals for reward and punishment in the ventral tegmental area. Nature *482*, 85-88.

Comoli, E., Coizet, V., Boyes, J., Bolam, J.P., Canteras, N.S., Quirk, R.H., Overton, P.G., and Redgrave, P. (2003). A direct projection from superior colliculus to substantia nigra for detecting salient visual events. Nat Neurosci *6*, 974-980.

Cooper, S., Robison, A.J., and Mazei-Robison, M.S. (2017). Reward Circuitry in Addiction. Neurotherapeutics : the journal of the American Society for Experimental NeuroTherapeutics *14*, 687-697.

Cossette, M., Lecomte, F., and Parent, A. (2005a). Morphology and distribution of dopaminergic neurons intrinsic to the human striatum. J Chem Neuroanat *29*, 1-11.

Cossette, M., Levesque, D., and Parent, A. (2005b). Neurochemical characterization of dopaminergic neurons in human striatum. Parkinsonism & related disorders *11*, 277-286.

Cossette, M., Parent, A., and Levesque, D. (2004). Tyrosine hydroxylase-positive neurons intrinsic to the human striatum express the transcription factor Nurr1. Eur J Neurosci *20*, 2089-2095.

Cox, B.A., and Johnson, S.W. (1998). Nitric oxide facilitates N-methyl-D-aspartate-induced burst firing in dopamine neurons from rat midbrain slices. Neurosci Lett *255*, 131-134.

Cragg, S.J., Baufreton, J., Xue, Y., Bolam, J.P., and Bevan, M.D. (2004). Synaptic release of dopamine in the subthalamic nucleus. European Journal of Neuroscience *20*, 1788-1802.

Crespo, C., Gracia-Llanes, F.J., Blasco-Ibanez, J.M., Gutierrez-Mecinas, M., Marques-Mari, A.I., and Martinez-Guijarro, F.J. (2003). Nitric oxide synthase containing periglomerular cells are GABAergic in the rat olfactory bulb. Neurosci Lett *349*, 151-154.

Dahlstrom, A., and Fuxe, K. (1964). Localization of monoamines in the lower brain stem. Experientia *20*, 398-399.

DeFelipe, J., Lopez-Cruz, P.L., Benavides-Piccione, R., Bielza, C., Larranaga, P., Anderson, S., Burkhalter, A., Cauli, B., Fairen, A., Feldmeyer, D.*, et al.* (2013). New insights into the classification and nomenclature of cortical GABAergic interneurons. Nat Rev Neurosci *14*, 202-216.

Del-Fava, F., Hasue, R.H., Ferreira, J.G., and Shammah-Lagnado, S.J. (2007). Efferent connections of the rostral linear nucleus of the ventral tegmental area in the rat. Neuroscience *145*, 1059-1076.

Demas, G.E., Kriegsfeld, L.J., Blackshaw, S., Huang, P., Gammie, S.C., Nelson, R.J., and Snyder, S.H. (1999). Elimination of aggressive behavior in male mice lacking endothelial nitric oxide synthase. J Neurosci *19*, RC30.

Di Chiara, G. (2002). Nucleus accumbens shell and core dopamine: differential role in behavior and addiction. Behav Brain Res *137*, 75-114.

Dobi, A., Margolis, E.B., Wang, H.L., Harvey, B.K., and Morales, M. (2010). Glutamatergic and nonglutamatergic neurons of the ventral tegmental area establish local synaptic contacts with dopaminergic and nondopaminergic neurons. J Neurosci *30*, 218-229.

Donato, F., Rompani, S.B., and Caroni, P. (2013). Parvalbumin-expressing basket-cell network plasticity induced by experience regulates adult learning. Nature *504*, 272-276.

Dougalis, A.G., Matthews, G.A., Bishop, M.W., Brischoux, F., Kobayashi, K., and Ungless, M.A. (2012). Functional properties of dopamine neurons and co-expression of vasoactive intestinal polypeptide in the dorsal raphe nucleus and ventro-lateral periaqueductal grey. Eur J Neurosci *36*, 3322-3332.

Dubach, M., Schmidt, R., Kunkel, D., Bowden, D.M., Martin, R., and German, D.C. (1987). Primate neostriatal neurons containing tyrosine hydroxylase: immunohistochemical evidence. Neurosci Lett *75*, 205-210.

Dussault, I., Fawcett, D., Matthyssen, A., Bader, J.-A., and Giguère, V. (1998). Orphan nuclear receptor RORα-deficient mice display the cerebellar defects of staggerer. Mechanisms of Development *70*, 147-153.

Eiden, L.E., Schafer, M.K., Weihe, E., and Schutz, B. (2004). The vesicular amine transporter family (SLC18): amine/proton antiporters required for vesicular accumulation and regulated exocytotic secretion of monoamines and acetylcholine. Pflugers Arch *447*, 636-640.

Eshel, N., Tian, J., Bukwich, M., and Uchida, N. (2016). Dopamine neurons share common response function for reward prediction error. Nat Neurosci *19*, 479-486.

Faget, L., Osakada, F., Duan, J., Ressler, R., Johnson, Alexander B., Proudfoot, James A., Yoo, Ji H., Callaway, Edward M., and Hnasko, Thomas S. (2016). Afferent Inputs to Neurotransmitter-Defined Cell Types in the Ventral Tegmental Area. Cell Reports *15*, 2796-2808.

Falck, B., Hillarp, N.A., Thieme, G., Torp, A. (1962). Fluorescence of catecholamines and related compounds condensed with formaldehyde. J Histochem Cytochem *10* 348–354.

Fallon, J.H., and Loughlin, S.E. (1982). Monoamine innervation of the forebrain: Collateralization. Brain Research Bulletin *9*, 295-307.

Fazzari, P., Paternain, A.V., Valiente, M., Pla, R., Lujan, R., Lloyd, K., Lerma, J., Marin, O., and Rico, B. (2010). Control of cortical GABA circuitry development by Nrg1 and ErbB4 signalling. Nature *464*, 1376-1380.

Fenno, L.E., Mattis, J., Ramakrishnan, C., Hyun, M., Lee, S.Y., He, M., Tucciarone, J., Selimbeyoglu, A., Berndt, A., Grosenick, L*., et al.* (2014). INTRSECT: single-component targeting of cells using multiple-feature Boolean logic. Nature methods *11*, 763-772.

Fishell, G., and Rudy, B. (2011). Mechanisms of Inhibition within the Telencephalon: "Where the Wild Things Are". Annual Review of Neuroscience *34*, 535-567.

Ford, B., Holmes, C.J., Mainville, L., and Jones, B.E. (1995). GABAergic neurons in the rat pontomesencephalic tegmentum: codistribution with cholinergic and other tegmental neurons projecting to the posterior lateral hypothalamus. J Comp Neurol *363*, 177-196.

Frank, M.J. (2005). Dynamic dopamine modulation in the basal ganglia: a neurocomputational account of cognitive deficits in medicated and nonmedicated Parkinsonism. Journal of cognitive neuroscience *17*, 51-72.

Franklin, K.B.J., and Paxinos, G. (2008). The mouse brain in stereotaxic coordinates ([Amsterdam] [u.a.: Acad. Press).

Freund, T.F., and Buzsaki, G. (1996). Interneurons of the hippocampus. Hippocampus *6*, 347-470.

Fu, Y., Yuan, Y., Halliday, G., Rusznák, Z., Watson, C., and Paxinos, G. (2012). A cytoarchitectonic and chemoarchitectonic analysis of the dopamine cell groups in the substantia nigra, ventral tegmental area, and retrorubral field in the mouse. Brain Structure and Function *217*, 591-612.

Fuentealba, P., Begum, R., Capogna, M., Jinno, S., Marton, L.F., Csicsvari, J., Thomson, A., Somogyi, P., and Klausberger, T. (2008). Ivy cells: a population of nitric-oxide-producing, slow-spiking GABAergic neurons and their involvement in hippocampal network activity. Neuron *57*, 917-929.

Furchgott, R.F. (1983). Role of endothelium in responses of vascular smooth muscle. Circ Res *53*, 557-573.

Furchgott, R.F., and Zawadzki, J.V. (1980). The obligatory role of endothelial cells in the relaxation of arterial smooth muscle by acetylcholine. Nature *288*, 373-376.

Gantz, S.C., Ford, C.P., Morikawa, H., and Williams, J.T. (2018). The Evolving Understanding of Dopamine Neurons in the Substantia Nigra and Ventral Tegmental Area. Annual Review of Physiology *80*, null.

Garthwaite, J. (1991). Glutamate, nitric oxide and cell-cell signalling in the nervous system. Trends Neurosci *14*, 60-67.

Garthwaite, J., Charles, S.L., and Chess-Williams, R. (1988). Endothelium-derived relaxing factor release on activation of NMDA receptors suggests role as intercellular messenger in the brain. Nature *336*, 385-388.

Gautier-Sauvigne, S., Colas, D., Parmantier, P., Clement, P., Gharib, A., Sarda, N., and Cespuglio, R. (2005). Nitric oxide and sleep. Sleep Med Rev *9*, 101-113.

Geffen, L.B., Jessell, T.M., Cuello, A.C., and Iversen, L.L. (1976). Release of dopamine from dendrites in rat substantia nigra. Nature *260*, 258-260.

Georges, F., and Aston-Jones, G. (2001). Potent Regulation of Midbrain Dopamine Neurons by the Bed Nucleus of the Stria Terminalis. The Journal of Neuroscience *21*, RC160-RC160.

Gerashchenko, D., Wisor, J.P., Burns, D., Reh, R.K., Shiromani, P.J., Sakurai, T., de la Iglesia, H.O., and Kilduff, T.S. (2008). Identification of a population of sleep-active cerebral cortex neurons. Proc Natl Acad Sci U S A *105*, 10227-10232.

Gerfen, C.R., Baimbridge, K.G., and Miller, J.J. (1985). The neostriatal mosaic: compartmental distribution of calcium-binding protein and parvalbumin in the basal ganglia of the rat and monkey. Proc Natl Acad Sci U S A *82*, 8780-8784.

German, D.C., and Manaye, K.F. (1993a). Midbrain dopaminergic neurons (nuclei A8, A9, and A10): three-dimensional reconstruction in the rat. J Comp Neurol *331*, 297-309.

German, D.C., and Manaye, K.F. (1993b). Midbrain dopaminergic neurons (nuclei A8, A9, and A10): Three-dimensional reconstruction in the rat. Journal of Comparative Neurology *331*, 297-309.

Gholami, A., Zarrindast, M.R., Sahraei, H., and Haerri-Rohani, A. (2003). Nitric oxide within the ventral tegmental area is involved in mediating morphine reward. Eur J Pharmacol *458*, 119-128.

Gholipour, T., Ghasemi, M., Riazi, K., Ghaffarpour, M., and Dehpour, A.R. (2010). Seizure susceptibility alteration through 5-HT(3) receptor: modulation by nitric oxide. Seizure *19*, 17-22.

Gibson, J.R., Beierlein, M., and Connors, B.W. (1999). Two networks of electrically coupled inhibitory neurons in neocortex. Nature *402*, 75-79.

Goldberg, E.M., Jeong, H.Y., Kruglikov, I., Tremblay, R., Lazarenko, R.M., and Rudy, B. (2011). Rapid developmental maturation of neocortical FS cell intrinsic excitability. Cereb Cortex *21*, 666-682.

Gonzalez-Hernandez, T., and Rodriguez, M. (2000). Compartmental organization and chemical profile of dopaminergic and GABAergic neurons in the substantia nigra of the rat. J Comp Neurol *421*, 107-135.

Goto, Y., Otani, S., and Grace, A.A. (2007). The Yin and Yang of dopamine release: a new perspective. Neuropharmacology *53*, 583-587.

Gotti, S., Sica, M., Viglietti-Panzica, C., and Panzica, G. (2005). Distribution of nitric oxide synthase immunoreactivity in the mouse brain. Microsc Res Tech *68*, 13-35.

Grace, A.A. (1991). Phasic versus tonic dopamine release and the modulation of dopamine system responsivity: a hypothesis for the etiology of schizophrenia. Neuroscience *41*, 1-24.

Grace, A.A., and Bunney, B.S. (1980). Nigral dopamine neurons: intracellular recording and identification with L-dopa injection and histofluorescence. Science *210*, 654-656.

Grace, A.A., and Bunney, B.S. (1984a). The control of firing pattern in nigral dopamine neurons: burst firing. J Neurosci *4*, 2877-2890.

Grace, A.A., and Bunney, B.S. (1984b). The control of firing pattern in nigral dopamine neurons: single spike firing. J Neurosci *4*, 2866-2876.

Grace, A.A., Skirboll, L.R., and Bunney, B.S. (1980). Dopamine auto- and postsynaptic receptors: possible interference by gallamine. Science *209*, 721.

Greene, J.G., Dingledine, R., and Greenamyre, J.T. (2005a). Gene expression profiling of rat midbrain dopamine neurons: implications for selective vulnerability in parkinsonism. Neurobiology of disease *18*, 19-31.

Greene, J.G., Dingledine, R., and Greenamyre, J.T. (2005b). Gene expression profiling of rat midbrain dopamine neurons: implications for selective vulnerability in parkinsonism. Neurobiol Dis *18*, 19-31.

Grimm, J., Mueller, A., Hefti, F., and Rosenthal, A. (2004a). Molecular basis for catecholaminergic neuron diversity. PNAS *101*, 13891-13896.

Grimm, J., Mueller, A., Hefti, F., and Rosenthal, A. (2004b). Molecular basis for catecholaminergic neuron diversity. Proc Natl Acad Sci U S A *101*, 13891-13896.

Guix, F.X., Uribesalgo, I., Coma, M., and Muñoz, F.J. (2005). The physiology and pathophysiology of nitric oxide in the brain. Progress in Neurobiology *76*, 126-152.

Gunaydin, L.A., Grosenick, L., Finkelstein, J.C., Kauvar, I.V., Fenno, L.E., Adhikari, A., Lammel, S., Mirzabekov, J.J., Airan, R.D., Zalocusky, K.A*., et al.* (2014). Natural neural projection dynamics underlying social behavior. Cell *157*, 1535-1551.

Gupta, A., Wang, Y., and Markram, H. (2000). Organizing Principles for a Diversity of GABAergic Interneurons and Synapses in the Neocortex. Science *287*, 273-278.

Halliday, G.M., and Tork, I. (1986). Comparative anatomy of the ventromedial mesencephalic tegmentum in the rat, cat, monkey and human. J Comp Neurol *252*, 423-445.

Hardingham, N., Dachtler, J., and Fox, K. (2013). The role of nitric oxide in pre-synaptic plasticity and homeostasis. Front Cell Neurosci *7*, 190.

Harris, H.W., and Nestler, E.J. (1996). Immunohistochemical studies of mesolimbic dopaminergic neurons in Fischer 344 and Lewis rats. Brain Research *706*, 1-12.

Hashimoto, T., Volk, D.W., Eggan, S.M., Mirnics, K., Pierri, J.N., Sun, Z., Sampson, A.R., and Lewis, D.A. (2003). Gene expression deficits in a subclass of GABA neurons in the prefrontal cortex of subjects with schizophrenia. J Neurosci *23*, 6315-6326.

Heiman, M., Schaefer, A., Gong, S., Peterson, J.D., Day, M., Ramsey, K.E., Suarez-Farinas, M., Schwarz, C., Stephan, D.A., Surmeier, D.J*., et al.* (2008). A translational profiling approach for the molecular characterization of CNS cell types. Cell *135*, 738-748.

Hibbs, J.B., Jr., Taintor, R.R., and Vavrin, Z. (1987). Macrophage cytotoxicity: role for L-arginine deiminase and imino nitrogen oxidation to nitrite. Science *235*, 473-476.

Higo, S., Akashi, K., Sakimura, K., and Tamamaki, N. (2009). Subtypes of GABAergic neurons project axons in the neocortex. Front Neuroanat *3*, 25.

Hikida, T., Jaaro-Peled, H., Seshadri, S., Oishi, K., Hookway, C., Kong, S., Wu, D., Xue, R., Andrade, M., Tankou, S*., et al.* (2007). Dominant-negative DISC1 transgenic mice display schizophrenia-associated phenotypes detected by measures translatable to humans. Proc Natl Acad Sci U S A *104*, 14501-14506.

Hikida, T., Kimura, K., Wada, N., Funabiki, K., and Nakanishi, S. (2010). Distinct roles of synaptic transmission in direct and indirect striatal pathways to reward and aversive behavior. Neuron *66*, 896-907.

Hikosaka, O. (2007). Basal ganglia mechanisms of reward-oriented eye movement. Ann N Y Acad Sci *1104*, 229-249.

Hippenmeyer, S., Vrieseling, E., Sigrist, M., Portmann, T., Laengle, C., Ladle, D.R., and Arber, S. (2005). A Developmental Switch in the Response of DRG Neurons to ETS Transcription Factor Signaling. PLoS Biology *3*, e159.

Hjelmstad, G.O., Xia, Y., Margolis, E.B., and Fields, H.L. (2013). Opioid modulation of ventral pallidal afferents to ventral tegmental area neurons. J Neurosci *33*, 6454-6459.

Hnasko, T.S., Hjelmstad, G.O., Fields, H.L., and Edwards, R.H. (2012). Ventral tegmental area glutamate neurons: electrophysiological properties and projections. J Neurosci *32*, 15076-15085.

Hochbaum, D.R., Zhao, Y., Farhi, S.L., Klapoetke, N., Werley, C.A., Kapoor, V., Zou, P., Kralj, J.M., Maclaurin, D., Smedemark-Margulies, N*., et al.* (2014). All-optical electrophysiology in mammalian neurons using engineered microbial rhodopsins. Nat Methods *11*, 825-833.

Hökfelt, T., Everitt, B.J., Theodorsson-Norheim, E., and Goldstein, M. (1984). Occurrence of neurotensinlike immunoreactivity in subpopulations of hypothalamic, mesencephalic, and medullary catecholamine neurons. The Journal of Comparative Neurology *222*, 543-559.

Hokfelt, T., Fuxe, K., Goldstein, M., and Joh, T.H. (1973). Immunohistochemical localization of three catecholamine synthesizing enzymes: aspects on methodology. Histochemie *33*, 231-254.

Hokfelt, T., Rehfeld, J.F., Skirboll, L., Ivemark, B., Goldstein, M., and Markey, K. (1980). Evidence for coexistence of dopamine and CCK in meso-limbic neurones. Nature *285*, 476-478.

Hong, S., Jhou, T.C., Smith, M., Saleem, K.S., and Hikosaka, O. (2011). Negative Reward Signals from the Lateral Habenula to Dopamine Neurons Are Mediated by Rostromedial Tegmental Nucleus in Primates. The Journal of Neuroscience *31*, 11457-11471.

Honsa, P., Pivonkova, H., Harantova, L., Butenko, O., Kriska, J., Dzamba, D., Rusnakova, V., Valihrach, L., Kubista, M., and Anderova, M. (2014). Increased expression of hyperpolarization-activated cyclic nucleotide-gated (HCN) channels in reactive astrocytes following ischemia. Glia *62*, 2004-2021.

Hontanilla, B., Parent, A., and Giménez-Amaya, J. (1995). Heterogeneous distribution of neurons containing calbindin D-28k and/or parvalbumin in the rat red nucleus. Brain research *696*, 121-126.

Hontanilla, B., Parent, A., and Giménez-Amaya, J.M. (1997). Parvalbumin and calbindin D-28k in the entopeduncular nucleus, subthalamic nucleus, and substantia nigra of the rat as revealed by double-immunohistochemical methods. Synapse *25*, 359-367.

Hope, B.T., Michael, G.J., Knigge, K.M., and Vincent, S.R. (1991). Neuronal NADPH diaphorase is a nitric oxide synthase. Proc Natl Acad Sci U S A *88*, 2811-2814.

Howes, O.D., McCutcheon, R., Owen, M.J., and Murray, R.M. (2017). The Role of Genes, Stress, and Dopamine in the Development of Schizophrenia. Biol Psychiatry *81*, 9-20.

Hu, H., Gan, J., and Jonas, P. (2014). Interneurons. Fast-spiking, parvalbumin(+) GABAergic interneurons: from cellular design to microcircuit function. Science *345*, 1255263.

Huang, P.L., Dawson, T.M., Bredt, D.S., Snyder, S.H., and Fishman, M.C. (1993). Targeted disruption of the neuronal nitric oxide synthase gene. Cell *75*, 1273-1286.

Huang, P.L., Huang, Z., Mashimo, H., Bloch, K.D., Moskowitz, M.A., Bevan, J.A., and Fishman, M.C. (1995). Hypertension in mice lacking the gene for endothelial nitric oxide synthase. Nature *377*, 239-242.

Ibanez-Sandoval, O., Tecuapetla, F., Unal, B., Shah, F., Koos, T., and Tepper, J.M. (2010). Electrophysiological and morphological characteristics and synaptic connectivity of tyrosine hydroxylase-expressing neurons in adult mouse striatum. J Neurosci *30*, 6999-7016.

Ibáñez-Sandoval, O., Tecuapetla, F., Unal, B., Shah, F., Koós, T., and Tepper, J.M. (2010). Electrophysiological and Morphological Characteristics and Synaptic Connectivity of Tyrosine Hydroxylase-Expressing Neurons in Adult Mouse Striatum. The Journal of Neuroscience *30*, 6999-7016.

Ikemoto, S. (2007). Dopamine reward circuitry: two projection systems from the ventral midbrain to the nucleus accumbens-olfactory tubercle complex. Brain Res Rev *56*, 27-78.

Isaacs, K.R., and Jacobowitz, D.M. (1994). Mapping of the colocalization of calretinin and tyrosine hydroxylase in the rat substantia nigra and ventral tegmental area. Experimental Brain Research *99*, 34-42.

J Garthwaite, a., and Boulton, C.L. (1995). Nitric Oxide Signaling in the Central Nervous System. Annual Review of Physiology *57*, 683-706.

Jackson-Lewis, V., and Smeyne, R.J. (2005). MPTP and SNpc DA neuronal vulnerability: role of dopamine, superoxide and nitric oxide in neurotoxicity. Minireview. Neurotoxicity research *7*, 193-202.

Jaglin, X.H., Hjerling-Leffler, J., Fishell, G., and Batista-Brito, R. (2012). The origin of neocortical nitric oxide synthase-expressing inhibitory neurons. Front Neural Circuits *6*, 44.

Jhou, T.C., Fields, H.L., Baxter, M.G., Saper, C.B., and Holland, P.C. (2009). The rostromedial tegmental nucleus (RMTg), a GABAergic afferent to midbrain dopamine neurons, encodes aversive stimuli and inhibits motor responses. Neuron *61*, 786-800.

Jiang, X., Shen, S., Cadwell, C.R., Berens, P., Sinz, F., Ecker, A.S., Patel, S., and Tolias, A.S. (2015). Principles of connectivity among morphologically defined cell types in adult neocortex. Science *350*.

Jin, H., Wu, H., Osterhaus, G., Wei, J., Davis, K., Sha, D., Floor, E., Hsu, C.C., Kopke, R.D., and Wu, J.Y. (2003). Demonstration of functional coupling between gamma -aminobutyric acid (GABA) synthesis and vesicular GABA transport into synaptic vesicles. Proc Natl Acad Sci U S A *100*, 4293-4298.

Jin, X., and Costa, R.M. (2010). Start/stop signals emerge in nigrostriatal circuits during sequence learning. Nature *466*, 457-462.

Johnson, S.W., and North, R.A. (1992a). Opioids excite dopamine neurons by hyperpolarization of local interneurons. J Neurosci *12*, 483-488.

Johnson, S.W., and North, R.A. (1992b). Two types of neurone in the rat ventral tegmental area and their synaptic inputs. J Physiol *450*, 455-468.

Joo, K.M., Chung, Y.H., Shin, C.M., Lee, Y.J., and Cha, C.I. (2004). Region-specific alterations of neuronal nitric oxide synthase (nNOS) expression in the amygdala of the aged rats. Brain Res *999*, 231-236.

Joseph-Bravo, P., Jaimes-Hoy, L., and Charli, J.L. (2015). Regulation of TRH neurons and energy homeostasis-related signals under stress. The Journal of endocrinology *224*, R139-159.

Joseph-Bravo, P., Jaimes-Hoy, L., and Charli, J.L. (2016). Advances in TRH signaling. Reviews in endocrine & metabolic disorders *17*, 545-558.

Kabanova, A., Pabst, M., Lorkowski, M., Braganza, O., Boehlen, A., Nikbakht, N., Pothmann, L., Vaswani, A.R., Musgrove, R., Di Monte, D.A.*, et al.* (2015). Function and developmental origin of a mesocortical inhibitory circuit. Nat Neurosci *18*, 872-882.

Kalk, E. (2015). DDAH1 and nNOS expression in the ventral tegmental area in relation to dopamine neurons (Imperial College London).

Kandel, E.R. (2013). Principles of neural science.

Kapur, S. (2003). Psychosis as a state of aberrant salience: a framework linking biology, phenomenology, and pharmacology in schizophrenia. The American journal of psychiatry *160*, 13-23.

Karagiannis, A., Gallopin, T., David, C., Battaglia, D., Geoffroy, H., Rossier, J., Hillman, E.M., Staiger, J.F., and Cauli, B. (2009). Classification of NPY-expressing neocortical interneurons. J Neurosci *29*, 3642-3659.

Kaufling, J., Veinante, P., Pawlowski, S.A., Freund-Mercier, M.J., and Barrot, M. (2010). gamma-Aminobutyric acid cells with cocaine-induced DeltaFosB in the ventral tegmental area innervate mesolimbic neurons. Biol Psychiatry *67*, 88-92.

Kawaguchi, Y., Katsumaru, H., Kosaka, T., Heizmann, C.W., and Hama, K. (1987). Fast spiking cells in rat hippocampus (CA1 region) contain the calcium-binding protein parvalbumin. Brain Res *416*, 369-374.

Kawaguchi, Y., and Kubota, Y. (1997). GABAergic cell subtypes and their synaptic connections in rat frontal cortex. Cereb Cortex *7*, 476-486.

Kawano, M., Kawasaki, A., Sakata-Haga, H., Fukui, Y., Kawano, H., Nogami, H., and Hisano, S. (2006). Particular subpopulations of midbrain and hypothalamic dopamine neurons express vesicular glutamate transporter 2 in the rat brain. The Journal of Comparative Neurology *498*, 581-592.

Kepecs, A., and Fishell, G. (2014). Interneuron cell types are fit to function. Nature *505*, 318-326.

Kilduff, T.S., Cauli, B., and Gerashchenko, D. (2011). Activation of cortical interneurons during sleep: an anatomical link to homeostatic sleep regulation? Trends Neurosci *34*, 10-19.

Kim, D., Pertea, G., Trapnell, C., Pimentel, H., Kelley, R., and Salzberg, S.L. (2013). TopHat2: accurate alignment of transcriptomes in the presence of insertions, deletions and gene fusions. Genome Biology *14*, R36.

Kim, J.I., Ganesan, S., Luo, S.X., Wu, Y.W., Park, E., Huang, E.J., Chen, L., and Ding, J.B. (2015). Aldehyde dehydrogenase 1a1 mediates a GABA synthesis pathway in midbrain dopaminergic neurons. Science *350*, 102-106.

Kirouac, G.J., Li, S., and Mabrouk, G. (2004). GABAergic projection from the ventral tegmental area and substantia nigra to the periaqueductal gray region and the dorsal raphe nucleus. J Comp Neurol *469*, 170-184.

Kita, H., Kosaka, T., and Heizmann, C.W. (1990). Parvalbumin-immunoreactive neurons in the rat neostriatum: a light and electron microscopic study. Brain Res *536*, 1-15.

Klausberger, T., and Somogyi, P. (2008a). Neuronal diversity and temporal dynamics: the unity of hippocampal circuit operations. Science *321*, 53-57.

Klausberger, T., and Somogyi, P. (2008b). Neuronal Diversity and Temporal Dynamics: The Unity of Hippocampal Circuit Operations. Science *321*, 53-57.

Klejbor, I., Domaradzka-Pytel, B., Ludkiewicz, B., Wojcik, S., and Morys, J. (2004). The relationships between neurons containing dopamine and nitric oxide synthase in the ventral tegmental area. Folia Histochem Cytobiol *42*, 83-87.

Klink, R., de Kerchove d'Exaerde, A., Zoli, M., and Changeux, J.P. (2001). Molecular and physiological diversity of nicotinic acetylcholine receptors in the midbrain dopaminergic nuclei. J Neurosci *21*, 1452-1463.

Knowles, R.G., Palacios, M., Palmer, R.M., and Moncada, S. (1989). Formation of nitric oxide from L-arginine in the central nervous system: a transduction mechanism for stimulation of the soluble guanylate cyclase. Proc Natl Acad Sci U S A *86*, 5159-5162.

Ko, C.H., and Takahashi, J.S. (2006). Molecular components of the mammalian circadian clock. Human Molecular Genetics *15*, R271-R277.

Kolk, S.M., Gunput, R.-A.F., Tran, T.S., van den Heuvel, D.M.A., Prasad, A.A., Hellemons, A.J.C.G.M., Adolfs, Y., Ginty, D.D., Kolodkin, A.L., Burbach, J.P.H.*, et al.* (2009). Semaphorin 3F Is a Bifunctional Guidance Cue for Dopaminergic Axons and Controls Their Fasciculation, Channeling,

Rostral Growth, and Intracortical Targeting. The Journal of neuroscience : the official journal of the Society for Neuroscience *29*, 12542-12557.

Kravitz, A.V., Freeze, B.S., Parker, P.R., Kay, K., Thwin, M.T., Deisseroth, K., and Kreitzer, A.C. (2010). Regulation of parkinsonian motor behaviours by optogenetic control of basal ganglia circuitry. Nature *466*, 622-626.

Kubota, Y. (2014). Untangling GABAergic wiring in the cortical microcircuit. Current Opinion in Neurobiology *26*, 7-14.

Kubota, Y., Hattori, R., and Yui, Y. (1994). Three distinct subpopulations of GABAergic neurons in rat frontal agranular cortex. Brain Res *649*, 159-173.

Kubota, Y., Shigematsu, N., Karube, F., Sekigawa, A., Kato, S., Yamaguchi, N., Hirai, Y., Morishima, M., and Kawaguchi, Y. (2011). Selective coexpression of multiple chemical markers defines discrete populations of neocortical GABAergic neurons. Cereb Cortex *21*, 1803-1817.

Kudo, T., Uchigashima, M., Miyazaki, T., Konno, K., Yamasaki, M., Yanagawa, Y., Minami, M., and Watanabe, M. (2012). Three types of neurochemical projection from the bed nucleus of the stria terminalis to the ventral tegmental area in adult mice. J Neurosci *32*, 18035-18046.

Kuhlman, S.J., Olivas, N.D., Tring, E., Ikrar, T., Xu, X., and Trachtenberg, J.T. (2013). A disinhibitory microcircuit initiates critical-period plasticity in the visual cortex. Nature *501*, 543-546.

Lacey, M.G., Mercuri, N.B., and North, R.A. (1987). Dopamine acts on D2 receptors to increase potassium conductance in neurones of the rat substantia nigra zona compacta. J Physiol *392*, 397-416.

Lahti, L., Achim, K., and Partanen, J. (2013). Molecular regulation of GABAergic neuron differentiation and diversity in the developing midbrain. Acta Physiol (Oxf) *207*, 616-627.

Lahti, L., Haugas, M., Tikker, L., Airavaara, M., Voutilainen, M.H., Anttila, J., Kumar, S., Inkinen, C., Salminen, M., and Partanen, J. (2016). Differentiation and molecular heterogeneity of inhibitory and excitatory neurons associated with midbrain dopaminergic nuclei. Development *143*, 516-529.

Lakshmanan, G., Lieuw, K.H., Lim, K.C., Gu, Y., Grosveld, F., Engel, J.D., and Karis, A. (1999). Localization of distant urogenital system-, central nervous system-, and endocardium-specific transcriptional regulatory elements in the GATA-3 locus. Mol Cell Biol *19*, 1558-1568.

Lamas, S., Marsden, P.A., Li, G.K., Tempst, P., and Michel, T. (1992). Endothelial nitric oxide synthase: molecular cloning and characterization of a distinct constitutive enzyme isoform. Proceedings of the National Academy of Sciences of the United States of America *89*, 6348-6352.

Lammel, S., Hetzel, A., Hackel, O., Jones, I., Liss, B., and Roeper, J. (2008). Unique properties of mesoprefrontal neurons within a dual mesocorticolimbic dopamine system. Neuron *57*, 760-773.

Lammel, S., Ion, D.I., Roeper, J., and Malenka, R.C. (2011). Projection-specific modulation of dopamine neuron synapses by aversive and rewarding stimuli. Neuron *70*, 855-862.

Lammel, S., Lim, B.K., and Malenka, R.C. (2014a). Reward and aversion in a heterogeneous midbrain dopamine system. Neuropharmacology *76 Pt B*, 351-359.

Lammel, S., Lim, B.K., Ran, C., Huang, K.W., Betley, M.J., Tye, K.M., Deisseroth, K., and Malenka, R.C. (2012). Input-specific control of reward and aversion in the ventral tegmental area. Nature *491*, 212-217.

Lammel, S., Steinberg, E.E., Foldy, C., Wall, N.R., Beier, K., Luo, L., and Malenka, R.C. (2015). Diversity of transgenic mouse models for selective targeting of midbrain dopamine neurons. Neuron *85*, 429-438.

Lammel, S., Tye, K.M., and Warden, M.R. (2014b). Progress in understanding mood disorders: optogenetic dissection of neural circuits. Genes Brain Behav *13*, 38-51.

Lavin, A., Nogueira, L., Lapish, C.C., Wightman, R.M., Phillips, P.E., and Seamans, J.K. (2005). Mesocortical dopamine neurons operate in distinct temporal domains using multimodal signaling. J Neurosci *25*, 5013-5023.

Lee, C.R., and Tepper, J.M. (2007). Morphological and physiological properties of parvalbumin- and calretinin-containing γ-aminobutyric acidergic neurons in the substantia nigra. The Journal of Comparative Neurology *500*, 958-972.

Lein, E.S., Hawrylycz, M.J., Ao, N., Ayres, M., Bensinger, A., Bernard, A., Boe, A.F., Boguski, M.S., Brockway, K.S., Byrnes, E.J*., et al.* (2007). Genome-wide atlas of gene expression in the adult mouse brain. Nature *445*, 168-176.

Letzkus, J.J., Wolff, S.B., Meyer, E.M., Tovote, P., Courtin, J., Herry, C., and Luthi, A. (2011). A disinhibitory microcircuit for associative fear learning in the auditory cortex. Nature *480*, 331-335.

Lewis, D.A. (2014). Inhibitory neurons in human cortical circuits: substrate for cognitive dysfunction in schizophrenia. Current Opinion in Neurobiology *26*, 22-26.

Li, X., Qi, J., Yamaguchi, T., Wang, H.L., and Morales, M. (2013). Heterogeneous composition of dopamine neurons of the rat A10 region: molecular evidence for diverse signaling properties. Brain Struct Funct *218*, 1159-1176.

Liang, C.L., Sinton, C.M., and German, D.C. (1996). Midbrain dopaminergic neurons in the mouse: co-localization with Calbindin-D28k and calretinin. Neuroscience *75*, 523-533.

Lin, L.H. (2009). Glutamatergic neurons say NO in the nucleus tractus solitarii. J Chem Neuroanat *38*, 154-165.

Lin, L.H., Edwards, R.H., Fremeau, R.T., Fujiyama, F., Kaneko, T., and Talman, W.T. (2004). Localization of vesicular glutamate transporters and neuronal nitric oxide synthase in rat nucleus tractus solitarii. Neuroscience *123*, 247-255.

Lindeberg, J., Usoskin, D., Bengtsson, H., Gustafsson, A., Kylberg, A., Soderstrom, S., and Ebendal, T. (2004). Transgenic expression of Cre recombinase from the tyrosine hydroxylase locus. Genesis *40*, 67-73.

Lindvall, O., and Björklund, A. (1979). Dopaminergic innervation of the globus pallidus by collaterals from the nigrostriatal pathway. Brain Research *172*, 169-173.

Lonart, G., and Johnson, K.M. (1994). Inhibitory effects of nitric oxide on the uptake of [3H]dopamine and [3H]glutamate by striatal synaptosomes. Journal of neurochemistry *63*, 2108-2117.

Loughlin, S.E., and Fallon, J.H. (1984). Substantia nigra and ventral tegmental area projections to cortex: Topography and collateralization. Neuroscience *11*, 425-435.

Love, M.I., Huber, W., and Anders, S. (2014). Moderated estimation of fold change and dispersion for RNA-seq data with DESeq2. Genome Biol *15*, 550.

Lu, Q., Harris, V.A., Rafikov, R., Sun, X., Kumar, S., and Black, S.M. (2015). Nitric oxide induces hypoxia ischemic injury in the neonatal brain via the disruption of neuronal iron metabolism. Redox Biol *6*, 112-121.

Ma, S., Bonaventure, P., Ferraro, T., Shen, P.J., Burazin, T.C.D., Bathgate, R.A.D., Liu, C., Tregear, G.W., Sutton, S.W., and Gundlach, A.L. (2007). Relaxin-3 in GABA projection neurons of nucleus incertus suggests widespread influence on forebrain circuits via G-protein-coupled receptor-135 in the rat. Neuroscience *144*, 165-190.

Ma, S., Smith, C.M., Blasiak, A., and Gundlach, A.L. (2017). Distribution, physiology and pharmacology of relaxin-3/RXFP3 systems in brain. British Journal of Pharmacology *174*, 1034-1048.

Madhavan, A., He, L., Stuber, G.D., Bonci, A., and Whistler, J.L. (2010). micro-Opioid receptor endocytosis prevents adaptations in ventral tegmental area GABA transmission induced during naloxone-precipitated morphine withdrawal. J Neurosci *30*, 3276-3286.

Magno, L., Oliveira, M.G., Mucha, M., Rubin, A.N., and Kessaris, N. (2012). Multiple embryonic origins of nitric oxide synthase-expressing GABAergic neurons of the neocortex. Front Neural Circuits *6*, 65.

Mansvelder, H.D., and McGehee, D.S. (2000). Long-term potentiation of excitatory inputs to brain reward areas by nicotine. Neuron *27*, 349-357.

Mao, L., Lau, Y.S., Petroske, E., and Wang, J.Q. (2001). Profound astrogenesis in the striatum of adult mice following nigrostriatal dopaminergic lesion by repeated MPTP administration. Brain research Developmental brain research *131*, 57-65.

Margolis, E.B., Lock, H., Chefer, V.I., Shippenberg, T.S., Hjelmstad, G.O., and Fields, H.L. (2006a). Kappa opioids selectively control dopaminergic neurons projecting to the prefrontal cortex. Proceedings of the National Academy of Sciences of the United States of America *103*, 2938-2942.

Margolis, E.B., Lock, H., Hjelmstad, G.O., and Fields, H.L. (2006b). The ventral tegmental area revisited: is there an electrophysiological marker for dopaminergic neurons? J Physiol *577*, 907-924.

Margolis, E.B., Mitchell, J.M., Ishikawa, J., Hjelmstad, G.O., and Fields, H.L. (2008). Midbrain dopamine neurons: projection target determines action potential duration and dopamine D(2) receptor inhibition. J Neurosci *28*, 8908-8913.

Margolis, E.B., Toy, B., Himmels, P., Morales, M., and Fields, H.L. (2012). Identification of rat ventral tegmental area GABAergic neurons. PLoS One *7*, e42365.

Marin, O. (2012). Interneuron dysfunction in psychiatric disorders. Nat Rev Neurosci *13*, 107-120.

Marín, O. (2012). Interneuron dysfunction in psychiatric disorders. Nat Rev Neurosci *13*, 107-120.

Markram, H., Toledo-Rodriguez, M., Wang, Y., Gupta, A., Silberberg, G., and Wu, C. (2004). Interneurons of the neocortical inhibitory system. Nat Rev Neurosci *5*, 793-807.

Marksteiner, J., Saria, A., and Krause, J.E. (1992). Comparative distribution of neurokinin B-, substance P- and enkephalin-like immunoreactivities and neurokinin B messenger RNA in the basal forebrain of the rat: Evidence for neurochemical compartmentation. Neuroscience *51*, 107-120.

Marshall, J.F., Levitan, D., and Stricker, E.M. (1976). Activation-induced restoration of sensorimotor functions in rats with dopamine-depleting brain lesions. Journal of comparative and physiological psychology *90*, 536-546.

Matsuda, K., and Yuzaki, M. (2011). Cbln family proteins promote synapse formation by regulating distinct neurexin signaling pathways in various brain regions. European Journal of Neuroscience *33*, 1447-1461.

Matsuda, W., Furuta, T., Nakamura, K.C., Hioki, H., Fujiyama, F., Arai, R., and Kaneko, T. (2009). Single Nigrostriatal Dopaminergic Neurons Form Widely Spread and Highly Dense Axonal Arborizations in the Neostriatum. The Journal of Neuroscience *29*, 444-453.

Matsumoto, M., and Hikosaka, O. (2009). Two types of dopamine neuron distinctly convey positive and negative motivational signals. Nature *459*, 837-841.

Mazloom, M., and Smith, Y. (2006). Synaptic microcircuitry of tyrosine hydroxylase-containing neurons and terminals in the striatum of 1-methyl-4-phenyl-1,2,3,6-tetrahydropyridine-treated monkeys. J Comp Neurol *495*, 453-469.

McCormick, D.A., Connors, B.W., Lighthall, J.W., and Prince, D.A. (1985). Comparative electrophysiology of pyramidal and sparsely spiny stellate neurons of the neocortex. Journal of Neurophysiology *54*, 782-806.

Meredith, G.E., Farrell, T., Kellaghan, P., Tan, Y., Zahm, D.S., and Totterdell, S. (1999). Immunocytochemical characterization of catecholaminergic neurons in the rat striatum following dopamine-depleting lesions. Eur J Neurosci *11*, 3585-3596.

Merrill, C.B., Friend, L.N., Newton, S.T., Hopkins, Z.H., and Edwards, J.G. (2015). Ventral tegmental area dopamine and GABA neurons: Physiological properties and expression of mRNA for endocannabinoid biosynthetic elements. *5*, 16176.

Meyer-Lindenberg, A., Kohn, P.D., Kolachana, B., Kippenhan, S., McInerney-Leo, A., Nussbaum, R., Weinberger, D.R., and Berman, K.F. (2005). Midbrain dopamine and prefrontal function in humans: interaction and modulation by COMT genotype. Nat Neurosci *8*, 594-596.

Mi, H., Huang, X., Muruganujan, A., Tang, H., Mills, C., Kang, D., and Thomas, P.D. (2017). PANTHER version 11: expanded annotation data from Gene Ontology and Reactome pathways, and data analysis tool enhancements. Nucleic acids research *45*, D183-D189.

Mi, H., Muruganujan, A., Casagrande, J.T., and Thomas, P.D. (2013). Large-scale gene function analysis with the PANTHER classification system. Nat Protoc *8*, 1551-1566.

Min, N., Joh, T.H., Kim, K.S., Peng, C., and Son, J.H. (1994). 5' upstream DNA sequence of the rat tyrosine hydroxylase gene directs high-level and tissue-specific expression to catecholaminergic neurons in the central nervous system of transgenic mice. Brain Res Mol Brain Res *27*, 281-289.

Mingote, S., Chuhma, N., Kusnoor, S.V., Field, B., Deutch, A.Y., and Rayport, S. (2015). Functional Connectome Analysis of Dopamine Neuron Glutamatergic Connections in Forebrain Regions. The Journal of Neuroscience *35*, 16259-16271.

Mitkovski, M., Padovan-Neto, F.E., Raisman-Vozari, R., Ginestet, L., da-Silva, C.A., and Del-Bel, E.A. (2012). Investigations into Potential Extrasynaptic Communication between the Dopaminergic and Nitrergic Systems. Front Physiol *3*, 372.

Miyazaki, T., and Lacey, M.G. (1998). Presynaptic inhibition by dopamine of a discrete component of GABA release in rat substantia nigra pars reticulata. J Physiol *513 (Pt 3)*, 805-817.

Moncada, S., Palmer, R.M., and Higgs, E.A. (1991). Nitric oxide: physiology, pathophysiology, and pharmacology. Pharmacological Reviews *43*, 109-142.

Morales, M., and Margolis, E.B. (2017). Ventral tegmental area: cellular heterogeneity, connectivity and behaviour. Nature reviews Neuroscience *18*, 73-85.

Morales, M., and Root, D.H. (2014). Glutamate neurons within the midbrain dopamine regions. Neuroscience *282*, 60-68.

Morley, J.E., and Flood, J.F. (1991). Evidence that nitric oxide modulates food intake in mice. Life Sci *49*, 707-711.

Morris, G., Berk, M., Klein, H., Walder, K., Galecki, P., and Maes, M. (2016). Nitrosative Stress, Hypernitrosylation, and Autoimmune Responses to Nitrosylated Proteins: New Pathways in Neuroprogressive Disorders Including Depression and Chronic Fatigue Syndrome. Molecular Neurobiology, 1-21.

Motahari, A.A., Sahraei, H., and Meftahi, G.H. (2016). Role of Nitric Oxide on Dopamine Release and Morphine-Dependency. Basic and clinical neuroscience *7*, 283-290.

Mura, A., Linder, J.C., Young, S.J., and Groves, P.M. (2000). Striatal cells containing aromatic L-amino acid decarboxylase: an immunohistochemical comparison with other classes of striatal neurons. Neuroscience *98*, 501-511.

Murray, A.J., Sauer, J.-F., Riedel, G., McClure, C., Ansel, L., Cheyne, L., Bartos, M., Wisden, W., and Wulff, P. (2011). Parvalbumin-positive CA1 interneurons are required for spatial working but not for reference memory. Nat Neurosci *14*, 297-299.

Musacchio, J.M. (1975). Enzymes Involved in the Biosynthesis and Degradation of Catecholamines. In Biochemistry of Biogenic Amines, L.L. Iversen, S.D. Iversen, and S.H. Snyder, eds. (Boston, MA: Springer US), pp. 1-35.

Nagai, T., McGeer, P.L., and McGeer, E.G. (1983). Distribution of GABA-T-intensive neurons in the rat forebrain and midbrain. J Comp Neurol *218*, 220-238.

Nair-Roberts, R.G., Chatelain-Badie, S.D., Benson, E., White-Cooper, H., Bolam, J.P., and Ungless, M.A. (2008). Stereological estimates of dopaminergic, GABAergic and glutamatergic neurons in the ventral tegmental area, substantia nigra and retrorubral field in the rat. Neuroscience *152*, 1024-1031.

Napier, T.C., Mitrovic, I., Churchill, L., Klitenick, M.A., Lu, X.Y., and Kalivas, P.W. (1995). Substance P in the ventral pallidum: Projection from the ventral striatum, and electrophysiological and behavioral cinsequences of pallidal substance P. Neuroscience *69*, 59-70.

Nardelli, J., Thiesson, D., Fujiwara, Y., Tsai, F.-Y., and Orkin, S.H. (1999). Expression and Genetic Interaction of Transcription Factors GATA-2 and GATA-3 during Development of the Mouse Central Nervous System. Developmental Biology *210*, 305-321.

Nelson, E.L., Liang, C.L., Sinton, C.M., and German, D.C. (1996). Midbrain dopaminergic neurons in the mouse: Computer-assisted mapping. Journal of Comparative Neurology *369*, 361-371.

Nieh, E.H., Matthews, G.A., Allsop, S.A., Presbrey, K.N., Leppla, C.A., Wichmann, R., Neve, R., Wildes, C.P., and Tye, K.M. (2015). Decoding neural circuits that control compulsive sucrose seeking. Cell *160*, 528-541.

Nieoullon, A., Cheramy, A., and Glowinski, J. (1977). Release of dopamine in vivo from cat substantia nigra. Nature *266*, 375-377.

Nishida, K., Harrison, D.G., Navas, J.P., Fisher, A.A., Dockery, S.P., Uematsu, M., Nerem, R.M., Alexander, R.W., and Murphy, T.J. (1992). Molecular cloning and characterization of the constitutive bovine aortic endothelial cell nitric oxide synthase. J Clin Invest *90*, 2092-2096.

Nugent, F.S., Penick, E.C., and Kauer, J.A. (2007). Opioids block long-term potentiation of inhibitory synapses. Nature *446*, 1086-1090.

O'Byrne, M.B., Bolam, J.P., Hanley, J.J., and Tipton, K.F. (2000). Tyrosine-hydroxylase immunoreactive cells in the rat striatum following treatment with MPP+. Adv Exp Med Biol *483*, 369-374.

Oades, R.D., and Halliday, G.M. (1987). Ventral tegmental (A10) system: neurobiology. 1. Anatomy and connectivity. Brain Research Reviews *12*, 117-165.

Ogawa, Sachie K., Cohen, Jeremiah Y., Hwang, D., Uchida, N., and Watabe-Uchida, M. (2014). Organization of Monosynaptic Inputs to the Serotonin and Dopamine Neuromodulatory Systems. Cell Reports *8*, 1105-1118.

Oh, Y.-M., Karube, F., Takahashi, S., Kobayashi, K., Takada, M., Uchigashima, M., Watanabe, M., Nishizawa, K., Kobayashi, K., and Fujiyama, F. (2017). Using a novel PV-Cre rat model to characterize pallidonigral cells and their terminations. Brain Structure and Function *222*, 2359-2378.

Okaty, B.W., Freret, M.E., Rood, B.D., Brust, R.D., Hennessy, M.L., deBairos, D., Kim, J.C., Cook, M.N., and Dymecki, S.M. (2015). Multi-Scale Molecular Deconstruction of the Serotonin Neuron System. Neuron *88*, 774-791.

Olson, V.G., and Nestler, E.J. (2007). Topographical organization of GABAergic neurons within the ventral tegmental area of the rat. Synapse *61*, 87-95.

Omelchenko, N., Bell, R., and Sesack, S.R. (2009). Lateral habenula projections to dopamine and GABA neurons in the rat ventral tegmental area. Eur J Neurosci *30*, 1239-1250.

Omelchenko, N., and Sesack, S.R. (2005). Laterodorsal tegmental projections to identified cell populations in the rat ventral tegmental area. J Comp Neurol *483*, 217-235.

Omelchenko, N., and Sesack, S.R. (2009). Ultrastructural analysis of local collaterals of rat ventral tegmental area neurons: GABA phenotype and synapses onto dopamine and GABA cells. Synapse *63*, 895-906.

Omelchenko, N., and Sesack, S.R. (2010). Periaqueductal gray afferents synapse onto dopamine and GABA neurons in the rat ventral tegmental area. Journal of neuroscience research *88*, 981-991.

Overstreet, L.S., and Westbrook, G.L. (2003). Synapse density regulates independence at unitary inhibitory synapses. J Neurosci *23*, 2618-2626.

Parra, P., Gulyas, A.I., and Miles, R. (1998). How many subtypes of inhibitory cells in the hippocampus? Neuron *20*, 983-993.

Perrenoud, Q., Geoffroy, H., Gauthier, B., Rancillac, A., Alfonsi, F., Kessaris, N., Rossier, J., Vitalis, T., and Gallopin, T. (2012a). Characterization of Type I and Type II nNOS-Expressing Interneurons in the Barrel Cortex of Mouse. Front Neural Circuits *6*, 36.

Perrenoud, Q., Rossier, J., Ferezou, I., Geoffroy, H., Gallopin, T., Vitalis, T., and Rancillac, A. (2012b). Activation of cortical 5-HT(3) receptor-expressing interneurons induces NO mediated vasodilatations and NPY mediated vasoconstrictions. Front Neural Circuits *6*, 50.

Petroske, E., Meredith, G.E., Callen, S., Totterdell, S., and Lau, Y.S. (2001). Mouse model of Parkinsonism: a comparison between subacute MPTP and chronic MPTP/probenecid treatment. Neuroscience *106*, 589-601.

Pfeffer, C.K., Xue, M., He, M., Huang, Z.J., and Scanziani, M. (2013). Inhibition of inhibition in visual cortex: the logic of connections between molecularly distinct interneurons. Nat Neurosci *16*, 1068-1076.

Phillipson, O.T. (1979a). The cytoarchitecture of the interfascicular nucleus and ventral tegmental area of tsai in the rat. The Journal of Comparative Neurology *187*, 85-98.

Phillipson, O.T. (1979b). A Golgi study of the ventral tegmental area of Tsai and interfascicular nucleus in the rat. The Journal of Comparative Neurology *187*, 99-115.

Pickel, V.M., Towle, A.C., Joh, T.H., and Chan, J. (1988). Gamma-aminobutyric acid in the medial rat nucleus accumbens: ultrastructural localization in neurons receiving monosynaptic input from catecholaminergic afferents. J Comp Neurol *272*, 1-14.

Pinal, C.S., and Tobin, A.J. (1998). Uniqueness and redundancy in GABA production. Perspectives on developmental neurobiology *5*, 109-118.

Pioli, E.Y., Dovero, S., Bioulac, B.H., Gross, C.E., and Bezard, E. (2004). Asymmetrically lesioned mesencephalon in healthy rodents: Call for caution. Brain Research *1022*, 251-253.

Porritt, M.J., Batchelor, P.E., Hughes, A.J., Kalnins, R., Donnan, G.A., and Howells, D.W. (2000). New dopaminergic neurons in Parkinson's disease striatum. Lancet (London, England) *356*, 44-45.

Poulin, J.F., Zou, J., Drouin-Ouellet, J., Kim, K.Y., Cicchetti, F., and Awatramani, R.B. (2014). Defining midbrain dopaminergic neuron diversity by single-cell gene expression profiling. Cell Rep *9*, 930-943.

Price, C.J., Cauli, B., Kovacs, E.R., Kulik, A., Lambolez, B., Shigemoto, R., and Capogna, M. (2005). Neurogliaform neurons form a novel inhibitory network in the hippocampal CA1 area. J Neurosci *25*, 6775-6786.

Przedborski, S., Jackson-Lewis, V., Yokoyama, R., Shibata, T., Dawson, V.L., and Dawson, T.M. (1996). Role of neuronal nitric oxide in 1-methyl-4-phenyl-1,2,3,6-tetrahydropyridine (MPTP)-induced dopaminergic neurotoxicity. Proc Natl Acad Sci U S A *93*, 4565-4571.

Pucak, M.L., and Grace, A.A. (1994). Evidence that systemically administered dopamine antagonists activate dopamine neuron firing primarily by blockade of somatodendritic autoreceptors. Journal of Pharmacology and Experimental Therapeutics *271*, 1181-1192.

Qi, J., Zhang, S., Wang, H.L., Barker, D.J., Miranda-Barrientos, J., and Morales, M. (2016). VTA glutamatergic inputs to nucleus accumbens drive aversion by acting on GABAergic interneurons. Nat Neurosci.

Qi, J., Zhang, S., Wang, H.L., Wang, H., de Jesus Aceves Buendia, J., Hoffman, A.F., Lupica, C.R., Seal, R.P., and Morales, M. (2014). A glutamatergic reward input from the dorsal raphe to ventral tegmental area dopamine neurons. Nat Commun *5*, 5390.

Radnikow, G., and Misgeld, U. (1998). Dopamine D₁ Receptors Facilitate GABA_ASynaptic Currents in the Rat Substantia Nigra Pars Reticulata. The Journal of Neuroscience *18*, 2009-2016.

Rajakumar, N., Elisevich, K., and Flumerfelt, B.A. (1994). Parvalbumin-containing GABAergic neurons in the basal ganglia output system of the rat. The Journal of Comparative Neurology *350*, 324-336.

Redgrave, P., Gurney, K., and Reynolds, J. (2008). What is reinforced by phasic dopamine signals? Brain Res Rev *58*, 322-339.

Reiner, A., and Anderson, K.D. (1993). Co-occurrence of γ-aminobutyric acid, parvalbumin and the neurotensin-related neuropeptide LANT6 in pallidal, nigral and striatal neurons in pigeons and monkeys. Brain Research *624*, 317-325.

Reinius, B., Blunder, M., Brett, F.M., Eriksson, A., Patra, K., Jonsson, J., Jazin, E., and Kullander, K. (2015). Conditional targeting of medium spiny neurons in the striatal matrix. Frontiers in Behavioral Neuroscience *9*.

Reyes, A., Lujan, R., Rozov, A., Burnashev, N., Somogyi, P., and Sakmann, B. (1998). Target-cell-specific facilitation and depression in neocortical circuits. Nat Neurosci *1*, 279-285.

Rice, M.E., and Patel, J.C. (2015). Somatodendritic dopamine release: recent mechanistic insights. Philos Trans R Soc Lond B Biol Sci *370*.

Robinson, D.L., Heien, M.L., and Wightman, R.M. (2002a). Frequency of dopamine concentration transients increases in dorsal and ventral striatum of male rats during introduction of conspecifics. J Neurosci *22*, 10477-10486.

Robinson, D.L., Heien, M.L.A.V., and Wightman, R.M. (2002b). Frequency of Dopamine Concentration Transients Increases in Dorsal and Ventral Striatum of Male Rats during Introduction of Conspecifics. The Journal of Neuroscience *22*, 10477-10486.

Robinson, T.E., and Berridge, K.C. (1993). The neural basis of drug craving: an incentive-sensitization theory of addiction. Brain Res Brain Res Rev *18*, 247-291.

Rodrigo, J., Springall, D.R., Uttenthal, O., Bentura, M.L., Abadia-Molina, F., Riveros-Moreno, V., Martinez-Murillo, R., Polak, J.M., and Moncada, S. (1994). Localization of Nitric Oxide Synthase in the Adult Rat Brain. Philosophical Transactions of the Royal Society of London Series B: Biological Sciences *345*, 175-221.

Rodŕiguez, M., and González-Hernández, T. (1999). Electrophysiological and Morphological Evidence for a GABAergic Nigrostriatal Pathway. The Journal of Neuroscience *19*, 4682-4694.

Roeper, J. (2013). Dissecting the diversity of midbrain dopamine neurons. Trends in Neurosciences *36*, 336-342.

Rogers, J.H. (1992). Immunohistochemical markers in rat cortex: co-localization of calretinin and calbindin-D28k with neuropeptides and GABA. Brain Res *587*, 147-157.

Root, D.H., Mejias-Aponte, C.A., Qi, J., and Morales, M. (2014a). Role of glutamatergic projections from ventral tegmental area to lateral habenula in aversive conditioning. J Neurosci *34*, 13906-13910.

Root, D.H., Mejias-Aponte, C.A., Zhang, S., Wang, H.L., Hoffman, A.F., Lupica, C.R., and Morales, M. (2014b). Single rodent mesohabenular axons release glutamate and GABA. Nat Neurosci *17*, 1543-1551.

Root, D.H., Wang, H.L., Liu, B., Barker, D.J., Mod, L., Szocsics, P., Silva, A.C., Magloczky, Z., and Morales, M. (2016). Glutamate neurons are intermixed with midbrain dopamine neurons in nonhuman primates and humans. Sci Rep *6*, 30615.

Rothermundt, M., Peters, M., Prehn, J.H., and Arolt, V. (2003). S100B in brain damage and neurodegeneration. Microsc Res Tech *60*, 614-632.

Salamone, J.D., and Correa, M. (2012). The mysterious motivational functions of mesolimbic dopamine. Neuron *76*, 470-485.

San Sebastián, W., Guillén, J., Manrique, M., Belzunegui, S., Ciordia, E., Izal-Azcárate, A., Garrido-Gil, P., Vázquez-Claverie, M., and Luquin, M.R. (2007). Modification of the number and phenotype of striatal dopaminergic cells by carotid body graft. Brain *130*, 1306-1316.

Sanchez-Catalan, M.J., Kaufling, J., Georges, F., Veinante, P., and Barrot, M. (2014). The antero-posterior heterogeneity of the ventral tegmental area. Neuroscience *282*, 198-216.

Santiago, M., and Westerink, B.H. (1991). Characterization and pharmacological responsiveness of dopamine release recorded by microdialysis in the substantia nigra of conscious rats. Journal of neurochemistry *57*, 738-747.

Sanz, E., Yang, L., Su, T., Morris, D.R., McKnight, G.S., and Amieux, P.S. (2009a). Cell-type-specific isolation of ribosome-associated mRNA from complex tissues. PNAS *106*, 13939-13944.

Sanz, E., Yang, L., Su, T., Morris, D.R., McKnight, G.S., and Amieux, P.S. (2009b). Cell-type-specific isolation of ribosome-associated mRNA from complex tissues. Proc Natl Acad Sci U S A *106*, 13939-13944.

Sato, T.K., Panda, S., Miraglia, L.J., Reyes, T.M., Rudic, R.D., McNamara, P., Naik, K.A., FitzGerald, G.A., Kay, S.A., and Hogenesch, J.B. (2004). A Functional Genomics Strategy Reveals Rora as a Component of the Mammalian Circadian Clock. Neuron *43*, 527-537.

Satoh, T., Nakai, S., Sato, T., and Kimura, M. (2003). Correlated coding of motivation and outcome of decision by dopamine neurons. J Neurosci *23*, 9913-9923.

Saunders, B.T., Richard, J.M., and Janak, P.H. (2015). Contemporary approaches to neural circuit manipulation and mapping: focus on reward and addiction. Philos Trans R Soc Lond B Biol Sci *370*, 20140210.

Savitt, J.M., Jang, S.S., Mu, W., Dawson, V.L., and Dawson, T.M. (2005). Bcl-x is required for proper development of the mouse substantia nigra. J Neurosci *25*, 6721-6728.

Schroeder, A., Mueller, O., Stocker, S., Salowsky, R., Leiber, M., Gassmann, M., Lightfoot, S., Menzel, W., Granzow, M., and Ragg, T. (2006). The RIN: an RNA integrity number for assigning integrity values to RNA measurements. BMC molecular biology *7*, 3.

Schultz, W. (1986). Activity of pars reticulata neurons of monkey substantia nigra in relation to motor, sensory, and complex events. J Neurophysiol *55*, 660-677.

Schultz, W. (2002). Getting formal with dopamine and reward. Neuron *36*, 241-263.

Schultz, W. (2007). Multiple dopamine functions at different time courses. Annual review of neuroscience *30*, 259-288.

Schultz, W., Dayan, P., and Montague, P.R. (1997). A neural substrate of prediction and reward. Science *275*, 1593-1599.

Seroogy, K., Ceccatelli, S., Schalling, M., Ho¨kfelt, T., Frey, P., Walsh, J., Dockray, G., Brown, J., Buchan, A., and Goldstein, M. (1988). A subpopulation of dopaminergic neurons in rat ventral mesencephalon contains both neurotensin and cholecystokinin. Brain Research *455*, 88-98.

Seroogy, K., Schalling, M., Brené, S., Dagerlind, Å., Chai, S.Y., Hökfelt, T., Persson, H., Brownstein, M., Huan, R., Dixon, J.*, et al.* (1989). Cholecystokinin and tyrosine hydroxylase messenger RNAs in neurons of rat mesencephalon: peptide/monoamine coexistence studies using in situ hybridization combined with immunocytochemistry. Experimental Brain Research *74*, 149-162.

Sgadò, P., Genovesi, S., Kalinovsky, A., Zunino, G., Macchi, F., Allegra, M., Murenu, E., Provenzano, G., Tripathi, P.P., Casarosa, S.*, et al.* (2013). Loss of GABAergic neurons in the hippocampus and cerebral cortex of Engrailed-2 null mutant mice: Implications for autism spectrum disorders. Experimental Neurology *247*, 496-505.

Shen, R.Y., Choong, K.C., and Thompson, A.C. (2007). Long-term reduction in ventral tegmental area dopamine neuron population activity following repeated stimulant or ethanol treatment. Biol Psychiatry *61*, 93-100.

Simon, H.H., Saueressig, H., Wurst, W., Goulding, M.D., and O'Leary, D.D.M. (2001). Fate of Midbrain Dopaminergic Neurons Controlled by the Engrailed Genes. The Journal of Neuroscience *21*, 3126-3134.

Simon, H.H., Thuret, S., and Alberi, L. (2004). Midbrain dopaminergic neurons: control of their cell fate by the engrailed transcription factors. Cell and Tissue Research *318*, 53-61.

Smiley, J.F., McGinnis, J.P., and Javitt, D.C. (2000). Nitric oxide synthase interneurons in the monkey cerebral cortex are subsets of the somatostatin, neuropeptide Y, and calbindin cells. Brain Res *863*, 205-212.

Smith, A.C.W., Scofield, M.D., Heinsbroek, J.A., Gipson, C.D., Neuhofer, D., Roberts-Wolfe, D.J., Spencer, S., Stankeviciute, N.M., Smith, R., Allen, N.P.*, et al.* (2016). Accumbens nNOS interneurons regulate cocaine relapse. The Journal of Neuroscience.

Smith, C.M., Shen, P.-J., Banerjee, A., Bonaventure, P., Ma, S., Bathgate, R.A.D., Sutton, S.W., and Gundlach, A.L. (2010). Distribution of relaxin-3 and RXFP3 within arousal, stress, affective, and cognitive circuits of mouse brain. The Journal of Comparative Neurology *518*, 4016-4045.

Sohal, V.S., Zhang, F., Yizhar, O., and Deisseroth, K. (2009). Parvalbumin neurons and gamma rhythms enhance cortical circuit performance. Nature *459*, 698-702.

Somogyi, J., Szabo, A., Somogyi, P., and Lamsa, K. (2012). Molecular analysis of ivy cells of the hippocampal CA1 stratum radiatum using spectral identification of immunofluorophores. Frontiers in Neural Circuits *6*.

Somogyi, P., and Klausberger, T. (2005). Defined types of cortical interneurone structure space and spike timing in the hippocampus. J Physiol *562*, 9-26.

Stamatakis, A.M., Jennings, J.H., Ung, R.L., Blair, G.A., Weinberg, R.J., Neve, R.L., Boyce, F., Mattis, J., Ramakrishnan, C., Deisseroth, K.*, et al.* (2013). A unique population of ventral tegmental area neurons inhibits the lateral habenula to promote reward. Neuron *80*, 1039-1053.

Stamatakis, A.M., and Stuber, G.D. (2012). Optogenetic strategies to dissect the neural circuits that underlie reward and addiction. Cold Spring Harb Perspect Med *2*.

Stark, E., Eichler, R., Roux, L., Fujisawa, S., Rotstein, H.G., and Buzsaki, G. (2013). Inhibition-induced theta resonance in cortical circuits. Neuron *80*, 1263-1276.

Steffensen, S.C., Svingos, A.L., Pickel, V.M., and Henriksen, S.J. (1998). Electrophysiological characterization of GABAergic neurons in the ventral tegmental area. J Neurosci *18*, 8003-8015.

Stewart, T.L., Michel, A.D., Black, M.D., and Humphrey, P.P. (1996). Evidence that nitric oxide causes calcium-independent release of [3H] dopamine from rat striatum in vitro. Journal of neurochemistry *66*, 131-137.

Stuber, G.D., Hnasko, T.S., Britt, J.P., Edwards, R.H., and Bonci, A. (2010). Dopaminergic terminals in the nucleus accumbens but not the dorsal striatum corelease glutamate. J Neurosci *30*, 8229-8233.

Stuber, G.D., Wightman, R.M., and Carelli, R.M. (2005). Extinction of cocaine self-administration reveals functionally and temporally distinct dopaminergic signals in the nucleus accumbens. Neuron *46*, 661-669.

Studler, J.-M., Kitabgi, P., Tramu, G., Herve, D., Glowinski, J., and Tassin, J.-P. (1988). Extensive Co-localization of neurotensin with dopamine in rat meso-cortico-frontal dopaminergic neurons. Neuropeptides *11*, 95-100.

Sugino, K., Hempel, C.M., Miller, M.N., Hattox, A.M., Shapiro, P., Wu, C., Huang, Z.J., and Nelson, S.B. (2006). Molecular taxonomy of major neuronal classes in the adult mouse forebrain. Nat Neurosci *9*, 99-107.

Sugrue, M.L., Vella, K.R., Morales, C., Lopez, M.E., and Hollenberg, A.N. (2010). The Thyrotropin-Releasing Hormone Gene Is Regulated by Thyroid Hormone at the Level of Transcription in Vivo. Endocrinology *151*, 793-801.

Sulzer, D., Joyce, M.P., Lin, L., Geldwert, D., Haber, S.N., Hattori, T., and Rayport, S. (1998). Dopamine Neurons Make Glutamatergic Synapses In Vitro. The Journal of Neuroscience *18*, 4588-4602.

Swanson, L.W. (1982). The projections of the ventral tegmental area and adjacent regions: a combined fluorescent retrograde tracer and immunofluorescence study in the rat. Brain Res Bull *9*, 321-353.

Szabo, B., Siemes, S., and Wallmichrath, I. (2002). Inhibition of GABAergic neurotransmission in the ventral tegmental area by cannabinoids. Eur J Neurosci *15*, 2057-2061.

Tan, K.R., Brown, M., Labouèbe, G., Yvon, C., Creton, C., Fritschy, J.-M., Rudolph, U., and Lüscher, C. (2010). Neural bases for addictive properties of benzodiazepines. Nature *463*, 769-774.

Tan, K.R., Yvon, C., Turiault, M., Mirzabekov, J.J., Doehner, J., Labouebe, G., Deisseroth, K., Tye, K.M., and Luscher, C. (2012). GABA neurons of the VTA drive conditioned place aversion. Neuron *73*, 1173-1183.

Tanaka, M., Yamaguchi, K., Tatsukawa, T., Nishioka, C., Nishiyama, H., Theis, M., Willecke, K., and Itohara, S. (2008). Lack of connexin43-mediated Bergmann glial gap junctional coupling does not affect cerebellar long-term depression, motor coordination, or eyeblink conditioning. Frontiers in Behavioral Neuroscience *2*.

Tandé, D., Höglinger, G., Debeir, T., Freundlieb, N., Hirsch, E.C., and François, C. (2006). New striatal dopamine neurons in MPTP-treated macaques result from a phenotypic shift and not neurogenesis. Brain *129*, 1194-1200.

Taniguchi, H., He, M., Wu, P., Kim, S., Paik, R., Sugino, K., Kvitsiani, D., Fu, Y., Lu, J., Lin, Y.*, et al.* (2011). A resource of Cre driver lines for genetic targeting of GABAergic neurons in cerebral cortex. Neuron *71*, 995-1013.

Taniguchi, H., Lu, J., and Huang, Z.J. (2013). The spatial and temporal origin of chandelier cells in mouse neocortex. Science *339*, 70-74.

Tashiro, Y., Sugimoto, T., Hattori, T., Uemura, Y., Nagatsu, I., Kikuchi, H., and Mizuno, N. (1989). Tyrosine hydroxylase-like immunoreactive neurons in the striatum of the rat. Neurosci Lett *97*, 6-10.

Tayfun Uzbay, I., and Oglesby, M.W. (2001). Nitric oxide and substance dependence. Neurosci Biobehav Rev *25*, 43-52.

Taylor, S.R., Badurek, S., Dileone, R.J., Nashmi, R., Minichiello, L., and Picciotto, M.R. (2014). GABAergic and glutamatergic efferents of the mouse ventral tegmental area. The Journal of comparative neurology *522*, 3308-3334.

Tecuapetla, F., Patel, J.C., Xenias, H., English, D., Tadros, I., Shah, F., Berlin, J., Deisseroth, K., Rice, M.E., Tepper, J.M*., et al.* (2010). Glutamatergic signaling by mesolimbic dopamine neurons in the nucleus accumbens. J Neurosci *30*, 7105-7110.

Tepper, J.M., Tecuapetla, F., Koós, T., and Ibáñez-Sandoval, O. (2010). Heterogeneity and Diversity of Striatal GABAergic Interneurons. Front Neuroanat *4*.

Tomioka, R., Okamoto, K., Furuta, T., Fujiyama, F., Iwasato, T., Yanagawa, Y., Obata, K., Kaneko, T., and Tamamaki, N. (2005). Demonstration of long-range GABAergic connections distributed throughout the mouse neocortex. Eur J Neurosci *21*, 1587-1600.

Torigoe, M., Yamauchi, K., Tamada, A., Matsuda, I., Aiba, A., Castellani, V., and Murakami, F. (2013). Role of neuropilin-2 in the ipsilateral growth of midbrain dopaminergic axons. European Journal of Neuroscience *37*, 1573-1583.

Torres, G.E., Gainetdinov, R.R., and Caron, M.G. (2003). Plasma membrane monoamine transporters: structure, regulation and function. Nat Rev Neurosci *4*, 13-25.

Tran, T.S., Rubio, M.E., Clem, R.L., Johnson, D., Case, L., Tessier-Lavigne, M., Huganir, R.L., Ginty, D.D., and Kolodkin, A.L. (2009). Secreted semaphorins control spine distribution and morphogenesis in the postnatal CNS. Nature *462*, 1065-1069.

Tremblay, R., Lee, S., and Rudy, B. (2016). GABAergic Interneurons in the Neocortex: From Cellular Properties to Circuits. Neuron *91*, 260-292.

Tricoire, L., Pelkey, K.A., Daw, M.I., Sousa, V.H., Miyoshi, G., Jeffries, B., Cauli, B., Fishell, G., and McBain, C.J. (2010). Common origins of hippocampal Ivy and nitric oxide synthase expressing neurogliaform cells. J Neurosci *30*, 2165-2176.

Tricoire, L., Pelkey, K.A., Erkkila, B.E., Jeffries, B.W., Yuan, X., and McBain, C.J. (2011). A blueprint for the spatiotemporal origins of mouse hippocampal interneuron diversity. J Neurosci *31*, 10948-10970.

Tricoire, L., and Vitalis, T. (2012). Neuronal nitric oxide synthase expressing neurons: a journey from birth to neuronal circuits. Front Neural Circuits *6*, 82.

Tritsch, N.X., Ding, J.B., and Sabatini, B.L. (2012). Dopaminergic neurons inhibit striatal output through non-canonical release of GABA. Nature *490*, 262-266.

Tritsch, N.X., Granger, A.J., and Sabatini, B.L. (2016). Mechanisms and functions of GABA co-release. Nat Rev Neurosci *17*, 139-145.

Tritsch, N.X., Oh, W.J., Gu, C., and Sabatini, B.L. (2014). Midbrain dopamine neurons sustain inhibitory transmission using plasma membrane uptake of GABA, not synthesis. Elife *3*, e01936.

Trivellin, G., Bjelobaba, I., Daly, A.F., Larco, D.O., Palmeira, L., Faucz, F.R., Thiry, A., Leal, L.F., Rostomyan, L., Quezado, M*., et al.* (2016). Characterization of GPR101 transcript structure and expression patterns. Journal of molecular endocrinology *57*, 97-111.

Trivellin, G., Daly, A.F., Faucz, F.R., Yuan, B., Rostomyan, L., Larco, D.O., Schernthaner-Reiter, M.H., Szarek, E., Leal, L.F., Caberg, J.H*., et al.* (2014). Gigantism and Acromegaly Due to Xq26 Microduplications and GPR101 Mutation. The New England journal of medicine *371*, 2363-2374.

Turiault, M., Parnaudeau, S., Milet, A., Parlato, R., Rouzeau, J.D., Lazar, M., and Tronche, F. (2007). Analysis of dopamine transporter gene expression pattern -- generation of DAT-iCre transgenic mice. FEBS J *274*, 3568-3577.

Tye, K.M., Mirzabekov, J.J., Warden, M.R., Ferenczi, E.A., Tsai, H.C., Finkelstein, J., Kim, S.Y., Adhikari, A., Thompson, K.R., Andalman, A.S.*, et al.* (2013). Dopamine neurons modulate neural encoding and expression of depression-related behaviour. Nature *493*, 537-541.

Tzschentke, T.M., and Schmidt, W.J. (2000). Functional relationship among medial prefrontal cortex, nucleus accumbens, and ventral tegmental area in locomotion and reward. Critical reviews in neurobiology *14*, 131-142.

Unal, B., Ibanez-Sandoval, O., Shah, F., Abercrombie, E.D., and Tepper, J.M. (2011). Distribution of tyrosine hydroxylase-expressing interneurons with respect to anatomical organization of the neostriatum. Frontiers in systems neuroscience *5*, 41.

Unal, B., Shah, F., Kothari, J., and Tepper, J.M. (2015). Anatomical and electrophysiological changes in striatal TH interneurons after loss of the nigrostriatal dopaminergic pathway. Brain Struct Funct *220*, 331-349.

Ungless, M.A., and Grace, A.A. (2012a). Are you or aren't you? Challenges associated with physiologically identifying dopamine neurons. Trends Neurosci *35*, 422-430.

Ungless, M.A., and Grace, A.A. (2012b). Are you or aren't you? Challenges associated with physiologically identifying dopamine neurons. Trends in neurosciences *35*, 422-430.

Ungless, M.A., Magill, P.J., and Bolam, J.P. (2004). Uniform inhibition of dopamine neurons in the ventral tegmental area by aversive stimuli. Science *303*, 2040-2042.

Van Bockstaele, E.J., and Pickel, V.M. (1995). GABA-containing neurons in the ventral tegmental area project to the nucleus accumbens in rat brain. Brain Res *682*, 215-221.

van Zessen, R., Phillips, J.L., Budygin, E.A., and Stuber, G.D. (2012). Activation of VTA GABA neurons disrupts reward consumption. Neuron *73*, 1184-1194.

Vashchinkina, E., Panhelainen, A., Aitta-Aho, T., and Korpi, E.R. (2014). GABAA receptor drugs and neuronal plasticity in reward and aversion: focus on the ventral tegmental area. Front Pharmacol *5*, 256.

Vincent, S.R., and Kimura, H. (1992). Histochemical mapping of nitric oxide synthase in the rat brain. Neuroscience *46*, 755-784.

Vives, V., Alonso, G., Solal, A.C., Joubert, D., and Legraverend, C. (2003). Visualization of S100B-positive neurons and glia in the central nervous system of EGFP transgenic mice. J Comp Neurol *457*, 404-419.

Vong, L., Ye, C., Yang, Z., Choi, B., Chua, S., Jr., and Lowell, B.B. (2011). Leptin action on GABAergic neurons prevents obesity and reduces inhibitory tone to POMC neurons. Neuron *71*, 142-154.

Vruwink, M., Schmidt, H.H., Weinberg, R.J., and Burette, A. (2001). Substance P and nitric oxide signaling in cerebral cortex: anatomical evidence for reciprocal signaling between two classes of interneurons. J Comp Neurol *441*, 288-301.

Wamsley, B., and Fishell, G. (2017). Genetic and activity-dependent mechanisms underlying interneuron diversity. Nat Rev Neurosci *18*, 299-309.

Wang, H., Treadway, T., Covey, D.P., Cheer, J.F., and Lupica, C.R. (2015a). Cocaine-Induced Endocannabinoid Mobilization in the Ventral Tegmental Area. Cell Rep *12*, 1997-2008.

Wang, H.L., Qi, J., Zhang, S., Wang, H., and Morales, M. (2015b). Rewarding Effects of Optical Stimulation of Ventral Tegmental Area Glutamatergic Neurons. J Neurosci *35*, 15948-15954.

Wang, M., Vijayraghavan, S., and Goidman-Rakic, P.S. (2004). Selective D2 Receptor Actions on the Functional Circuitry of Working Memory. Science *303*, 853-856.

Wang, X., Liu, C., Wang, X., Gao, F., and Zhan, R.Z. (2017). Density and neurochemical profiles of neuronal nitric oxide synthase-expressing interneuron in the mouse basolateral amygdala. Brain Res *1663*, 106-113.

Wang, Y., and Marsden, P.A. (1995). Nitric oxide synthases: gene structure and regulation. Adv Pharmacol *34*, 71-90.

Watabe-Uchida, M., Zhu, L., Ogawa, S.K., Vamanrao, A., and Uchida, N. (2012). Whole-brain mapping of direct inputs to midbrain dopamine neurons. Neuron *74*, 858-873.

Wei, P., Pattarini, R., Rong, Y., Guo, H., Bansal, P.K., Kusnoor, S.V., Deutch, A.Y., Parris, J., and Morgan, J.I. (2012). The Cbln family of proteins interact with multiple signaling pathways. Journal of neurochemistry *121*, 717-729.

Wiszniak, S., Scherer, M., Ramshaw, H., and Schwarz, Q. (2015). Neuropilin-2 genomic elements drive cre recombinase expression in primitive blood, vascular and neuronal lineages. genesis *53*, 709-717.

Wolff, S.B., Grundemann, J., Tovote, P., Krabbe, S., Jacobson, G.A., Muller, C., Herry, C., Ehrlich, I., Friedrich, R.W., Letzkus, J.J*., et al.* (2014). Amygdala interneuron subtypes control fear learning through disinhibition. Nature *509*, 453-458.

Woodruff, A.R., McGarry, L.M., Vogels, T.P., Inan, M., Anderson, S.A., and Yuste, R. (2011). State-dependent function of neocortical chandelier cells. J Neurosci *31*, 17872-17886.

Wu, C.-S., Zhu, J., Wager-Miller, J., Wang, S., O'Leary, D., Monory, K., Lutz, B., Mackie, K., and Lu, H.-C. (2010). Requirement of cannabinoid CB1 receptors in cortical pyramidal neurons for appropriate development of corticothalamic and thalamocortical projections. European Journal of Neuroscience *32*, 693-706.

Xenias, H.S., Ibanez-Sandoval, O., Koos, T., and Tepper, J.M. (2015a). Are striatal tyrosine hydroxylase interneurons dopaminergic? J Neurosci *35*, 6584-6599.

Xenias, H.S., Ibáñez-Sandoval, O., Koós, T., and Tepper, J.M. (2015b). Are Striatal Tyrosine Hydroxylase Interneurons Dopaminergic? The Journal of Neuroscience *35*, 6584-6599.

Xie, Q.W., Cho, H.J., Calaycay, J., Mumford, R.A., Swiderek, K.M., Lee, T.D., Ding, A., Troso, T., and Nathan, C. (1992). Cloning and characterization of inducible nitric oxide synthase from mouse macrophages. Science *256*, 225-228.

Yamaguchi, T., Qi, J., Wang, H.L., Zhang, S., and Morales, M. (2015). Glutamatergic and dopaminergic neurons in the mouse ventral tegmental area. Eur J Neurosci *41*, 760-772.

Yamaguchi, T., Sheen, W., and Morales, M. (2007a). Glutamatergic neurons are present in the rat ventral tegmental area. The European journal of neuroscience *25*, 106-118.

Yamaguchi, T., Sheen, W., and Morales, M. (2007b). Glutamatergic neurons are present in the rat ventral tegmental area. The European journal of neuroscience *25*, 106-118.

Yamaguchi, T., Wang, H.L., Li, X., Ng, T.H., and Morales, M. (2011). Mesocorticolimbic glutamatergic pathway. J Neurosci *31*, 8476-8490.

Yamaguchi, T., Wang, H.L., and Morales, M. (2013). Glutamate neurons in the substantia nigra compacta and retrorubral field. Eur J Neurosci *38*, 3602-3610.

Yan, X.X., Jen, L.S., and Garey, L.J. (1996). NADPH-diaphorase-positive neurons in primate cerebral cortex colocalize with GABA and calcium-binding proteins. Cereb Cortex *6*, 524-529.

Yardan, T., Erenler, A.K., Baydin, A., Aydin, K., and Cokluk, C. (2011). Usefulness of S100B protein in neurological disorders. JPMA The Journal of the Pakistan Medical Association *61*, 276-281.

Zahm, D.S., and Heimer, L. (1988). Ventral striatopallidal parts of the basal ganglia in the rat: I. Neurochemical compartmentation as reflected by the distributions of neurotensin and substance P immunoreactivity. J Comp Neurol *272*, 516-535.

Zahniser, N.R., and Sorkin, A. (2004). Rapid regulation of the dopamine transporter: role in stimulant addiction? Neuropharmacology *47 Suppl 1*, 80-91.

Zeisel, A., Muñoz-Manchado, A.B., Codeluppi, S., Lönnerberg, P., La Manno, G., Juréus, A., Marques, S., Munguba, H., He, L., Betsholtz, C.*, et al.* (2015). Cell types in the mouse cortex and hippocampus revealed by single-cell RNA-seq. Science *347*, 1138-1142.

Zhang, J., Lanuza, Guillermo M., Britz, O., Wang, Z., Siembab, Valerie C., Zhang, Y., Velasquez, T., Alvarez, Francisco J., Frank, E., and Goulding, M. (2014). V1 and V2b Interneurons Secure the Alternating Flexor-Extensor Motor Activity Mice Require for Limbed Locomotion. Neuron *82*, 138-150.

Zhang, S., Qi, J., Li, X., Wang, H.L., Britt, J.P., Hoffman, A.F., Bonci, A., Lupica, C.R., and Morales, M. (2015). Dopaminergic and glutamatergic microdomains in a subset of rodent mesoaccumbens axons. Nat Neurosci *18*, 386-392.

Zhou, F.-M., and Lee, C.R. (2011). Intrinsic and integrative properties of substantia nigra pars reticulata neurons. Neuroscience *198*, 69-94.

Zhou, F.-W., Jin, Y., Matta, S.G., Xu, M., and Zhou, F.-M. (2009). An Ultra-Short Dopamine Pathway Regulates Basal Ganglia Output. The Journal of Neuroscience *29*, 10424-10435.

Zsiros, V., and Maccaferri, G. (2005). Electrical coupling between interneurons with different excitable properties in the stratum lacunosum-moleculare of the juvenile CA1 rat hippocampus. J Neurosci *25*, 8686-8695.

Appendix 1: RNA-Seq candidate checklist

Gene Symbol	Fold-enrichment	P-Adj	Mean RPKM GABA-IP	Mean RPKM DA-IP	PANTHER	ABA density	ABA ISH	Cre-Driver
Nacc2	1.79	2.84E-25	3231.74	911.3267	✓	✓		
Penk	2.81	7.18E-25	1796.75	228.77	✓			
Chga	2.15	6.29E-24	4896.917	1049.323	✓			
Kcng4	3.32	4.06E-19	1389.357	106.44	✓	✓		
Lhx5	2.81	1.55E-18	318.82	39.03333	✓	✓		
Kcna6	1.28	1.80E-18	1464.79	593.5133	✓	✓		
Gata3	**2.44**	**9.03E-18**	**365.6367**	**61.13**	✓	✓	✓	✓
Laptm4b	1.66	6.37E-17	1168.67	357.1167	✓			
Arl4c	1.63	3.74E-15	1518.903	472.9867	✓			
Ranbp6	1.15	6.47E-15	809.07	362.4967	✓			
Gjd2	1.82	1.86E-14	192.1167	51.12	✓	✓		
Pnoc	2.82	3.01E-14	386.61	43.27	✓	✓	✓	
Cox5a	2.26	1.08E-13	4193.673	784.3333	✓			
Scn4b	2.21	2.66E-13	2957.637	576.26	✓	✓		
Slc32a1	2.55	3.38E-13	1914.253	274.8567	✓			
Slc25a4	1.57	1.05E-12	8989.233	2907.3	✓			
Atp5g3	1.94	1.18E-12	6655.607	1611.4	✓			
Esrrg	2.25	3.15E-12	1354.817	251.96	✓	✓		
Cox4i1	1.70	3.48E-12	8413.47	2471.823	✓			
Cited1	2.53	3.77E-12	137.5733	19.28	✓	✓		
Epn3	1.97	3.85E-12	264.1567	62.79333	✓	✓		
Htr7	1.46	5.38E-12	284.9833	100.4	✓			
Lgi2	1.88	9.14E-12	2850.133	722.42	✓	✓		
Fgf9	1.56	9.49E-12	542.7533	175.7933	✓			
Esrrb	2.65	1.20E-11	158.5267	19.49333	✓	✓		
Paqr4	1.56	1.23E-11	1279.427	414.3	✓	✓		
Htr2c	1.42	1.32E-11	1269.547	460.8033	✓			
Atp5b	1.54	2.13E-11	18696.36	6189.863	✓			
Tmem130	1.67	2.29E-11	6612.5	1980.813	✓			
Atp5a1	1.73	2.84E-11	16712.08	4761.343	✓			
Asic4	1.90	2.85E-11	569.2467	140.4267	✓			
Cdc42ep2	1.65	5.84E-11	203.4067	60.59667	✓			
Dner	2.20	6.87E-11	4871.447	931.2533	✓			
Vdac3	1.18	1.03E-10	2422.273	1052.277	✓			
Hcn2	1.13	2.12E-10	2742.597	1235.527	✓			
Gabra1	1.35	3.58E-10	4683.343	1789.973	✓			
Cd59a	1.57	4.37E-10	350.3333	113.65	✓			
Cabp7	1.07	4.70E-10	1465.123	685.67	✓	✓	✓	
Nxph1	1.87	4.94E-10	681.9033	169.6567	✓	✓	✓	
Nrtn	2.49	6.32E-10	137.3333	19.12667	✓			
Kcnh2	1.36	6.57E-10	1056.453	398.18	✓			
Gabarapl2	1.80	7.16E-10	3506.833	928.1567	✓			
SOM	**2.20**	**7.93E-10**	**2331.097**	**433.47**	✓	✓	✓	✓
Nxph4	2.09	1.13E-09	164.6833	32.59	✓	✓		
Atp5o	1.72	1.13E-09	3584.743	1014.373	✓			
Edf1	1.53	1.21E-09	1683.71	552.6267	✓			
Atp1a3	1.48	1.23E-09	28744.88	9889.833	✓			
Atp5g1	1.64	1.35E-09	2301.66	691.9267	✓			
Atp6v0c	1.66	1.39E-09	10728.09	3181.683	✓			
Slc25a11	1.30	1.43E-09	1535.81	605.8767	✓			
Sp9	2.44	1.55E-09	138.32	20.07667	✓			
Timm17a	1.52	2.51E-09	1041.037	344.2733	✓			
Kcnab2	1.04	2.81E-09	4554.973	2185.977	✓	✓		
Cand1	0.89	3.30E-09	1747.043	936.9867	✓			
Glra1	2.59	3.39E-09	459.71	57.52667	✓	✓		
Rcan2	1.48	4.43E-09	4398.79	1504.743	✓			
Rom1	1.50	5.88E-09	154.58	52.08	✓	✓		

Gene Symbol	Fold-enrichment	P-Adj	Mean RPKM GABA-IP	Mean RPKM DA-IP	PANTHER	ABA density	ABA ISH	Cre-Driver
Lrrc38	2.37	5.88E-09	84.26333	12.63	✓			
B3galt5	0.92	6.69E-09	686.4667	358.4333	✓	✓		
Kcnk3	1.17	6.87E-09	539.1467	233.5933	✓			
Strap	1.07	7.16E-09	1677.287	785.7	✓			
Slc35g2	1.72	7.60E-09	462.16	129.8433	✓			
Kcnip1	1.47	8.31E-09	482.15	165.0667	✓	✓		
Ctnnbip1	1.12	9.05E-09	782.7133	351.03	✓	✓		
Vdac2	0.97	1.01E-08	2453.1	1235.567	✓	✓		
Atp5j2	1.90	1.11E-08	3096.203	743.7867	✓	✓		
Sall2	0.96	1.34E-08	918.24	465.3133	✓	✓		
Park7	1.55	1.57E-08	2516.723	807.8633	✓			
Wbp5	1.76	1.78E-08	1506.433	406.15	✓			
BC031181	1.43	1.90E-08	1549.63	547.4567	✓	✓		
Ndrg4	1.19	1.90E-08	28873.88	12361.5	✓			
Diras1	1.66	2.33E-08	3018.373	883.7033	✓			
Slc1a6	2.08	2.50E-08	512.3767	103.5867	✓	✓		
Hpcal1	1.69	2.76E-08	1352.763	385.6033	✓	✓		
Atp5e	1.93	2.87E-08	1497.373	346.45	✓			
Cib2	1.47	3.19E-08	611.9167	209.97	✓			
Vdac1	1.17	3.29E-08	6534.077	2829.883	✓			
Gnl1	1.02	3.49E-08	2654.463	1282.653	✓	✓		
Atp6v1h	1.04	3.93E-08	2108.567	1010.333	✓			
Irx3	1.92	4.34E-08	121.7167	27.62667	✓			
Akt1	0.81	4.53E-08	2237.667	1262.777	✓			
Spryd3	1.27	4.65E-08	2634.163	1056.483	✓			
Tal1	1.63	4.74E-08	351.97	105.65	✓			
Gpr62	1.65	4.84E-08	198.0867	57.5	✓			
Ap2m1	0.94	5.04E-08	6138.733	3151.987	✓			
Fgf18	2.00	6.27E-08	60.66	12.98333	✓	✓		
Mtch1	1.15	6.68E-08	5388.947	2364.867	✓			
Scn1b	1.18	6.86E-08	4537.47	1946.817	✓			
Vps45	0.98	9.58E-08	418.0267	207.5967	✓			
Fkbp2	1.38	1.13E-07	1623.637	598.25	✓			
Tac1	1.54	1.17E-07	392.32	126.58	✓			
Slc25a5	1.44	1.22E-07	2508.937	877.3267	✓			
Slc41a3	1.84	1.33E-07	203.89	49.90667	✓	✓		
Cacng5	1.47	1.46E-07	208.45	70.36	✓	✓		
Pink1	1.01	1.49E-07	3796.13	1844.77	✓			
Arl3	1.26	1.59E-07	1120.197	449.7633	✓			
Tceal1	1.61	1.63E-07	619.2367	186.3733	✓			
Srp9	1.34	2.05E-07	1469.057	553.12	✓			
Atp6v1a	1.11	2.17E-07	6673.747	3011.87	✓			
Zc3h15	0.97	2.18E-07	1838.573	924.09	✓			
Gnas	1.34	2.65E-07	20626.89	7791.087	✓			
Crhbp	1.52	3.04E-07	206.07	66.22	✓	✓	✓	
Hgs	0.89	3.19E-07	956.4967	509.55	✓			
Scn2b	1.07	3.63E-07	3641.967	1695.46	✓			
Nell1	1.57	4.01E-07	962.4	301.4933	✓			
Pitpna	1.02	4.06E-07	4970.797	2406.947	✓			
Atp5d	1.34	4.15E-07	2996.69	1126.387	✓			
Map1lc3a	1.45	4.40E-07	2539.693	874.2067	✓	✓		
Slc6a1	0.67	4.56E-07	3715.207	2325.19	✓	✓		
Cdip1	0.95	5.16E-07	3498.31	1777.973	✓			
Eef1e1	1.41	5.65E-07	461.84	162.8133	✓			
Tceb2	1.54	6.08E-07	1577.92	504.0033	✓			
Nfe2l1	0.87	8.16E-07	4413.38	2381.94	✓			
Fgf1	1.29	8.59E-07	1267.853	493.4033	✓			
Acp1	1.07	8.88E-07	896.7633	417.82	✓	✓		

Gene Symbol	Fold-enrichment	P-Adj	Mean RPKM GABA-IP	Mean RPKM DA-IP	PANTHER	ABA density	ABA ISH	Cre-Driver
Lrrc49	0.89	1.04E-06	1231.783	652.9367	✓			
Chrna2	2.28	1.19E-06	50.75333	7.256667	✓	✓		
Nr2f2	1.15	1.24E-06	607.7667	265.5767	✓	✓		
Tomm7	1.57	1.29E-06	815.01	249.9167	✓			
Timm22	1.32	1.33E-06	457.6533	174.0367	✓			
Kcnk1	1.03	1.53E-06	879.43	418.1467	✓			
Fzd1	1.09	1.56E-06	210.48	95.46	✓	✓		
Timm10	1.52	1.59E-06	313.2467	99.81667	✓	✓		
Clpp	0.91	1.67E-06	726.94	380.6033	✓			
Zfp385a	1.33	1.67E-06	1533.727	580.79	✓			
Leprotl1	1.18	1.68E-06	1050.467	445.77	✓			
Lrrn2	1.14	1.73E-06	1247.713	547.2733	✓			
Chrm2	1.48	1.73E-06	325.0467	108.2167	✓	✓		
Gabrg2	0.92	1.82E-06	2167.853	1131.097	✓			
Nkiras1	1.03	1.85E-06	1891.387	905.7367	✓	✓		
Kcnc1	1.04	1.87E-06	3686.31	1756.373	✓			
Irx1	1.33	1.96E-06	104.5567	38.53333	✓	✓	✓	
Zfp521	1.45	1.97E-06	341.6333	115.4867	✓	✓		
Ddt	1.68	1.99E-06	426.1567	118.0633	✓	✓		
Relt	1.02	2.00E-06	338.6033	163.5467	✓	✓		
Slc25a33	1.19	2.10E-06	718.0433	303.9233	✓			
Nenf	1.55	2.27E-06	669.8533	209.4033	✓	✓	✓	
Cntnap2	1.29	2.32E-06	856.9733	334.55	✓			
Sfrp2	2.29	2.35E-06	67.23	8.67	✓	✓		
Tspan3	1.32	2.38E-06	3959.87	1503.787	✓			
Tomm40	0.72	2.49E-06	999.0767	600.76	✓			
Emc6	1.20	2.51E-06	526.0533	218.27	✓			
Kcna1	1.22	2.57E-06	2886.007	1193.697	✓			
Bag3	1.22	2.73E-06	232.7433	94.52667	✓	✓		
Clec2l	1.09	2.75E-06	998.82	455.4633	✓			
Rcan3	1.12	2.77E-06	920.5133	411.1733	✓	✓		
Gnal	1.00	2.78E-06	1889.363	922.7533	✓	✓		
Hbegf	1.04	3.10E-06	172.3633	82.69667	✓			
Nkx6-1	2.17	3.18E-06	37.62	5.993333	✓	✓		
Bcap31	1.03	3.23E-06	805.65	385.5267	✓			
Iltifb	2.68	3.32E-06	67.34333	5.076667	✓			
Prelid1	1.16	3.38E-06	1476.883	635.3233	✓			
Spcs1	1.33	3.39E-06	1104.093	415.1767	✓			
Slc39a6	0.87	3.46E-06	640.35	344.1033	✓			
Cited2	1.26	3.76E-06	533.2567	212.2933	✓			
Smyd2	0.93	4.06E-06	1194.53	613.3133	✓			
Lhx1	2.09	4.23E-06	221.4	40.24667	✓	✓		
Gpr101	**1.24**	**4.25E-06**	**188.53**	**76.74**	✓	✓	✓	✓
Cerk	1.09	4.36E-06	1784.507	811.5367	✓	✓		
Nectin2	1.31	4.41E-06	164.9533	61.85	✓			
Thy1	1.36	4.52E-06	6444.94	2361.82	✓			
Asph	1.19	4.52E-06	1538.113	650.4233	✓	✓		
Gng3	1.31	4.58E-06	2507.127	958.01	✓			
Cadm4	1.28	4.78E-06	3546.777	1388.463	✓			
Slc25a25	0.90	4.83E-06	1287.3	679.1767	✓			
Dach1	1.34	4.86E-06	153.8433	57.37	✓	✓		
Uqcr10	1.34	4.91E-06	1377.41	513.97	✓			
Slmo2	1.16	4.93E-06	762.94	327.32	✓	✓		
Ctbp1	0.87	5.11E-06	2779.237	1493.28	✓			
Pax2	2.64	5.23E-06	54.68333	3.886667	✓			
Scg2	1.54	5.79E-06	7920.59	2481.303	✓			
Atg101	1.14	6.44E-06	367.67	159.59	✓			
Mapk8ip2	0.79	6.64E-06	3794.153	2177.583	✓			
Znhit2	1.45	6.66E-06	319.8733	107.14	✓			

Gene Symbol	Fold-enrichment	P-Adj	Mean RPKM GABA-IP	Mean RPKM DA-IP	PANTHER	ABA density	ABA ISH	Cre-Driver
Chgb	1.25	6.94E-06	5116.217	2054.723	✓			
Hap1	0.91	7.08E-06	4457.197	2340.453	✓			
Tceal3	1.20	7.42E-06	1337.217	555.2367	✓			
Otp	2.55	7.46E-06	41.39667	3.24	✓	✓		
Atp6v1c1	1.08	7.53E-06	2846.98	1310.343	✓			
Slc27a4	0.72	7.60E-06	1475.85	887.3567	✓			
Gprc5b	0.92	7.75E-06	1869.51	965.48	✓			
Btbd11	1.10	7.95E-06	698.3933	317.52	✓			
Colq	1.84	8.09E-06	62.17	14.92667	✓			
Grid2	2.12	8.11E-06	416.38	71.31333	✓	✓		
Snw1	0.73	8.41E-06	801.76	478.49	✓	✓		
Srprb	1.00	9.15E-06	441.48	215.34	✓	✓		
Psap	0.97	9.71E-06	19073.8	9504.007	✓			
Cox7a2l	1.09	9.71E-06	1533.68	699.64	✓			
Naca	1.07	9.96E-06	2137.707	983.9333	✓			
Pepd	0.94	1.05E-05	426.6633	217.26	✓			
Pax8	2.38	1.11E-05	32.95	3.44	✓			
Cacng2	1.51	1.33E-05	2555.06	816.9867	✓	✓		
Cbln4	**1.28**	**1.42E-05**	**339.7667**	**131.8633**	✓	✓	✓	✓
Lrrc4b	0.85	1.52E-05	1687.767	920.4467	✓			
Glrb	0.97	1.61E-05	2723.977	1357.263	✓			
Scg5	1.15	1.63E-05	2101.147	911.8933	✓			
Slc38a1	1.07	1.70E-05	3379.11	1561.937	✓			
Akr1a1	1.19	1.70E-05	4543.883	1910.65	✓			
Psmd14	0.80	1.70E-05	972.7867	550.4533	✓			
Ngb	1.38	1.73E-05	225.2767	80.41667	✓	✓	✓	
Hoxb5	2.28	1.81E-05	22.59667	2.336667	✓	✓		
Kcnmb2	1.58	1.81E-05	94.18	27.83333	✓			
Pgrmc2	0.91	1.84E-05	1209.97	631.37	✓			
Necap1	1.15	2.04E-05	2958.043	1280.097	✓			
Htr3a	1.46	2.17E-05	93.14667	30.74333	✓			
Nova1	0.97	2.20E-05	1816.893	908.99	✓			
Aes	0.98	2.20E-05	4328.98	2139.803	✓			
Lmo1	1.15	2.26E-05	181.6033	78.05333	✓			
Gal	2.12	2.45E-05	33.43333	5.063333	✓			
Gpr149	1.68	2.49E-05	48.46333	13.17667	✓			
Bsg	1.12	2.51E-05	6583.403	2907.047	✓			
Bag5	1.32	2.61E-05	644.6333	241.16	✓	✓		
Cltc	1.02	2.64E-05	7775.373	3737.97	✓			
Chrnb2	0.68	2.79E-05	1083.363	670.3367	✓	✓		
Hoxa5	2.47	2.90E-05	14.18333	0.883333	✓			
Taf7	1.23	2.94E-05	140.5267	56.36333	✓	✓		
Caln1	1.25	3.04E-05	655.6133	261.8833	✓			
Snd1	0.68	3.05E-05	950.0433	588.1633	✓			
Calca	1.87	3.06E-05	63.31333	13.29333	✓			
Atp9a	0.70	3.18E-05	3789.78	2309.207	✓	✓		
Panx2	0.60	3.21E-05	1658.003	1085.027	✓	✓		
Zbtb4	0.55	3.39E-05	1783.443	1212.36	✓			
Slco3a1	0.80	3.51E-05	601.0267	341.35	✓			
Atp6v1b2	1.26	3.95E-05	11193.88	4421.313	✓			
Hmgb3	1.28	3.97E-05	305.1033	116.6367	✓			
Cplx1	1.35	4.52E-05	15033.27	5501.977	✓			
Rxfp3	**1.71**	**4.59E-05**	**82.16333**	**21.23667**	✓	✓	✓	✓
Btf3	1.16	4.68E-05	1527.66	653.36	✓			
Gnb5	0.82	4.69E-05	1492.13	829.49	✓	✓		
Eif3h	0.92	4.73E-05	1038.55	534.65	✓			
Sox14	1.98	4.76E-05	70.85	13	✓	✓	✓	
Gpr176	1.04	4.93E-05	197.9633	93.30667	✓	✓		
Ramp3	1.52	5.00E-05	235.15	72.57	✓			

Gene Symbol	Fold-enrichment	P-Adj	Mean RPKM GABA-IP	Mean RPKM DA-IP	PANTHER	ABA density	ABA ISH	Cre-Driver
Ctnna2	0.95	5.15E-05	1276.057	643.28	✓	✓		
Bcl2l1	1.00	5.15E-05	1476.957	716.1333	✓			
Arf6	0.91	5.21E-05	703.47	364.58	✓	✓		
Pam16	0.91	5.38E-05	330.6133	171.5067	✓			
Ik	0.93	5.43E-05	1972.033	1014.18	✓			
Disp2	0.59	5.60E-05	4852.68	3208.393	✓			
0610009B22Rik	1.08	5.72E-05	218.84	98.33	✓			
Eef1g	0.86	5.78E-05	3423.557	1857.813	✓			
Alpk2	2.46	6.29E-05	48.64333	3.29	✓			
Timm8b	1.23	6.47E-05	778.6867	311.3033	✓			
Tspan9	0.94	6.56E-05	641.6967	325.4167	✓	✓	✓	
Gsto1	1.07	6.69E-05	325.92	148.0367	✓	✓	✓	
Snx3	1.21	6.88E-05	1684.897	689.5133	✓			
Fxyd6	1.33	7.00E-05	1755.023	645.71	✓			
Vmp1	0.75	7.04E-05	923.6567	542.3367	✓			
Pax7	1.81	7.31E-05	124.3933	27.73667	✓	✓		
Sik3	0.55	7.47E-05	1458.633	992.9033	✓			
Impad1	1.01	7.61E-05	1848.75	889.7733	✓			
Gbx2	1.54	9.13E-05	32.96333	9.763333	✓			
Reep1	0.78	9.40E-05	1601.527	918.1867	✓			
Morf4l1	0.91	9.67E-05	5902.477	3069.507	✓			
Paqr9	1.08	9.93E-05	180.81	80.47333	✓			
Megf11	1.35	1.01E-04	433.2133	156.28	✓	✓	✓	
Gne	0.76	1.02E-04	453.86	263.2	✓	✓		
Kcnc4	0.86	1.04E-04	1002.367	539.33	✓	✓	✓	
Khdrbs1	0.69	1.06E-04	1461.263	895.4133	✓			
Timm17b	1.07	1.08E-04	277.39	126.1333	✓			
Tfam	0.78	1.10E-04	556.86	319.0967	✓			
Cuta	1.14	1.22E-04	703.3333	302.54	✓			
Fbxo45	0.74	1.24E-04	842.4567	495.66	✓	✓		
Tceal6	1.31	1.25E-04	838.9233	311.0567	✓			
Pex14	1.03	1.27E-04	524.7767	246.7467	✓	✓	✓	
Atg9b	0.88	1.27E-04	134.04	71.11333	✓			
Gabarapl1	1.07	1.30E-04	6984.357	3204.983	✓			
Mcfd2	0.97	1.30E-04	897.2667	443.8433	✓			
Map1lc3b	0.95	1.33E-04	2240.5	1127.513	✓			
Dusp10	1.41	1.35E-04	156.53	52.71333	✓	✓		
Slc35e4	0.96	1.35E-04	294.6433	145.5433	✓			
Bnip3	1.01	1.35E-04	1233.073	593.3567	✓			
Sfrp1	1.52	1.41E-04	140.29	42.04	✓	✓		
Uncx	1.33	1.44E-04	85.23667	31.48333	✓	✓		
Arhgdig	1.01	1.53E-04	841.82	402.8067	✓			
Smad9	1.08	1.59E-04	314.5167	141.8967	✓			
Cdipt	0.68	1.63E-04	1183.453	728.5567	✓			
Gabrb2	1.11	1.66E-04	2918.663	1288.993	✓	✓	✓	
Gdf11	0.92	1.66E-04	307.6333	157.8633	✓	✓		
Edil3	1.02	1.68E-04	1479.59	703.5467	✓	✓		
Rhd	2.32	1.68E-04	11.21667	0.823333	✓			
Atp6v1f	1.20	1.69E-04	1224.943	498.81	✓			
B3gnt5	2.03	1.71E-04	48.46333	7.896667	✓			
Cbln1	1.58	1.74E-04	196.9833	55.74333	✓			
Cops8	0.75	1.80E-04	1130.863	663.8067	✓			
Gdi2	0.69	1.81E-04	2364.52	1445.08	✓			
Cckar	2.18	1.82E-04	24.53333	2.65	✓	✓	✓	
Slc25a12	0.75	1.91E-04	2217.16	1296.007	✓			
C1d	1.11	1.95E-04	686.4033	303.3833	✓	✓		
Pitx2	1.48	1.96E-04	77.17	24.45	✓			
Panx1	1.00	1.96E-04	221.53	106.43	✓	✓	✓	

Gene Symbol	Fold-enrichment	P-Adj	Mean RPKM GABA-IP	Mean RPKM DA-IP	PANTHER	ABA density	ABA ISH	Cre-Driver
Jund	1.30	1.98E-04	2244.913	838.9933	✓			
Cnr1	0.66	2.00E-04	1286.257	807.8967	✓			
Hdgf	0.64	2.04E-04	2251.333	1430.737	✓			
Erh	1.16	2.07E-04	758.85	318.45	✓	✓		
Pqbp1	1.00	2.08E-04	808.69	388.0933	✓	✓		
Nrxn3	1.26	2.08E-04	4975.547	1928.163	✓			
Atp6v0d1	0.96	2.18E-04	2391.237	1195.013	✓			
Dpp6	0.66	2.19E-04	2533.46	1587.083	✓	✓		
Asic2	0.71	2.20E-04	629.2033	380.73	✓			
Inhbb	1.16	2.36E-04	142.3667	59.46	✓			
Kcnab1	0.96	2.39E-04	884.7233	440.2667	✓	✓		
Cnih1	1.15	2.46E-04	887.16	376.83	✓			
Plcl1	0.88	2.47E-04	203.13	107.3933	✓	✓	✓	
Abcf1	0.68	2.48E-04	1274.323	786.6967	✓	✓		
Atp6ap1	0.76	2.51E-04	3972.157	2303.657	✓			
Fam195b	0.96	2.53E-04	1106.237	550.2367	✓			
G3bp2	0.72	2.56E-04	3296.087	1973.32	✓			
Cgref1	0.91	2.66E-04	308.3067	159.6867	✓			
Slc35e1	0.63	2.74E-04	698.37	447.2067	✓			
Slc24a2	0.61	2.74E-04	3619.533	2354.457	✓			
Supt4a	1.06	2.93E-04	559.6867	256.5367	✓			
Arf1	0.87	2.99E-04	3511.007	1869.167	✓			
Chp1	0.88	3.00E-04	1897.157	1009.077	✓			
Zmat2	0.99	3.03E-04	2444.21	1186.443	✓			
Ppargc1a	0.96	3.12E-04	883.72	438.67	✓	✓		
Nts	**1.47**	**3.40E-04**	**81.83**	**25.08333**	✓	✓	✓	✓
Tceal8	1.05	3.41E-04	473.6733	217.14	✓	✓	✓	
Fam58b	1.16	3.42E-04	164.44	68.34	✓			
Cdc5l	0.78	3.53E-04	723.5967	415.57	✓	✓		
Esrra	0.89	3.63E-04	1153.583	607.19	✓	✓		
Gjc2	1.12	3.78E-04	375.46	163.3933	✓			
Apoa2	1.63	3.99E-04	25.18	6.5	✓			
Atp6v1g1	0.90	4.02E-04	934.7	486.4667	✓			
Htr1b	1.62	4.11E-04	38.77333	10.05667	✓	✓		
Apbb1	0.67	4.23E-04	3730.757	2320.99	✓			
Apol8	1.23	4.39E-04	144.6133	56.91667	✓			
G0s2	1.25	4.67E-04	95.10333	36.44667	✓	✓		
Paqr7	0.97	4.83E-04	776.7967	381.5867	✓			
Slc25a39	0.85	4.84E-04	921.8667	501.1333	✓	✓		
Rora	**1.10**	**4.95E-04**	**1535.063**	**680.19**	✓	✓	✓	✓
Wnt9b	1.56	4.99E-04	28.17	7.94	✓			
Fgf12	1.16	5.29E-04	1472.06	618.8333	✓	✓	✓	
Lgi3	0.69	5.39E-04	2366.433	1448.927	✓			
Sac3d1	1.15	5.40E-04	171.9333	71.91333	✓			
Elmo1	1.09	5.44E-04	1636.043	725.8767	✓			
Csk	0.67	5.45E-04	571.7067	357.7767	✓			
Grm1	1.38	5.49E-04	864.7967	295.3433	✓	✓		
Noa1	0.66	5.55E-04	263.7533	165.3467	✓			
M6pr	0.63	5.59E-04	1182.927	756.2	✓	✓		
Praf2	1.08	5.61E-04	923.4167	414.9967	✓			
Zbtb7a	0.91	5.61E-04	1189.33	613.8433	✓			
Tspan12	0.84	5.63E-04	221.7667	119.69	✓			
Olfm3	1.01	5.87E-04	455.1633	216.8167	✓			
Znhit1	0.85	6.00E-04	558.29	302.75	✓	✓		
Slc5a1	2.19	6.10E-04	22.69667	1.003333	✓	✓	✓	
Maf	0.85	6.11E-04	514.4	278.7067	✓			
Abcg1	0.74	6.12E-04	483.5333	282.0833	✓	✓		
Tomm22	0.92	6.22E-04	806.0767	412.58	✓	✓		
Lrfn3	0.81	6.22E-04	201.8967	111.81	✓			

Gene Symbol	Fold-enrichment	P-Adj	Mean RPKM GABA-IP	Mean RPKM DA-IP	PANTHER	ABA density	ABA ISH	Cre-Driver
Atp2a3	1.72	6.22E-04	493.4833	115.8267	✓	✓		
Mapk6	0.79	6.55E-04	1043.05	592.1533	✓			
Unc119	0.90	7.00E-04	559.1533	290.1333	✓			
Pdcd2	0.79	7.01E-04	252.2967	143.34	✓	✓		
Arl8b	0.75	7.01E-04	1564.757	910.5367	✓	✓		
Tigd2	0.92	7.27E-04	203.0833	103.9833	✓			
Pgr15l	1.47	7.49E-04	26.95667	8.676667	✓			
Ptger4	1.56	7.49E-04	30.26667	8.606667	✓	✓		
Plcl2	0.67	7.59E-04	776.8	483.1733	✓			
Asna1	0.90	7.66E-04	934.27	483.12	✓			
Cabp1	0.97	8.06E-04	1818.407	896.1433	✓			
Pura	0.78	8.11E-04	4653.777	2662.423	✓			
Fxn	0.93	8.91E-04	93.88333	47.27667	✓			
Nkx6-2	1.28	9.17E-04	363.7667	134.8333	✓			
Opn3	1.01	9.25E-04	84.17667	40.46667	✓	✓		
Isl1	1.79	9.29E-04	55.11	11.6	✓	✓		
Il17d	0.85	9.39E-04	119.14	63.30333	✓			
Vegfb	0.60	9.45E-04	637.6233	415.87	✓	✓		
Zbtb7b	0.54	9.74E-04	288.44	197.47	✓	✓		
Cox8b	2.08	9.75E-04	16.19333	1.073333	✓	✓		
Lrrn1	1.01	9.89E-04	629.9467	298.37	✓	✓		
Zfp536	1.01	9.96E-04	507.0133	241.96	✓			
Aqp6	2.00	1.01E-03	34.78667	3.96	✓			
Tsc22d3	0.79	1.02E-03	1926.167	1089.613	✓	✓		
Pdlim2	1.44	1.02E-03	284.85	88.49333	✓	✓	✓	
Drap1	0.91	1.02E-03	1440.077	743.3333	✓			
Atp6v0e2	0.92	1.04E-03	3619.613	1846.297	✓			
Tm9sf3	0.60	1.07E-03	1918.803	1256.297	✓			
Glra2	1.13	1.08E-03	195.2333	82.62333	✓	✓	✓	
Tnfrsf21	0.93	1.08E-03	1061.733	534.5933	✓			
Tmco3	0.54	1.16E-03	480.0133	329.0967	✓	✓		
Rltpr	0.52	1.16E-03	906.9067	628.8533	✓	✓	✓	
Akr1b3	0.72	1.18E-03	417.51	247.77	✓			
Orai1	1.07	1.18E-03	86.63667	38.39333	✓			
Homer3	1.90	1.18E-03	1046.507	166.94	✓	✓		
Zfp771	0.71	1.23E-03	452.27	271.2467	✓	✓		
Kcnd2	0.58	1.26E-03	934.73	619.31	✓	✓		
Shroom2	0.76	1.27E-03	1078.467	627.3033	✓	✓		
Hoxc4	1.65	1.28E-03	17.80667	4.353333	✓			
Scp2	0.81	1.30E-03	1188.877	657.9433	✓	✓		
Taf10	0.83	1.34E-03	630.9633	345.1	✓			
Arl6ip5	1.01	1.34E-03	1394.297	656.8667	✓			
Tmem147	0.65	1.43E-03	765.3667	483	✓	✓		
Nos1	**0.98**	**1.45E-03**	**955.4967**	**461.21**	✓	✓	✓	✓
Msl3l2	0.91	1.46E-03	139.2633	69.96	✓			
Nfatc2	0.86	1.47E-03	390.91	208.89	✓			
Nr2f6	0.72	1.54E-03	547.3767	326.95	✓			
Tom1l2	0.76	1.57E-03	4047.91	2345.077	✓			
Hcrtr2	1.09	1.58E-03	60.08667	26.91667	✓			
Myh7b	0.95	1.61E-03	239.2433	119.16	✓			
Tm9sf2	0.63	1.61E-03	1083.71	693.76	✓			
Polr2g	0.81	1.64E-03	754.91	418.9867	✓			
Slc35d3	1.15	1.65E-03	33.30667	14.09333	✓	✓	✓	
Trh	**1.50**	**1.67E-03**	**132.47**	**37.27**	✓	✓	✓	✓
Grin3a	0.66	1.67E-03	522.47	326.4633	✓			
Pex7	0.72	1.69E-03	320.0933	191.8267	✓			
Kat5	0.46	1.75E-03	720.8967	519.85	✓	✓		
Nfkbib	0.89	1.76E-03	233.3433	120.3733	✓			
Zfpm2	0.83	1.80E-03	219.63	120.2067	✓	✓		

Gene Symbol	Fold-enrichment	P-Adj	Mean RPKM GABA-IP	Mean RPKM DA-IP	PANTHER	ABA density	ABA ISH	Cre-Driver
Kcnk15	2.01	1.85E-03	10.45	0.593333	✓			
Cdc42	0.65	1.89E-03	3326.693	2095.673	✓			
Arf5	0.84	1.90E-03	1332.203	721.5167	✓			
Kcnj12	0.90	1.93E-03	131.2967	67.07	✓			
Pgrmc1	0.87	1.99E-03	3332.887	1759.613	✓	✓	✓	
Grb2	0.85	2.02E-03	1632.727	875.31	✓	✓		
Gabbr1	0.50	2.06E-03	7030.54	4929.707	✓			
Gnai1	0.67	2.09E-03	1456.833	900.4267	✓	✓	✓	
Grm8	0.94	2.14E-03	151.8833	75.27	✓	✓	✓	
Gabarap	0.93	2.14E-03	1608.097	807.4933	✓			
Grm4	0.88	2.15E-03	588.3333	310.1733	✓			
Scg3	0.88	2.16E-03	1990.707	1045.157	✓			
Taf13	0.91	2.17E-03	525.6767	270.0533	✓	✓		
Jkamp	0.77	2.17E-03	750.8233	431.85	✓	✓		
Nlrp10	1.98	2.18E-03	17.38	1.03	✓			
Zmynd19	0.82	2.19E-03	403.9433	222.5867	✓			
Doc2b	0.73	2.20E-03	556.0867	328.03	✓	✓		
En2	**1.14**	**2.21E-03**	**186.8033**	**78.50333**	✓	✓	✓	✓
Gnb1	0.62	2.21E-03	5601.103	3601.1	✓			
Arl8a	0.66	2.24E-03	1744.92	1085.063	✓			
Mbp	1.01	2.24E-03	23680.86	11094.05	✓			
Casz1	1.34	2.25E-03	144.3333	50.28	✓	✓		
Mlf2	0.64	2.41E-03	3581.83	2267.243	✓			
Gabrg1	0.81	2.56E-03	329.9467	183.72	✓	✓	✓	
Htr1d	1.39	2.73E-03	27.95667	8.99	✓			
Sbds	0.67	2.78E-03	855.57	526.6	✓			
Nfic	0.76	2.79E-03	1088.21	629.36	✓	✓		
Nectin4	1.11	2.83E-03	151.41	64.64	✓			
Zfp423	0.72	2.87E-03	401.5667	238.1167	✓			
Cox16	1.21	2.90E-03	107.1167	41.12667	✓			
Tac2	1.28	2.95E-03	59.62333	20.99333	✓	✓		
Slc17a8	1.06	3.08E-03	86.48667	38.95333	✓	✓		
Slc7a14	0.44	3.09E-03	951.87	700.5567	✓	✓		
Tom1	0.50	3.11E-03	560.3067	395.5133	✓			
Cops5	0.50	3.13E-03	946.6433	669.03	✓			
Slc12a8	1.46	3.17E-03	33.21	9.506667	✓			
Ifit2	0.97	3.23E-03	146.37	69.35333	✓			
Nppc	1.30	3.31E-03	58.18333	19.61333	✓			
Tacr1	0.92	3.34E-03	116.58	59.58	✓			
Sema7a	0.88	3.41E-03	2001.83	1044.547	✓	✓		
Faf2	0.52	3.48E-03	628.5833	432.62	✓			
Irx5	1.18	3.50E-03	39.05	15.36333	✓			
Rxra	0.62	3.54E-03	528.46	338.7233	✓	✓		
App	0.93	3.55E-03	16463.24	8269.9	✓			
Dirc2	0.70	3.56E-03	567.68	341.44	✓	✓		
Fblim1	1.30	3.65E-03	46.82667	16.43333	✓			
Txndc17	0.82	3.67E-03	351.3	192.5233	✓	✓		
Reep2	0.42	3.67E-03	1510.333	1124.58	✓			
P2ry1	1.02	3.71E-03	117.3633	53.76	✓	✓		
Npy	1.02	3.78E-03	225.1633	103.5067	✓	✓		
Arhgap12	0.73	3.78E-03	889.65	526.33	✓	✓	✓	
Npffr1	1.79	3.80E-03	13.24667	1.736667	✓			
1190002N15Rik	0.84	3.80E-03	378.8233	204.0167	✓			
Atg3	0.70	3.81E-03	517.9067	310.7933	✓	✓	✓	
Armc1	0.63	3.85E-03	989.36	631.12	✓			
Zbtb11	0.53	3.87E-03	2622.32	1801.423	✓			
Derl1	0.62	3.91E-03	876.5	561.78	✓			
Sarnp	0.74	3.94E-03	514.4467	300.37	✓			
Mrgpre	1.07	3.98E-03	162.0667	71.53667	✓			

Gene Symbol	Fold-enrichment	P-Adj	Mean RPKM GABA-IP	Mean RPKM DA-IP	PANTHER	ABA density	ABA ISH	Cre-Driver
Ehd1	0.62	4.06E-03	468.8833	300.87	✓	✓		
Nup50	0.64	4.07E-03	719.2733	455.9467	✓	✓		
Wnt7a	1.00	4.08E-03	152.1333	70.67333	✓			
Gas6	0.46	4.08E-03	1797.367	1299.04	✓			
Atp6v1g2	0.89	4.12E-03	4794.81	2476.973	✓			
Cox8a	0.99	4.18E-03	2475.88	1177.637	✓			
Kcnn1	0.78	4.47E-03	220.86	124.9933	✓			
Kpna2	0.59	4.56E-03	311.2033	204.78	✓			
Ascl4	1.84	4.58E-03	38.84667	3.14	✓			
Cux1	0.66	4.61E-03	474.2567	295.85	✓	✓		
Rgmb	0.78	4.62E-03	1384.78	783.9833	✓			
Gsk3b	0.67	5.01E-03	2130.727	1316.22	✓			
Dcbld1	0.72	5.13E-03	134.3233	79.09667	✓			
Slc22a23	0.45	5.24E-03	745.4667	540.0867	✓	✓		
Bmp2	0.99	5.46E-03	66.47	31.37333	✓			
Dap	1.25	5.62E-03	119.93	42.99333	✓			
Wnt3	0.95	5.64E-03	115.7867	57.22667	✓			
Foxj1	0.84	5.67E-03	141.7533	76.33	✓	✓		
Grina	0.54	5.82E-03	4422.32	3007.477	✓	✓		
Kcnip4	0.80	5.88E-03	826.3267	459.7567	✓	✓	✓	
Pole4	0.75	5.92E-03	358.2867	206.09	✓	✓		
Emb	0.67	6.10E-03	383.2767	236.9467	✓	✓		
Elmod1	0.48	6.49E-03	1536.313	1095.003	✓			
Lrrn3	0.78	6.51E-03	550.69	311.5733	✓			
Fgf11	0.75	6.51E-03	838.5267	485.3233	✓			
Ctnnb1	0.53	6.61E-03	4017.4	2754.667	✓			
Mnat1	0.62	6.87E-03	202.0133	129.69	✓			
Ppp1r1b	0.95	7.08E-03	769.6367	376.86	✓	✓		
Dpf3	0.96	7.25E-03	66.08	31.29	✓	✓		
Tspan7	0.86	7.36E-03	6819.003	3611.833	✓			
Negr1	0.73	7.50E-03	1527.843	896.31	✓			
Spry4	0.72	7.65E-03	226.7533	134.1567	✓			
Gtf2b	0.70	7.80E-03	425.21	254.9833	✓	✓		
Nrg1	0.77	8.09E-03	74.47	42.90333	✓	✓		
Tmeff2	0.60	8.11E-03	788.2367	513.3767	✓			
Sema3e	0.68	8.34E-03	257.4333	158.27	✓	✓		
Btbd2	0.46	8.50E-03	711.68	513.9267	✓	✓		
S100b	**1.45**	**8.54E-03**	**2834.257**	**747.01**	✓	✓	✓	✓
Dscr3	0.51	8.63E-03	583.93	408.8033	✓			
Aatf	0.68	8.66E-03	211.9067	130.2833	✓			
Btbd3	0.46	8.66E-03	1330.523	962.0767	✓	✓		
Cntnap4	0.74	8.79E-03	528.0233	310.1667	✓			
Oxa1l	0.39	8.89E-03	509.2467	386.9	✓			
Arhgef4	0.44	9.09E-03	2563.777	1880.757	✓			
Unc5b	0.69	9.17E-03	448.47	271.7367	✓	✓	✓	
Cacng4	0.87	9.22E-03	718.96	376.19	✓	✓		
Nkx2-2	0.83	9.25E-03	89.52333	48.72333	✓	✓		
Atg5	0.65	9.31E-03	301.96	188.3633	✓	✓		
Lgr5	0.86	9.42E-03	105.37	56.86667	✓	✓		
Slc8a3	0.62	9.43E-03	371.51	237.8933	✓			
Ptprm	0.84	9.43E-03	519.17	278.2567	✓			
Gtf2e2	0.73	9.43E-03	237.2	138.6933	✓			
Cort	1.17	9.58E-03	40.36667	15.66	✓			
Stx18	1.23	9.86E-03	702.75	256.72	✓			
Dtx1	0.52	9.87E-03	822.4733	565.8933	✓			
Adcyap1	0.91	9.98E-03	279.0333	139.7133	✓			
Kcnk12	0.97	1.01E-02	95.35	44.81333	✓			
Lsamp	0.71	1.01E-02	3144.223	1881.777	✓	✓	✓	
Psip1	0.42	1.02E-02	3052.007	2278.067	✓			

Gene Symbol	Fold-enrichment	P-Adj	Mean RPKM GABA-IP	Mean RPKM DA-IP	PANTHER	ABA density	ABA ISH	Cre-Driver
Bnip3l	0.74	1.02E-02	1437.62	835.99	✓	✓	✓	
Tfap2b	1.22	1.03E-02	193.18	70.76333	✓			
Crtam	1.61	1.05E-02	47.90667	7.903333	✓			
Cbx4	0.69	1.05E-02	680.4433	411.8333	✓			
Ngf	1.26	1.06E-02	28.19667	9.54	✓			
Cntn1	0.63	1.07E-02	3445.753	2183.01	✓	✓	✓	
Zfp787	0.65	1.07E-02	200.1033	124.0633	✓			
Tbl3	0.54	1.13E-02	433.35	296.0567	✓	✓		
Gjb1	1.10	1.14E-02	200.7367	83.43	✓			
Zfp597	0.57	1.15E-02	285.8433	189.5833	✓	✓		
Olig1	1.04	1.18E-02	1514.32	672.6267	✓			
Arhgdia	0.66	1.18E-02	2164.75	1336.117	✓			
Irx4	1.61	1.19E-02	13.65	1.836667	✓			
Gata2	0.73	1.20E-02	155.69	90.44	✓			
Abcf3	0.59	1.21E-02	1291.573	849.0333	✓			
Lpar1	1.04	1.22E-02	351.8667	154.2467	✓	✓	✓	
Gdf10	0.95	1.22E-02	65.18333	30.48333	✓			
Tsc22d1	0.58	1.23E-02	4098.153	2704.167	✓			
Leng1	0.62	1.24E-02	193.67	123.6933	✓			
Nrip3	0.68	1.25E-02	2677.5	1638.907	✓			
Fam43b	0.74	1.27E-02	285.14	166.6567	✓			
Atf4	0.49	1.27E-02	1722.967	1214.483	✓			
Socs5	0.54	1.28E-02	1493.47	1015.81	✓			
Hoxb4	1.52	1.31E-02	10.94	1.91	✓	✓		
Rcan1	0.57	1.31E-02	616.48	407.9233	✓			
Asic1	0.45	1.32E-02	761.1767	556.6133	✓			
Bud31	0.56	1.34E-02	435.7	291.9833	✓			
Lrrc8d	0.65	1.36E-02	315.34	195.3333	✓			
Dgkg	0.72	1.37E-02	520.5233	307.0433	✓	✓		
Gtf2f2	0.79	1.37E-02	133.6567	72.79333	✓			
Gnl3l	0.52	1.38E-02	2335.713	1614.063	✓			
Pth1r	0.73	1.38E-02	133.9067	77.89	✓	✓		
Kpnb1	0.41	1.39E-02	1753.96	1317.593	✓	✓	✓	
Kcnj5	0.97	1.40E-02	37.44	17.95333	✓			
Nacc1	0.44	1.46E-02	1029.327	750.9267	✓	✓		
Abcf2	0.60	1.46E-02	995.8333	646.71	✓			
Atp5g2	0.85	1.50E-02	732.2367	386.09	✓			
Lrrtm3	0.72	1.50E-02	362.2667	214.0167	✓			
Gid8	0.68	1.51E-02	466.18	282.4667	✓			
Sdc3	0.61	1.56E-02	2516.153	1618.02	✓			
Lrp12	0.61	1.56E-02	394.9633	254.4167	✓			
Abtb2	0.62	1.56E-02	178.7867	112.9767	✓			
Serinc1	0.51	1.56E-02	4858.543	3382.35	✓			
Taf9	0.55	1.60E-02	425.1967	285.3433	✓			
Thra	0.54	1.64E-02	6484.623	4401.097	✓	✓		
4930452B06Rik	0.73	1.65E-02	139.66	81.88	✓	✓		
Tpr	0.76	1.66E-02	1582.54	900.8633	✓	✓		
Btg1	0.64	1.66E-02	380.7967	238.3	✓	✓		
Lrsam1	0.64	1.68E-02	613.7933	385.69	✓	✓	✓	
Mapk8ip1	0.42	1.71E-02	4261.11	3176.757	✓			
Srpr	0.49	1.73E-02	706.9833	500.5733	✓	✓	✓	
Tspan2	0.73	1.74E-02	1686.29	984.9367	✓			
Zhx1	0.53	1.75E-02	641.5367	437.2367	✓	✓		
Cbx5	0.46	1.77E-02	2102.827	1521.293	✓	✓		
Yaf2	0.63	1.77E-02	751.4367	474.8033	✓	✓		
Cd81	0.73	1.77E-02	2664.823	1555.86	✓			
Kdelr2	0.57	1.79E-02	282.05	185.7267	✓			
Cadm3	0.60	1.80E-02	3352.033	2181.43	✓			

Gene Symbol	Fold-enrichment	P-Adj	Mean RPKM GABA-IP	Mean RPKM DA-IP	PANTHER	ABA density	ABA ISH	Cre-Driver
Zhx3	0.43	1.80E-02	668.62	491.46	✓			
Mpnd	0.55	1.80E-02	1304.997	877.38	✓			
Wif1	1.18	1.81E-02	17.05667	6.406667	✓			
Ehd4	0.61	1.82E-02	220.6967	142.7267	✓	✓		
Agrp	1.52	1.82E-02	16.79333	3.023333	✓			
B3galt4	0.75	1.84E-02	48.69	27.87667	✓			
Foxb1	1.25	1.86E-02	48.4	15.87	✓	✓		
Nxph2	1.11	1.89E-02	34.47667	14.32333	✓			
Igfbp4	0.68	1.90E-02	588.56	355.8733	✓	✓	✓	
Slc12a5	0.53	1.90E-02	6176.3	4233.6	✓			
Tspan4	0.75	1.94E-02	258.66	147.3567	✓			
Zfp37	0.58	1.95E-02	188.51	123.8067	✓			
Bok	0.79	1.97E-02	318.3867	176.8767	✓	✓		
Polr3h	0.66	2.00E-02	469.4167	289.8133	✓	✓		
Atp2a1	1.24	2.04E-02	22.76	7.46	✓			
Elfn1	0.68	2.06E-02	227.48	137.4667	✓	✓	✓	
Prmt5	0.34	2.07E-02	564.1633	443.64	✓			
Clcn5	0.58	2.08E-02	360.38	239.8167	✓	✓	✓	
Fam19a2	0.81	2.09E-02	589.7867	321.5733	✓			
Uso1	0.44	2.12E-02	1112.87	813.2633	✓			
Bcl2	0.68	2.12E-02	263.03	158.7167	✓	✓		
Sorl1	0.69	2.13E-02	3487.53	2106.27	✓			
Arhgap26	0.65	2.19E-02	1179.553	732.74	✓	✓		
Slc25a2	1.51	2.20E-02	9.623333	1.536667	✓			
Ogfrl1	0.71	2.21E-02	2044.653	1213.25	✓	✓		
Cyb5d2	0.62	2.21E-02	137.5833	87.32667	✓			
Nhlh2	0.75	2.29E-02	91.50333	53.29333	✓	✓		
Xpr1	0.47	2.29E-02	886.0133	632.0067	✓	✓		
Hoxb2	1.46	2.35E-02	9.966667	1.72	✓	✓		
Nectin1	0.54	2.37E-02	557.7067	378.82	✓			
Smyd3	0.53	2.37E-02	403.4133	275.2067	✓			
Chrac1	0.59	2.51E-02	141.29	91.48	✓	✓		
C3	1.17	2.52E-02	21.53333	8.116667	✓			
Creld1	0.55	2.58E-02	1141.957	769.56	✓			
Irs1	0.61	2.59E-02	307.2367	197.0033	✓			
Stat5b	0.54	2.64E-02	466.7167	316.8133	✓	✓		
Hspa12a	0.62	2.68E-02	2730.873	1745.787	✓			
Acsf3	0.53	2.75E-02	265.5467	181.6433	✓	✓		
Gucy1a3	0.59	2.75E-02	671.4467	439.7667	✓	✓	✓	
Mafa	1.44	2.81E-02	13.48	2.066667	✓			
Rbm43	0.49	2.81E-02	242.7833	171.47	✓	✓		
G3bp1	0.35	2.82E-02	886.06	693.49	✓	✓		
Hoxb3	1.41	2.99E-02	12.2	2.283333	✓			
Bloc1s1	0.88	3.00E-02	172.83	86.1	✓			
Tceal5	0.57	3.01E-02	664.11	439.9167	✓			
Svop	0.48	3.04E-02	1515.28	1072.097	✓			
Esr1	0.91	3.08E-02	56.19	26.95	✓			
Camta1	0.40	3.09E-02	4724.483	3568.28	✓			
Tmeff1	0.58	3.10E-02	843.09	552.85	✓	✓	✓	
Apbb2	0.50	3.13E-02	538.8633	376.8233	✓	✓		
Jup	0.65	3.13E-02	401.95	248.3633	✓	✓		
Calcr	1.25	3.23E-02	22.9	7.043333	✓			
Kcna5	0.94	3.27E-02	40.52333	19.13333	✓			
Sp8	1.30	3.29E-02	26.94333	7.903333	✓			
Jun	0.59	3.30E-02	667.1933	432.3233	✓			
Slc45a1	0.40	3.30E-02	761.2267	573.4	✓	✓		
Scfd2	0.56	3.32E-02	153.8333	102.5267	✓			
Slc17a6	0.74	3.37E-02	1073.203	615.3	✓			

Gene Symbol	Fold-enrichment	P-Adj	Mean RPKM GABA-IP	Mean RPKM DA-IP	PANTHER	ABA density	ABA ISH	Cre-Driver
Stk24	0.71	3.37E-02	460.7367	270.9967	✓	✓		
Slc38a10	0.38	3.41E-02	831.0867	636.4233	✓			
Homez	0.55	3.41E-02	171.94	115.0367	✓			
Zmynd12	1.41	3.42E-02	20.06667	2.67	✓			
Vdr	1.37	3.44E-02	11.19333	2.06	✓	✓		
Six3	1.40	3.44E-02	5.78	0.706667	✓			
Slc25a38	0.47	3.48E-02	339.3833	242.7633	✓			
Atp2a2	0.50	3.51E-02	6564.203	4576.683	✓			
Zfp385b	0.68	3.51E-02	227.3233	137.1067	✓	✓		
Grid1	0.61	3.59E-02	509.1833	324.9133	✓			
Sparcl1	0.71	3.63E-02	11640.02	6837.187	✓			
Tceal7	1.30	3.69E-02	40.93333	10.79333	✓			
Oxtr	0.69	3.70E-02	82.26667	48.74	✓	✓		
SOMr5	1.22	3.81E-02	11.68	3.533333	✓			
Tcea1	0.44	3.91E-02	938.42	689.0533	✓			
Pgf	0.86	3.92E-02	68.12667	34.02	✓	✓		
Ifit3b	0.85	3.95E-02	51.41667	25.64	✓			
Slc22a17	0.42	3.98E-02	5498.957	4093.96	✓			
Gabre	0.96	4.00E-02	24.98	12.22333	✓	✓	✓	
Gpr37	0.80	4.04E-02	405.57	218.9667	✓	✓		
Tmem241	0.72	4.07E-02	71.84333	41.20667	✓			
Nrp2	**0.42**	**4.10E-02**	**356.91**	**264.8933**	✓	✓	✓	✓
Slc5a3	0.50	4.11E-02	478.4367	334.8233	✓	✓		
Atf2	0.49	4.15E-02	1090.033	764.8333	✓			
Btbd1	0.42	4.17E-02	1382.643	1022.57	✓			
Tnfrsf11b	0.91	4.20E-02	30.86333	14.34667	✓	✓		
Foxp4	0.53	4.22E-02	493.02	334.8267	✓	✓	✓	
Foxp2	0.82	4.31E-02	429.23	229.2567	✓	✓	✓	
Foxo3	0.45	4.36E-02	695.6433	501.12	✓			
Hoxa2	1.35	4.36E-02	6.626667	1.046667	✓			
Kcnk13	0.79	4.39E-02	86.76667	46.82	✓	✓		
Cit	0.50	4.43E-02	2091.9	1460.26	✓			
Pax3	1.09	4.43E-02	22.39333	8.916667	✓	✓		
Nkiras2	0.61	4.44E-02	126.7733	80.38	✓	✓		
Ell3	1.26	4.47E-02	5.14	0	✓			
Tada2b	0.55	4.51E-02	333.5167	222.5767	✓	✓		
Ucn	1.30	4.54E-02	45.24	9.57	✓	✓		
Asgr1	1.13	4.59E-02	57.04333	20.16	✓	✓		
Scarb2	0.49	4.59E-02	350.5933	245.33	✓			
Zmat4	0.62	4.68E-02	602.7167	381.7967	✓	✓		
Slc43a2	0.49	4.68E-02	885.3633	622.33	✓	✓		
Bcam	0.58	4.71E-02	280.7233	183.31	✓	✓	✓	
Med27	0.41	4.76E-02	172.2067	128.5267	✓			
Gng11	0.89	4.78E-02	179.9233	87.80667	✓			
Kdelr1	0.56	4.79E-02	427.0667	282.36	✓	✓	✓	
Psen2	0.41	4.88E-02	229.2667	172.1067	✓	✓		
Mapk10	0.58	4.96E-02	3243.447	2129.17	✓			